

THE UNIVERSITY OF CALGARY

Investigations in Glacial Hydrology Through the Use of Ground-Penetrating Radar

by

Amy Lyttle

A THESIS

SUBMITTED TO THE FACULTY OF GRADUATE STUDIES
IN PARTIAL FULFILLMENT OF THE REQUIREMENTS FOR THE
DEGREE OF MASTER OF SCIENCE

DEPARTMENT OF GEOGRAPHY

CALGARY, ALBERTA

JUNE 2001

© Amy Lyttle 2001



National Library
of Canada

Acquisitions and
Bibliographic Services

395 Wellington Street
Ottawa ON K1A 0N4
Canada

Bibliothèque nationale
du Canada

Acquisitions et
services bibliographiques

395, rue Wellington
Ottawa ON K1A 0N4
Canada

Your file Votre référence

Our file Notre référence

The author has granted a non-exclusive licence allowing the National Library of Canada to reproduce, loan, distribute or sell copies of this thesis in microform, paper or electronic formats.

The author retains ownership of the copyright in this thesis. Neither the thesis nor substantial extracts from it may be printed or otherwise reproduced without the author's permission.

L'auteur a accordé une licence non exclusive permettant à la Bibliothèque nationale du Canada de reproduire, prêter, distribuer ou vendre des copies de cette thèse sous la forme de microfiche/film, de reproduction sur papier ou sur format électronique.

L'auteur conserve la propriété du droit d'auteur qui protège cette thèse. Ni la thèse ni des extraits substantiels de celle-ci ne doivent être imprimés ou autrement reproduits sans son autorisation.

0-612-65115-0

Canada

ABSTRACT

To date, most glacial hydrology research has been limited to the use of dye tracer experiments, hydrograph separation, and hydrochemistry. New ground-penetrating radar (GPR) systems have recently been shown to be very effective in imaging detailed hydrological features such as conduits and cavities of glaciers. This research has utilized GPR to investigate the existence and structure of englacial and subglacial conduits and cavities within a glacier in the Canadian Arctic.

The glacier studied, informally named Stagnation Glacier, is located on the south side of Bylot Island, Nunavut Territory. Previous research suggests that the glacier may be polythermal. An extensive GPR survey was conducted on the lower part of the glacier and was used to model the hydrologic and thermal structure. GPR interpretation indicates the presence of hydrologic networks, zones of warm-ice and sediment accretion. This work provides further evidence that the ablation zone of Stagnation Glacier may be polythermal, and might be capable of forming, if not at least maintaining, extensive hydrologic networks and warm-ice zones.

ACKNOWLEDGEMENTS

I would like to thank those individuals whose contributions made this project possible. First and foremost, Dr. Brian Moorman, a truly great teacher and friend, provided countless hours of support, assistance and, above all, inspiration. His willingness to assist and provide guidance is indescribably appreciated.

This project would not be possible had it not been for the support and aid from various people. I would like to express my gratitude to Darren Sjogren, Masaki Hayashi, Shawn Marshall, Regina Shedd, Len Hills, Carolyn Deacock, the Department of Geography, and the Department of Geology and Geophysics.

This research was supported by the Department of Indian and Northern Affairs through the Northern Scientific Training Program, the Faculty of Graduate Studies, the Polar Continental Shelf Project, and the Town of Pond Inlet, Nunavut.

Finally, I would like to thank my friends, my family, and Steve Daca for their continuous support and encouragement.

TABLE OF CONTENTS

Acceptance Page.....	ii
Abstract.....	iii
Acknowledgements.....	iv
Table of Contents.....	v
List of Figures.....	viii
CHAPTER 1 INTRODUCTION.....	1
1.1 BACKGROUND.....	1
1.2 GLACIER CLASSIFICATION.....	2
1.3 WATER SOURCES.....	4
1.4 GLACIAL HYDROLOGY.....	6
1.4.1 Microscale Hydrology.....	6
1.4.2 Macroscale Hydrology.....	7
1.4.2.1 <i>Supraglacial Hydrology</i>	8
1.4.2.2 <i>Englacial Hydrology</i>	9
1.4.2.3 <i>Subglacial Hydrology</i>	15
1.4.3 Hydrological Dynamics.....	18
1.4.4 Ground-Penetrating Radar and Glacial Hydrology.....	20
1.5 OBJECTIVES.....	21
CHAPTER 2 STUDY AREA.....	22

CHAPTER 3	METHODOLOGY	27
3.1	GROUND-PENETRATING RADAR.....	27
3.2	GEOPHYSICAL SPECIFICATIONS.....	28
3.3	GPR PARAMETERIZATION.....	32
3.3.1	System Parameters.....	33
3.4	ANCILLARY DATA.....	35
CHAPTER 4	SURFICIAL HYDROLOGY	37
4.1	SUPRAGLACIAL HYDROLOGY.....	37
4.2	PERIGLACIAL HYDROLOGY.....	40
4.3	MORAINIE HYDROLOGY.....	42
CHAPTER 5	SUBSURFACE HYDROLOGY: RESULTS	44
5.1	GPR DATA PROCESSING.....	44
5.2	GPR DATA INTERPRETATION.....	46
5.3	SUBSURFACE HYDROLOGY RESULTS.....	58
5.3.1	Lower Section.....	58
5.3.2	Middle Section.....	67
5.3.3	Upper Section.....	72
CHAPTER 6	DISCUSSION: SUBSURFACE HYDROLOGY	82
6.1	HYDROLOGICAL NETWORKING.....	82
6.2	THERMAL CHARACTER.....	90

6.3 SUBGLACIAL SEDIMENTATION.....	96
CHAPTER 7 CONCLUSIONS.....	99
7.1 SUMMARY.....	99
7.2 RECOMMENDATIONS FOR FUTURE WORK.....	101
BIBLIOGRAPHY	103
APPENDIX GPR PROFILES.....	108

LIST OF FIGURES AND ILLUSTRATIONS

Figure 1.1	Schematic representation of glacial thermal regimes. Grey line represents the annual temperature range within the glacier.....	3
Figure 1.2	Lowering of the melting point of pure ice due to increases in pressure with depth.....	5
Figure 1.3	Schematic cross section of a vein formed from the junction of three grains (Raymond and Harrison, 1975).....	7
Figure 1.4	Drainage tunnels extending from moulines dipped 0 – 45 ° from vertical in the down-glacier direction (Holmlund, 1988).....	10
Figure 1.5	Theoretical direction of englacial flow based on Shreve (1972) (Adapted from Hooke, 1989).....	13
Figure 1.6	Schematic of changing conduit shape with age due to the preferential melting and subsequent vertical deepening.....	14
Figure 1.7	Schematic showing gradient from debris-free ice to debris-rich ice to ice-rich debris.....	15
Figure 1.8	Equipotential contours near highs on glacier bed (adapted from Hooke, 1989).....	16
Figure 2.1	Map of Canada and Greenland showing location of Bylot Island.....	23
Figure 2.2	Satellite image of study site on Bylot Island, Nunavut Territory.....	23

Figure 2.3	Oblique aerial photograph of Stagnation Glacier, Bylot Island.....	24
Figure 3.1	Ground-penetrating radar on the surface of Stagnation Glacier.....	29
Figure 3.2	Relationship of centre frequency (f_c) and bandwidth (Δf) (Annan, 1992).....	31
Figure 3.3	Schematic of GPR antennae orientation and radar footprint. Note this type of data collection orients the radar footprint such that the shape is elongated in the direction of travel.....	36
Figure 3.4	Organization of collected data. Shaded boxes indicate field-based work.....	36
Figure 4.1	Map of the lower portion of Stagnation Glacier, the locations of surficial features, and GPR lines.....	39
Figure 5.1	GPR system consisting of a transmitter (Tx) and a receiver (Rx) (left), and single wavelet formed from the reflection of radio waves off of a boundary between differing materials.....	47
Figure 5.2	Topographic map of Stagnation Glacier and the surrounding area. Elevations are in metres above sea level.....	51
Figure 5.3	DEM of Stagnation Glacier and surrounding area.....	52

Figure 5.4	GPR Profile 99-1/2 between the intersections of 99-37 and 99-34. Note the rise in basal topography upstream (to the right) of the hyperbolic reflections. Glacier flow is from right to left.....	54
Figure 5.5	GPR Profile 99-27. Note the thickening in glacier ice as a result of a decrease in elevation of the base, and an increase in elevation of the glacier surface.....	55
Figure 5.6	Map of Stagnation Glacier divided into upper, middle and lower sections. GPR line numbers and direction of travel are indicated as well.....	56
Figure 5.7	GPR profiles 99-34 and 99-35. Note the circled continuous reflections at 60 metres depth (75 – 100 metre position). The reflections have a positive polarity, indicating the feature producing the reflection is either sediment or water. Glacier flow is out of the page (towards the reader).....	59
Figure 5.8	GPR Profile 99-36. Glacier flow is from left to right. Note the large positive-polarity hyperbolae from positions 130 metres to 250 metres. These have been interpreted as water-filled conduits. The high frequency reflections seen from positions 123 metres to 200 metres (25 metres depth) are probably from a zone of sealed crevasses. The beginning of a warm-ice zone (circled) is also interpreted, starting at 90 metres (70 metres depth). The reflection becomes weaker near the 50 metre position.....	61

Figure 5.9	GPR Profile 99-33. Note the change in the circled basal reflection along positions 75 – 100 metres (70 metres depth). This change could indicate the presence of water flow at the base. Glacier flow is from right to left. A strong reflection from 0 – 24 metres along the profile is interpreted as the upper layer of basal sedimentation.....	62
Figure 5.10	Schematic of Stagnation Glacier showing proposed conduit orientation as interpreted from GPR data from profiles 99-1/2, 33, 34, 35 and 36.	63
Figure 5.11	Schematic showing the regelation of plucked bedrock material into basal ice.....	64
Figure 5.12	GPR Profile 99-32 showing debris entrainment into basal ice at the glacier margin. The sedimentation at the eastern portion of the profile is observed at the northern portion of 99-33 (Figure 5.9). Glacier flow is out of the page (towards the reader).....	66
Figure 5.13	GPR Profile 99-1/2 between 99-43 and 99-10. Note the extension of the zero-degree isotherm through the glacier to the bedrock/till (circled). Glacier flow is from right to left.....	69
Figure 5.14	GPR Profile 99-46. Note the reflector dipping downstream from 145 to 155 metres, which has been interpreted as a reach of a water-filled conduit. Glacier flow is from right to left.....	71

Figure 5.15	GPR Profile 99-25, showing the type of reflection generated from what is thought to be a warm-ice zone. The zone starts at 78 m depth (position 0 metres) and thins out down to 106 metres depth (approximately 70 metres in position). Where the zone becomes thinner than 20 metres, the cold-ice/warm-ice interface becomes less obvious. 99-25 was surveyed along a traverse diagonal to glacier flow. Glacier flow is into the page (away from the reader).....	74
Figure 5.16	GPR Profile 99-1/2, in the vicinity of 99-14, in the upper section of Stagnation Glacier. Note the steep rise in basal topography. Glacier flow is from right to left.....	76
Figure 5.17	Map of the interpreted hydrologic features within the lower section of Stagnation Glacier. Note the content, depth and elevation (if known) of the interpreted GPR reflections. Refer to Appendix for map of entire glacier.....	77
Figure 5.18	Map of the interpreted hydrologic features within the middle section of Stagnation Glacier. Note the content, depth and elevation (if known) of the interpreted GPR reflections. Refer to Appendix for map of entire glacier.....	78
Figure 5.19	Map of the interpreted hydrologic features within the upper section of Stagnation Glacier. Note the content, depth and elevation (if known) of the interpreted GPR reflections. Refer to Appendix for map of entire glacier.....	79
Figure 5.20	Map of the warm-ice zones in the upper section interpreted from the GPR data. Refer to Appendix for map of entire glacier.....	80

Figure 5.21	Map of the warm-ice zones on the lower and middle sections of Stagnation Glacier. Refer to Appendix for map of entire glacier.....	81
Figure 6.1	GPR profiles of the experimental ice cube. The top profile was obtained while the PVC tube was empty, similar to an air-filled conduit in a glacier. The bottom profile was obtained after the tube was filled with liquid water. At position 0.96 m, the top of the air-filled tube is seen at 4.25 ns (0.7 m depth) by a reflection with negative polarity (- + -). The top of the water-filled tube is seen at the same position, time and depth, but is represented by a reflection with positive polarity (+ - +).....	84
Figure 6.2	Schematic of glacial ice extending into the moraine, showing the process of ice-cored moraine formation.....	88
Figure 6.3	Map of generalized hydrologic and thermal structures within Stagnation Glacier. Englacial / subglacial water is forced to flow towards the margins upstream due to a downstream blockage of flow. This is due to thinner ice and colder ice temperatures.....	93

CHAPTER ONE

INTRODUCTION

1.1 BACKGROUND

The movement of water within glaciers is highly complex, and is subject to variations in atmospheric conditions, glacial mechanics, ice composition, and glacial thermal conditions. Attempts to understand the hydrological processes at work within glaciers have been made, primarily on temperate (warm-based), subpolar glaciers. Much theoretical research, and somewhat inconclusive field research, in glacial hydrology (particularly supraglacial and subglacial hydrology) has been conducted for nearly a century. However, the inaccessibility of the englacial and subglacial networks has limited our full understanding of glacial hydrology. Use of geophysical tools in glaciology research have been developed as a non-intrusive method of imaging the glacial subsurface.

One such tool is ground-penetrating radar (GPR). Modern GPR systems are particularly successful in producing detailed images of the glacial-hydrological features.

This thesis describes the results of a research program in which GPR was employed to map drainage conduits in order to provide a better understanding of the hydrology of a glacier on Bylot Island in the Canadian High Arctic.

1.2 GLACIER CLASSIFICATION

Traditional glacier classification schemes were based on geomorphological characteristics and originated the piedmont, valley, and cirque glacier terminology. It became apparent that the shape of a glacier indicated very little about the composition and mechanics of individual glaciers. Glacier classifications based on climate and temperature also proved to be insufficient once glaciologists recognized that entire glaciers are not homogeneous in their shape, mechanics or thermal structure. As a result, a classification of areas or zones within glaciers was developed.

Polar, or cold-based glaciers are glaciers that are below the melting point throughout. Temperate glaciers are at the melting point everywhere throughout the glacier except for a surface layer that is subject to seasonal and diurnal temperature changes. Subpolar or polythermal glaciers are temperate glaciers with cold regions, often at the base (Figure 1.1). This type of classification was deemed too simplistic by glaciologists in the 1970's and has since been replaced by classifications of the ice within glaciers. Cold ice is below the melting point, whereas temperate ice, or warm ice, is at the melting point.

Polythermal glacier temperature regimes have been studied by Fowler (1984), Blatter (1987), Blatter and Hutter (1991), and Jansson (1996). The new research conducted

on High Arctic Canadian glaciers and Svalbard glaciers is indicating our previous understanding of the hydrology of non-temperate ice is incomplete.

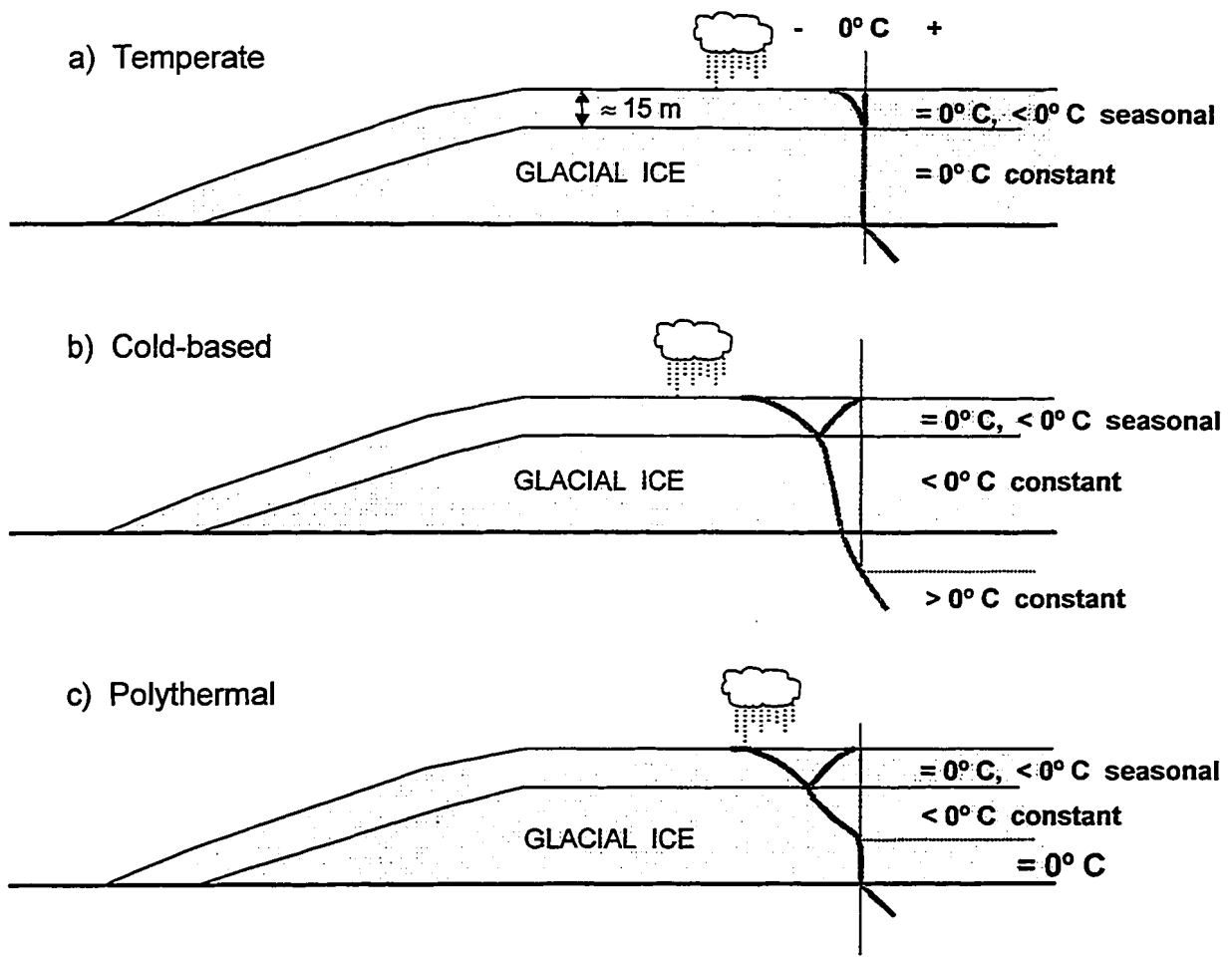


Figure 1.1 Schematic representation of glacial thermal regimes. Grey line represents the annual temperature range within the glacier.

1.3 WATER SOURCES

The liquid water in a glacier originates from many sources. Meltwater is produced at the surface, internally and at the glacier bed. Meltwater is produced at the glacier surface from warmer atmospheric temperatures, solar radiation, and melting from rain falling directly on the glacier (Shreve, 1972). Surficial meltwater is a major component of glacial runoff for temperate and alpine glaciers. Due to low temperatures and minimal rainfall, surface meltwater is relatively minimal on cold or polar glaciers.

Surface meltwater may travel across a glacier surface in a similar manner to meandering fluvial systems. Surface meltwater enters the glacier's hydrologic system by percolating through permeable snow and firn layers in the accumulation area, or through crevasses and moulins anywhere on the glacier.

Internal and subglacial melting occurs from heat production associated with ice deformation and viscous dissipation, the lowering of the melting point of ice due to increases in pressure or solute concentration, and geothermal heat absorption. Deformation melting is produced from internal friction and is calculated from the difference between total work of glacier motion and the portion of work required to exceed the sliding friction at the bed (Zotikov, 1986).

Viscous dissipation is the frictional force of water along a conduit wall or drainage surface as the water flows through it (Shreve, 1972). Melting due to viscous dissipation can be calculated with theoretical values for conduit size, shape, hydraulic gradient, discharge, hydraulic pressure and the temperature of water (Shreve, 1972). These values are difficult to measure within a glacier and at best provide a rough estimate of melting due to viscous dissipation.

A third source of meltwater is created when the melting point of ice is lowered from an increase in pressure. A gradient of $0.072^{\circ}\text{C}/\text{MPa}$ has been calculated in laboratory conditions and does not take into account the effect of impurities or solutes in ice on the melting point.

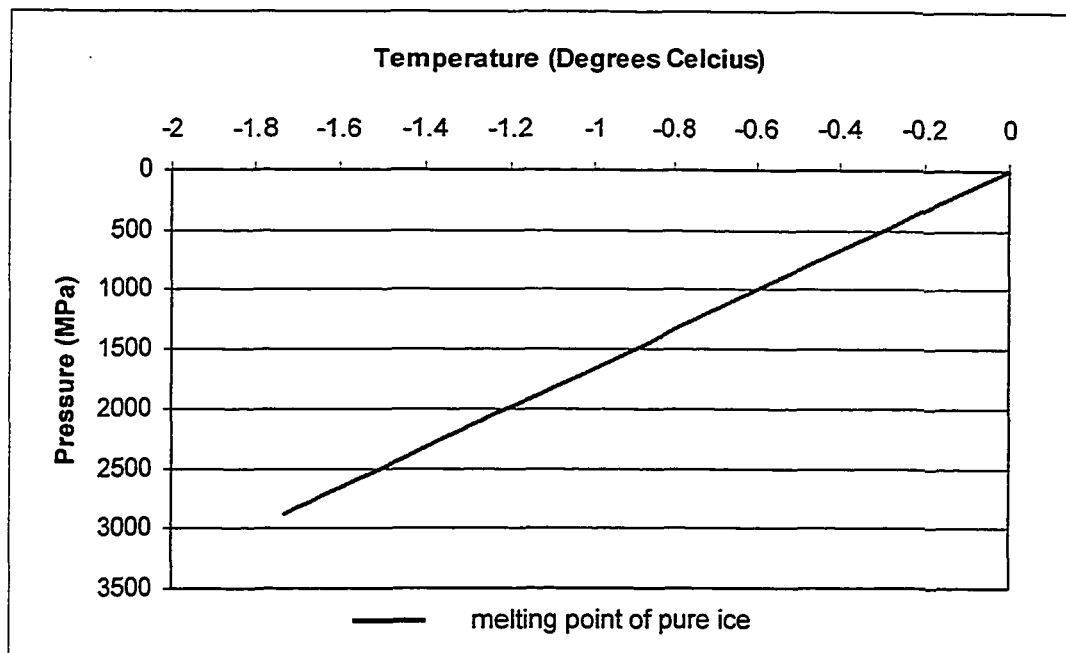


Figure 1.2 Lowering of the melting point of pure ice due to increases in pressure with depth.

Examples of impurities found in ice are particulate matter (e.g. salts) and air. The melting point of sea ice is reduced by salt concentration and is approximately -2°C at atmospheric pressure (Benn and Evans, 1998). Meltwater can be produced from geothermal heat sources at the bed of a glacier. The geothermal gradient ranges from $0.04 \text{ W}/\text{m}^2$ in the continental shield to $0.09 \text{ W}/\text{m}^2$ in areas of recent volcanic activity. The global average of $0.0599 \text{ W}/\text{m}^2$ can melt up to 6 mm of ice per year (Patterson, 1994).

1.4 GLACIAL HYDROLOGY

The movement of liquid water generated within a glacier is governed by the hydraulic gradient and the permeability of the ice. The hydraulic gradient is the rate at which the hydraulic potential changes from an area of high hydraulic potential to low hydraulic potential. Hydraulic potential is not only determined by elevation but by water pressure as well. R.L. Shreve (1972) determined the hydraulic potential (Φ) as:

$$\Phi = \Phi_0 + \rho_w g Z + \rho_i g (H - Z) + p(r) \quad (1)$$

where ρ_w and ρ_i are the densities of water and ice, g is the gravitational acceleration, H and Z are the elevations of the points on the glacier, and r is the rate of conduit closure by plastic flow, and $p(r)$ is the effect of pressure or potential on the closure rate. Conduit closure and formation will be discussed later.

There are two forms of glacial permeability: microscale and macroscale. Microscale glacial hydrology is the movement of water between granular interfaces and veins. Macroscale glacial hydrology is the movement of water through conduits.

1.4.1 Microscale Hydrology

Nye and Frank (1973) postulated that veins should be present at three-grain intersections, and should join other veins at four-grain intersections of temperate ice (Figure 1.3).

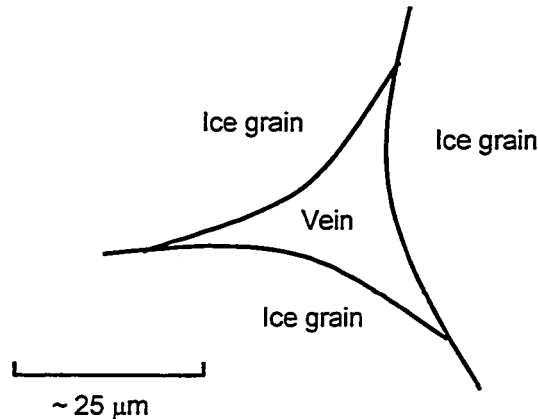


Figure 1.3 Schematic cross section of a vein formed from the junction of three grains (Raymond and Harrison, 1975)

The presence of veins as seen by Raymond and Harrison (1975) is attributed to temporary hydrostatic pressures forcing meltwater through the drainage system. Despite the existence of veins in ice cores, Raymond and Harrison (1975) conclude that the permeability of glacier ice and its ability to transport water on a microscopic scale are too ineffective to sustain the hydrological systems of glaciers. Instead, the formation of conduits is necessary to effectively transport meltwater given the fluctuations in discharge and water pressure.

1.4.2 Macroscale Hydrology

Glacial hydrology research on large-scale systems such as conduits and tunnels is extensive. Our understanding of supraglacial hydrology is comprehensive because the system operates above ground, allowing us to observe the processes at work. However, englacial and subglacial hydrology has been a topic of debate because of the inaccessibility

of the systems and processes at work. Previously, only borehole hydrochemistry, runoff stage studies and post-glacial examination of glacier beds allowed scientists an indirect view of the englacial and subglacial hydrology.

1.4.2.1 Supraglacial Hydrology

When meltwater is produced on the surface of a glacier, it is governed by gravity, flowing from areas of higher elevations to lower elevations (Röthlisberger, 1972). Depending on the ice conditions, it may percolate through the upper layer of the glacier where it will enter the englacial hydrological system, or it may behave like a fluvial system and meander down the glacier until it enters the englacial system through crevasses, or run off the side or terminus of the glacier. Water travelling on the surface of glacier entering the englacial system through a crevasse, creates a moulin. Water within a moulin may drain to the glacier bed or where the moulin intersects a tributary of the englacial drainage system. The meltwater within a moulin may also form new drainage channels in the glacier if none exist and if the meltwater carries enough heat.

Similar to a crevasse, moulins may begin to close in areas of compressional stress. However, they may remain open or maintain space within the glacier as a conduit or cavity due to the heat produced from meltwater and from viscous dissipation. These sites may be the beginning of dendritic or channelized drainage networks with the englacial system (Holmlund, 1988).

Moulins become inactive when the supply of meltwater decreases such that melting rates do not exceed the rate of deformation, or the connection to the drainage system is shut. When water-filled moulins are isolated from the drainage network, snow may collect

in the moulin and freeze with the water to form wedges of superimposed ice (Holmlund, 1988). Where snow is absent from the isolated moulin, the deeper water freezes and forms small, shallow pools on the glacier surface (Holmlund, 1988). Eventually, all water within the isolated moulin freezes in concentric patterns, called “crystal quirkes” (Stenborg, 1968) or fossil moulins, (Holmlund, 1988).

1.4.2.2 Englacial Hydrology

Much theory has been developed to model the formation, maintenance, and closure of englacial and subglacial conduits within ice (Röthlisberger, 1972; Paterson, 1981; Lliboutry, 1983; Hooke, 1984; Kamb, 1987; Seaberg et al., 1988, Walder and Fowler, 1994). Similarly, several assumptions have been made in the formation of those theories, and as a result, the understanding of englacial and subglacial hydrology has relied on the direct (and now indirect) observation of hydrological systems within glaciers.

The crevasse-based origin of moulins is generally accepted and is probably a major source of englacial conduit formation in temperate ice. Theoretically, englacial drainage cannot occur in truly polar glaciers under steady-state conditions because the glacier ice is below the melting point. Polythermal glaciers will therefore contain preferential melting through zones of temperate ice. The mapping of englacial drainage networks will provide insight into the distribution and magnitude of temperate zones within polythermal ice.

Holmlund (1988) mapped the moulins of Storglaciären, Sweden, and found that most moulins are drained by two drainage tunnels. The first tunnel was oriented horizontally and located at the bottom of the original crevasse, while the second and lowest

tunnel was located at the bottom of the moulin. Drainage tunnels extending from there were oriented $0 - 45^\circ$ from vertical in the down-glacier direction (Holmlund, 1988).

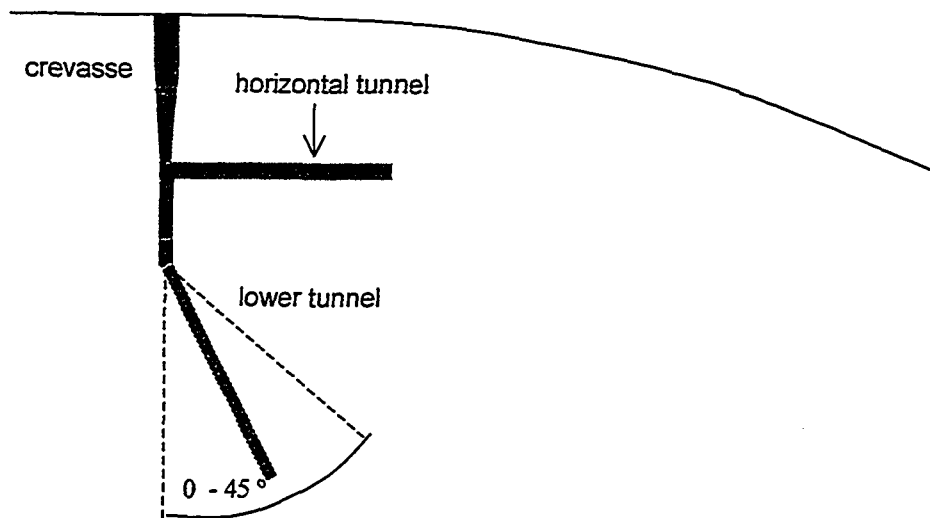


Figure 1.4 Drainage tunnels extending from moulins dipped $0 - 45^\circ$ from vertical in the down-glacier direction (Holmlund, 1988).

There was a tendency for moulins to widen with depth, which has been explained by high melt rates from the meltwater. The pressure-melting point would change negligibly within a moulin, so the heat exchange between the glacial ice and meltwater is the only explanation for the widening of the moulin at depth (Holmlund, 1988).

Englacial drainage systems have been a highly debated topic in glacial hydrology. Our understanding of englacial hydrology to date has been limited to overly simplistic theories and obscured observations. The understanding of englacial drainage requires an in-depth knowledge of the stratigraphic composition of a glacier, three-dimensional channel geometry and degree of sediment inclusions.

The formation of englacial conduits is most likely through the enlargement of englacial veins and moulins. The transition from vein to conduit theoretically occurs when discharge approximates 10^{-3} - 10^{-4} m³/s (Röthlisberger and Lang, 1987), generating enough heat from the meltwater and viscous dissipation to enlarge vein diameters. Theories of conduit formation, enlargement and closure based on the water pressure within a steady-state glacier have been developed and will be applied to conditions within Stagnation Glacier, although the theories make several assumptions about the local conditions.

Hooke (1984) postulated that conduit diameter, D_c , can be obtained with:

$$D_c = \left[\frac{8 f Q^2}{g \pi^2 \sin \beta} \right]^{1/5} \quad (2)$$

where f is the friction coefficient of water, Q is discharge, g is gravitational acceleration, and β is the slope of the glacier bed. This equation assumes that the conduits are full of water and are in steady-state conditions, specifically, the melt rate of conduit walls is equal to the rate of conduit closure due to the pressure of the overlying ice.

The rate of conduit closure (\dot{r}) was also addressed by Nye (1953) as:

$$\frac{\dot{r}}{r} = A n^{-n} (P_i - P_w)^n \quad (3)$$

where r is the conduit radius and A and n are ice flow parameters determined for randomly-oriented polycrystalline ice. A range of values for the ice deformation coefficient A have been supplied by different authors. Röthlisberger (1972) gives a value of $1.00 \text{ bar}^{-3} \text{ a}^{-1}$,

Paterson (1981) a value of 0.167, Lliboutry (1983) a value of 0.232, and Hooke (1984) a value of 0.244. The ice deformation coefficient n has a value of 3.00 m⁻³. The ice pressure (P_i) or cryostatic pressure, is the pressure exerted by the weight of the overlying ice. The water pressure (P_w) can vary between atmospheric pressure and the cryostatic pressure, depending on whether conduits are empty, full or semi-full of water.

The ice pressure (P_i) can be found using the weight and thickness of the ice:

$$P_i = \rho_i g (H - z) \quad (4)$$

where ρ_i is the density of ice (900 kg m⁻³), g is gravitational acceleration (9.807 m s⁻²), H is the elevation of the ice surface, and z is the elevation of the conduit within the glacier.

Englacial conduits have been seen in borehole video experiments by Harper and Humphrey (1995). Conduits ranged in size from 8 – 12 cm and were observed between 26 – 97 m below the surface of the glacier. Shreve (1972) envisioned an arborescent network of tunnels fingering through the ice, occasionally meeting the glacier bed, where the drainage would then become subglacial. Shreve (1972) calculated that equipotential planes dip up-glacier at an angle 11 times the slope of the glacier surface as given by the equation:

$$\alpha = \arctan \left[\frac{\rho_i |grad H|}{|\rho_w - \rho_i|} \right] \quad (5)$$

where α is the angle, and ρ_i is the density of ice. Water should flow normal to the equipotential planes when under hydrostatic pressure, hence an estimation of a conduit dip angle to surface elevation ratio of 11 is given.

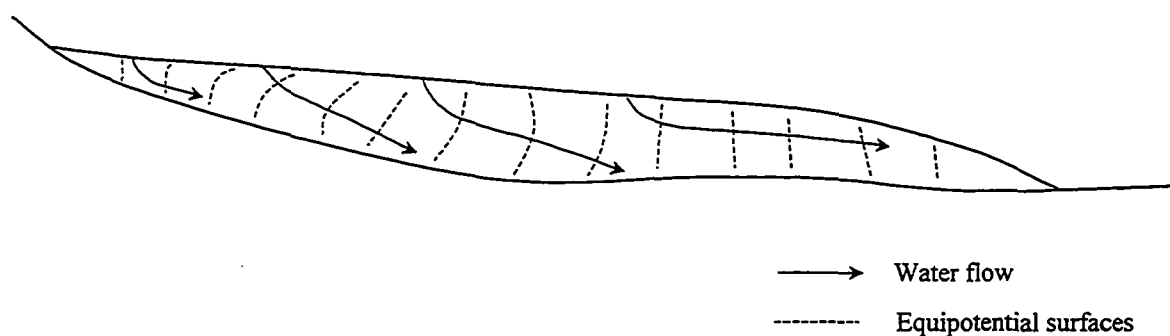


Figure 1.5 Theoretical direction of englacial flow based on Shreve (1972) (Adapted from Hooke, 1989)

However, recent glacial research suggests that conduits are not restricted to theoretical dip angles or water pressures. Several borehole experiments conducted by Pohjola (1994) suggest that englacial conduits in temperate ice exist with pressure ranges from atmospheric to cryostatic. Active englacial conduits were not found in the top 50 m of the glacier in their study.

Hooke (1984) calculated that after conduits reach a size of 3 - 4 mm in diameter, the viscous dissipation energy is capable of melting the conduit walls at a rate that exceeds the plastic flow rate of warm ice. Conduits would thus trend nearly vertical because the water flow would melt the bottom of the conduit first. Melt rates would rapidly increase as the

diameter of the conduit increases, hence the creation of nearly vertical conduits with age (Figure 1.6).

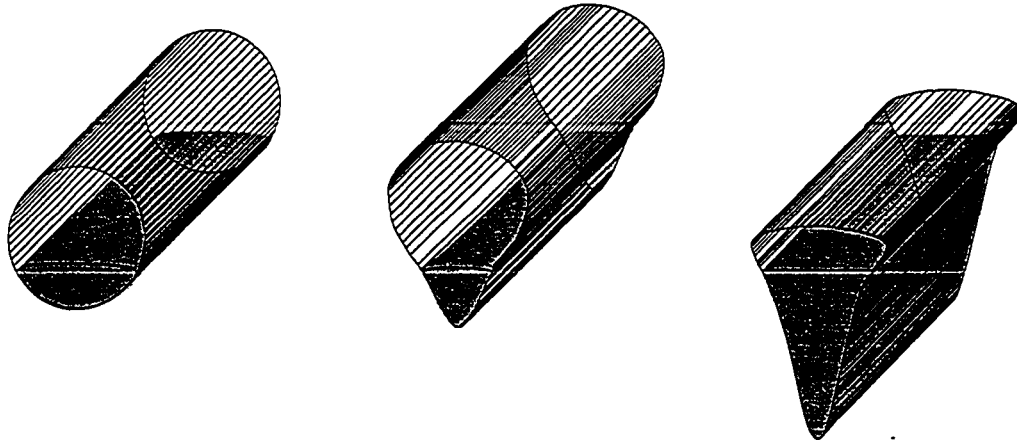


Figure 1.6 Schematic of changing conduit shape with age due to the preferential melting and subsequent vertical deepening.

The shape of englacial conduits cannot be calculated theoretically unless the local ice conditions are known. Under steady-state flow, englacial conduits maintain a circular diameter (Röthlisberger and Lang, 1987). Variations in conduit shape arise from the orientation anisotropic ice, anisotropic stress on the conduit, and sediment load within the conduit (Röthlisberger and Lang, 1987). Borehole video analysis by Harper and Humphrey (1995) showed circular conduit shapes. However, the shape of englacial conduits continues to be debated.

Englacial voids have been seen in borehole analyses (Pohjola, 1994) and interpreted from ground penetrating radar surveys (Moorman and Michel, 2000). Isolated englacial voids are likely remnants from disconnected englacial conduits (Pohjola, 1994).

1.4.2.3 Subglacial Hydrology

Where englacial drainage systems (microscopic veins and macroscopic conduits) meet the glacier bed, the water movement becomes governed by subglacial drainage patterns. A key factor in how the subglacial system will operate depends on the material of the glacier bed (glacial bed refers to the surface on which the glacier sits). The contact between glacial ice and the bed is not always distinct. Often, particularly where glaciers override conformable, unconsolidated sediments, the glacial ice/bed contact is gradual. A transition from sediment-free ice to sediment-rich ice to ice-rich sediment to ice-free sediment can occur, complicating the ice-bed contact within the basal zone of the glacier (Figure 1.7).

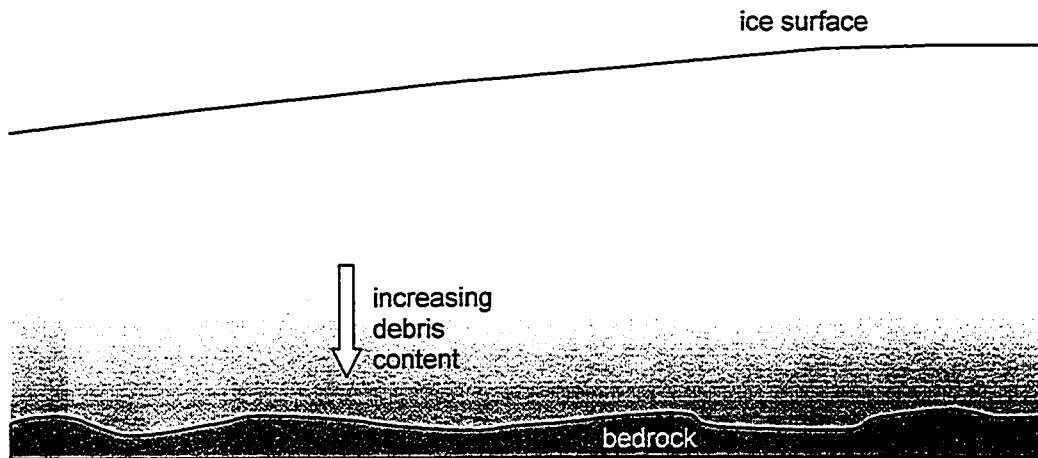


Figure 1.7 Schematic showing gradient from debris-free ice to debris-rich ice to ice-rich debris.

This sediment, or debris, can be entrained by processes involving thermal, hydraulic and strain conditions at the base. Numerous theories have been developed to explain the various forms in which entrainment takes place. The two most prominent theories are that

sediment is incorporated by thrusting of bed material along shear zones up into the ice, and that debris is entrained by regelation of meltwater (Weertman, 1964).

Hooke (1989) agreed with Shreve (1972) that subglacial drainage is subject to flow along contours that intersect equipotential planes along the glacier bed. What distinguishes subglacial flow from englacial flow is complexity introduced by variations in the ice-bed contact. Bed topography, high cryostatic pressures, and cold zones can alter the equipotential planes of water flow.

Bed topography is the most influential factor in subglacial flow. “Obstacles” or topographic highs on the glacier bed surface create dimples in the equipotential contours from the increased pressure on up-glacier sides of “highs” (Figure 1.8).

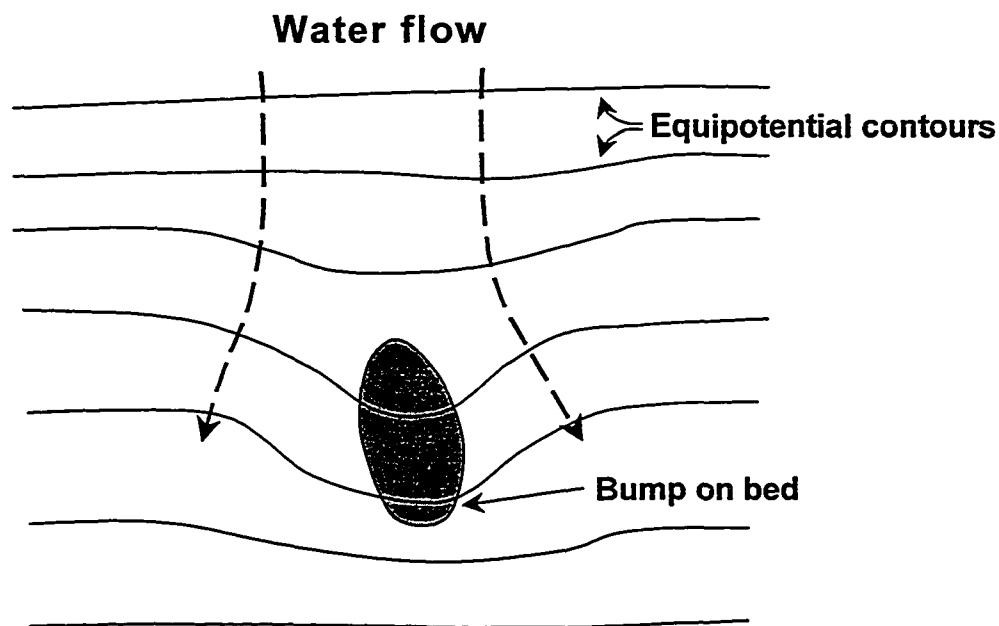


Figure 1.8 Equipotential contours near highs on glacier bed (adapted from Hooke, 1989).

How water flows over the surface of the bed also depends on the strength and degree of consolidation of the glacier bed. Where water flows over deformable material (e.g. unconsolidated sediment), water cuts into the bed surface, forming Nye-channels or N-channels (Paterson, 1994). Where water flows over non-deformable material, it erodes up into the ice, forming R othlisberger-channels or R-channels (Paterson, 1994). These types of subglacial flow are linked-tunnel systems (Paterson, 1994). Ice is assumed to be in contact with the bed except where tunnels exist. Water pressures in a linked-tunnel system decrease as discharge increases. Because the relationship between discharge and pressure is negative, tunnels of larger size tend to draw water away from tunnels of smaller size (Hooke, 1989). This is because larger tunnels have lower pressures than smaller ones with higher pressures, and water flows from high to low pressure. Thus, linked-tunnel systems tend to consist of large tunnels with smaller, linked tributaries.

Subglacial flow can also occur as a linked-cavity system where the ice is not always in contact with the bed. Here, cavities are maintained by glacier sliding as well as by melting from water flow. However, water pressure varies directly with discharge in a linked-cavity system. Water flow has no preferential flow through larger or smaller linked cavities (Hooke, 1989).

Glaciers underlain by till or other unconsolidated material do not usually have distinct subglacial drainage patterns. Instead, water enters the bed and flows under normal hydrological laws. However, the ground underneath a non-temperate glacier may contain a layer of permafrost and thus the downward flow of meltwater maybe restricted. Where regions of basal ice are at the pressure-melting point, permafrost in the underlying sediments can become discontinuous, and the sediment can become subject to deformation.

The shape of subglacial tunnels or cavities has yet to be established by glacial hydrologists. Hooke (1989) discussed Shoemaker's (unpublished) theory that drag on the glacier bed will counteract the widening of semicircular tunnels by melting of the ice walls by water movement. Due to drag on the bed, the inward flow of ice is higher on the sides of tunnel walls than on the ice along the bed. As a result, tunnels will tend to be semicircular in shape, tending to form broad, low openings under certain pressures (Hooke, 1989).

1.4.3 Hydrological Dynamics

The closure of englacial conduits is not completely understood because the water pressure and conduit shape parameters required are difficult to obtain. Nye (1953) determined theoretical equations for calculation of the rate of tunnel closure by contraction and the rate of melting along a unit length of a tunnel.

Röthlisberger and Lang (1987) also determined the rate of tunnel closure by volume from the plastic flow of ice. Many assumptions on the rate of conduit closure are made in these equations (steady-state conditions, circular cross-section, 100% water fill of conduits) and unfortunately the field of glaciology continues to lack an appreciable understanding of conduit closure.

The drainage network of a glacier is not static: it must respond to diurnal and seasonal fluctuations in temperature and precipitation. Ultimately, the system must be able to accommodate fluctuations in meltwater discharge. By examining glacial discharge hydrographs, it is possible to identify multiple drainage systems. Nienow et al. (1996) identified dual drainage systems during periods of high discharge through dye tracer

experiments on the Haut Glacier D'Arolla, Switzerland. They concluded that a major drainage system develops as a response to dramatic increases in runoff during the summer melt season. The increase in runoff was due to the seasonal up-glacier migration of the snow line. The high water pressures that resulted from increased discharges instigated the switch from a subglacial drainage system to a drainage system utilizing both englacial and subglacial drainage networks.

By examining dye injection at various moulins, a relationship between discharge and velocity was developed and indicates the existence of both channelized and distributed drainage systems. They conclude that the measurements made at moulins suggested how the moulin was connected to a secondary drainage network during periods of high discharge. When discharges increased such that the water head in moulins reached a particular height, the water entered a second drainage system through englacial conduits. When discharges are low, runoff is automatically routed to a distributed subglacial drainage system. Clarke (1996) presented a unique and effective comparison of a multi-routed subglacial drainage system to an electrical circuit. By using the mathematical-circuit relationships in a lumped-element model, Clarke was able to simulate the observed responses in water pressure, turbidity and conductivity to a 1990 subglacial hydrological event on Trapridge Glacier, Yukon. Through comparison to an electrical circuit, the model suggested that the event was the result of a formed connection to stored subglacial water, and the subsequent fluctuation between the pre-existing and newly-formed conduits.

Fischer et al. (1999) looked at the mechanical and hydrological coupling of the basal ice of Trapridge Glacier, Yukon, Canada, and its bed. By comparing ploughmeter data (that measures the Newtonian force and direction of sliding at the bed) with subglacial

water pressure, they observed a direct correlation between the mechanical and hydrological signals observed in the data. They proposed that high-water pressure induces the formation of a lubricating film of water, engaging a basal sliding response. Low-pressure conditions result in the absence of such a film, hence increasing the basal slip resistance. “Sticky spots” or stick-slip sliding has yet to be fully understood, particularly the role englacial and subglacial water has on glacial flow.

The coexistence of englacial and subglacial drainage systems are probably more frequent than have been reported to date. Although our understanding of englacial hydrology is still very limited, more research is being conducted and a more in-depth comprehension of englacial processes is likely to be found in the future.

1.4.4 Ground-Penetrating Radar and Glacial Hydrology

Ground penetrating radar (GPR) has recently been shown to be very effective in imaging sub-surface features within glaciers such as conduits, cavities and sediment stratification (Nobes et al., 1994; Arcone et al., 1995; Hamran et al., 1996; Kohler et al., 1997; Murray et al., 1997; Moorman, 1998; Woodward et al., in press;)

GPR operates by emitting a pulse of electromagnetic (EM) energy into the ground and recording the reflections of the EM pulse off of features within the subsurface. A reflection occurs when the EM pulse encounters material of a differing dielectric constant. The strength of reflections received by the GPR unit are dependent on many things including the configuration of the GPR unit, the depth of the contact (or reflector), and the nature of the contact itself. These factors and how they influence the response of GPR to hydrological features of glaciers will be discussed in chapter three.

1.5 OBJECTIVES

The use of GPR as a method for identifying small-scale features of glaciers was first tested in the Ph. D. research conducted by Moorman (1998). This research extends and refines Moorman's initial work and applies it to a detailed description of a glacial hydrological network.

The specific objectives of this thesis are to:

1. conduct a detailed GPR survey in order to determine the size, density and orientation of hydrological features within the glacier.
2. determine the morphology and structure of the hydrological network(s) of an subpolar glacier using GPR.
3. propose a model of hydrological drainage based on GPR data and field observations.
4. infer thermal conditions within or below the glacier from GPR data.

CHAPTER 2

STUDY AREA

Bylot Island, Nunavut is located in the Canadian Arctic, north of Baffin Island, at 73° N, 78° W (Figure 2.1). The Byam Martin Mountains extend across the length of Bylot Island and are extensively glaciated. A 4500 km² ice field is contained across the centre of the island, from which valley and piedmont glaciers extend out onto the lowlands. The glacier chosen for study, B28 (Inland Waters Branch, 1969) (informally named Stagnation Glacier), is a valley glacier located on the south side of the island (Figure 2.2). It was chosen on the basis of its accessibility and smaller size, making the survey program easier to implement and the hydrological model easier to construct.

Stagnation Glacier is approximately 10 kilometers long and is fed from the central icefield. It is flanked on both margins by large (up to 200 m tall) ice-cored lateral moraines (Moorman, 1998) (Figure 2.3). At the terminus, the glacier is approximately 200 m wide and gradually widens to 400 m in the survey area. Mountain ridges surround the glacier



Figure 2.1 Map of Canada and Greenland showing location of Bylot Island

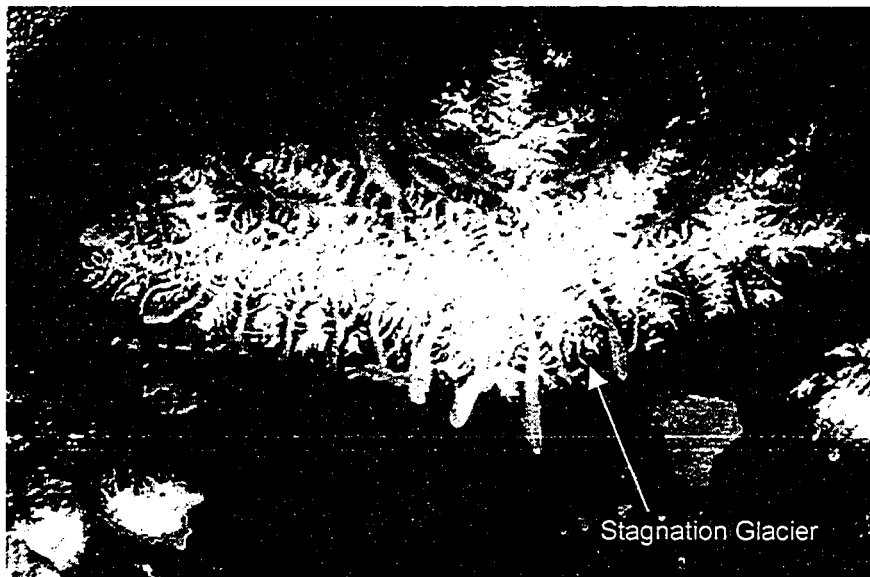


Figure 2.2 Satellite image of study site on Bylot Island, Nunavut Territory.



Figure 2.3 Oblique aerial photograph of Stagnation Glacier, Bylot Island

valley, limiting the length of time of direct irradiation, despite 24-hour sunlight in the summer. Stagnation Glacier is south-facing and experiences approximately 12 hours of direct solar radiation per day during the summer, generating diurnal meltwater discharge cycles. Ice-cored eskers (approximately 1.5 m in height) and kame deltas (approximately 2-3 m in height) can be found on the outwash plain.

The along-glacier surface profile of the terminus of Stagnation Glacier is roughly linearly angled at approximately 12°. This is characteristic for termini of receding glaciers. Aerial photographs taken since the 1950's show that Stagnation Glacier has been in recession.

The surface topography of the lower 2 kilometres of the glacier is hummocky with large longitudinal ridges and valleys. A steep rise in the surface topography was seen on the middle section of the glacier, approximately 600 m up glacier from the terminus. A second rise was observed at the end of the surveyed section, causing the heavily-crevassed region that hampered data collection.

The glacier has incorporated subglacial sediment into the lower 5 m of the glacier and appears frozen to its base as indicated by the relative lack of basal sedimentation and observation in the field. Unstratified layers of debris-rich ice (although not overly rich), bubbly, and bubble-free ice were seen in local areas. Shear planes of stratified ice varying in crystal size and air bubble content can be seen dipping in an up-glacier direction, striking transverse to glacier flow.

Small-amounts of debris can be found on the surface of the glacier and is most likely deposited from avalanches or rockfalls up-glacier in or near the accumulation zone.

Supraglacial meltwater streams were flowing down some of the valleys during the period of this research, which took place July 1999.

The climate of Bylot Island is arctic desert, with a mean annual air temperature of -15°C and mean annual precipitation of approximately 225 mm. Average daily maximum and minimum air temperatures during the last three weeks of July 1999 were 9.7°C and 2.1°C , respectively.

CHAPTER 3

METHODOLOGY

3.1 GROUND-PENETRATING RADAR

GPR and radio-echo sounding was originally used for determination of ice thickness. Dowdeswell et al. (1984), Jacobel and Raymond (1984), Walford et al. (1986), Walford and Kennett (1989), Kennett (1989), and Hagen and Sætrang (1991) were first to interpret reflections and echoes as englacial conduits and even recognized the temporal variation in echoes as temporal movement of meltwater on a variety of temperate and non-temperate glaciers in Alaska, Spitsbergen, and Sweden.

Oswald and Robin (1973), Shoemaker (1990, 1991), Ridley et al. (1993), Arcone et al. (1995), and Arcone (1996) have used radio-echo sounding to identify and map up to 57 subglacial lakes beneath the Antarctic Ice Sheet, located primarily in northern Victoria

Land. GPR was used by Clarke and Bentley (1994) to determine ice strain history from buried crevasses on Ice Stream B2, Antarctica.

Arcone et al. (1995) used the differences in dielectric constants of englacial and basal ice in order to identify and model reflection sources. Arcone (1996) used GPR to show the brine migration through an ice stream on the Ross Ice Shelf, Antarctica. Moorman (1998) tested the ability of GPR to identify englacial conduits and cavities on the lower part of Stagnation Glacier, Bylot Island.

This research employs those advances to use GPR to locate and identify englacial conduits and their thermal and stratigraphic setting.

3.2 GEOPHYSICAL SPECIFICATIONS

The components of a GPR system include: two antennas connected to a transmitter and digital receiver, the console which processes data received, and a computer that acts as the user interface for the GPR operation, data storage and display (Figure 3.1). The antennas are designed such that one transmits the radiowave pulse, and the second receives the reflected pulse. The console's purpose is to relay timing commands to the transmitter and receiver and process received signals. The processed data is then relayed to a computer, where the information is recorded and displayed in graphical format for interpretation by the user.



Figure 3.1 Ground-penetrating radar on the surface of Stagnation Glacier.

The propagation of a radar pulse in the ground is determined by two factors: the electrical properties of the subsurface and the configuration of the GPR system. GPR operates by emitting a pulse of electromagnetic (EM) energy into the ground and recording the timing and magnitude of reflections off features within the subsurface. A reflection occurs when the EM pulse encounters material of a differing dielectric constant from that of the previous material. Strength of reflections received by the GPR unit are dependent on many things including the configuration of the GPR unit, the position of the reflecting interface (or reflector), and the nature of the reflector itself. These factors and how they influence the response of GPR to hydrological features of glaciers will be discussed.

An EM pulse is generated when an alternating current (AC) is run along a wire. The frequency and duration of the pulse are selected depending on the GPR application. GPR frequencies in glacial applications generally range from 1 – 100 MHz (in the radio range), while pulse duration is in the order of ten's of nanoseconds (ns). The centre frequency (f_c) is commonly referred to when describing a GPR survey (Figure 3.2). For the pulseEKKO IV, the bandwidth is equal to the centre frequency. Hence, a 50 MHz antenna would generate a radiowave with a centre frequency of 50 MHz and a bandwidth of 50 MHz. The frequency is variable with different antennae, and the ratio of the centre frequency to the bandwidth will always remain constant.

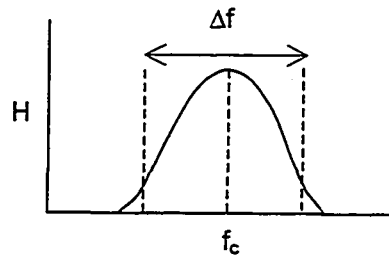


Figure 3.2 Relationship of centre frequency (f_c) and bandwidth (Δf) (Annan, 1992).

The bandwidth is the inverse of the pulse width, which describes the length of time the antennas generates the radiowave.

Example: bandwidth $50 \text{ MHz} = 50 \times 10^6$ cycles per second

pulse width $1 / 50 \times 10^6 = 0.00000002$ seconds = 20 ns

The dielectric constant (K) is a measure of a material's ability to store an electrical charge. Ice has a dielectric constant of 3 - 4, air has a dielectric constant of 1, and the dielectric constant of water is 81. The proportion of the incident energy reflected back to the receiving antenna from a planar interface (called the reflection coefficient R) is given by:

$$R = \frac{\sqrt{K_1} - \sqrt{K_2}}{\sqrt{K_1} + \sqrt{K_2}} \quad (6)$$

An ice/air contact would generate a reflection coefficient of 0.30, whereas a ice/water contact would generate a reflection coefficient of -0.65. The amplitude and polarity of the reflected energy received by the antenna is also dependant on many factors including the type of signal generated (frequency), the efficiency of the antennas, the attenuation coefficient of the ground (or ice), the speed at which the signal travels through the ground (propagation velocity), the distance to the reflection, the character of the material between the source and the reflector of interest, and the shape of the reflector.

3.3 GPR PARAMETERIZATION

The most important parameter in GPR surveying, other than the conductivity of the material being surveyed, is the frequency of the signal. The frequency at which signals are generated defines three main values: the depth to which geophysical information may be gathered, the size of the target to be imaged (resolution) and the reflectivity of the target. Moorman (1998) showed that during reconnaissance glacial hydrology studies for GPR use, a 50 MHz PulseEKKO IV TM system achieved a penetration depth of 145 m. Ice is a very effective medium for radar wave propagation because the attenuation coefficient is so low.

The minimum target size (δZ) is a function of the frequency and dielectric constant, and is given by (Annan, 1992):

$$\delta Z > 75 / (f \sqrt{K}) \quad (7)$$

where δZ is an estimate of the minimum target resolution, f is frequency and K is the dielectric constant.

The depth of penetration (D) is also a function of the frequency and dielectric constant, and a guideline for estimating this is given by (Annan, 1992):

$$D < 1200\sqrt{K}/f \quad (8)$$

Clutter is the reflection of radar from within the host material, without reflecting off of the desired targets. The maximum size of clutter (δL) is estimated by (Annan, 1992):

$$\delta L < 30 / (f \sqrt{K}) \quad (9)$$

3.3.1 System Parameters

Through forward modelling with the radar range equation and previous experience of the anticipated conditions, the following survey parameters were determined to be most effective in the imaging of subsurface glacial features of Stagnation Glacier.

Survey Parameter	50 MHz	100 MHz
Transmitter voltage	1000V	400V
Time window	800 ns	400 ns
Sampling interval	1.7 ns	0.83 ns
Station spacing	2 m	1 m

Antenna separation	1 m	1 m
Antenna Orientation	Parallel-parallel	Parallel-parallel
Anticipated Results	50 MHz	100 MHz
Minimum target size (δZ)	0.84 m	0.42 m
Maximum depth of target detection (D) (for maximum size target)	43 m	21 m
Maximum clutter size (δL)	0.3 m	0.17 m

The GPR surveys were conducted using the pulseEKKO IV™, a digital GPR system manufactured by Sensors & Software Inc. 51 GPR lines were run on the lower 2 kilometres of Stagnation Glacier in order to maximize the detail with which hydrological features are imaged. One to two line-kilometres of GPR data were obtained per day by towing the GPR behind a person walking, while a second carried the GPR console and laptop, and a third collected GPS data.

A majority of lines were oriented perpendicular to the long axis of the glacier, as this is thought to be perpendicular to the orientation of the majority of glacial conduits, thus yielding the greatest possibility of intersecting as many features as possible.

The orientation of the antennas allows the antennas to be easily pulled (sliding on the glacier surface) and it greatly increases the rate at which measurements may be made. The elongate footprint pattern results in a small cross-sectional survey area in an orientation perpendicular to the direction of travel and a larger cross-sectional survey area

in the direction parallel to the direction of travel. This results in a resampling of positions in the direction of travel, thus increasing station-to-station correlation (Figure 3.3).

3.4 ANCILLARY DATA

Positional measurements were collected by a Trimble Differential Global Positioning System (DGPS) so that the GPR data could be located and corrected topographically. In order to create a map of the glacier bed, the ice thickness (interpreted from the radar data) is subtracted from GPS data of the glacier surface. A partial knowledge of the glacier bed surface is useful when considering the hydraulic potential of meltwater and its route through glacial ice.

Dye tracer experiments involving fluorescent dye (uranine) injections into meltwater were conducted in three separate incidents. These experiments were purely qualitative, supplying information on meltwater routing.

Figure 3.4 provides a summary of data collected and how it will be organized into the model of glacial hydrology of Stagnation Glacier.

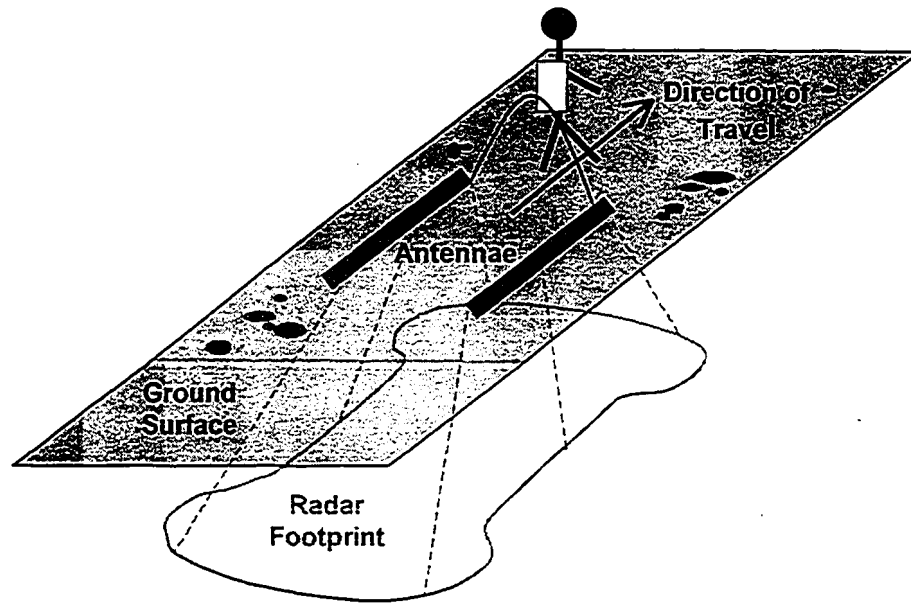


Figure 3.3 Schematic of GPR antennae orientation and radar footprint. Note this type of data collection orients the radar footprint such that the shape is elongated in the direction of travel.

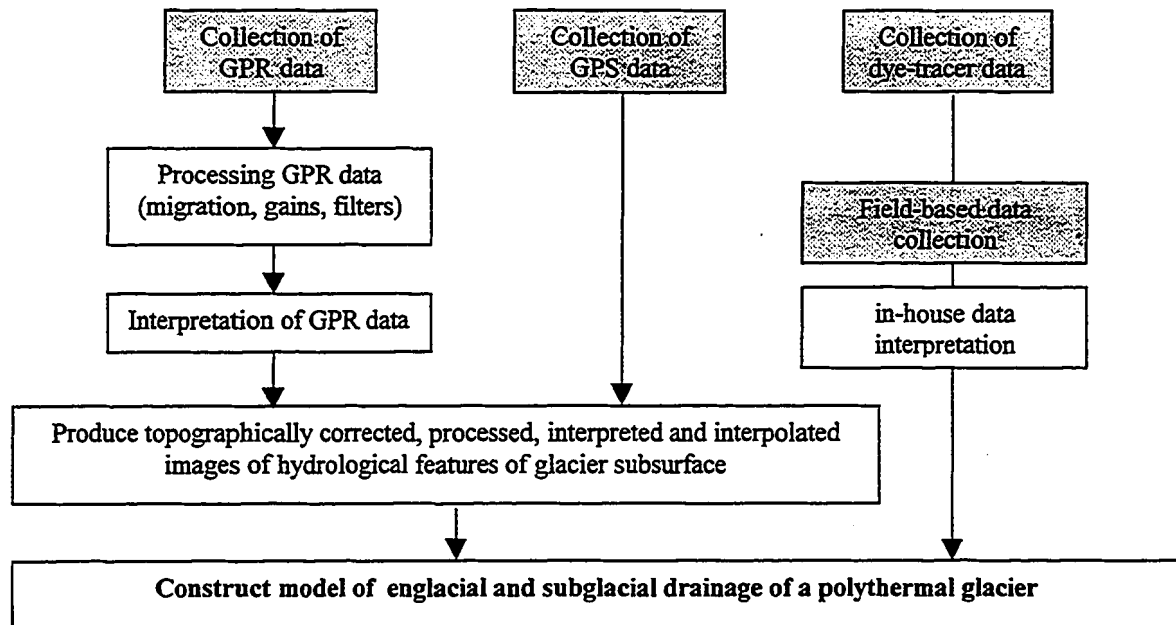


Figure 3.4 Organization of collected data. Shaded boxes indicate field-based work.

CHAPTER FOUR

SURFICIAL HYDROLOGY

The hydrology of the periglacial environment around Stagnation Glacier was directly observed both on the surface of the glacier (supraglacial), in front and beside the glacier, and around the ice-cored moraines.

4.1 SUPRAGLACIAL HYDROLOGY

Several supraglacial streams flowing on the surface of the glacier were observed. Similar to meandering rivers, supraglacial streams transport meltwater across the glacier where they may meet lateral streams along the side of the glacier, or proglacial streams at the front of the glacier near the terminus. Supraglacial stream widths measured up to 1 m across and up to 0.3 m in depth (approximately). Water movement occurs over the entire surface of the glacier, but becomes channeled through the development of

supraglacial streams. Meltwater carried in a stream may flow off the glacier, or enter the glacier through a moulin.

A moulin was observed on the western side of Stagnation Glacier that collected water from a nearby supraglacial stream. The moulin was approximately 30 cm in diameter, and was observed to reach at least 10 m below the surface of the glacier. The moulin was located in a heavily crevassed region, and was most likely formed from the intersection of a crevasse and the nearby stream. In fact, the abandoned channel left by the formation of the moulin could still be seen. The relative change in elevation of the abandoned stream bed and the active stream bed was minimal, thus the formation of the crevasse was most likely very recent, probably within the current meltseason.

Although not measured, the discharge of the stream was estimated to average 0.1 - 0.5 m³/s. Discharge peaked typically mid-afternoon, several hours after the sun reached it's highest altitude and therefore, strongest intensity. Applying Hooke's (1984) equation for the diameter of a conduit (D_c), the diameter of a conduit at depth could be calculated as:

$$D_c = \left[\frac{8fQ^2}{g\pi^2 \sin \beta} \right]^{1/5} \quad (10)$$

where $f = 0.025$ (for a partially-filled conduit)

$$Q = 0.1 \text{ m}^3/\text{s}$$

$$\beta = \text{slope of bed} \approx 0.1^\circ \text{ (as estimated from GPR interpretation)}$$

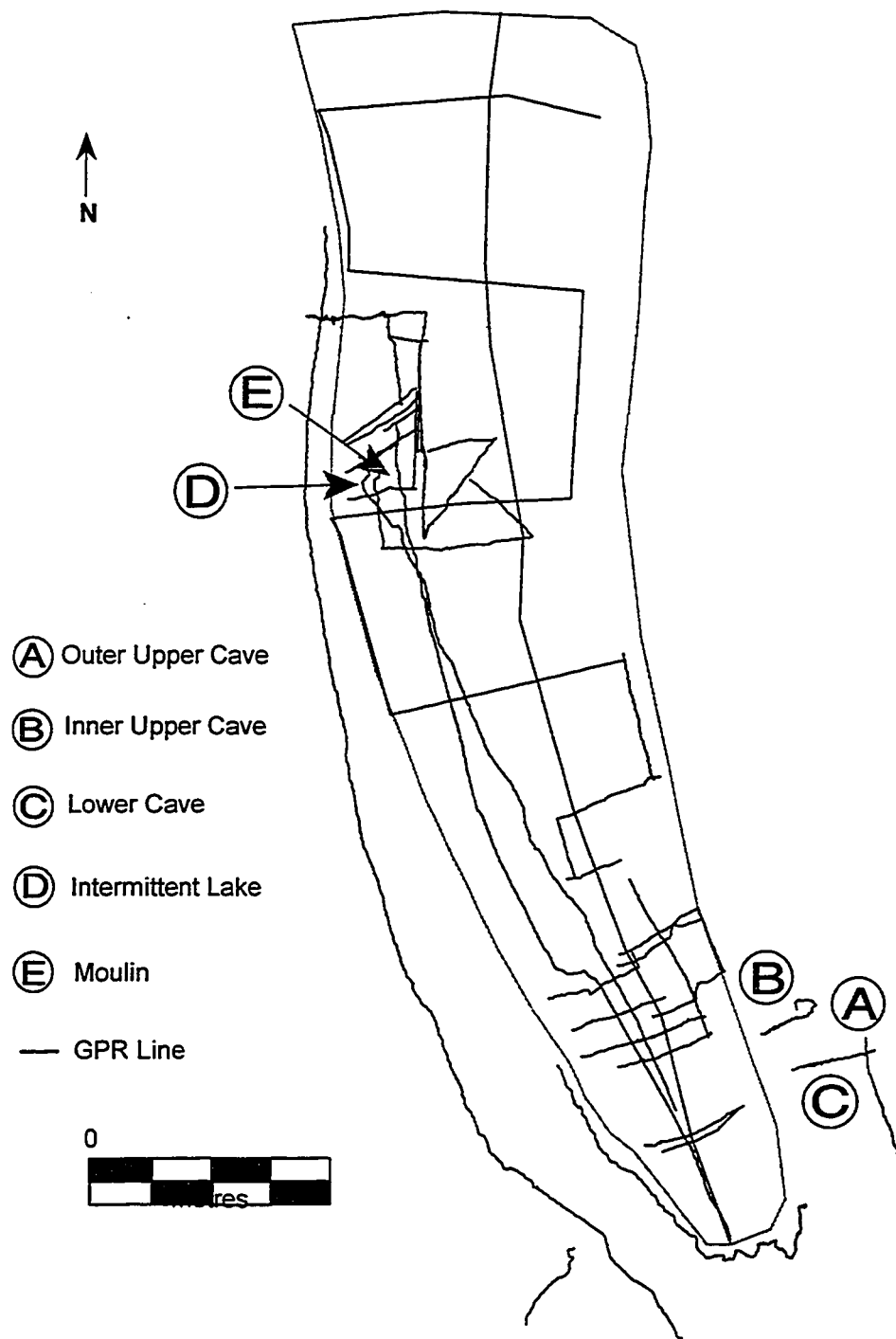


Figure 4.1 Map of the lower portion of Stagnation Glacier, the locations of surficial features, and GPR lines.

Equation (10) gives a conduit diameter of 0.41 m, which seems reasonable, and within the spatial resolution of the GPR.

An intermittent pond was observed within the vicinity of the moulin, on a topographic depression in the western region of Stagnation Glacier. In this area, the remnants of a prior crevasse field were present in the form of ridges and valleys. The pond measured 100 m² in area and was approximately 10 m deep. The pond was filled and emptied diurnally, at least during the study period. The pond was first observed to fill from a source at its base shortly after 12:00 p.m. Once the pond was completely filled, water would pour over the side of the glacier. The fill/empty cycle occurred again between 5 and 6 p.m. Prior to being filled with water, loud, deep boom-like sounds could be heard, as shifts in the ice were felt at the surface.

During data interpretation, a rise in surface topography was noted to have taken place over the four day period from July 17-21. The largest rise was 3.5 m, while the smallest measured rise was 1 m. This occurred in the vicinity of the moulin and intermittent lake area.

4.2 PERIGLACIAL HYDROLOGY

Lateral streams flowing along the sides of the glacier were observed along most portions of the glacier margin, except where they undercut the glacier, and flowed partially beneath where they flowed beneath the lateral moraines for a short distance. The lateral streams are joined mostly by alpine streams and to a lesser degree, moraine meltwater. At the terminus of Stagnation Glacier, lateral streams joined to form a single channel that later spread out into a braid plain.

An ice-cored esker, the relict of past fluvial hydrology, was observed extending out from the terminus of Stagnation Glacier for approximately 50 m to a bedrock bench in the valley bottom. A kame terrace was observed 30 m beyond the current terminus and indicates the presence of delta formation at a previous terminus location. The presence of an esker, more importantly than a kame terrace, indicates that at least previously, subglacial or englacial water movement occurred within Stagnation Glacier.

An icing was also observed in the proglacial area of Stagnation Glacier. Since winter temperatures do not allow for the movement of liquid water at the surface, water movement must be occurring beneath the glacier surface. Surface meltwater production does not occur during the winter, so the water used to form icings must originate from stored water within or below the glacier. Icing growth was gradual from the slow release of water as indicated by the crystal orientation within icing layers. Crystallographic evidence indicates that pressurized water was injected between pre-existing layers within the icing. As the water froze, it pushed the two layers apart, forming columnar crystals growing in a vertical orientation. Had the release of water been rapid, such a process could not occur. The portion of the icing observed at Stagnation Glacier was approximately (150 - 200) m² in size, and 0.5 - 1 m in thickness. A more extensive icing has been observed and studied by Moorman (1998) at nearby Fountain Glacier on Bylot Island. Although different in size, both icings indicate the presence of liquid water within the glaciers during the winter.

4.3 MORaine HYDROLOGY

The moraines surrounding Stagnation Glacier are ice-cored, as a result of glacial ice being covered in debris, and consequently being incorporated into the moraine. These ice-cored moraines have been subject to hydrological routing within them, as evidenced by the presence of several water-cut caves. Cave C, located on the eastern moraine approximately 200 m upstream from the glacier terminus, extended approximately 30 m into the moraine before it got too small to explore further. At the entrance, the cave was 4 m wide and over 3 m high. Due to its orientation (facing the side of the glacier) very little direct sunlight entered the cave. The walls of the cave were composed of ice, since the moraine is ice-cored. A frozen, abandoned stream ran through and exited out the entrance of the cave. Rounded boulders of ice, and portions of the cave ceiling laid in piles along the edge of the cave. The cave was mostly likely used to transport meltwater from the glacier. Due to the size of the cave, it is unlikely that it was created by meltwater from the moraine, due to the diameter of the cave (4 m wide x 3 m high). It is possible that the cave was formed as a tunnel before the glacial ice was abandoned as a moraine. Unless meltwater from the glacier was re-routed through a moraine network, this is the most likely explanation.

Accretionary ice surfaces were observed at the entrance to the cave and extending approximately 5 - 10 m into the cave. Ice layers, approximately 0.10 - 0.15 m in thickness, lined the ceiling and walls of the cave, indicating that stored still water had frozen onto the cave interior. Multiple layers indicate multiple storage events. Accretionary ice is absent at the back of the cave, which is also shorter. This suggests that the weight of the overlying ice is too great to maintain the opening and the cave is slowly collapsing in on itself. In

cold ice environments, glacier thickness greater than 35 m provide enough overlying pressure to collapse air cavities at atmospheric pressure (Dolgoff, 1998). Water pressure, if high enough, may provide an equal but opposite pressure, maintaining the cavity.

Approximately 200 m from Cave C, a set of caves extending into the east moraine on both sides was observed. Cave A entered the mountain side of the moraine, and was broad and shallow in shape. The cave extended 15 m into the moraine, as far as could be safely entered, at which point an alpine stream entering the moraine disappeared beneath the till. Inside the cave, light could be seen through cracks from the other side of the moraine. Directly on the other side of the moraine, Cave B was observed. Large volumes of water flowed out of this cave. Large boulders obscured the entrance to the cave, as well as the joining of a lateral stream with the water exiting the moraine, but it appeared that the stream exiting the cave is augmented from additional meltwater from within the moraine, as well as the lateral stream.

CHAPTER FIVE

SUBSURFACE HYDROLOGY: RESULTS

5.1 GPR DATA PROCESSING

Investigation into the subsurface hydrology of Stagnation Glacier was aided by the use of ground-penetrating radar. Processing of GPR and GPS data was required in order to interpret the results. GPS data processing involved differential correction between rover (field) files and base station data transmitted by satellites. Certain periods during the day were inopportune for GPS data collection and resulted in lower measures of positional accuracy. Typical horizontal errors ranged from 0.1 – 0.25 m. Vertical errors were larger and ranged from 0.3 m to 1.8 m in height. Accuracy values were recorded with each data point.

The GPS and GPR data were collected simultaneously. Since GPR data are collected along traverses, GPS data are made up of locational points forming a line. The

uncertainty associated with the location of the GPR traverses is affected by a) GPS positioning; b) mismatching of GPR and GPS traverses; c) two-dimensional GPS line length calculation errors. Because some of the sources of uncertainty will over-estimate the error while others will under-estimate, these errors are thought to cancel each other out and the overall positional uncertainty is estimated to be less than one metre. The position of each transect was recorded. Individual trace locations were not.

The true station-spacing varied according to the slope of the glacier surface being traversed, with slower rates of travel on up slope directions, and higher rates of travel on down slope directions. To determine the average station-spacing for a particular line of GPR data collected, the length of the line as shown in the GPS data was divided by the total number of traces collected in the line. This results in a station-spacing of n metres per trace. This procedure was done for every GPR line to correct the station-spacing with the PulseEkko system. Keeping in mind that this procedure assumes a constant velocity along the line, which was not always feasible, depending on field conditions. The centre line, consisting of 99-1 and 99-2, however, incorporated changing data collection velocities as calculated from the GPS data. A simple experiment to find out the length of time between traces was performed and used to calculate the changing rate of data collection along the centre line. This allowed for a greater rate of data coherency between lines 99-1 and 99-2 and intersecting traverses. For the sake of simplicity, the centre line will now be referred to as 99-1/2.

Since radio waves emitted from the GPR antennae do not only radiate in a truly vertical direction, but in all directions, the area reached by a particular sequence of waves, is called the footprint. The footprint of the GPR used is elongate with widened lobes at the

ends. The horizontal area of a footprint increases with depth, and is aligned parallel with antennae direction, such that the elongated shape is oriented in the direction of travel. As long as the relative antennae orientation is held constant during data collection, it can be assumed that positive and negative reflection coefficients are representative of subsurface interface characteristics.

Radar processing occurred in a series of steps. A procedure called signal de-WOW was used at the time of data collection to reduce the effect of receiver saturation of reflection amplitudes from features at the near surface (less than 5 m from the surface). Duplicate traces were deleted, and a procedure to re-calibrate the position of the zero time line was used on some profiles. To aid in GPR interpretation, various filters, gains and migration techniques were used. High-pass and low-pass filters were used in junction with various mathematical gains on GPR traces. Migration is a technique that collapses or reduces the diffraction tails on hyperbolic reflections back to the apex. This aids in interpreting the character of the reflection.

5.2 GPR DATA INTERPRETATION

A reflected signal, consisting of a minimum of one wavelet, has three characteristics; the length, the phase, and amplitude of the signal. The length of the wavelet is a function of the resolvable size of the reflector and the propagation velocity of the host material. Objects whose size is less than that of the wavelength of the radar wave pulse, have shown to generate a single reflection, consisting of one and one-half cycles (Arcone et al., 1995), given the dielectric constant of the reflector is different enough from that of the ice. Objects that are larger in size (vertically) than the wavelength of the radar

wave pulse are resolvable in size, and will be represented by longer reflections (two or more cycles).

Examining a portion of a radar trace (Figure 5.1), the black areas of the wavelet are called 'peaks' or 'positives', while the white areas are called 'troughs' or 'negatives'. The phase of the reflected signal depends on the polarity of the antennae configuration and

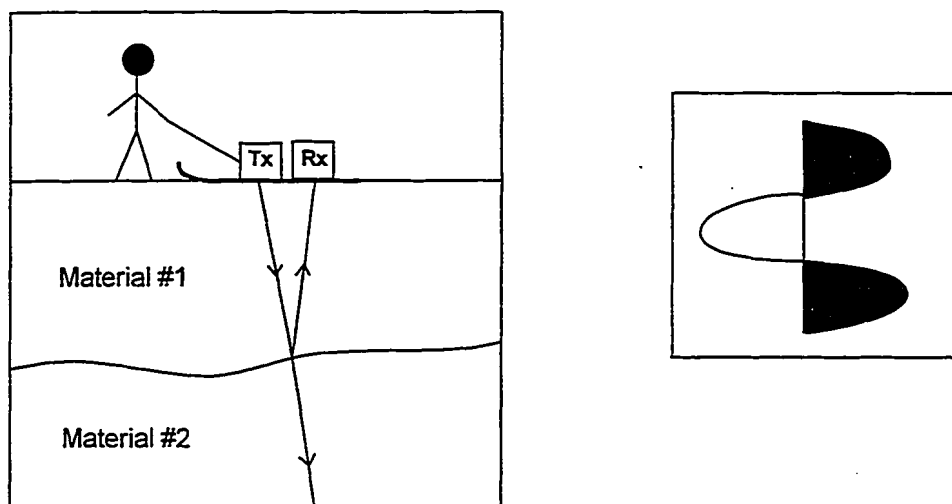


Figure 5.1 GPR system consisting of a transmitter (Tx) and a receiver (Rx) (left), and single wavelet formed from the reflection of radio waves off of a boundary between differing materials.

whether the reflector's dielectric constant is greater or less than that of ice ($K_{ice} = 3$).

With the system configuration used, a wavelet with a positive reflection coefficient (+ - +) is generated when the EM pulse is reflected from a material with a higher dielectric constant than that of the material the pulse was traveling through. The dielectric constant of ice ranges from 3 -4, and thus a reflection with a positive reflection coefficient is generated by features with dielectric constants greater than 3 or 4, such as the materials comprising till (sand, silt, clay), bedrock, or water. Water has the highest dielectric constant ($K = 81$), and therefore generates the largest reflection coefficient.

Negative reflection coefficients (- + -) indicate that the reflector material has a dielectric constant lower than that of the previous material. The only natural material to have a dielectric constant lower than that of ice is air ($K = 1$). Thus, negatively-phased reflections are generated by air-filled cavities within ice.

Upon data interpretation, the polarity of internal reflections are compared to those generated from a known surface, such as the ice/sediment interface at the glacier bottom. Keeping in mind that the antennae configuration remained constant throughout data collection, a positive polarity could be definitively defined as being generated from a surface in which the host material's dielectric constant was higher than that of the reflecting material.

The shape and size of objects that will be imaged by GPR will produce different types of reflections, given the size of the reflector is greater than one-quarter of the wavelength of the radio waves. Point source objects, such as air-filled, water-filled or small sediment-filled cavities, will generate hyperbolae or diffractions, on a radar profile.

Due to the low dielectric constant of glacial ice, the size of the radar pulse footprint increases dramatically with depth. The theory behind antennae wave directivity is complex, given the unknown composition of glacial ice with respect to differing air, water and sediment compositions. To estimate the maximum size of the footprint, we can inspect the length of a diffraction tail. Diffraction tails are formed when a point source object is detected by the radiating waves before and after the GPR antennae. The hyperbolic shape of the reflection is formed as the travel time to and from the object decreases as the antennae approach, and as the travel times increase again as the antennae move further away.

The centre of the GPR waves respond somewhat differently to conduits and tunnels, depending on the orientation of the GPR traverse with respect to the orientation of the conduit. Traverses that intersect the conduit at right angles, or close to right angles, will produce hyperbolic reflections. Traverses that run parallel with the conduit will produce continuous reflections along the length of the conduit. Any meandering of the conduit will result in the continuous reflections to seemingly undulate in elevation. This is an effect of the changing travel times to and from the conduit by the radio waves.

Analysis of the GPR profiles from Stagnation Glacier revealed that the size of the signal footprint increases with depth, to a maximum of approximately 50 m. This suggests that objects at a maximum distance of 50 m away in any radial direction from the GPR

antennae will generate a reflection. This is a significant factor to keep in mind during data analysis, and will be discussed in section 5.3.1.

The first returns to reach the receiver are the direct air and ground waves. The basal reflection, is seen as single wavelet of positive-negative-positive (+ - +) polarity. The source of this reflection was verified by running GPR traverses across the glacier to its edge.

Topographic maps and a digital elevation model were constructed from the GPS data within Golden Software's SURFER program. Figure 5.2 shows the topographic map of the surface elevation. A digital elevation model (DEM) was constructed from this data within Golden Software's SURFER mapping program (Figure 5.3).

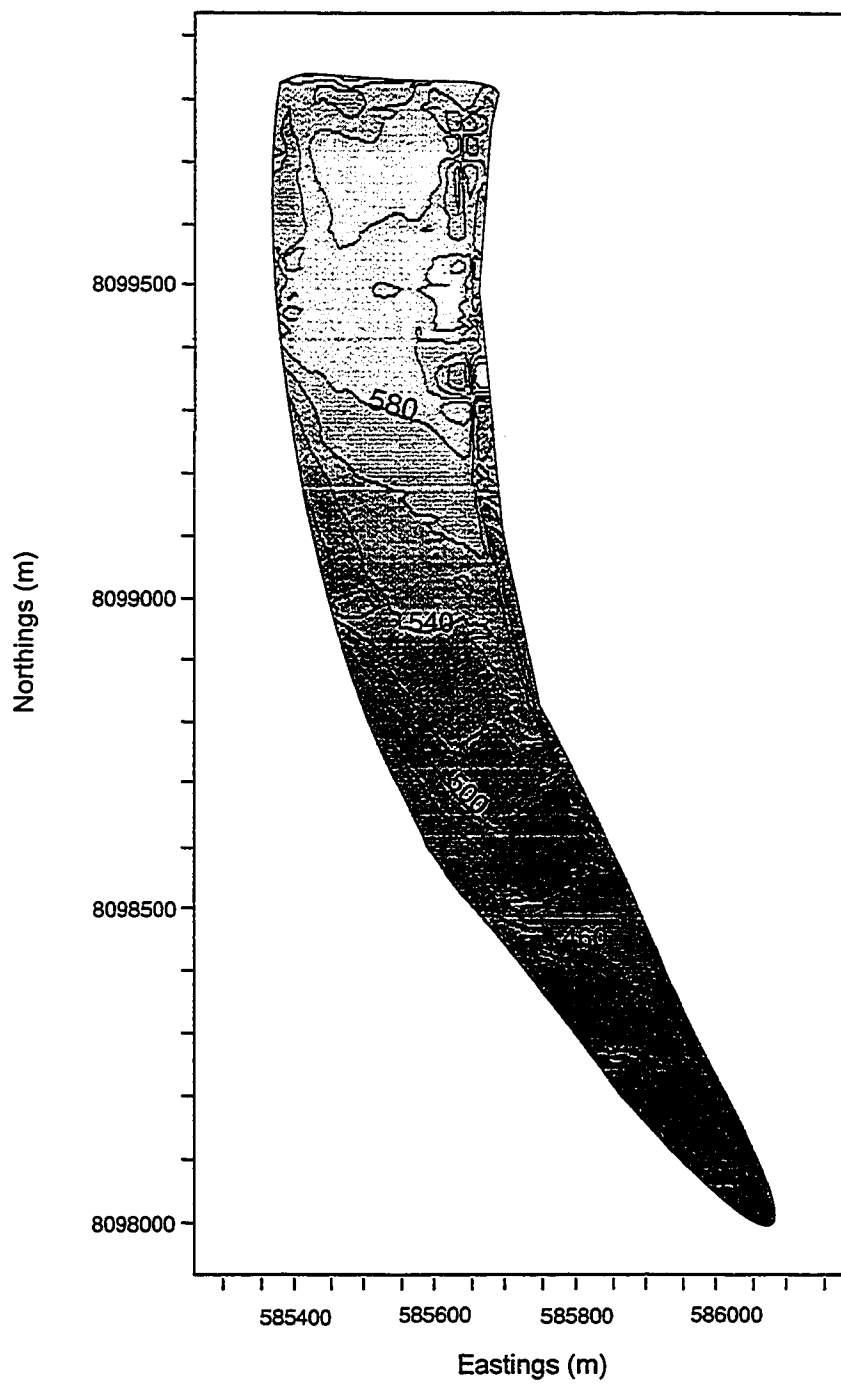


Figure 5.2 Topographic map of Stagnation Glacier and the surrounding area. Elevations are in metres above sea level.

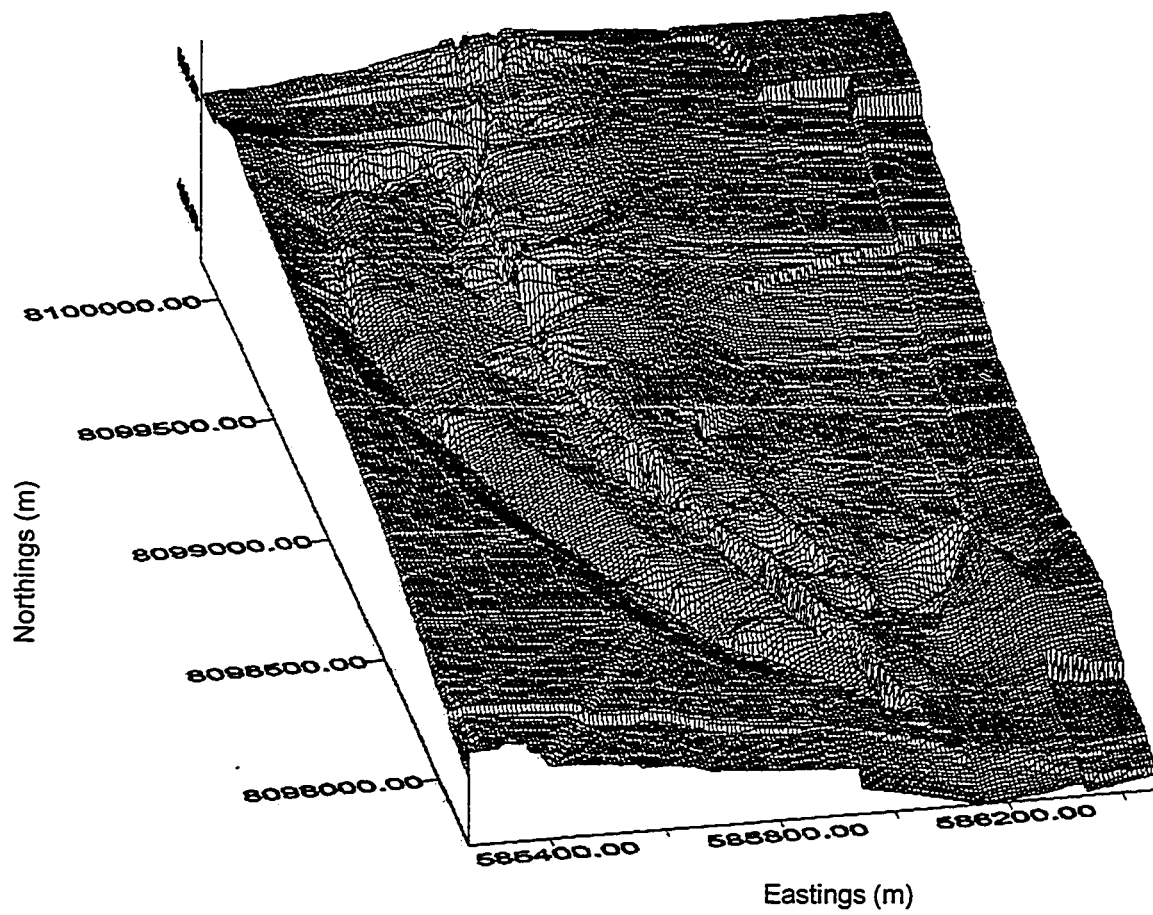


Figure 5.3 DEM of Stagnation Glacier and surrounding area.

The elevation of the base of the glacier (interpreted as the interface between ice and sediment on bedrock) was calculated by subtracting the thickness of the glacier from the surface elevation, thus all elevations are in metres above sea level (MASL).

Data was gridded using the Kriging technique. Kriging was selected for its tendency to connect high points as ridges and low points as valleys. A resolution of 8 m was used to minimize mapping times while revealing significant detail on the DEM. Due to the variation of data density over the mapped portion of the glacier, areas with low data points are estimated by triangulation of the nearest surrounding data points. Figure 4.1 shows the location of GPR lines. Kriging can also have a tendency to overestimate elevations in areas of low data density, hence producing an inaccurate DEM of the glacial surfaces. This can not be avoided without further collection of GPS data, and thus the DEM should be used, but not without consideration of the limitations of the data set and modelling program.

In areas of higher data density, it was observed that the bedrock/till base elevation varies greatly, indicating an undulating surface of valleys, ridges, hills and depressions. The effect this has on glacier thickness and the resulting hydrology will be discussed later.

Figure 5.4 shows how the basal elevation on GPR profile 99-1 decreases by 10 m over a distance of 50 m, suggesting a dipping slope of 12°- 13° while the slope of the ice surface remains constant. A similar overdeepening can be seen at the top of 99-1 and at the end of 99-27. A thickening of 40 m over a distance of 250 m was observed on 99-27. Figure 5.5 shows the thickening in glacier ice for a portion of this zone.

The area studied within the ablation zone on Stagnation Glacier will be discussed in three sections: the lower, middle and upper sections (Figure 5.6). The GPR results and

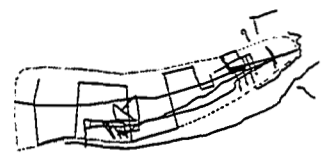
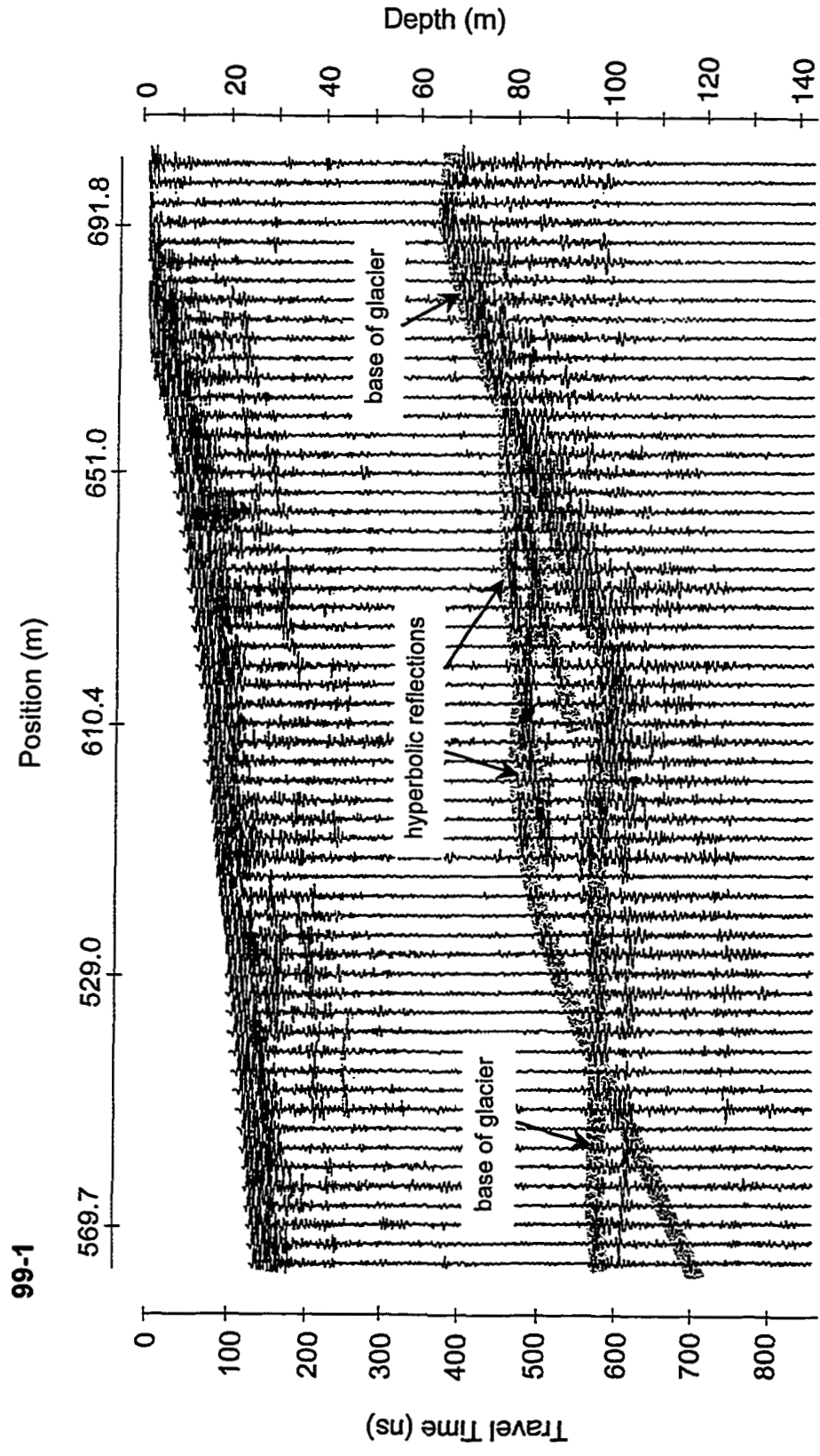


Figure 5.4 GPR Profile 99-1/2 between the intersections of 99-37 and 99-34. Note the rise in basal topography upstream (to the right) of the hyperbolic reflections. Glacier flow is from right to left.

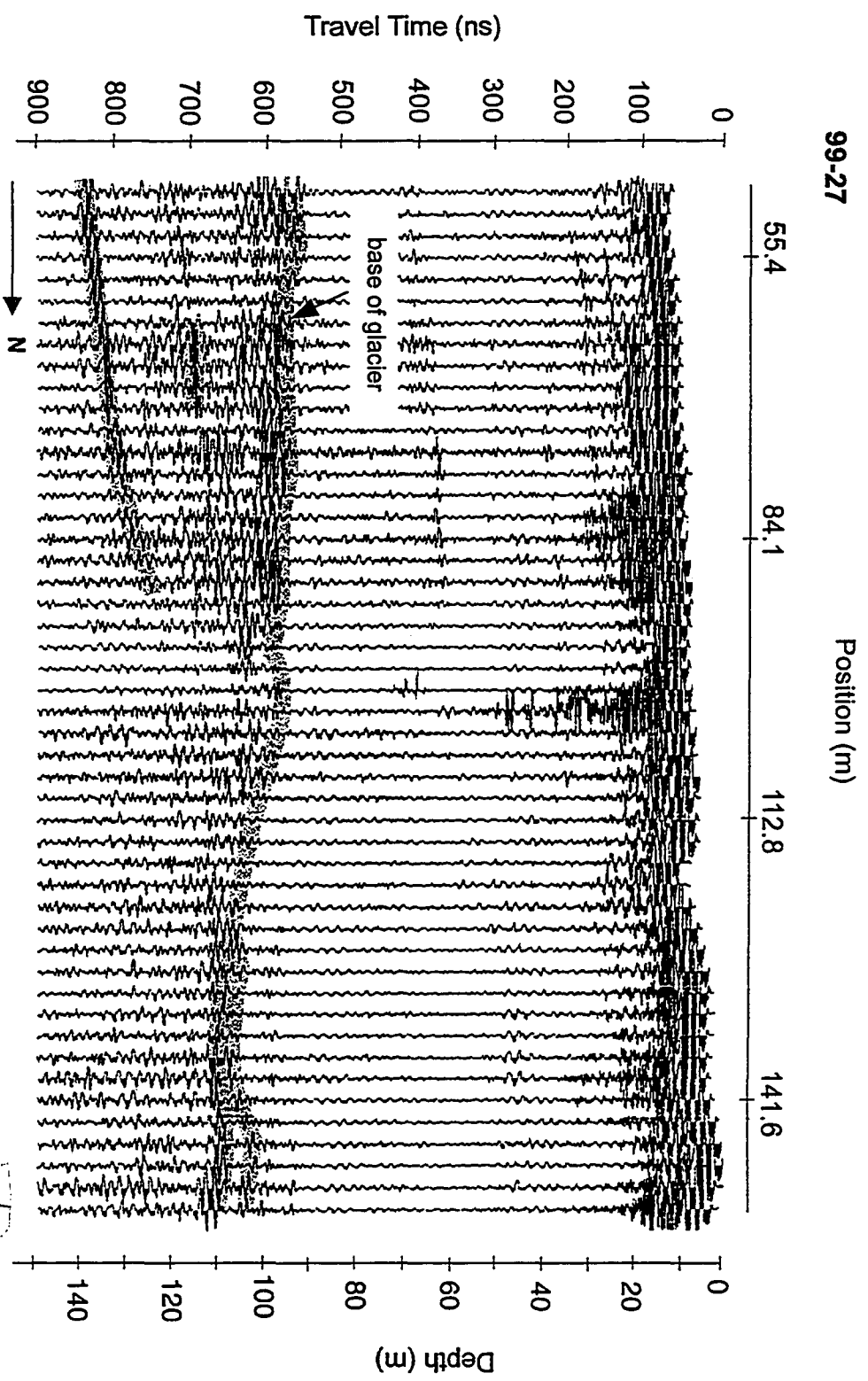


Figure 5.5 GPR Profile 99-27. Note the thickening in glacier ice as a result of a decrease in elevation of the base, and an increase in elevation of the glacier surface.

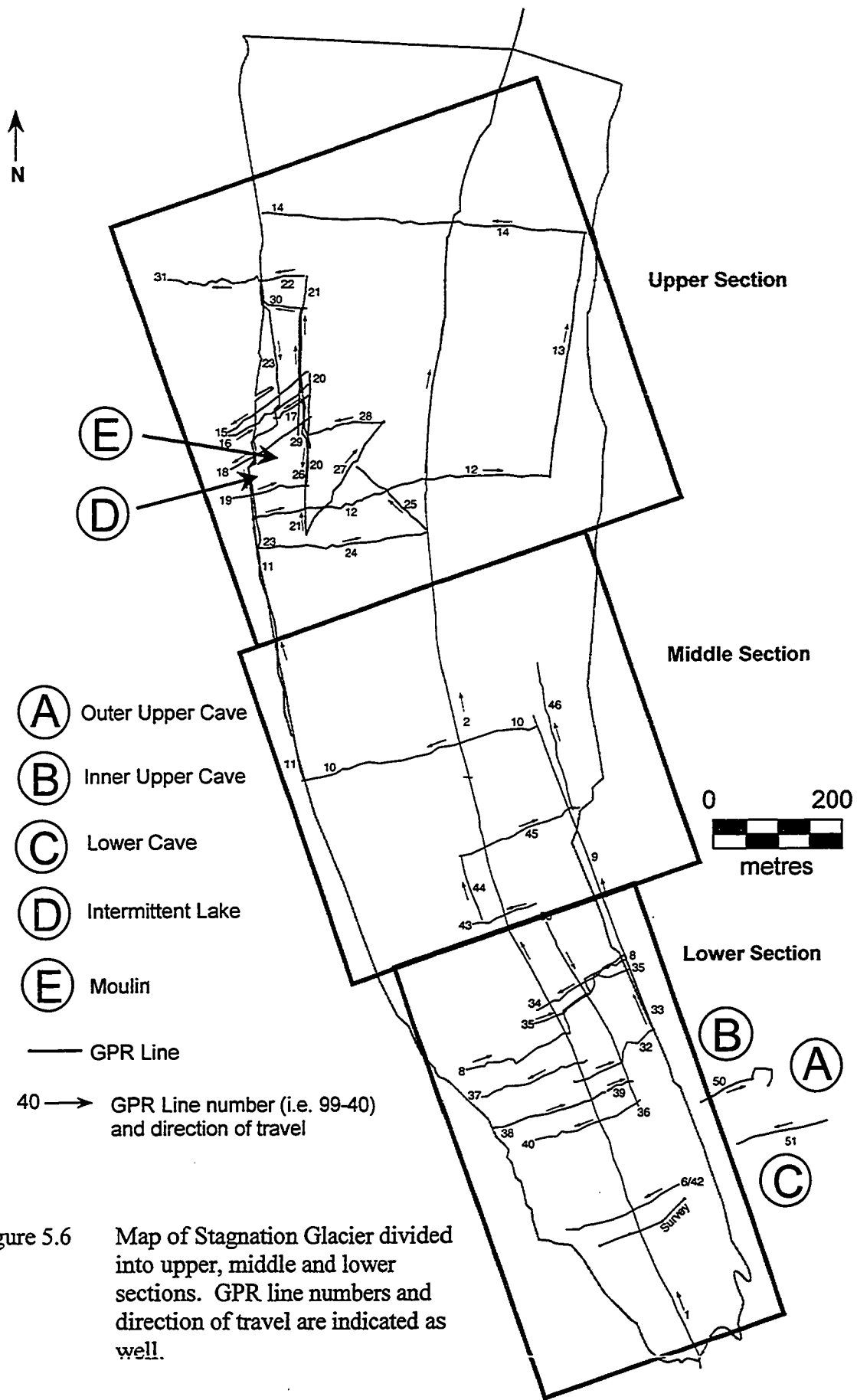


Figure 5.6 Map of Stagnation Glacier divided into upper, middle and lower sections. GPR line numbers and direction of travel are indicated as well.

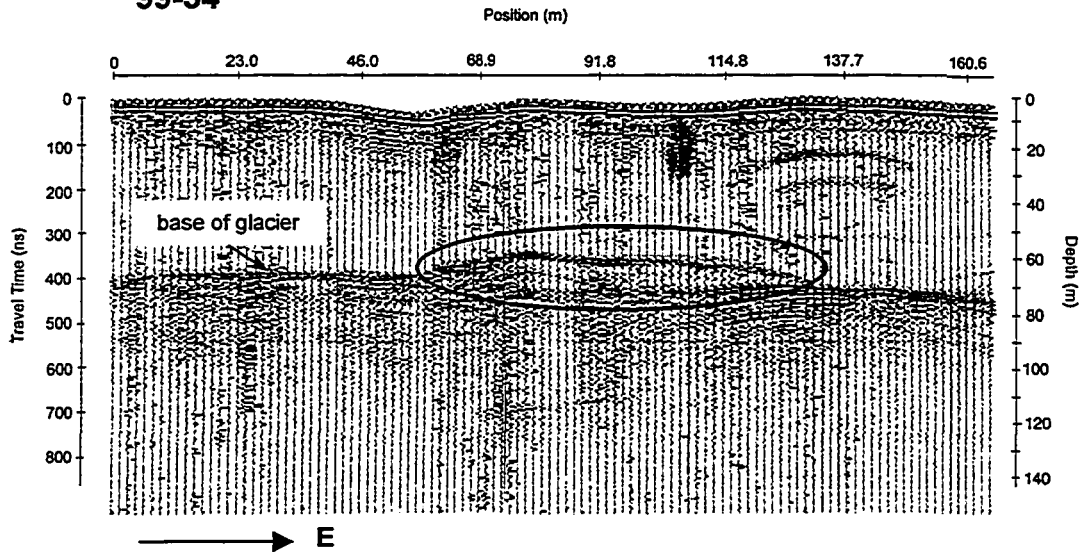
primary interpretation from each section will now be highlighted so as to demonstrate the typical findings from each section. The thermal and hydrological character of Stagnation Glacier will be discussed later when the results of the GPR data are collectively interpreted and modeled.

5.3 SUBSURFACE HYDROLOGY RESULTS

5.3.1 Lower Section

Beginning at the terminus of the glacier, and moving up-glacier along the centre line, the following describes the features as interpreted from the GPR data. In the lower section of Stagnation Glacier several interesting features were interpreted: large conduit system running perpendicular to glacier flow, sediment drapes at the base of the glacier, shear zones, numerous air-filled and water-filled conduits, and the beginning of a warm-ice zone at the base near the top of the lower section.

The large conduit system is indicated by the presence of distinctive types of radar reflections. These different types are the result of the orientation of the numerous radar lines collected in the vicinity of the conduit system, with respect to the orientation of the conduit system. Every reflection suggests that the object is water- or sediment-filled, due to the positive reflection coefficient. The interpolation of the reflections across the GPR traverses and the geometry of the reflections suggest that the feature is water-filled. Numerous hyperbolae are observed on GPR traverses running parallel to glacier flow, indicating conduit orientation is perpendicular to glacier flow. For simplicity, this type of orientation will be described as “cross-glacier”, where as flow parallel to glacier flow will be termed “along-glacier”. Continuous reflections are seen on 99-34 and 99-35 at approximately 60 m depth (Figure 5.7).



99-35

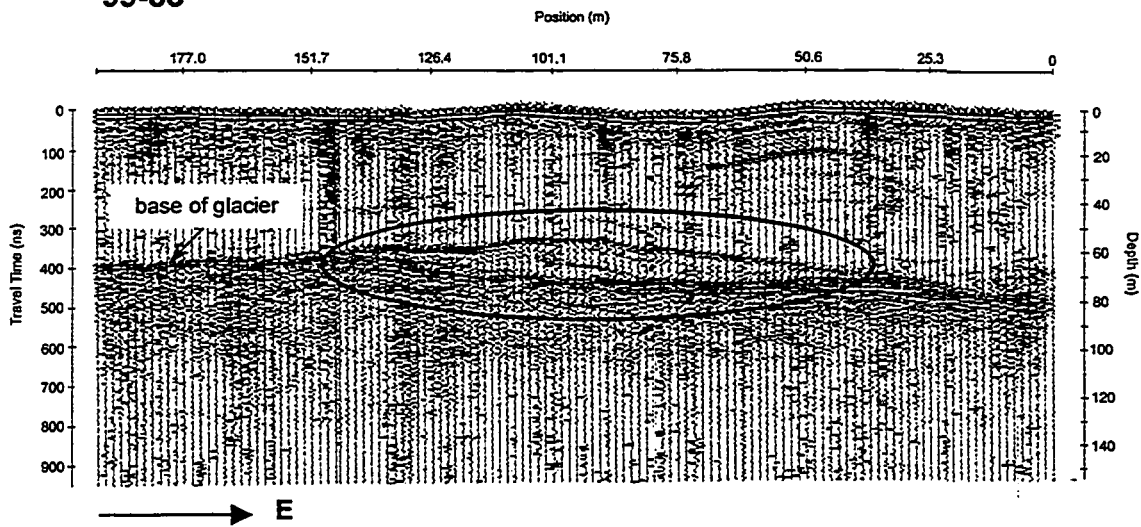
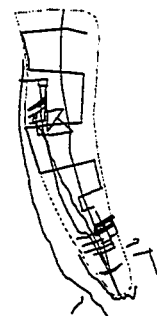


Figure 5.7 GPR profiles 99-34 and 99-35. Note the circled continuous reflections at 60 metres depth (75 – 100 metre position). The reflections have a positive polarity, indicating the feature producing the reflection is either sediment or water. Glacier flow is out of the page (towards the reader).



Both reflections are remarkably similar in shape and character, except that the reflection on 99-34 has a longer travel time, suggesting that the conduit is at a lower depth. Since no reflections were observed on the nearby portion of 99-1/2, these continuous reflections have been interpreted as diffractions from a conduit system down-glacier from the line. The furthest upglacier line, 99-34, supports this theory if we remember that the plotted depth is a function of time, and not vertical distance. The suggestion that these are diffractions is supported by other reflections “beneath” the conduit diffraction. If the continuous reflection is indeed directly below the traverse, it is unlikely radio waves would reflect off of features below the conduit, due to the high reflection coefficient of the water-ice interface.

Hyperbolae are observed on 99-36 (Figure 5.8), which again suggest conduit orientation across-glacier. However, the elevation of these hyperbolae, when migrated, suggest the conduits gain elevation as they run offglacier. A third GPR traverse, 99-33 (Figure 5.9), running parallel to glacier flow and 99-1/2 and 99-36, does not contain hyperbolic returns. At the base, however, it is possible that broad conduits are being detected, as indicated by the change in the character of the basal reflection in the vicinity of the proposed conduit.

The elevations of the hyperbolae along 99-36 are close to, and occasionally higher than the elevations of the hyperbolae observed on 99-1/2. Figure 5.10 displays a schematic of the interpreted conduit geometry.

99-36

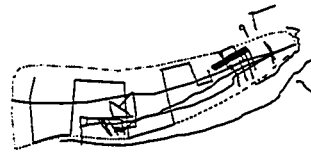
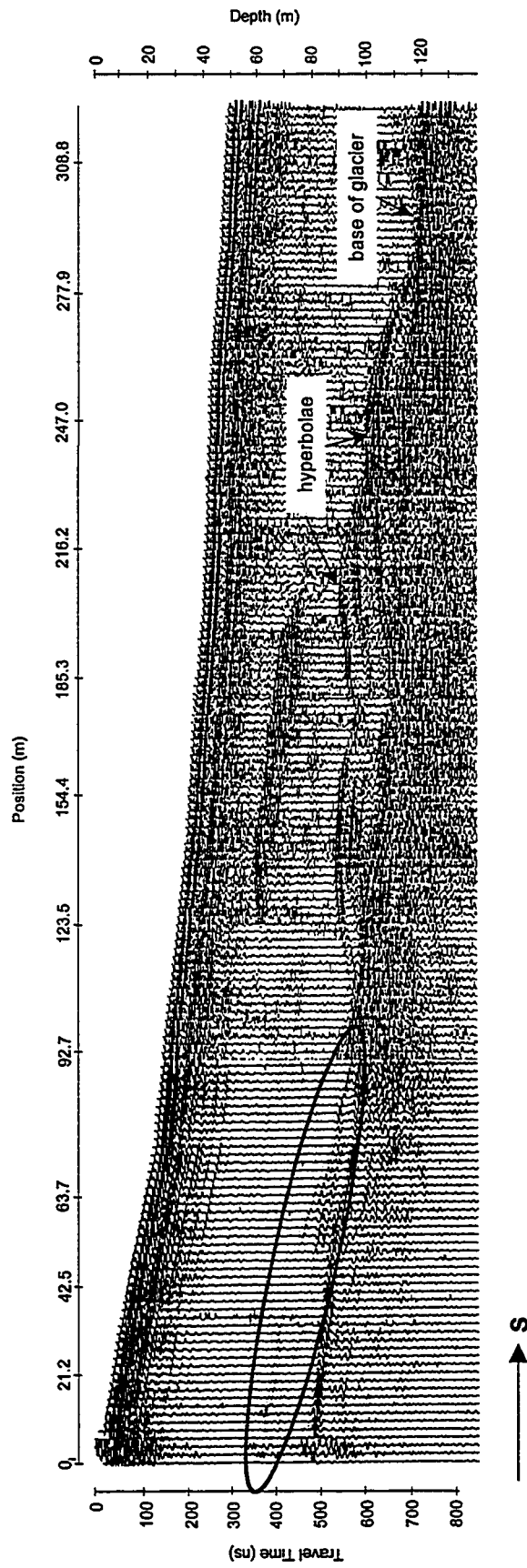


Figure 5.8 GPR Profile 99-36. Glacier flow is from left to right. Note the large positive-polarity hyperbolae from positions 130 metres to 250 metres. These have been interpreted as water-filled conduits. The high frequency reflections seen from positions 123 metres to 200 metres (25 metres depth) are probably from a zone of sealed crevasses. The beginning of a warm-ice zone (circled) is also interpreted, starting at 90 metres (70 metres depth). The reflection becomes weaker near the 50 metre position.

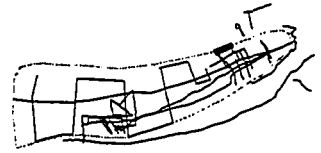
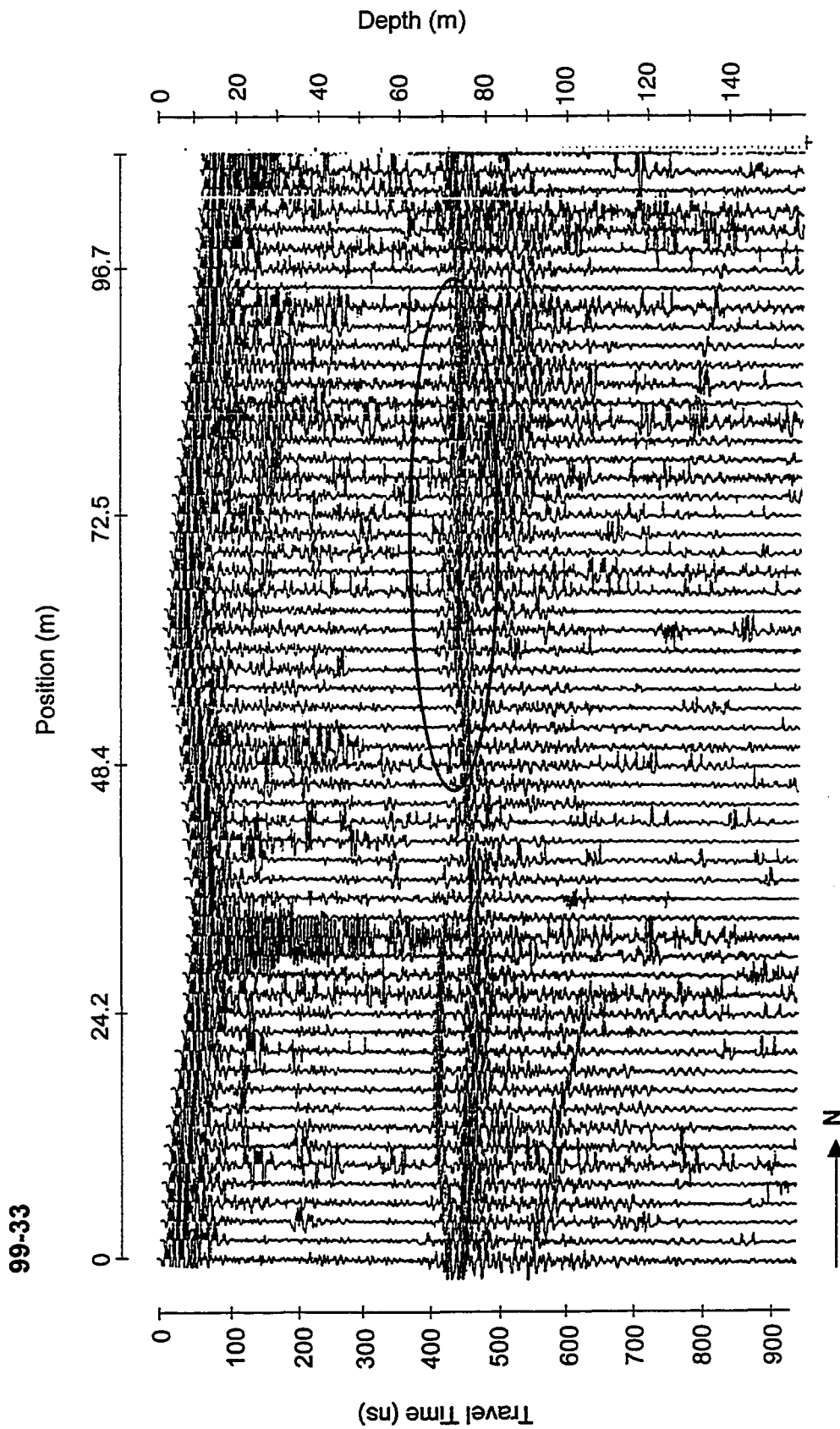


Figure 5.9 GPR Profile 99-33. Note the change in the circled basal reflection along positions 75 – 100 metres (70 metres depth). This change could indicate the presence of water flow at the base. Glacier flow is from right to left. A strong reflection from 0 – 24 metres along the profile is interpreted as the upper layer of basal sedimentation.

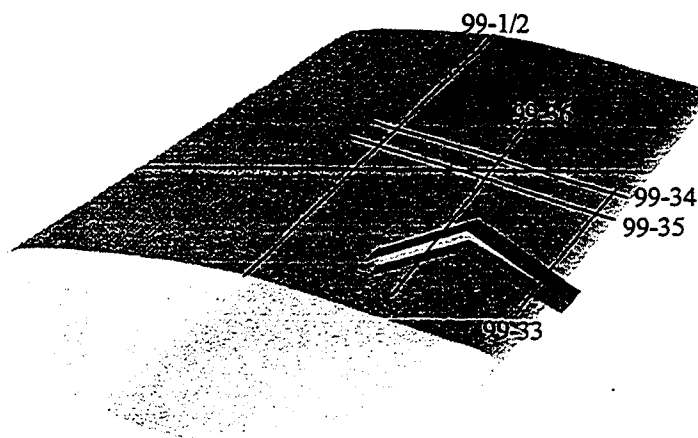


Figure 5.10 Schematic of Stagnation Glacier showing proposed conduit orientation as interpreted from GPR data from profiles 99-1/2, 33, 34, 35 and 36.

A second feature observed in lower portion of Stagnation Glacier is interpreted as a sediment drape over the bedrock/till, in the area down-glacier from a high in bedrock topography (Figure 5.11). These are indicated by weaker continuous reflections observed 0 - 10 m above the base of the glacier (not shown in figures). The drape is observed to gradually increase in thickness towards the centre of the glacier (increasing in both elevation and thickness), and pinch out towards the sides. The reflection is weaker and has a positive reflection coefficient. There are also random discontinuous returns between the continuous return and the basal reflection, which are typical of reflections from poorly sorted coarse grained sediment such as till (Moorman, 1998).

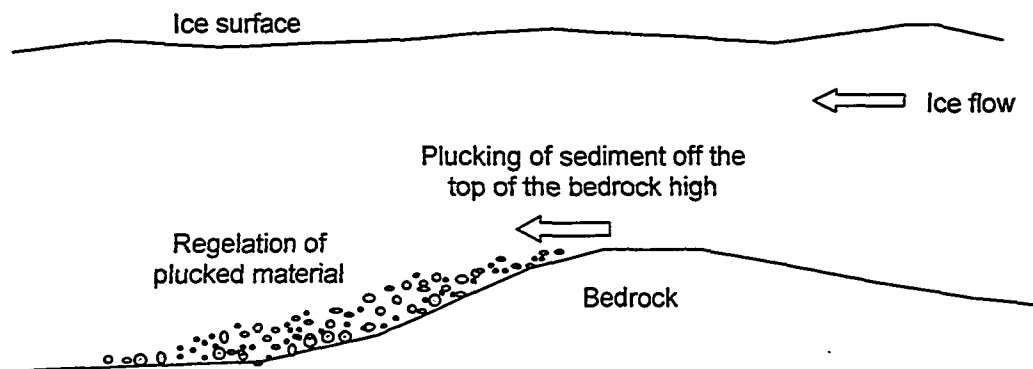


Figure 5.11 Schematic showing the regelation of plucked bedrock material into basal ice.

Continuous reflectors that dip towards the centre of the glacier are also observed.

The reflectors are often multi-layered, have a positive reflection coefficient, and follow the topography of the rising bedrock toward the edge of the glacier as it thins, as seen on profile 99-32 in figure 5.12. These reflections have been interpreted as debris trains incorporated into basal ice.

Numerous hyperbolae were also observed throughout the lower portion of Stagnation Glacier. Most are generated by objects too small and thus their lateral extent cannot be resolved (i.e. less than 2 - 3 m). A total of 16 hyperbolae were mapped, 9 of which were air-filled, 6 that were water-filled, and one that was possibly air- and water-filled. Such a conduit could form if the water level throughout the conduit remains lower than full-capacity such that an opening to the surface is maintained, keeping the conduit at atmospheric pressure. The air filled voids are most likely unconnected cavities formed from the closure of crevasses. The water filled objects could be connected conduits or isolated water-filled cavities. Determining the connectivity of the conduits is difficult due to the sparse distribution of the reflections over the glacier.

On Figure 5.8, the top of 99-36 reveals what might be the beginning of a warm-ice zone with Stagnation Glacier. The northern most 100 m of the traverse reveals a continuous positive reflection, weakening and strengthening along the traverse, that pinches out towards the south. A discontinuous positive reflection is observed above the base. Together, these reflections indicate the beginning of a warm-ice zone, formed from the transition between cold and temperate ice. This warm-ice zone is discussed in the next section 5.3.2.

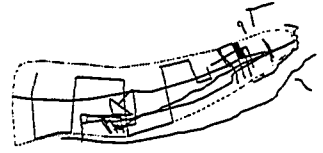
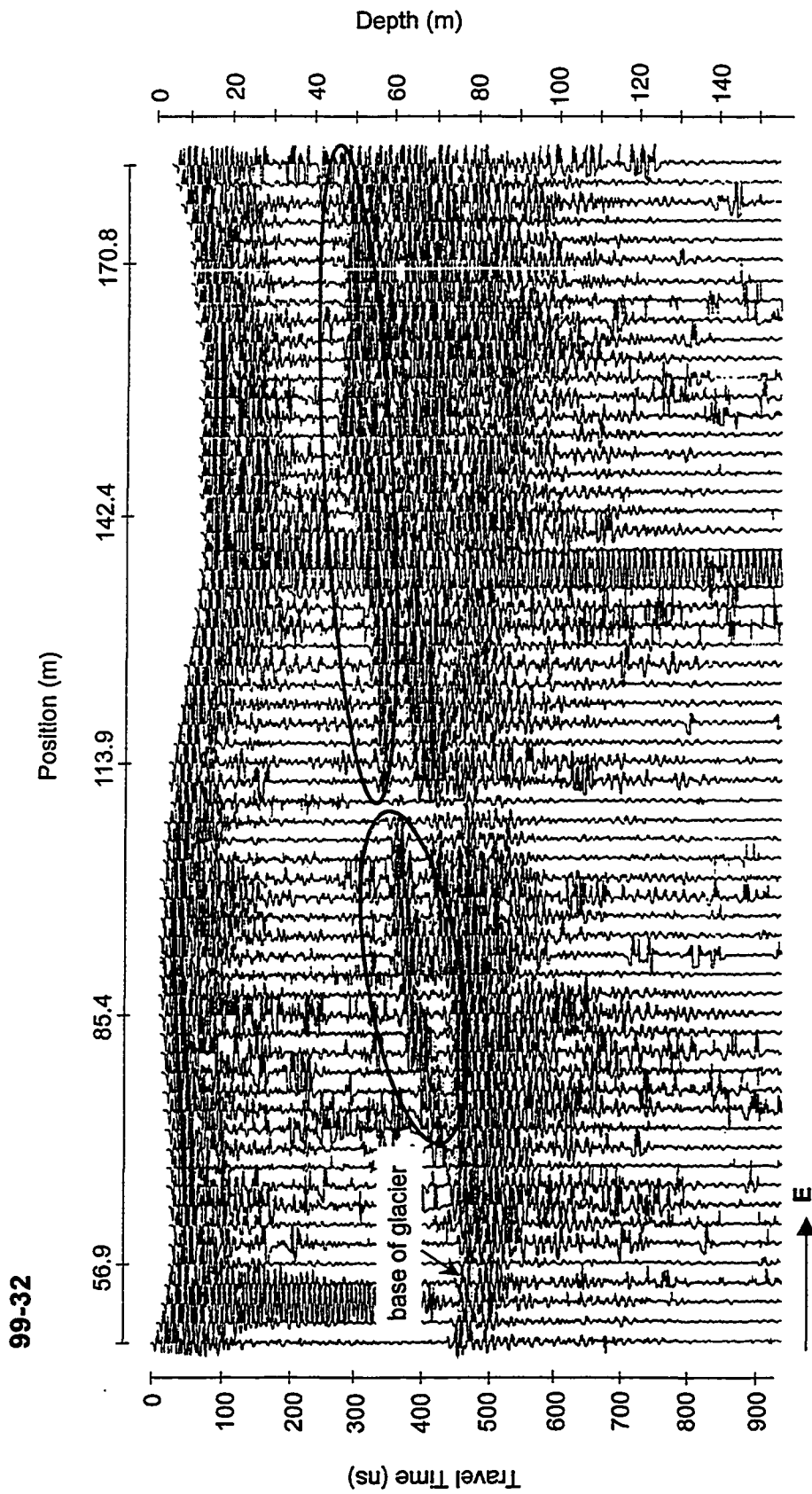


Figure 5.12 GPR Profile 99-32 showing debris entrainment (circled) into basal ice at the glacier margin. The sedimentation at the eastern portion of the profile is observed at the northern portion of 99-33 (Figure 5.9). Glacier flow is out of the page (towards the reader)

The basal topography of the lower section, as computed by the subtraction of ice thickness as indicated on radar data, from surface elevation data, shows a steep ridge over which glacial ice thins as it flows over. An overdeepening below the ridge is seen in the local depression on the lee side of the ridge, and the subsequent thickening of ice above.

5.3.2 Middle Section

The middle section of Stagnation Glacier, starting approximately 800 m from the terminus, and extending for a distance of 500 m, is the least surveyed of the three sections due to treacherous terrain, and the fact that the fewer features were observed during initial reconnaissance surveys. One prominent feature interpreted in post-field analysis however, is the presence of a large zone of warm ice above the base of the glacier. Relatively few (less than five) water-filled conduits were observed, although numerous air-filled cavities were observed in the near surface of this section.

The warm-ice zone is particularly interesting in the middle section because it is marked by the zero-degree isotherm, as indicated by the type-reflection for warm-ice ice being a continuous reflection with positive polarity (+ - +). The zero-degree isotherm is a line of constant zero-degree temperature, where ice above is below the pressure-melting point and ice below is at the pressure-melting point. The zero-degree isotherm would theoretically increase the water content of the ice since the temperature is at the pressure-melting point. The water content at the zone surrounding a zero-degree isotherm is likely to be gradual, and may not be observable with GPR as a result of the detection limits of the GPR system. This will be discussed in further in section 6.2. As observed on GPR profile

99-1/2 in Figure 5.13, the zero-degree isotherm extends into the till below the glacier, suggesting the presence of active, deformable unfrozen till.

The zone of temperate ice was mapped according to the similar reflections on both 99-1/2 and 99-33. The warm-ice zone is 18 m thick at its maximum, and pinches out to zero down glacier where the zero-degree isotherm passes beneath the basal ice/till boundary.

A second warm-ice zone is observed further down glacier from 99-43 to 99-36. Figure 5.8 showed the beginning of the warm-ice zone on GPR profile 99-36. The zone is 11 m thick at its maximum, and pinches out to zero as well. An extension of the zero-degree isotherm is not observed here. It appears that the two warm-ice zones, although located proximally to each other, are not connected. A distance of 50 m separates the isolated zones.

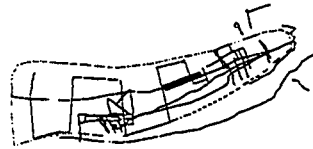
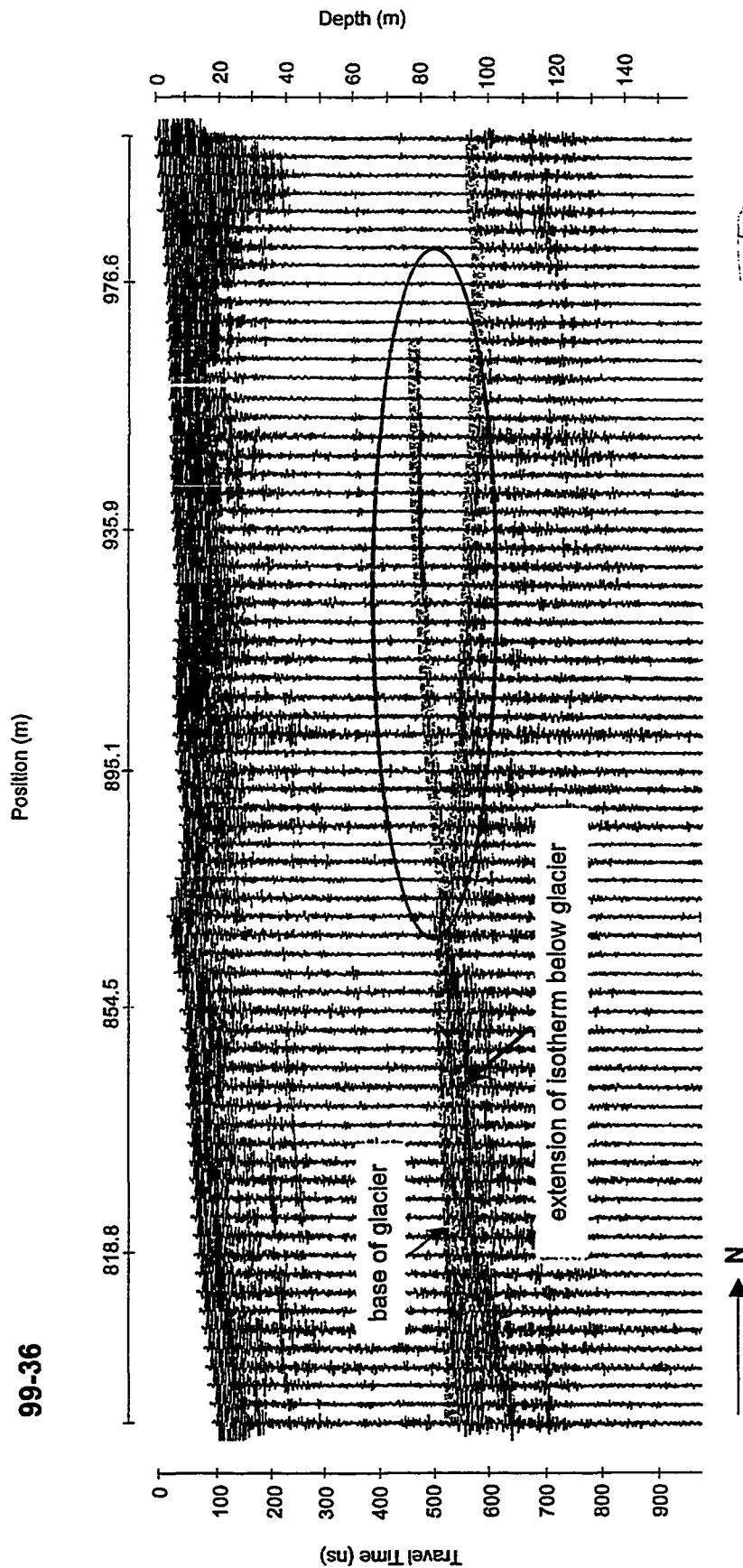


Figure 5.13 GPR Profile 99-1/2 between 99-43 and 99-10. Note the extension of the zero-degree isotherm through the glacier to the bedrock/fill (circled). Glacier flow is from right to left.

Several areas of possible water-filled conduits were detected, indicating the flow of water in a down-glacier orientation. At the upper boundary of the middle section, two continuous reflections (positive polarity) were observed. One reflection, located on 99-10 is 11 m wide and suggests water flow down glacier. The feature is observed at 107 m depth, located just above the base of the glacier, in the deepest part of the valley-shaped cross-section of the glacier. A second, smaller water-filled feature (hyperbola) was observed directly 16 m above. Along 99-10, two other water-filled tunnels or cavities were observed between 20 and 30 m depth.

The second continuous reflection is located on 99-46 (Figure 5.14). The reflector is dipping down glacier, and is unlike the character of sediment-derived reflections observed below. The continuous reflector dips down glacier where it meets the base. This may suggest water flow towards the glacier terminus.

99-46

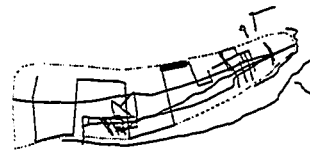
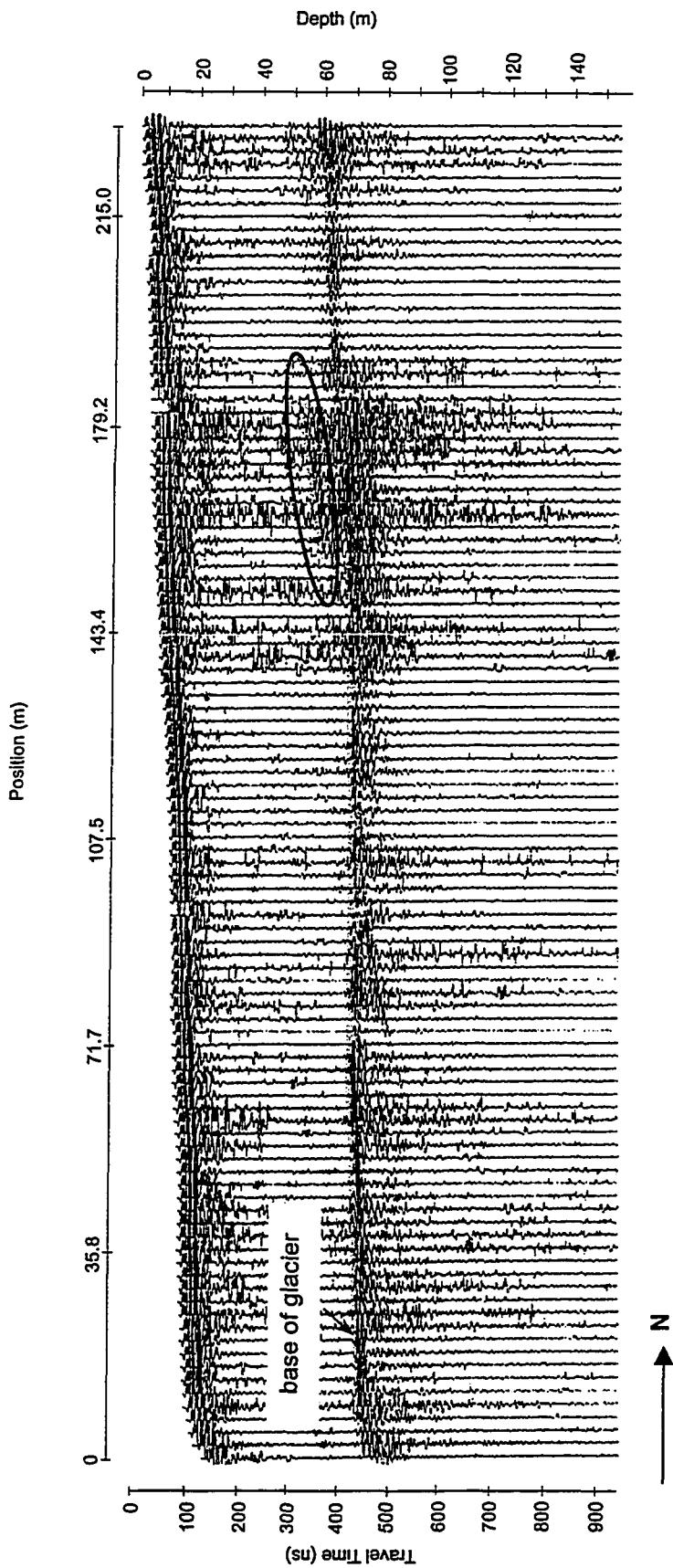


Figure 5.14 GPR Profile 99-46. Note the reflector dipping downstream from 145 to 155 metres, which has been interpreted as a reach of a water-filled conduit. Glacier flow is from right to left.

Another hyperbola with positive polarity was observed near the edge of Stagnation Glacier, on 99-9 at a depth of 42 m. Several air-filled cavities were observed in the near surface and are most likely the relicts of closed crevasses.

The middle section begins at the crest of the large basal ridge below the ice. The ridge flattens towards the top, and begins to form a depression up glacier. This depression forms another glacier overdeepening, which might have an effect on the formation of the zero-degree isotherm.

5.3.3 Upper Section

The upper section contained the greatest number of surface and subsurface features. One additional warm-ice zone, numerous air-filled and water-filled cavities and conduits, and basal sedimentation were observed from the GPR data. Each type of feature was observed in both the lower and middle sections of Stagnation Glacier.

The uppermost group of three warm-ice zones were detected in the upper section of Stagnation Glacier. The zones, ending approximately 1400 m up from the terminus for no more than 200 - 300 m. The eastern and northern boundaries of the warm-ice zone are unmappable due to lack of GPR data. The zone is marked by a weaker positively-polarized reflection above noisy high-frequency reflections to the base. The warm-ice zone is 30 m thick, where the glacier ice is at it's thickest (110 m thick). The zone pinches out to the north where the glacier flows over another topographic high in the bedrock/till. Up glacier from the high, glacier ice thins to 50 m.

The character of the reflection from the warm-ice zones varies between the zones within the lower sections of Stagnation Glacier. Signal strength and the extent of higher-

frequency “noise” below can differ slightly. The typical reflection from a warm-ice zone can be seen on 99-25 (Figure 5.15)

During GPS and GPR data processing, a rise in surface topography was observed in the vicinity of the moulin and intermittent lake. At the intersection of 99-15 and 99-23, an increase in surface elevation of 3.5 m over 4 days was observed. An increase of 1.3 and 1.5 m was observed down-glacier at the intersections of 99-16 and 99-18 with 99-23. This increase is not a measure of error in data collection. This was confirmed by examination of GPS point records, since multiple points are usually taken for at one location, depending on the pace of data collection.

The northernmost area of the survey indicated another thinning of the glacier as it flowed over another rise in bedrock topography. The basal high is seen on 99-1/2 in the vicinity of the intersection with 99-14 (Figure 5.16).

An increase in the thickness and distribution of backscattering noise in the near surface of the glacier was noted, particularly in the area surrounding the moulin and intermittent lake. This noise has been interpreted as returns from sealed or open crevasses in the 0-15 m below the glacier surface.

The surface topography above 99-14 rose in elevation and contained greater numbers of surface crevasses (Figure 5.16).

Air-filled and water filled conduits were observed throughout the thickness of Stagnation Glacier. Figures 5.17, 5.18 and 5.19 show the location of various air-filled and water-filled conduits with the lower, middle and upper sections of Stagnation Glacier, respectively. The connectivity of the conduits and cavities cannot be determined due to

99-25

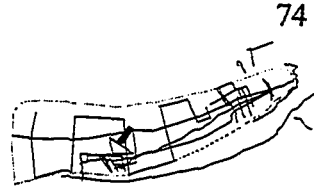
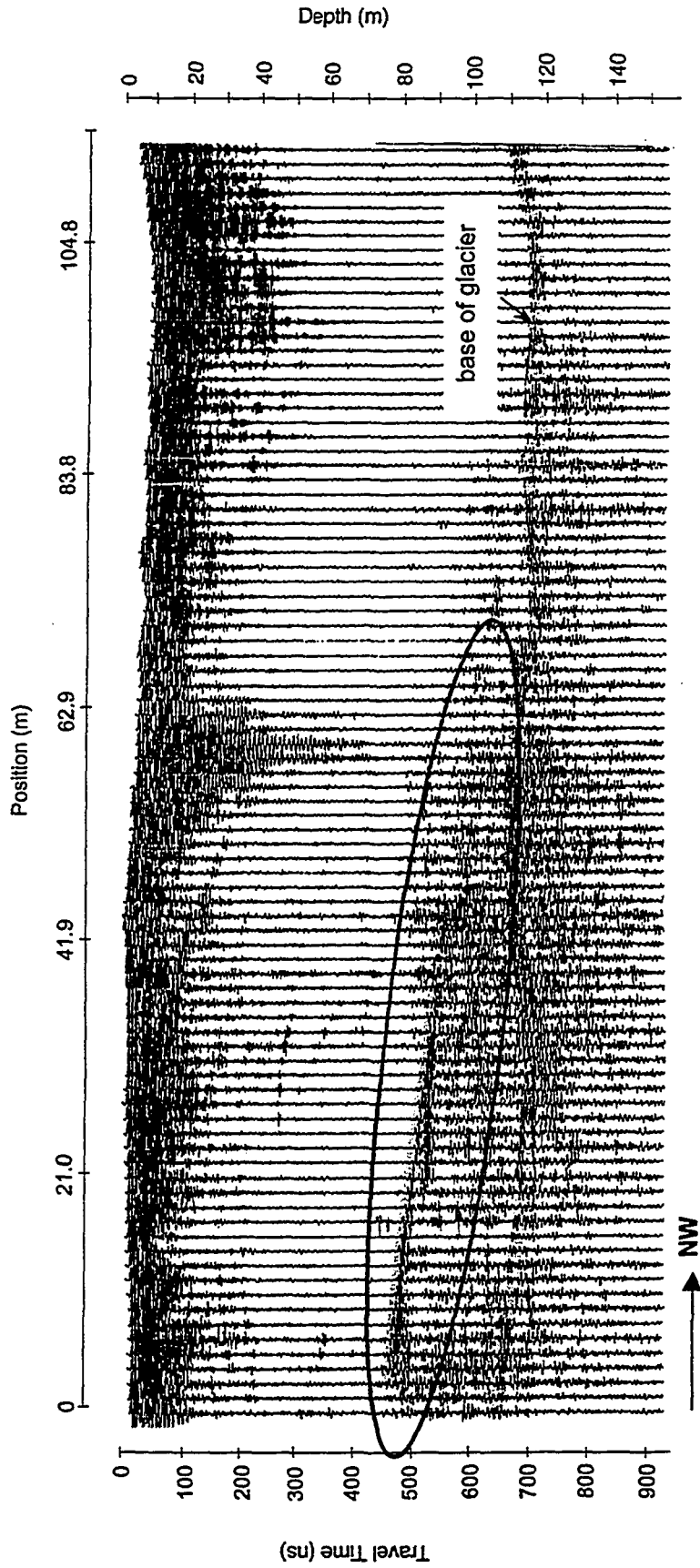


Figure 5.15 GPR Profile 99-25, showing the type of reflection generated from what is thought to be a warm-ice zone. The zone starts at 78 m depth (position 0 metres) and thins out down to 106 metres depth (approximately 70 metres in position). Where the zone becomes thinner than 20 metres, the cold-ice/warm-ice interface becomes less obvious. 99-25 was surveyed along a traverse diagonal to glacier flow. Glacier flow is into the page (away from the reader)

complexity associated with the different depths and sizes of the features. However, it can be speculated that water flow occurs in both the down-glacier and cross-glacier orientations. Figure 5.20 provides a map of the warm-ice zones within Stagnation Glacier.

By applying various processing techniques such as migration, temporal and spatial filters, and gains, the GPR data was interpreted, suggesting complexity in both the hydrologic and thermal characteristics of Stagnation Glacier. These interpretations have been presented, and will now be discussed with reference to each other, and with respect to the surficial observations made while in the field. The implications on the large scale hydrology and thermal character of Stagnation Glacier, will now be discussed, particularly it's application to the study of polythermal sub-arctic glaciers.

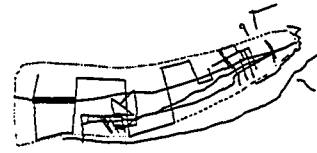
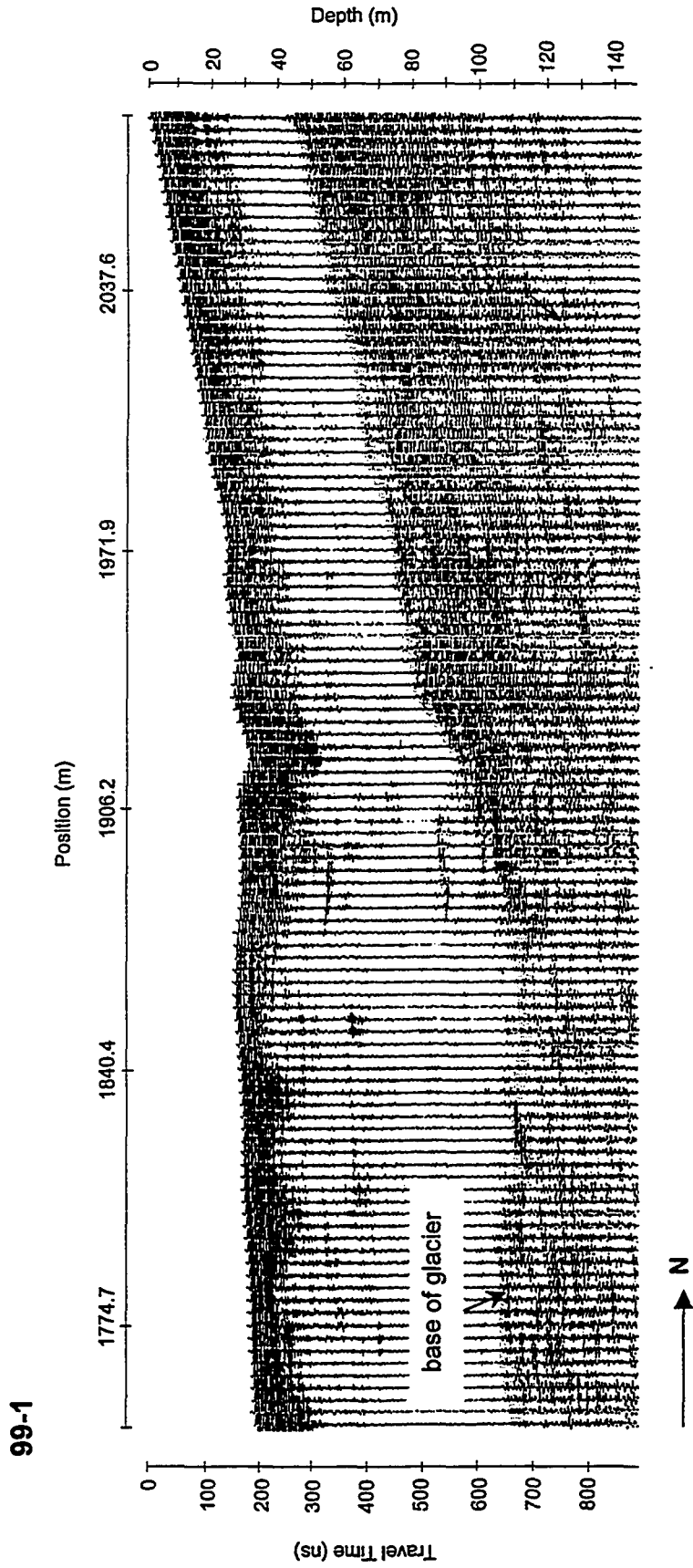


Figure 5.16 GPR Profile 99-1/2, in the vicinity of 99-14, in the upper section of Stagnation Glacier. Note the steep rise in basal topography. Glacier flow is from right to left.

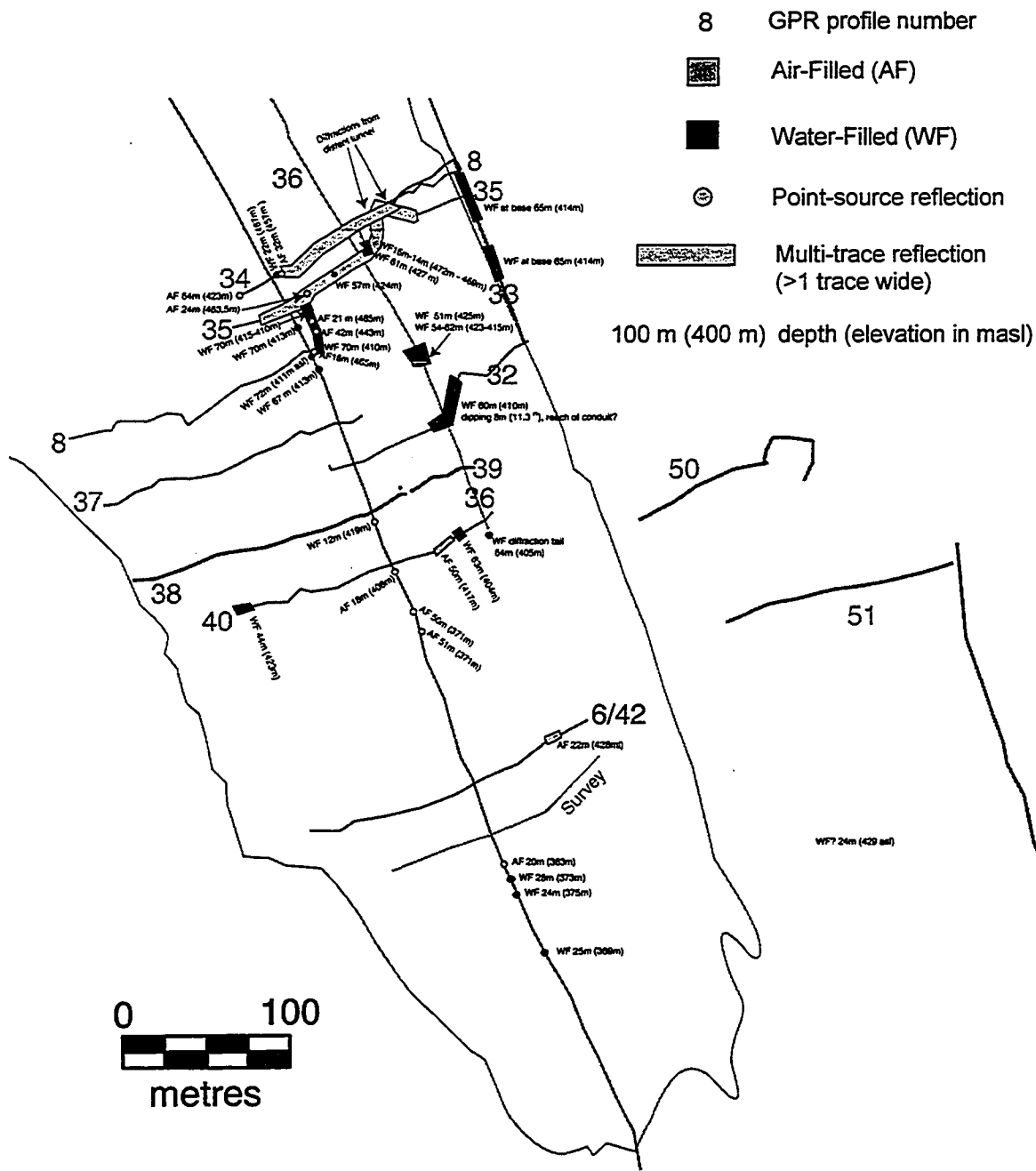


Figure 5.17 Map of the interpreted hydrologic features within the lower section of Stagnation Glacier. Note the content, depth and elevation (if known) of the interpreted GPR reflections. Refer to Appendix for map of entire glacier.

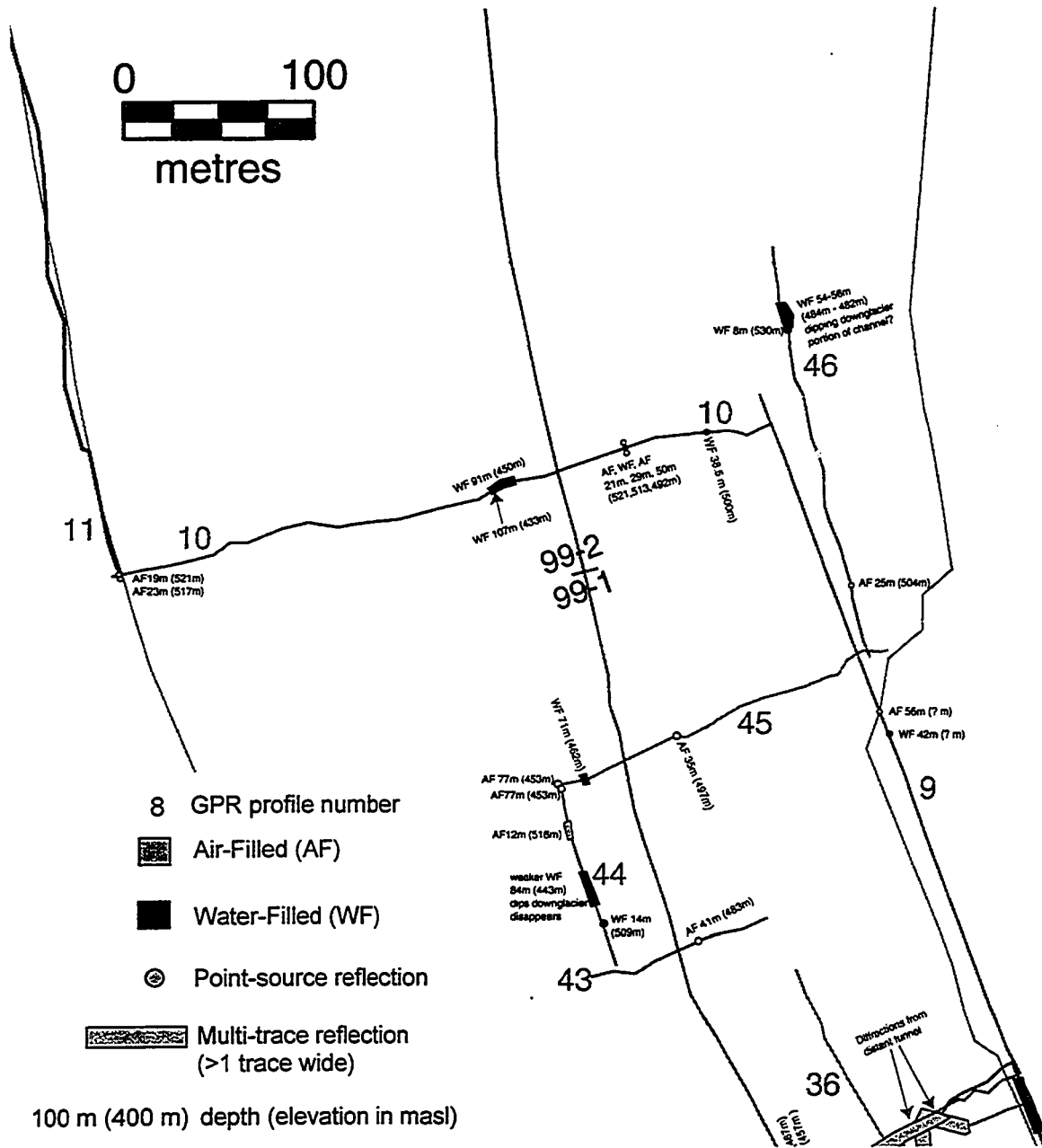


Figure 5.18 Map of the interpreted hydrologic features within the middle section of Stagnation Glacier. Note the content, depth and elevation (if known) of the interpreted GPR reflections. Refer to Appendix for map of entire glacier.

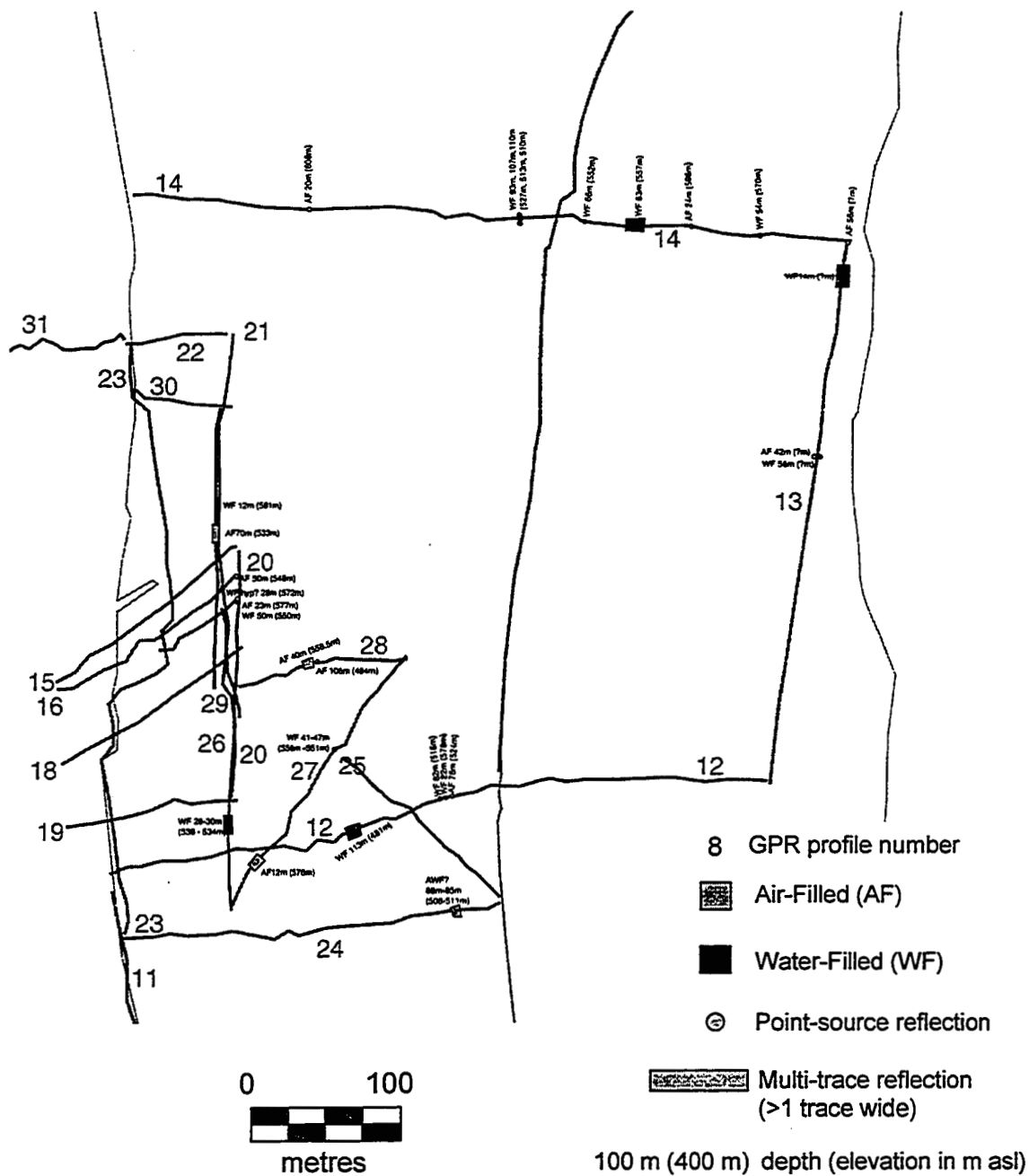


Figure 5.19 Map of the interpreted hydrologic features within the upper section of Stagnation Glacier. Note the content, depth and elevation (if known) of the interpreted GPR reflections. Refer to Appendix for map of entire glacier.

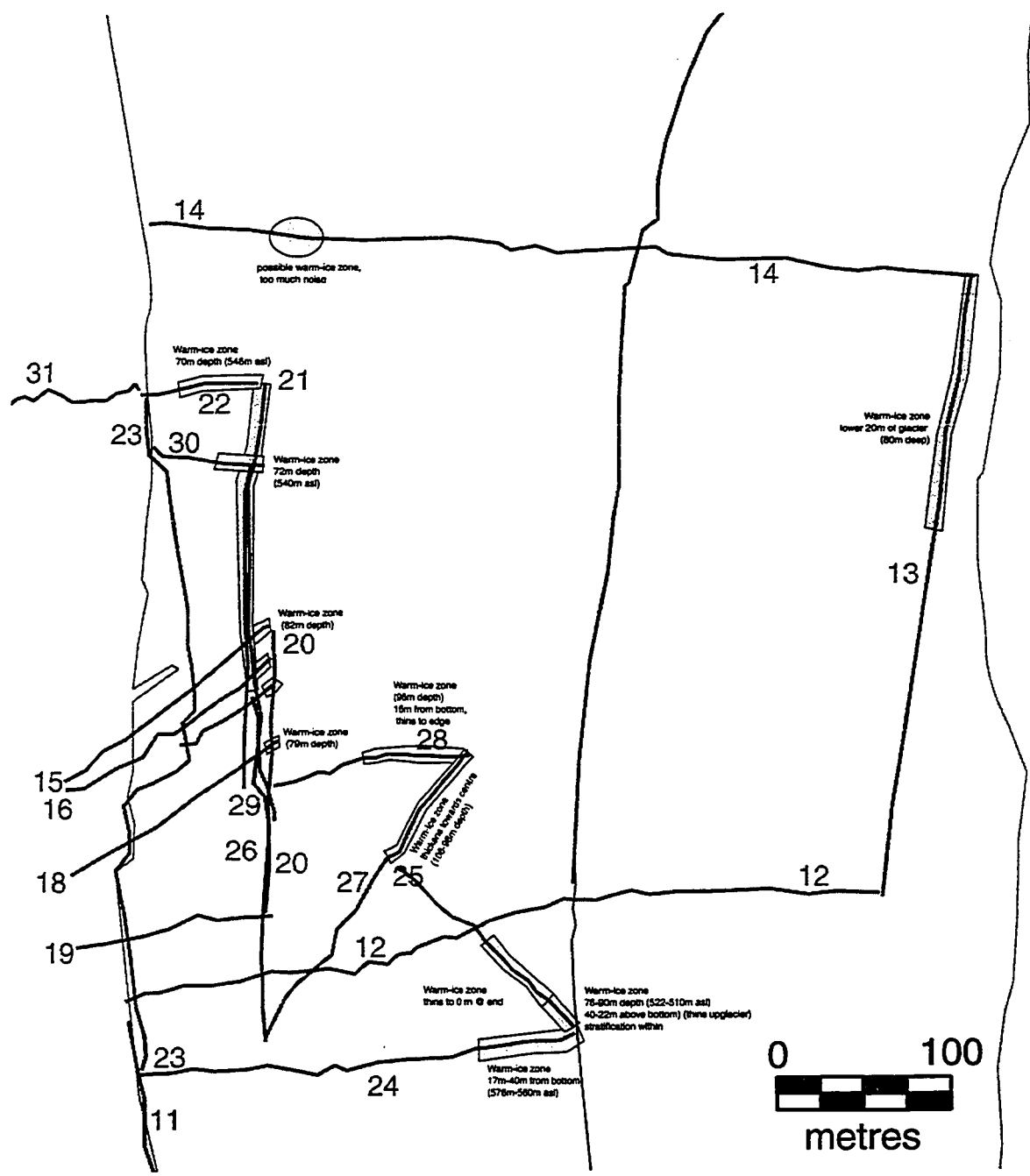


Figure 5.20 Map of the warm-ice zones in the upper section interpreted from the GPR data. Refer to Appendix for map of entire glacier.

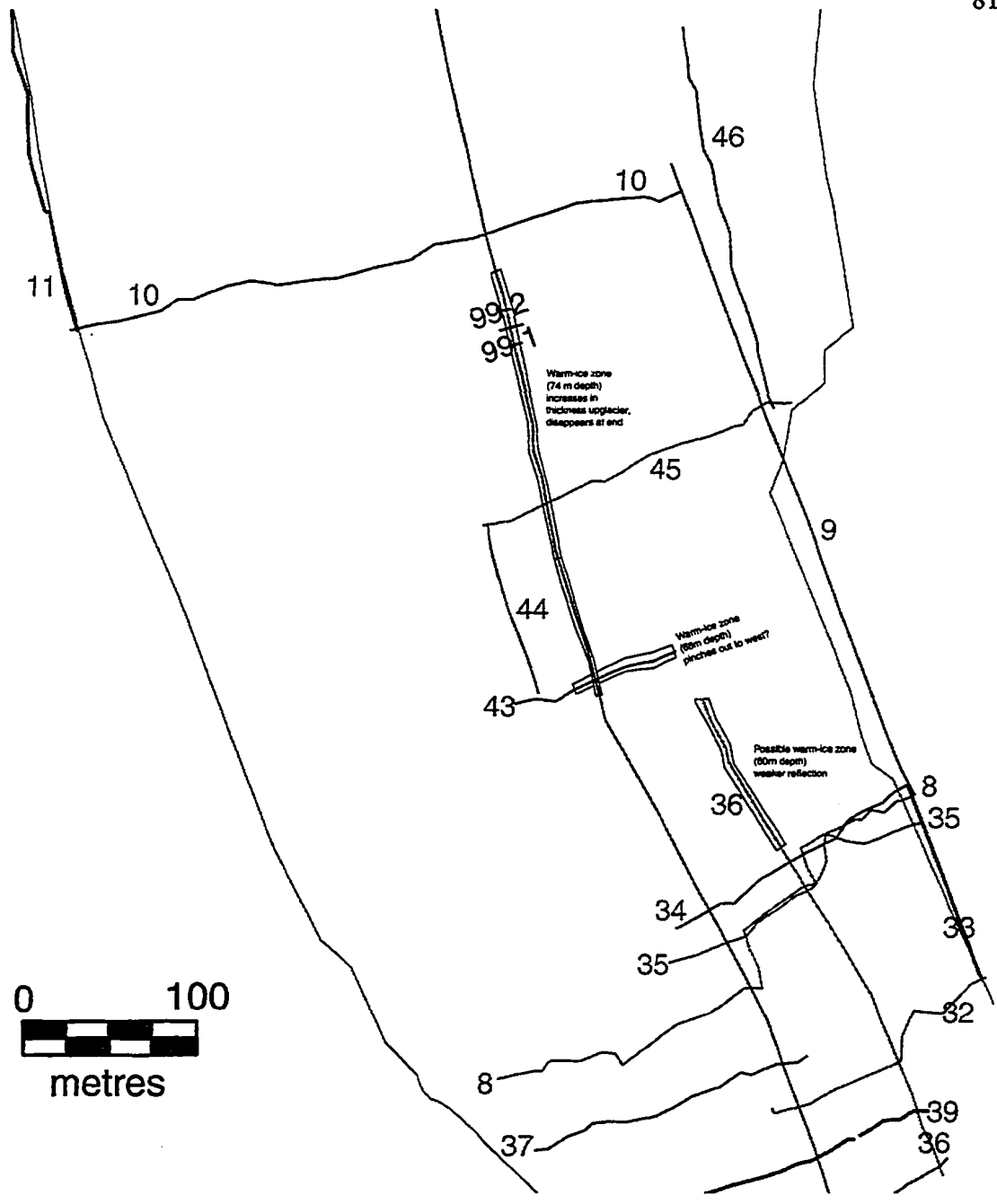


Figure 5.21 Map of the warm-ice zones on the lower and middle sections of Stagnation Glacier. Refer to Appendix for map of entire glacier.

CHAPTER SIX

DISCUSSION: SUBSURFACE HYDROLOGY

During the analysis of GPR and field-obtained data, three major categories of observations were made about the surface and internal conditions within Stagnation Glacier: the presence and nature of hydrological conduits within the ice, the evidence for temperate zones within the ice, and the incorporation of sediment into the basal ice. These three categories will now be discussed with respect to the implications of these features to other aspects of Stagnation Glacier, and how this study relates to the collective and current understanding of polythermal hydrology.

6.1 HYDROLOGICAL NETWORKING

As discussed previously, the presence of hydrological conduits was indicated by the interpretation from GPR data. The resolution of the GPR suggests that the minimum

size of resolvable conduits is 0.4 m. Conduits smaller than 0.4 m may be detected and are represented by a hyperbolic reflection in the GPR data. The polarity of the reflection, when compared to a known reflection, indicates whether the conduit is water- or air-filled. In total, 25 hyperbolae with positive polarity's were recorded, suggesting the presence of 25 smaller (less than 0.4 m in any plane) water-filled conduits. Where the hyperbolae were generated from features larger than 0.4 m, their size may be resolvable. Seventeen resolvable features were interpreted as water-filled conduits and ranged in size from 0.4 m up to 20 m across. Seven were interpreted as air-filled features and ranged from 0.4 to 15 m long. The vertical resolution in conduit geometry contained less variability: reflections were typically composed of one to two wavelets. For water-filled features this translates to a height of 0.49 m - 0.66 m. The vertical resolution, however, is more difficult to determine due to the complexity of receiver timing of signals travelling at various speeds due to the difference in the electrical properties of the various materials.

An experiment was carried out by Moorman (2000, personal communication) to isolate the type of reflections generated by water- and air-filled conduits in a block of ice, with GPR. Although the GPR system used was operated at a much higher frequency (1000 MHz), the physical and electrical components of the GPR remained the same. The block of ice was 1 m wide \times 1 m deep \times 3 m long, and was constructed in a cold laboratory. Two-inch diameter, empty PVC tubing was frozen into the ice cube as it was formed, simulating an air-filled englacial conduit. Once fully frozen, a GPR survey was conducted across the block. As seen in Figure 6.1, the reflection generated by the PVC tubing was negative in polarity, as compared with a survey conducted once the PVC tubing was filled

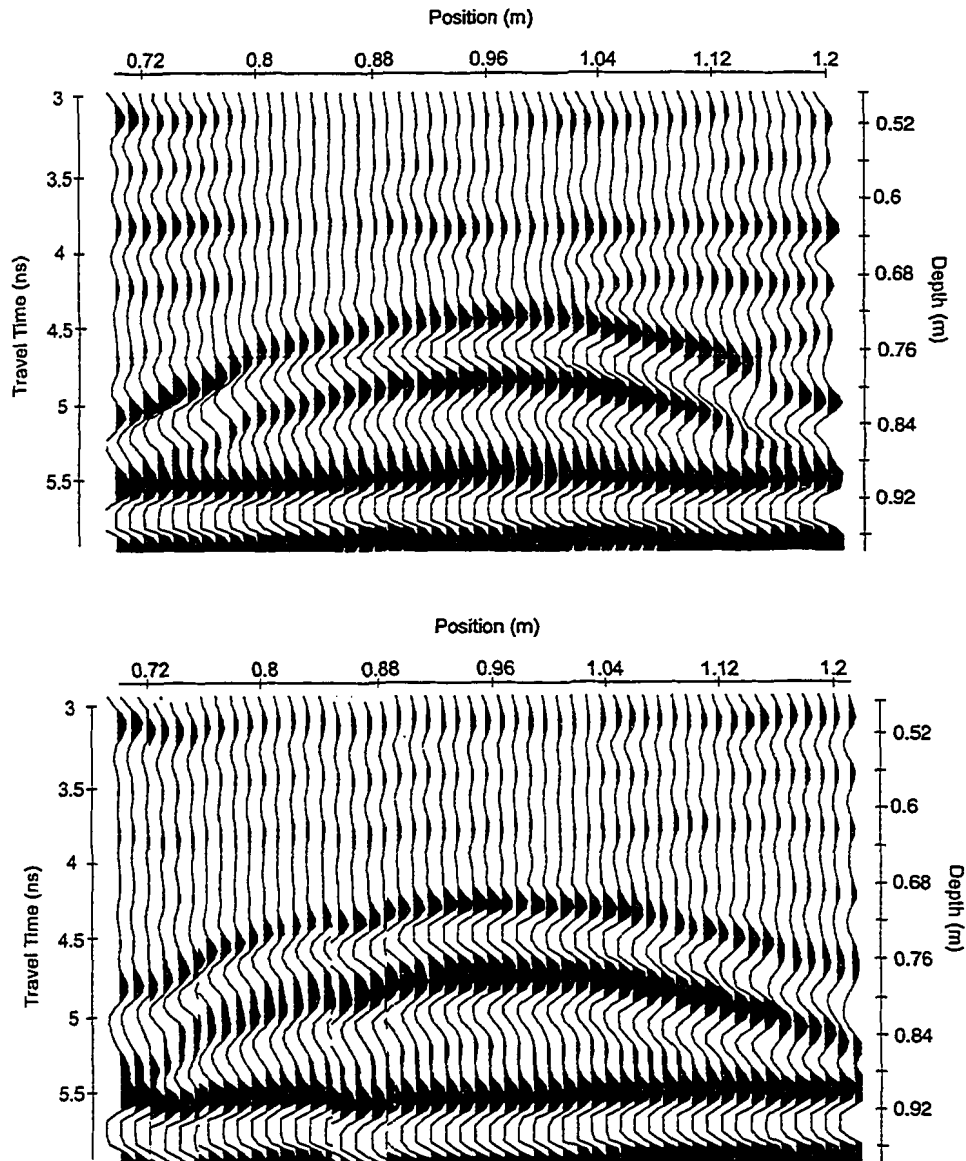


Figure 6.1 GPR profiles of the experimental ice cube. The top profile was obtained while the PVC tube was empty, similar to an air-filled conduit in a glacier. The bottom profile was obtained after the tube was filled with liquid water. At position 0.96 m, the top of the air-filled tube is seen at 4.25 ns (0.7 m depth) by a reflection with negative polarity (- + -). The top of the water-filled tube is seen at the same position, time and depth, but is represented by a reflection with positive polarity (+ - +).

with water. Moorman's experiment proved the reversal in polarity that occurs between air-filled and water-filled conduits when surveyed with GPR.

The inference of the network hydrology from interpreted GPR data was possible only where areas of dense data collection permitted interpolation beyond a reasonable doubt. This occurred once in the vicinity of 99-36 and 99-33, where a conduit system is theorized to link to a system within the moraine, and will be discussed ahead. More often than not, however, GPR lines were surveyed at such large distances from other lines that conduit connectivity could not be inferred with confidence. The slope of the portion of a conduit interpreted on 99-46 (Figure 5.14), has in fact a slope approximately 3 X the surface slope. Future studies involving larger-scale, detailed data collection will be necessary in order to more confidently pose hydrological connectivities of conduits. This could help prove or disprove Shreve's 1972 theory that the dip angles of conduits are approximately 11 X the dip angle of the surface topography. Shreve has theorized that the conduit dip angles are related to the surface topography as a function of the flow being governed by the equipotential contouring and the rate of closure by a function of 11.

The majority of interpreted englacial conduits were typically located within 20 m above the glacier base, although conduits were interpreted at all depths within the glacier (from 12 m depth - 113 m depth). At times, the conduits appeared to be located subglacially, that is, at the base of the glacier. Due to the lack of understanding about basal ice conditions (specifically the transition between englacial ice and subglacial ice), a separation between englacial and subglacial hydrology is problematic, and will be disregarded. A distinct reflection within the basal region was observed on nearly every

profile and was used to distinguish the basal zone, and will be discussed in the following sections.

Hydrological flow direction was determined, if possible, given the elevations of the conduits connecting a mappable hydrological network, assuming a general down hill trend in flow. Flow appears to follow all directions, however, both cross- and along-glacier, and even flow uphill, when pressurized, as is suggested in the vicinity of GPR profile 99-33 in the Lower Section of Stagnation Glacier. The mapping of the conduits suggests that water flows from the centre of the glacier to the edge, where it would presumably, convalesce with the surficial marginal hydrology. This theory, however, implies that water flow from 99-1/2 uphill to 99-36, and then downhill to the base of the glacier, forming a thin or broad channel beneath 99-33, and then to the glacier edge. According to Shreve (1972) the equipotential contours formed by the combination of water pressure, ice and water densities and overburden pressures govern the flow of water, and can force pressurized water to flow uphill. This theory, however, assumes a circular conduit shape, and the absence of flow at atmospheric pressure.

Another explanation is that the conduit bypasses the marginal stream, and enters a hydrological network that extends out to the moraine. This is feasible if we consider that moraine ice was at one time a part of the glacier. Relict hydrological networks that were at one time used prior to glacial recession (and subsequent moraine formation) could be maintained, and used during times of high flow given that the conduit closure rate is no greater than the pressure exerted by water in a pressurized conduit and the rate of conduit wall melting. Moorman (1998) showed the eastern moraine of Stagnation Glacier was ice-

cored, and supports the incorporation of moraine drainage into the englacial hydrology of Stagnation Glacier (Figure 6.2).

A connection between the moraine hydrology and englacial hydrology is also supported by observations made in the field of the three caves within the eastern moraine of Stagnation Glacier. A battery of simple, qualitative dye-trace tests were carried out to identify the connection between the inner and outer moraine caves. Slugs of a photosensitive, fluorescent dye called uranine, were added to a stream entering the terrestrial side of the eastern moraine. The stream leaving the moraine, and coalescing with a lateral stream, was observed for the appearance of the dye, indicating a connection between the two streams. No such observation was made, nor was any dye ever detected in the proglacial streams of Stagnation Glacier.

The lower cave extending up into the moraine also suggests the presence of moraine hydrology. The large diameter (2 - 3 m vertically, >5 m horizontally) of the cave and the large diameters of the ice boulders suggests that at one point, large quantities of water flowed through the cave (forming a conduit). In order to remain open and not close in on itself under the pressure of the overlying ice, water, particularly if it is pressurized, must have occupied the cave at some time. Unless the ice above is considerably thinner than estimated by Moorman (1998), the cave could currently be in the process of closure. Regardless, as evidenced by the open cave, we can conclude that the cave was a remnant of some hydrological network. It is unlikely this conduit has formed since the moraine ice was separated from the glacier in the formation of the ice-cored moraine.

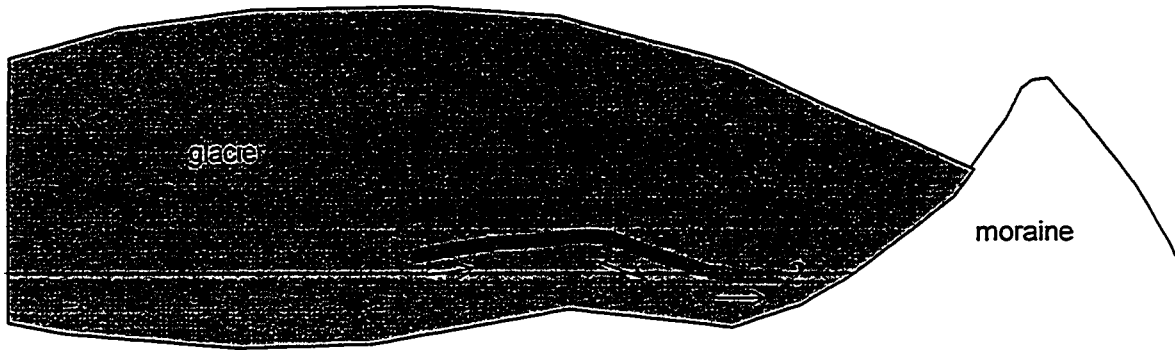
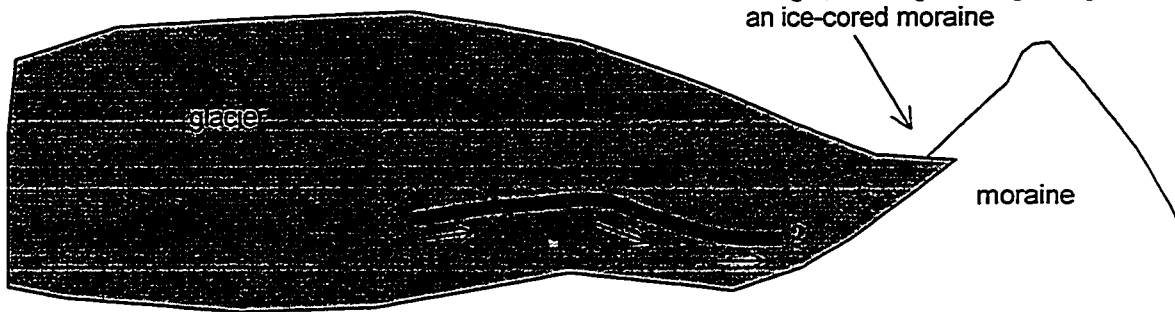
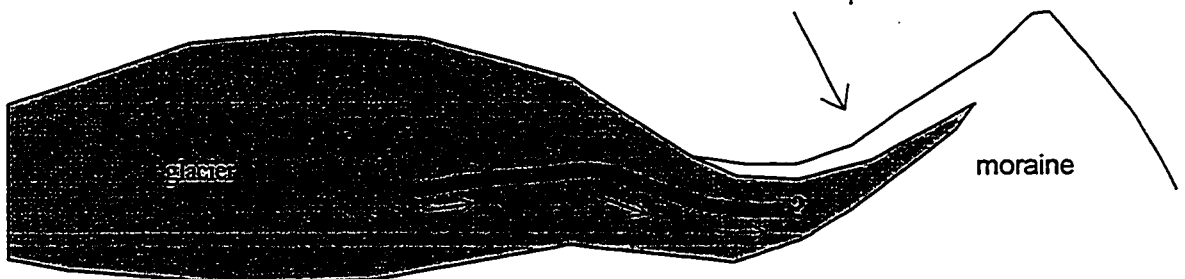
GLACIAL MAXIMUM – time series 1**GLACIAL RECESSION – time series 2****GLACIAL RECESSION – time series 3**

Figure 6.2 Schematic of glacial ice extending into the moraine, showing the process of ice-cored moraine formation.

A second test was conducted to test the connectedness of the moulin, the intermittent pond, and the surrounding hydrology. A slug of dye was added to meltwater entering the moulin, and was not seen in water entering the intermittent pond, or in the lateral or proglacial streams. From this we can conclude that at least the moulin and intermittent pond are not connected, although located proximal to each other (approximately 75 m away). In the event that the water flowing into the moulin is entering an englacial or subglacial hydrological system, the dispersivity must be so large that dye detection would not be possible. A large dispersivity index can indicate the magnitude of the connectedness of the moulin to a large hydrological network. A future quantitative dye-trace experiment could detect minute quantities of uranine, and could provide more information on the characteristics of the system.

The complex connectivity as indicated by several dye-trace experiments could be explained by a connection of the glacial and moraine hydrological networks.

The diurnal filling of the intermittent pond could be due to a release of stored water. A blockage within the local hydrological network could temporarily store water until the water pressure builds to the point where one or more blocks of crevassed ice are uplifted and release the stored water until water pressures wane and the uplifted block subsides. Although this theory is speculative, it is also supported by the indications of cracking and the shifting both heard and felt by the author and other researchers.

The interpreted conduit orientations from the GPR data suggest flow in multi-directions: cross-glacier, along-glacier and presumably, in any angle between the two directions. This may be due in part or whole to two factors: equipotential contouring, as previously discussed, or flow impedance within down-glacier (downstream) ice or at the

margins. Flow impedance can occur where ice no longer supports the conditions required for water percolation, and the subsequent formation of conduits, and eventually the development of a hydrological network.

In order for water to move through ice, the temperature of the ice must be at the pressure-melting point, as discussed in chapter two. It is imperative that we accept the relationship, although not mutually exclusive, between the presence of hydrological conduits and temperate zones of ice within a glacier. The following section discusses the thermal character of Stagnation Glacier, the evidence for temperate zones, and their significance to the glacial hydrology of Stagnation Glacier.

6.2 THERMAL CHARACTER

The presence of warm-ice zones were indicated by several types of reflections observed in the GPR data. These reflections were unlike that of the type of reflection generated from what is thought to be sediment incorporation into the marginal areas of the glacier. The reflection from a warm-ice zone is usually continuous, relatively weaker than a reflection from sediment, has a smaller amplitude, and can often lie above even weaker, discontinuous reflections (called scatter). Moore et al (1999) showed through borehole thermometry and water depths that the scattered returns as seen in their 50 MHz GPR data indicate the presence of a cold-temperate ice transition zone on Hansbreen, a polythermal Spitzbergen glacier. Water inclusions at both the micro- and macroscopic levels scatter the GPR signals, producing a distinctive type of return that indicates the presence of temperate ice. Hamran et al. (1996) used the strength of scattered radar energy to calculate the liquid water content of Uvérsbreen, a polythermal glacier in Svalbard. Their study found that the

water content increased gradually with depth below the cold-temperate transition. Their technique, although impractical due to the difference in the GPR systems used, yielded key information about the hydrothermal nature of a polythermal glacier. Macheret and Moskalevsky (1993) used a similar technique on the radio wave velocities from various Radio-Echo Sounding (RES) surveys of three Svalbard glaciers. RES equipment uses high frequency to ultra-high frequency signals with much larger centre frequencies and smaller bandwidths than GPR surveying equipment, resulting in much larger (deeper) penetration depths and coarser resolution. RES surveys have been typically used to investigate internal ice conditions in Antarctica and very large glaciers. Macheret's calculations of radio wave velocities within three Svalbard glaciers were used in theoretical mathematical models to estimate water content. Their findings showed the sensitivity of radio waves to small water content within glacier ice (0.22 % - 3.83%) and indicated that hydrothermal conditions could be inferred from the data.

Björnsson et al. (1996) also conducted a RES survey on four Svalbard glaciers and observed distinct reflections from basal layers containing water inclusions, as confirmed by borehole drilling. These strong reflections were observed in the ablation zone, but could not be followed into the accumulation zone. The ablation zone of one glacier was underlain by a temperate layer in the vicinity of a supraglacial depression where meltwater accumulates during the summer.

Ødegård et al. (1997) showed using RES that Finsterwalderbeen, a polythermal surge-type glacier in south Spitsbergen, has a basal layer at the pressure-melting point above 500 m above the terminus. Their results in the accumulation zone indicated a strong relationship between thermal conditions and snow accumulation, where temperate ice

zones are associated wet-snow zones, and cold ice zones underlain by a thinner temperate ice layer are associated with superimposed ice zones

Five possible warm-ice zones were interpreted from the radar data in this study (Figure 6.3). The total areal distribution of each zone can only be estimated due to the low density of data collected in some of the zones. The actual limits of zones are difficult to delineate from the GPR data. However, the largest warm-ice zone is approximately 250 m long, by 150 m wide and approximately 13,500 m² (0.013 km²) in area. Stronger reflections have been used to indicate the presence of a liquid water content within glacial ice, but due to the resolution of the GPR system used, temperate-cold ice boundary zones may not be detected. Water inclusions, although present at micro- to macroscopic scales, are detectable depending on the GPR frequency used. High frequency noise observed in the upper warm-ice zone could indicate the presence of sub-resolution water inclusions (Arcone et al., 1995). The theorized minimum size of backscatter was calculated to be 0.17 m. This indicates that water inclusions smaller than 0.17 m will not be detected. Therefore an underestimation of the depth of the cold-temperate boundary will result. The GPR data, however, still provided excellent indication of the presence of temperate ice within Stagnation Glacier.

Temperate ice zones appeared to be detached and distributed across the lower 2 kilometres of the glacier, however they appeared to be restricted from the lower 100 m of the ablation zone. The formation of temperate zones is theorized to be unique to local conditions: ice thickness, glacier surface and bed slope, connectivity to supraglacially-derived meltwater via moulins and crevasses, and relic thermal conditions incorporated into

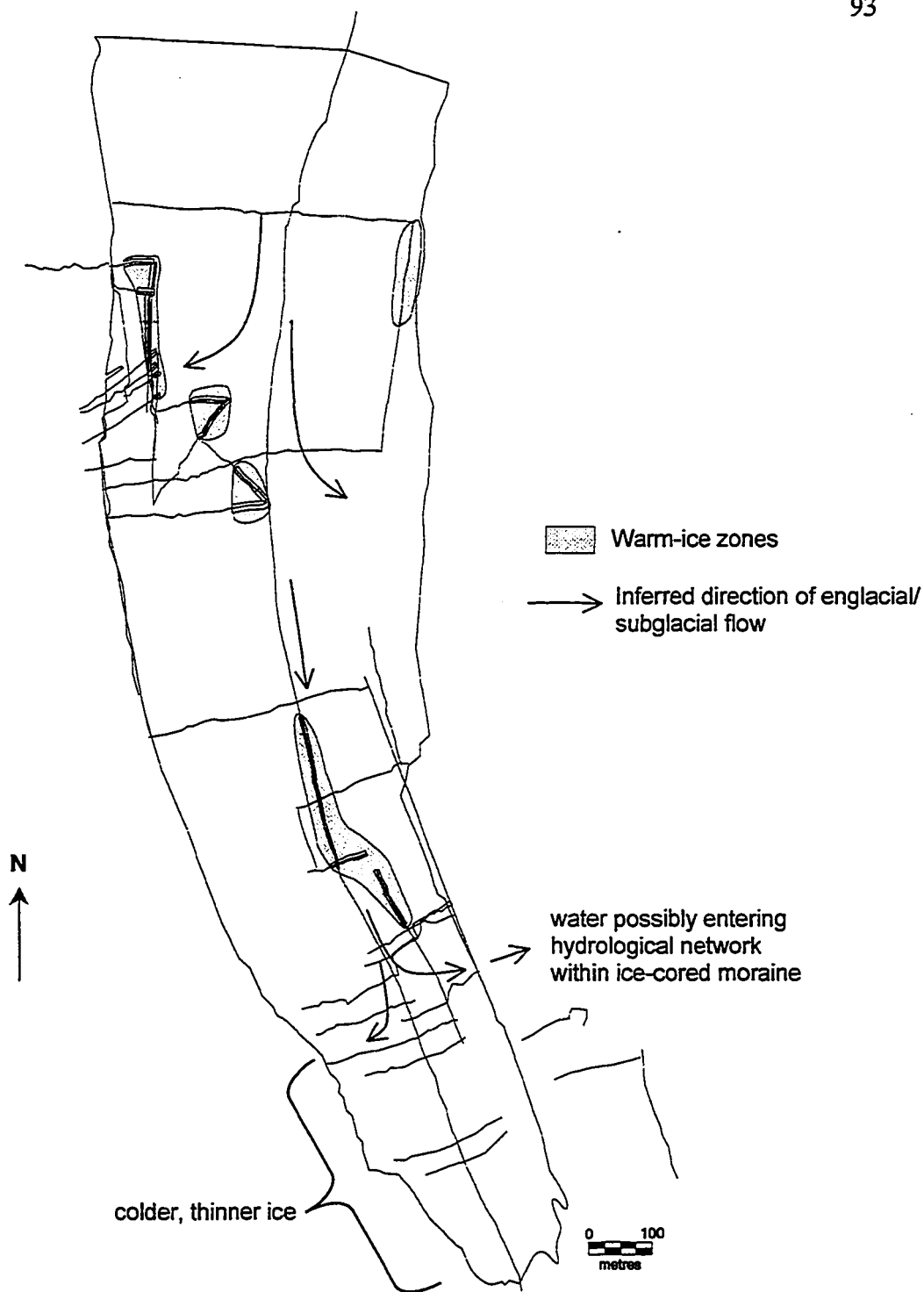


Figure 6.3 Map of generalized hydrologic and thermal structures within Stagnation Glacier. Englacial / subglacial water is forced to flow towards the margins upstream due to a downstream blockage of flow. This is due to thinner ice and colder ice temperatures.

the ice from the climate in which the glacial ice was formed. The term “sticky spots” was coined by Fischer et al. (1999) to describe the distributed areas of low water pressure that produce high basal drag at the base of Trapridge Glacier, Yukon Territory. Their findings suggest that the presence of a thin film of water serves as lubrication in areas on the ice-bed interface, which serves to promote local basal sliding. Marginal drag was modeled and estimated to be equal in magnitude to basal drag within sticky spots. This suggests that a lack of water (and hence a lack of temperate ice) at the margins produces marginal drag. Relatively lower amounts of sediment inclusion along the glacier margin also provides evidence for dryer and colder ice at the margins. This is feasible due to the reduced thickness at the margin, which normally provides the source of pressure for lowering the ice melting point and producing temperate ice.

For most of the zones, the northern and southern (upper and lower, respectively) limits were approximated, and thus the average length for warm-ice zones was approximated to be 200 m. Figure 6.4 shows the distribution of temperate zones across the lower portion of Stagnation Glacier. An intriguing feature is the proximity of the upper temperate zone to the margin of the glacier. Two smaller, rounder temperate zones were approximately 125 m in length, while the two longest, and skinniest temperate zones were both approximately 250 m in length.

The findings from other glacial studies seem to provide support for the existence of discontinuous, and distributed warm-ice zones at the base of Stagnation Glacier (Blatter, 1987; Rabus and Echelmeyer, 1997)

A mathematical model was presented by Blatter and Hutter (1991) to calculate the position of the cold-temperate transition surface (CTS). Their model suggested that the

polythermal nature of Laika Glacier, Coburg Island, Canada is a result of remnant climatic conditions, for their model predicted cold-based conditions.

Numerous studies involving sediment and structural analysis, and hydrochemistry have assumed polythermal conditions, without the capability of examining the distribution of the temperate ice (Hambrey and Huddart, 1995; Vatne et al., 1995; Jansson, 1996; Hambrey and Dowdeswell, 1997; Wadham et al., 1997). The concept of polythermal glaciology has been accepted, but not fully understood.

It is reasonable to expect that a gradational boundary would exist between cold ice and warm ice within the glacier. Where the geothermal heat flux is considered insignificant, as in the case for Stagnation Glacier, melting from the viscous dissipation of water forms the “mushy” zone of co-existing water and ice.

Where cold ice overlies warm ice, it is theorized that the heat gradient between the two zones sets up a flux such that the heat contained in the liquid water entering the two zones is released into the surrounding ice, freezing the water. This is called regelation ice, and can form below temperate zones.

Hubbard and Sharp (1989, 1993) showed that regelation ice is usually found to be less than several centimetres thick, and is formed from the re-freezing of ice on the stoss side of obstacles due to the higher water pressure, which results in a local lowering of the melting point. This water is melted and flows around the obstacle, where it encounters cold ice again, and re-freezes. This type of ice would not be seen with GPR, but could provide a small-scale explanation for local basal conditions where debris-rich ice is absent. Hubbard and Sharp (1995) describe the presence of clear ice below temperate glaciers. This ice is formed by internal melting and refreezing, and hence, recrystallization with

increased rates of strain, say for instance, at the bed. A distinct possibility exists that this type of ice can exist below polythermal glaciers, being restricted to forming below temperate regions, and re-freezing below up-glacier from bedrock obstacles, in a thinner, colder region of the glacier. This is seen on Stagnation Glacier on the Lower Section, in the regions of GPR lines 37, 38 and 40.

The extension of a zero-degree isotherm from the glacier ice into the till can be seen in Figure 5.13. The entrainment of till into the basal ice, both in the form of shear planes and basal debris layers, is possible near transition zones between warm ice and cold ice, due to regelation. Although largely absent, areas of basal sedimentation were observed, both in the field, and interpreted from the GPR data. The observation of basal sedimentation, therefore can be used to provide information about the thermal characteristics of a glacier.

6.3 SUBGLACIAL SEDIMENTATION

The basal sediment conditions of Stagnation Glacier can be inferred from both observations in the field, and interpretation from GPR data.

The weight of the ice can cause the squeezing of subglacial sediment or till into basal crevasses. A discussion of basal crevassing is discussed by Sharp (1985), and noted by Clarke et al. (1984). Sharp argued that sediment from unfrozen, deformable till is squeezed upward into the cavities of basal crevasses when the glacier stagnated. Basal crevasses are formed from the extension of ice during glacier flow at the base of the glacier. Typically crevasses are formed at the surface, but can form at the base where topographical constraints on glacier thickness compromise the tensile strength of basal ice

during flow. The small (up to several traces wide) reflections observed in the GPR data across the base of Stagnation glacier are theorized to be from basal crevasse-fill ridges. Although not mapped for their connectivity across the base of the glacier, they can indicate the presence of subglacial water content and the subsequent sediment deformation.

Often the extension of basal-crevasse fill ridges can be observed from the glacier terminus out onto the foreland. Flutings, if observed on the foreland, can indicate the presence of subglacial sediment deformation. Although not explicitly observed and researched in this study, future examination of sediment deformation patterns within the proglacial area could provide more information on the subglacial hydrological conditions.

Sediment drapes at the margins of Stagnation Glacier were observed, and suggest the ploughing of subglacial sediment off bedrock or till during flow conditions, and the subsequent deposition along subglacial valley walls upon stagnation. These sediment drapes (up to 10 m in thickness) suggest that the sediment beneath Stagnation Glacier is unconsolidated and deformable. This is also supported by the observation of infill sediments from the GPR data. Topographic lows in the bedrock/till surface become filled with infill sediments as the glacier flows over the bedrock.

Thrust planes observed both at the surface and interpreted within the glacier also provide evidence for unconsolidated, unfrozen subglacial sediments.

The basal ice, both in field observation and GPR interpretation, was found to contain in local areas, very little to relatively large amounts of sediment. Glacier ice debris content varied on a local scale, and hence the subglacial forces resulting in debris content, occur on a local scale. Clarke et al. (1984) suggest that the thermal flux gradients observed with the Trapridge Glacier, a surge-type glacier in the Canadian Yukon, are formed from

the water percolation through permeable subglacial material. The permeability, and hence distribution of temperate basal ice, depended on the geological characteristics of the bedrock material. This linkage between thermal conditions and local bedrock geology show how varying thermal conditions can be.

CHAPTER SEVEN

CONCLUSIONS

7.1 SUMMARY

The objective of this thesis was to examine the internal structural and hydrologic characteristics of a sub-polar glacier in the Canadian Arctic. Ground-penetrating radar was used as the principal means of subsurface data collection.

GPR data was collected, processed, and corrected in order to gain information about the hydrological, thermal and subglacial sedimentation characteristics of Stagnation Glacier. The data and subsequent interpretation indicated the following:

- hydrological conduits and cavities may be detected by GPR. Water-filled and air-filled conduits and cavities were present. The majority (approximately 54) of detected features were less than 0.4 m, whereas only a few features ranging in size

from 0.4 m to 20 m across were detected. The latter features were interpreted as large-diameter conduits and portions of conduit reaches. Most features were detected within 20 m above the base of the glacier.

- The conduits appeared to exist in all orientations, however the overall flow of englacial and subglacial water was out towards the margins.
- Water flow is believed to be obstructed within the ablation zone due to colder conditions, and is forced out to the sides where it may be entering relict hydrological networks within the ice-cored moraines, and/or coalescing with the lateral streams.
- Distributed, discontinuous zones of temperate ice were interpreted to be present across the lower 2 kilometres of the glacier. The frequency of the temperate zones increased with distance up the glacier and were detected within 20 m of the glacier base. Ice thickness appears to be the governing factor in temperate ice formation.
- Basal ice conditions ranged from debris-rich to ice-rich, suggesting the pressures responsible for the entrainment of debris are not constant throughout the surveyed portion of the glacier. Examples of sedimentation included shear zones, depression infills and sediment drapes. These features support the theory that Stagnation Glacier contains some degree of englacial and subglacial hydrology, which may be due in part, to zones of warm ice.

- The presence of several supraglacial and periglacial hydrological features also support the hypothesis that there may exist a complex hydrological and thermal structure within Stagnation Glacier.

7.2 RECOMMENDATIONS FOR FUTURE WORK

The glacial hydrology of Stagnation Glacier is indeed complex. The thermal dynamics of polythermal glaciers are largely unknown. Regarding the primary technique used in this thesis, GPR applications to glaciological studies are still in an preliminary stage. The following are suggested topics for future investigation:

1. A detailed GPR survey should be conducted on smaller key areas where this work highlighted the presence in complex glacial hydrology. One such area would be on the southeast portion of the surveyed area, where the hydrological network appeared to flow upwards and outwards towards the margin, and possibly entering networks within the ice-cored moraine. Another area to investigate is the warm-ice zones in the northwest region of Stagnation Glacier (near the moulin).
2. A detailed GPR survey operated at a higher frequency could also be conducted to further investigate the morphology of any of the temperate zones thought to be present within Stagnation Glacier.

3. Quantitative dye-trace analyses could be conducted where supraglacial water enters the glacier to understand the nature of the hydrological system, and similarly for the possible network(s) within the ice-cored moraines.

BIBLIOGRAPHY

- Annan, A.P., 1992. Ground-Penetrating Radar Workshop Notes. Sensors & Software Inc., Mississauga, ON.
- Arcone, S.A., 1996. High resolution of glacial ice stratigraphy: A ground-penetrating radar survey of Pegasus Runway, McMurdo Station, Antarctica. *Geophysics*, vol. 61 (6), pg. 1653 – 1663.
- Arcone, S.A., Lawson, D.E. and Delaney, A.J., 1995. Short-pulse radar wavelet recovery and resolution of dielectric constants in englacial and basal ice at Matanuska Glacier, Alaska. *Journal of Glaciology* vol. 41, pg. 68 – 86.
- Benn, D.I. and Evans, D.J.A., 1998. *Glaciers and Glaciation*. Arnold, London. 734 pg.
- Björnsson, H., Gjessing, Y., Hamran, S.-E., Hagen, J.O., Liestol, O., Pálsson, F. and Erlingsson, B., 1996. The thermal regime of sub-polar glacier mapped by multi-frequency radio-echo sounding. *Journal of Glaciology* vol. 42, pg. 23 – 32.
- Blatter, H. 1987. On the thermal regime of an Arctic valley glacier: a study of White Glacier, Axel Heiberg Island, N.W.T., Canada. *Journal of Glaciology* vol. 33, pg. 200– 211.
- Blatter, H. and Hutter, K., 1991. Polythermal conditions in Arctic glaciers. *Journal of Glaciology* vol. 37, pg. 261 – 269.
- Clarke, T.S. and Bentley, C.R., 1994. High-resolution radar on Ice Stream B2, Antarctica: measurements of electromagnetic wave speed in firn and strain history from buried crevasses. *Annals of Glaciology* vol. 20, pg. 153 – 159.
- Clarke, G.K.C., 1996. Lumped-element model for subglacial transport of solute and suspended sediment. *Annals of Glaciology* vol. 22, pg. 152 – 159.
- Clarke, G.K.C., Collins, S.G. and Thompson, D.E., 1984. Flow, thermal structure, and subglacial conditions of a surge-type glacier. *Canadian Journal of Earth Sciences* vol. 21, pg. 232 – 240.
- Dolgoff, A. 1998. *Physical Geology*. Houghton Mifflin of Boston, 638 pg.
- Dowdeswell, J.A., Drewry, D.J., Liestøl, O. and Orheim, O. 1984. Radio-echo sounding of Spitsbergen glaciers: problems in the interpretation of layer and bottom returns. *Journal of Glaciology* vol. 30, pg. 16 – 21.

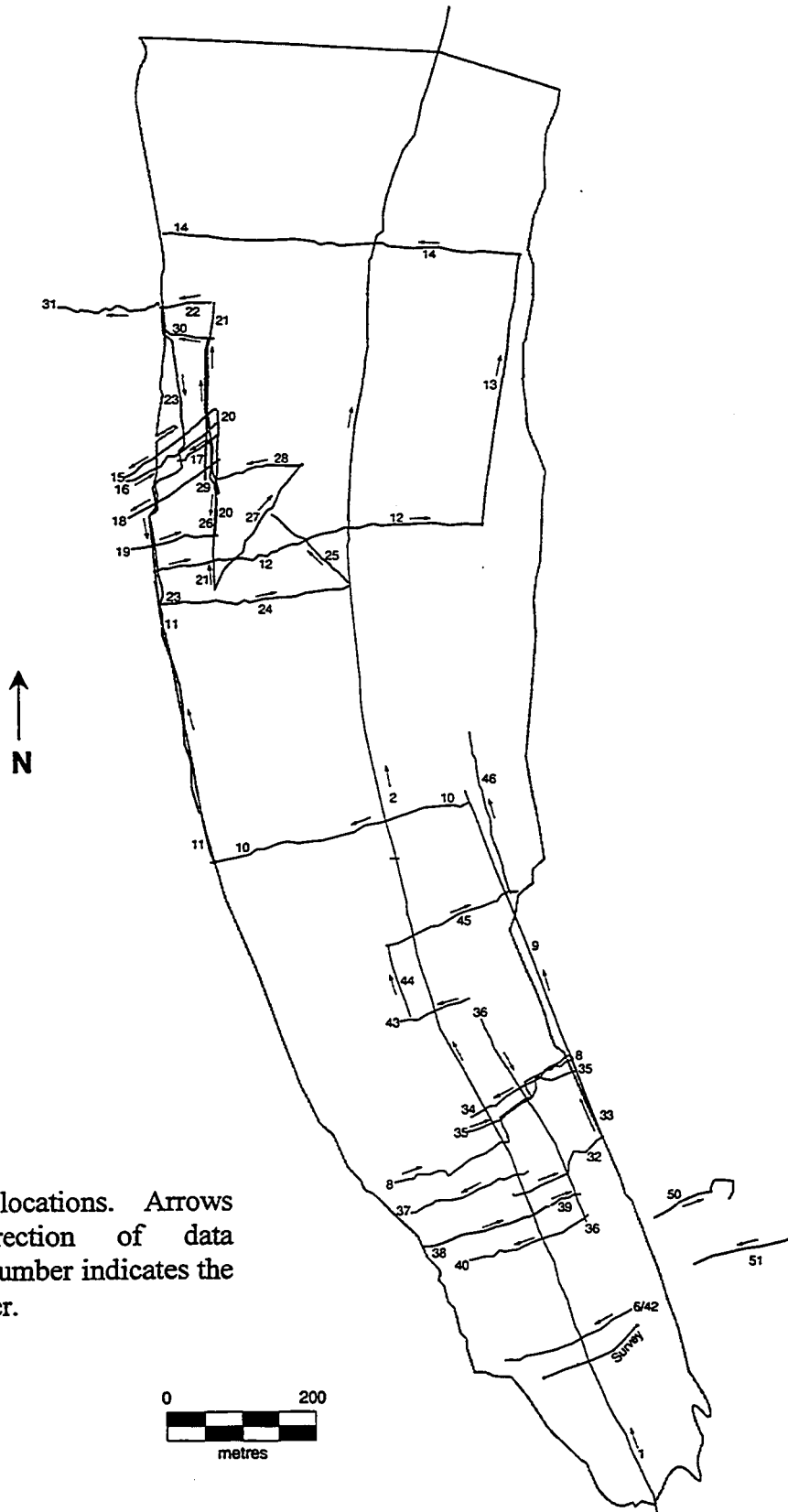
- Fischer, U.H., Clarke, G.K.C., and Blatter, H., 1999. Evidence for temporally varying “sticky spots” at the base of Trapridge Glacier, Yukon Territory, Canada. *Journal of Glaciology* vol. 45, pg. 352 – 360.
- Fowler, A.C. 1984. On the transport of moisture in polythermal glaciers. *Geophysical and Astrophysical Fluid Dynamics*, vol. 28, pg. 99 – 140.
- Hagen, J.O. and Sætrang, A., 1991. Radio-echo soundings of sub-polar glaciers with low-frequency radar. *Polar Research* vol. 9, pg. 99 – 107.
- Hambrey, M.J. and Dowdeswell, J.A., 1997. Structural evolution of a surge-type polythermal glacier: Hessbreen, Svalbard. *Annals of Glaciology* vol. 24, pg. 375 – 381.
- Hambrey, M.J. and Huddart, D., 1995. Englacial and proglacial glaciotectonic processes at the snout of a thermally complex glacier in Svalbard. *Journal of Quaternary Science* vol. 10, pg. 313 – 326.
- Hamran, S.-E., Aarholt, E., Hagen, J.O., and Mo, P., 1996. Estimation of relative water content in a sub-polar glacier using surface-penetration radar. *Journal of Glaciology* vol. 42, pg. 533 – 537.
- Harper, J.T. and Humphrey, N.F., 1995. Borehole video analysis of a temperate glacier’s englacial and subglacial structure: implications for glacier flow models. *Geology* vol. 23 (10), pg. 901 – 904.
- Holmlund, P., 1988. Internal geometry and evolution of moulines, Storglaciären, Sweden. *Journal of Glaciology* vol. 34, pg. 242 – 248.
- Hooke, R. Le B., 1984. On the role of mechanical energy in maintaining subglacial water conduits at atmospheric pressure. *Journal of Glaciology* vol. 30, pg. 180 – 187.
- Hooke, R. Le B., 1989. Englacial and subglacial hydrology: a qualitative review. *Arctic and Alpine Research* vol. 21 (3), pg. 221 – 233.
- Inland Waters Branch, Canada, 1969. *Glacier Atlas of Canada*. Surveys and Mapping Branch, Dept. of Energy, Mines and Resources, Canada.
- Jacobel, R. and Raymond, C., 1984. Radio echo-sounding studies of englacial water movement in Variegated Glacier, Alaska. *Journal of Glaciology* vol. 30, pg. 22 – 29.
- Jansson, P., 1996. Dynamics and hydrology of a small polythermal valley glacier. *Geografiska Annaler*, vol. 78A, (2-3), pg. 171 – 180.

- Kohler, J., Moore, J., Kennett, M., Engeset, R., and Elvehøy, H., 1997. Using ground-penetrating radar to image previous years' summer surfaces for mass-balance measurements. *Annals of Glaciology* vol. 24, pg. 355 – 360.
- Kamb, W.B., 1987. Glacier surge mechanism based on lined cavity configuration of the basal conduit system. *Journal of Geophysical Research* vol. 92, pg. 9083 – 9100.
- Kennett, M.I., 1989. A possible radio-echo method of locating englacial and subglacial waterways. *Annals of Glaciology* vol. 13, pg. 135 – 139.
- Macheret, Y.Y., and Moskalevsky, M.Y., 1993. Velocity of radio waves in glaciers as an indicator of their hydrothermal state, structure and regime. *Journal of Glaciology* vol. 39, (132), pg. 373 – 384.
- Moore, J.C., Pälli, A., Ludwig, F., Blatter, H., Jania, J., Gadek, B., Glowacki, P., Mochnecki, D., and Isaksson, E., 1999. High-resolution hydrothermal structure of Hansbreen, Spitsbergen, mapped by ground-penetrating radar. *Journal of Glaciology* vol. 45 (151), pg. 184 – 189.
- Moorman, B.J., 1998. The Development and Preservation of Tabular Massive Ground Ice in Permafrost Regions. Ph. D. Thesis, Carleton University, Ottawa.
- Moorman, B.J., and Michel, F.A., 2000. Glacial hydrological system characterization using ground-penetrating radar. *Hydrological Processes* vol. 14, pg. 2645 – 2667.
- Murray, T., Gooch, D.L., and Stuart, G.W., 1997. Structures within the surge front at Bakaninbreen, Svalbard, using ground-penetrating radar. *Annals of Glaciology* vol. 24, pg. 122 – 129.
- Nienow, P.W., Sharp, M.J., and Willis, I.C., 1996. Sampling-rate effects on the properties of dye breakthrough curves from glaciers. *Journal of Glaciology* vol. 42, pg. 184 – 189.
- Nobes, D.C., Leary, S.F., Hochstein, M.P., and Henry, S.A., 1994. Ground-penetrating radar profiles of rubble-covered temperate glaciers: Results from the Tasman and Mueller glaciers of the southern Alps of New Zealand. Society of Exploration Geophysicists, 64th Annual International Meeting, expanded abstracts with biographies, Tulsa, OK, pg. 826-829.
- Nye, J.F. 1953. The flow law of ice from measurements in glacier tunnels, laboratory experiments, and the Jungfraufirn borehole experiment. *Proceedings of the Royal Society of London, Series A*, vol. 219, (1139), pg. 477 – 489.
- Nye, J.F. and Frank, F.C., 1973. Hydrology of the intergranular veins in a temperate glacier. Symposium at Cambridge 1969. *International Association of Scientific Hydrology Publication* vol. 95, pg. 157 – 161.

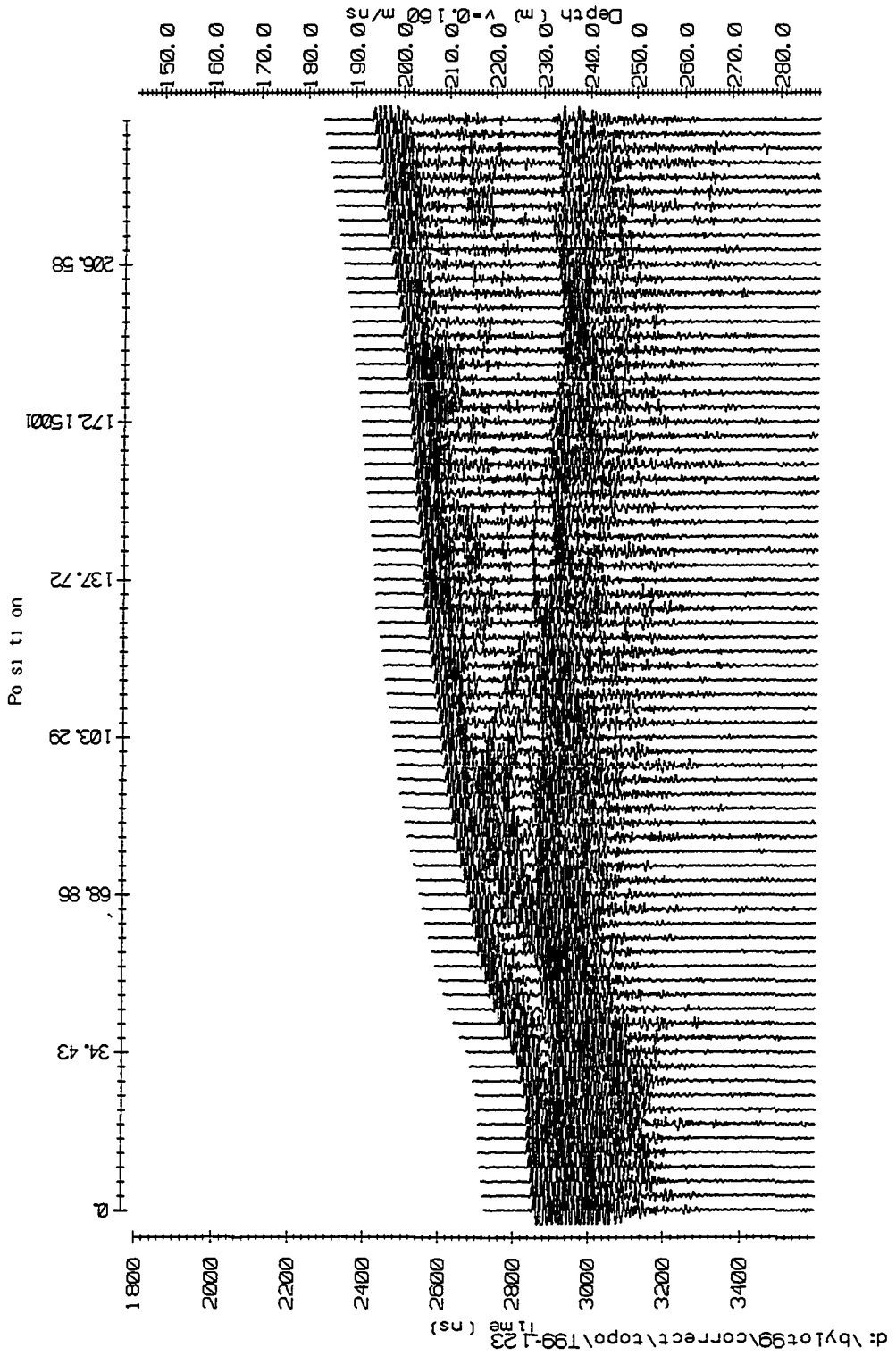
- Ødegård, R.S., Hagen, J.O., and Hamran, S.-E., 1997. Comparison of radio-echo sounding (30-1000 MHz) and high-resolution borehole-temperature measurements at Finsterwalderbreen, southern Spitsbergen, Svalbard. *Annals of Glaciology* vol. 24, pg. 262 – 267.
- Oswald, G.K.A and Robin, G. de Q., 1973. Lakes beneath the Antarctic Ice Sheet. *Nature* vol. 245, pg. 251 – 254.
- Patterson, W.S.B., 1994. *The Physics of Glaciers*. Pergamon, New York, 480 pg.
- Pohjola, V.A., 1994. TV-video observations of englacial voids in Storglaciären, Sweden. *Journal of Glaciology* vol. 40 (135), pg. 231 – 240.
- Rabus, B.T. and Echelmeyer, K.A., 1997. The flow of a polythermal glacier: McCall Glacier, Alaska, U.S.A. *Journal of Glaciology* vol. 43, no. 145, pg. 522 – 536.
- Raymond, C.F. and Harrison, W.D., 1975. Some observations on the behavior of the liquid and gas phases in temperate glacier ice. *Journal of Glaciology* vol. 14, pg. 213 – 233.
- Ridley, J.K., Cudlip, W. and Laxon, S.W., 1993. Identification of subglacial lakes using ERS-1 radar altimeter. *Journal of Glaciology* vol. 39, pg. 625 – 634.
- Röthlisberger, H., 1972. Water pressure in intra- and subglacial channels. *Journal of Glaciology* vol. 11, pg. 177 – 203.
- Röthlisberger, H. and Lang, H. 1987. Glacial Hydrology. In: *Glacio-fluvial Sediment Transfer: An Alpine Perspective*, eds. A.M. Gurnell and M.J. Clark, Wiley, Chichester, pg. 207 – 284.
- Seaberg, S.Z., Seaberg, J.Z., Hooke, R. Le B., and Wiberg, D.W., 1988. Character of the englacial and subglacial drainage system in the lower part of the ablation area of Storglaciären, Sweden, as revealed by dye-trace studies. *Journal of Glaciology* vol. 34, pg. 217 – 227.
- Shoemaker, E.M., 1990. The ice topography over subglacial lakes. *Cold Regions Science and Technology* vol. 18 (3), pg. 323 – 329.
- Shoemaker, E.M., 1991. On the formation of large subglacial lakes. *Canadian Journal of Earth Sciences*, vol. 28 (12), pg. 1975 – 1981.
- Shreve, R.L., 1972. Movement of water in glaciers. *Journal of Glaciology* vol. 11, pg. 205 – 214.

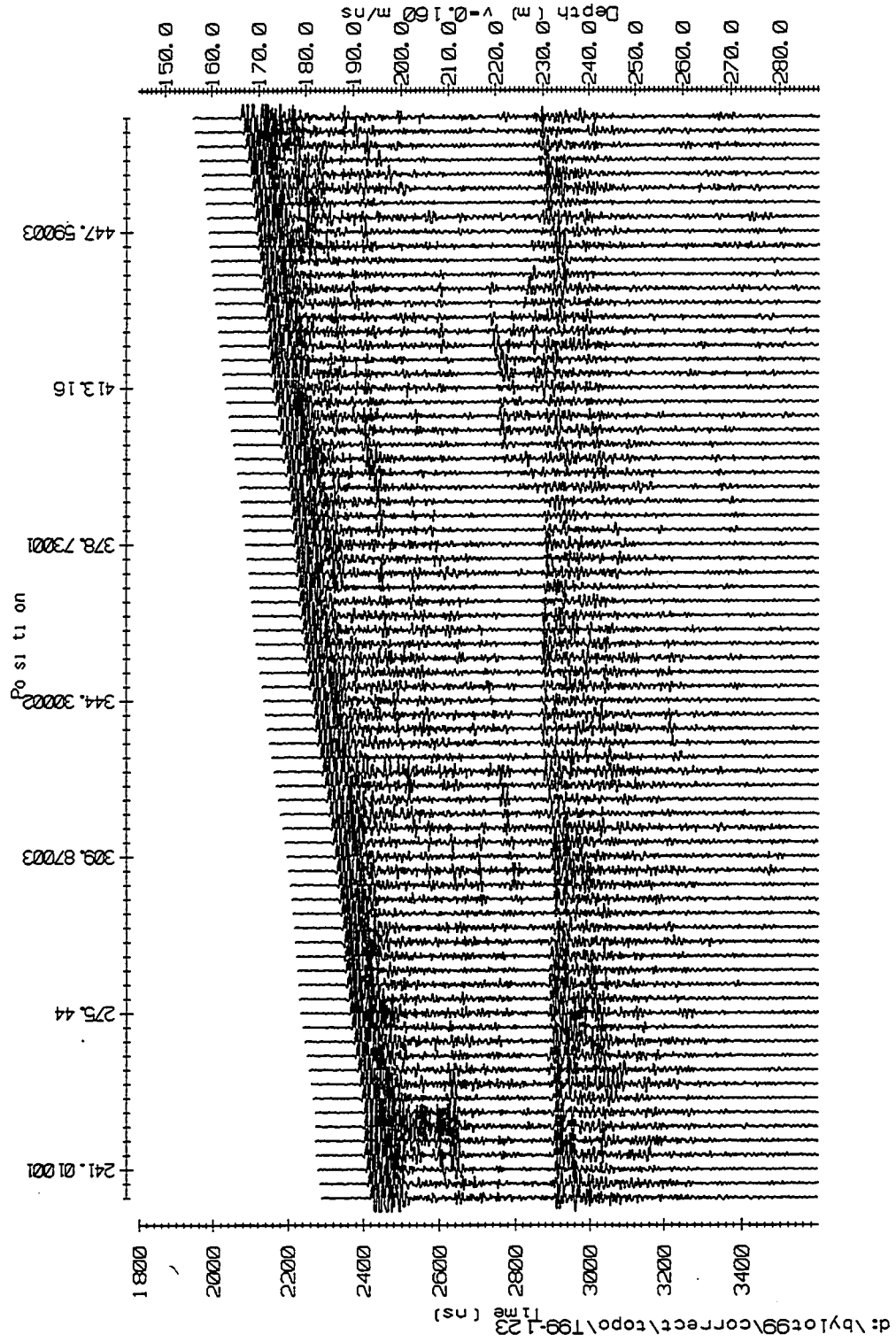
- Vatne, G., Etzelmüller, Sollid, J.L., 1995. Hydrology of a polythermal glacier, Erikbreen, Northern Spitsbergen. *Nordic Hydrology* vol. 26, pg. 169-190.
- Wadham, J.L., Hodson, A.J., Tranter, M. and Dowdeswell, J.A., 1997. The rate of chemical weathering beneath a quiescent, surge-type, polythermal-based glacier, southern Spitsbergen, Svalbard. *Annals of Glaciology* vol. 24, pg. 27 – 31.
- Walder, J.S. and Fowler, A. 1994. Channelized subglacial drainage over a deformable bed. *Journal of Glaciology*, vol. 40, pg. 3 - 15.
- Walford, M.E.R. and Kennett, M.I., 1989. A synthetic-aperture radio-echo experiment at Storglaciären, Sweden. *Journal of Glaciology* vol. 35, pg. 43 – 47.
- Walford, M.E.R., Kennett, M.I, and Holmlund, P., 1986. Interpretation of radio echoes from Storglaciären, Northern Sweden. *Journal of Glaciology* vol. 32, pg. 39 – 49.
- Weertman, J., 1964. The theory of glacier sliding. *Journal of Glaciology* vol. 5, pg. 287 – 303.
- Zotikov, I.A., 1986. *The Thermophysics of Glaciers*. D. Reidel Publishing Company, Boston, 275 pg.

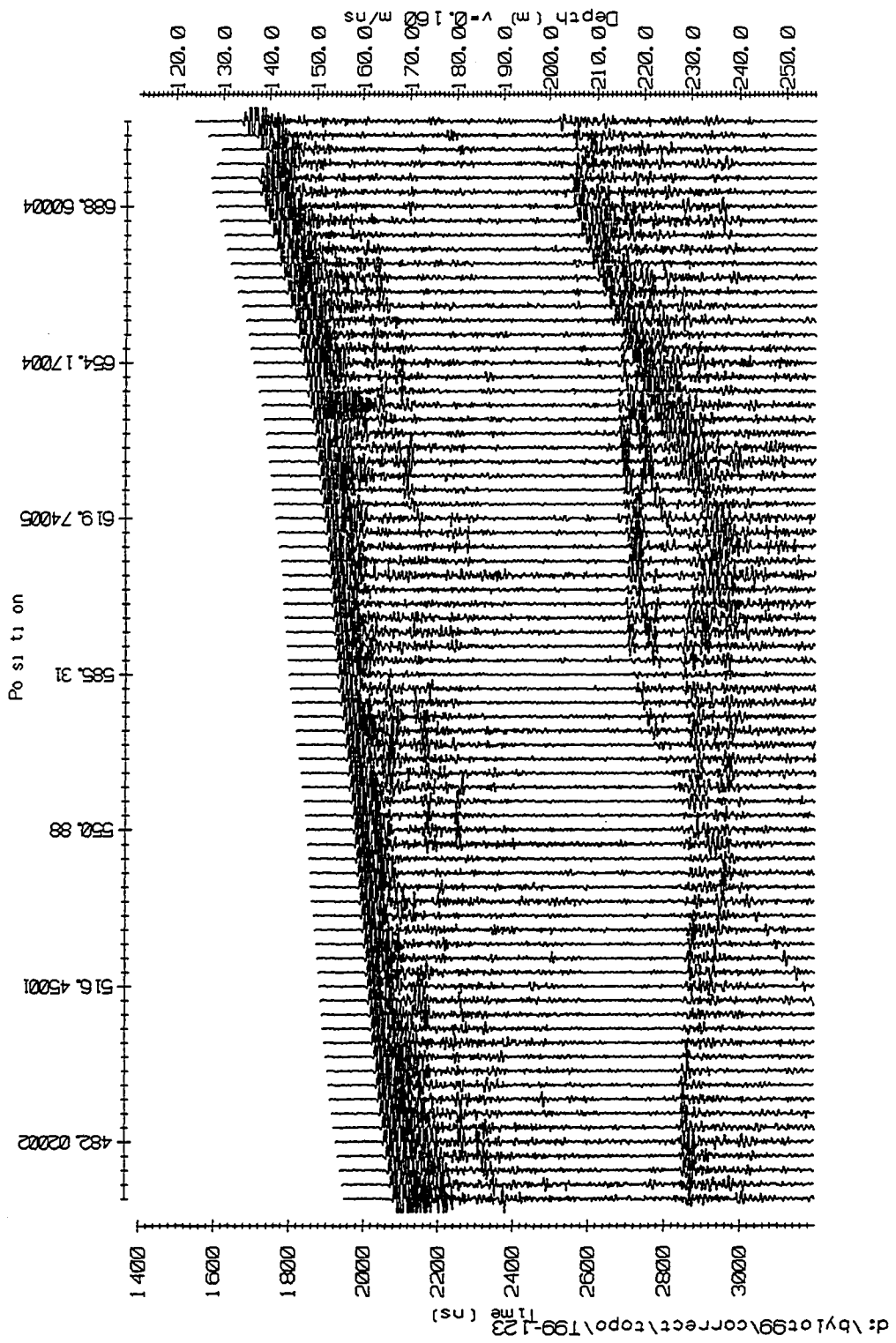
APPENDIX
GPR PROFILES

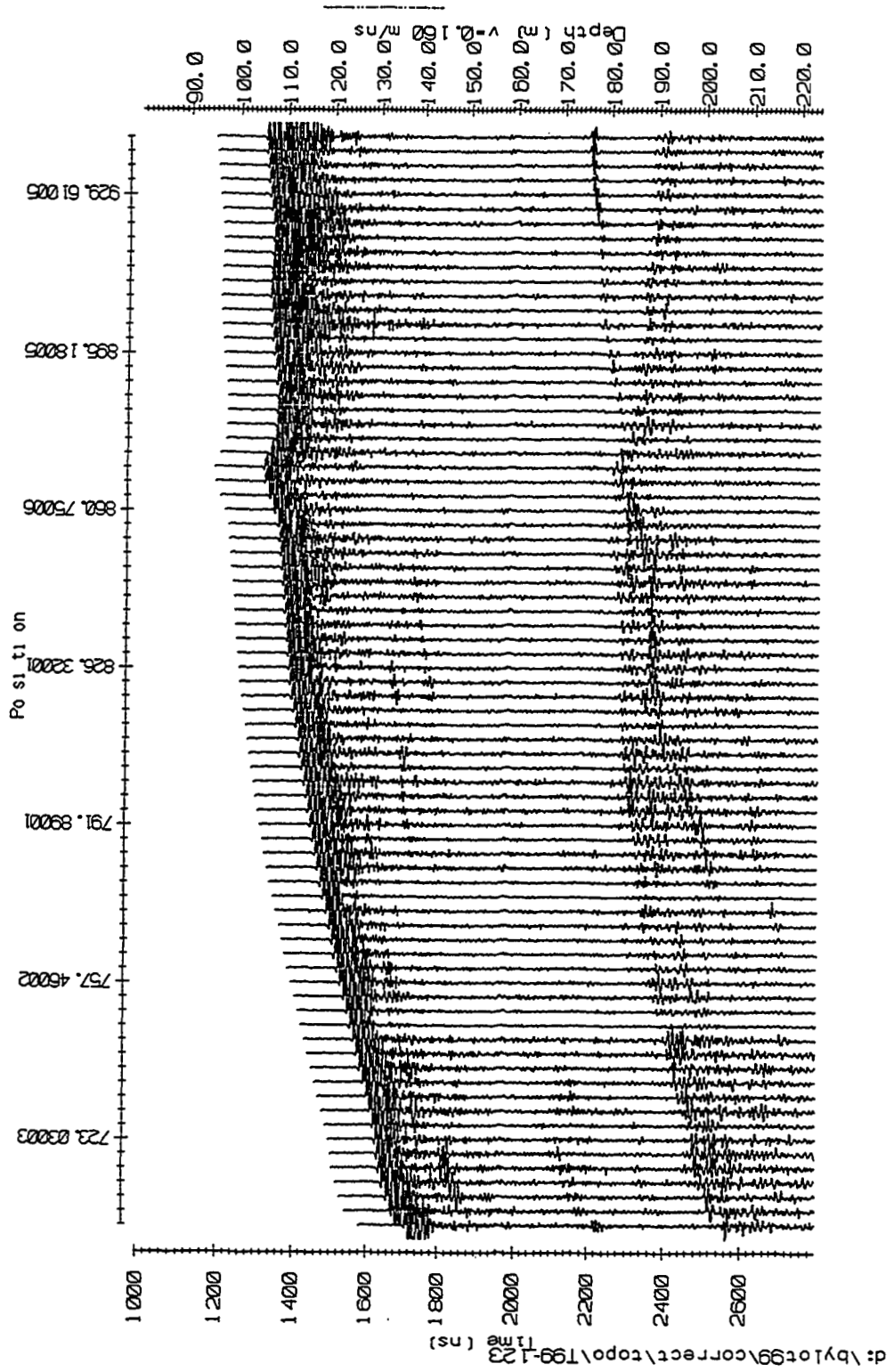


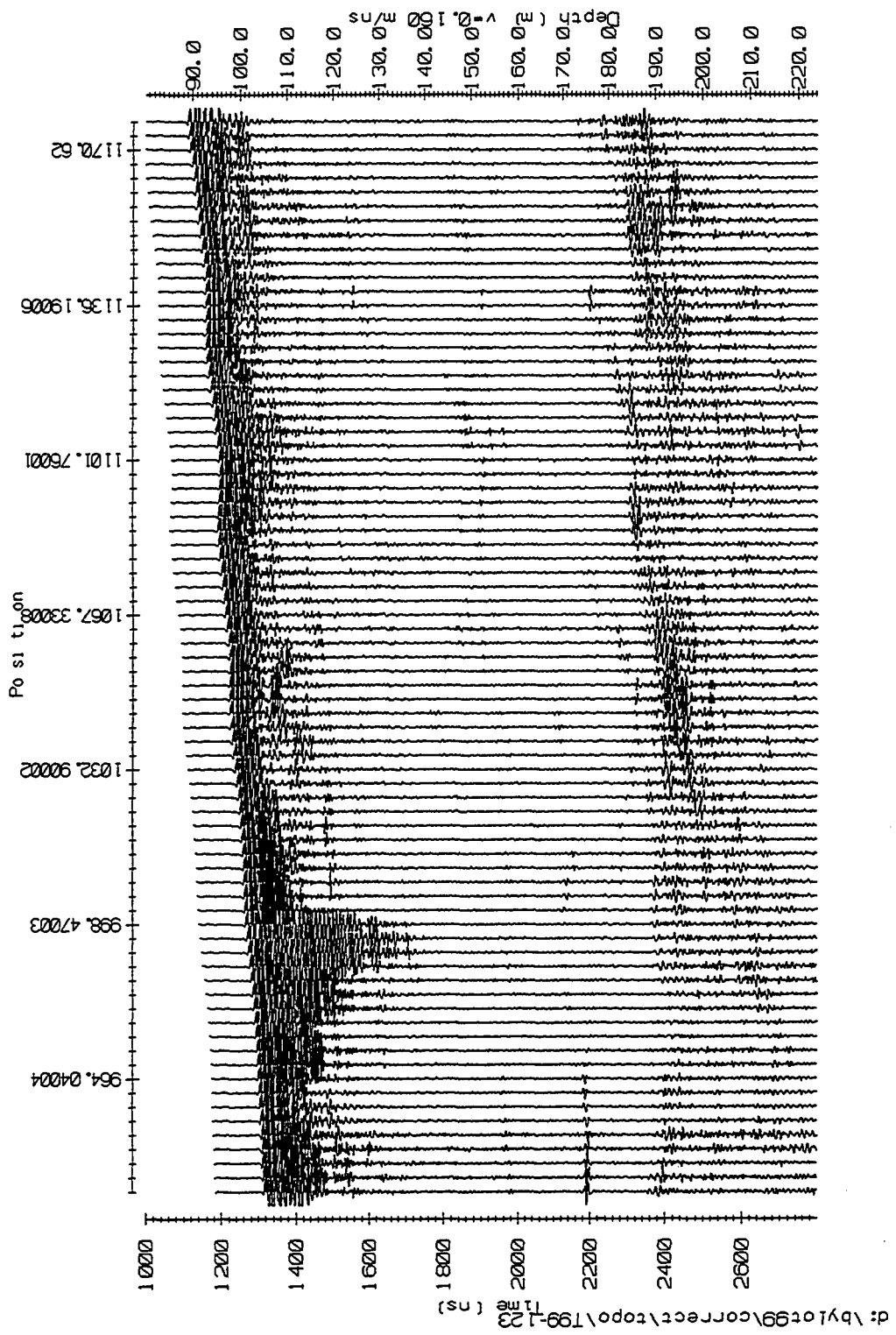
GPR profile locations. Arrows indicate direction of data collection. Number indicates the profile number.

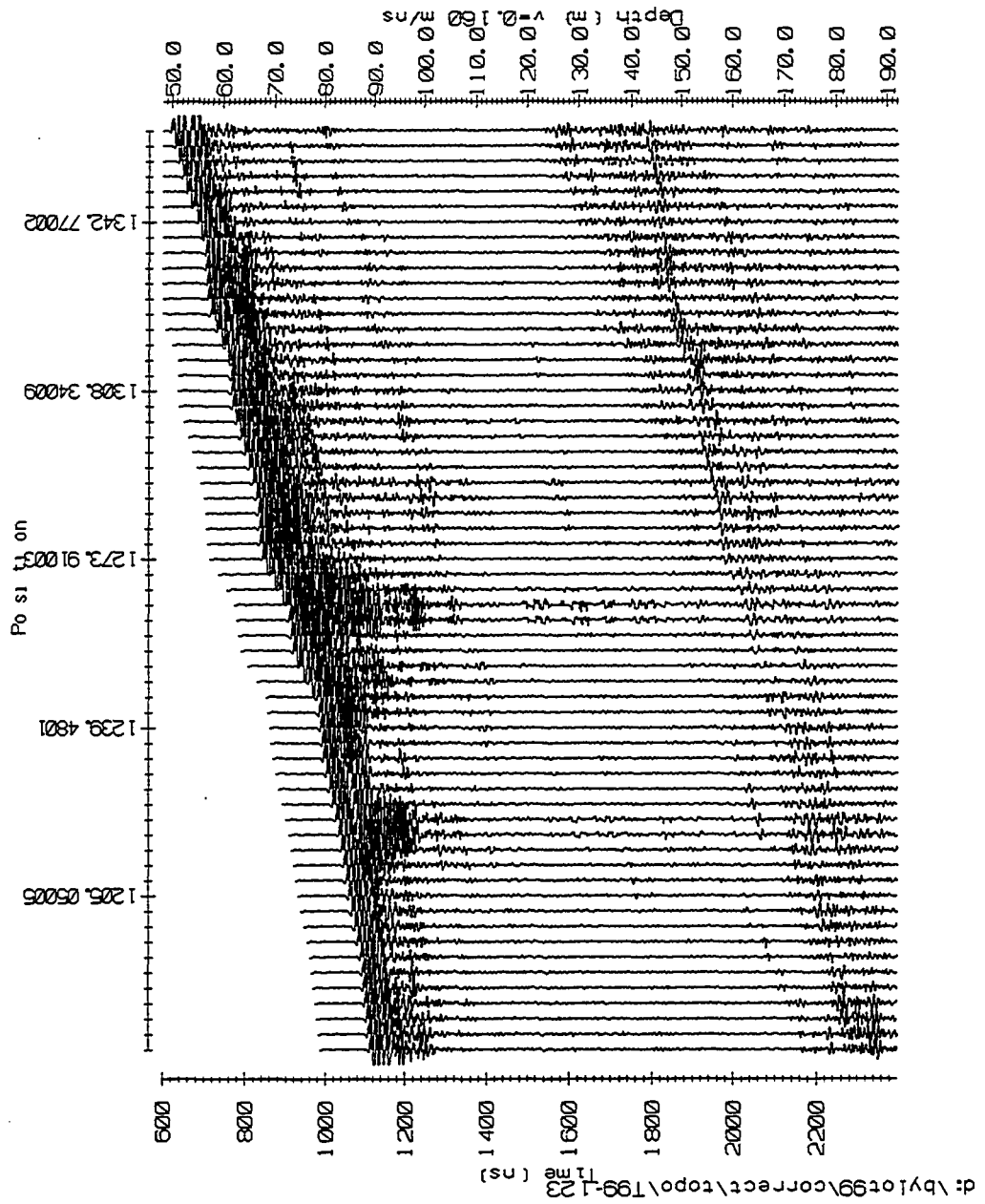




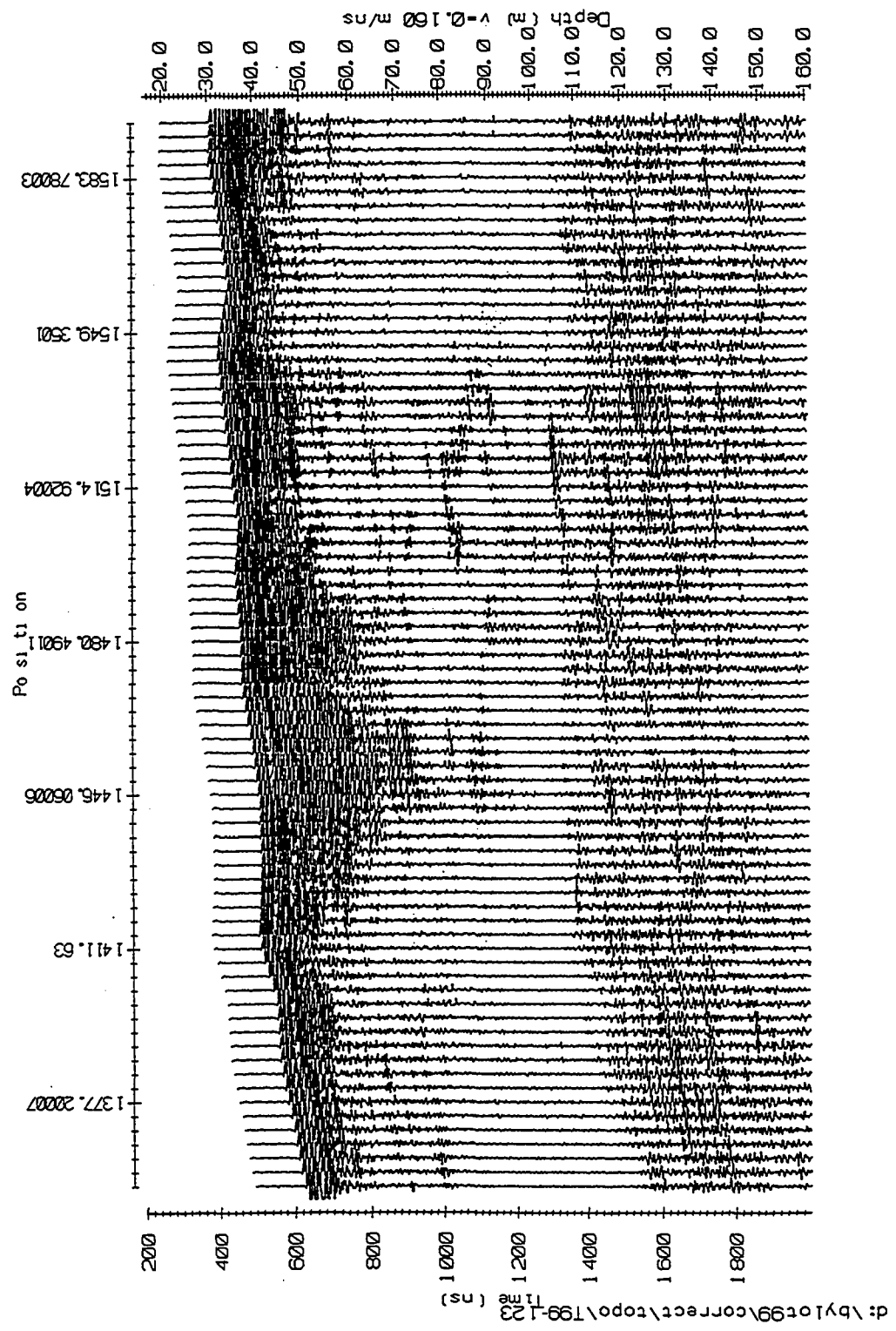


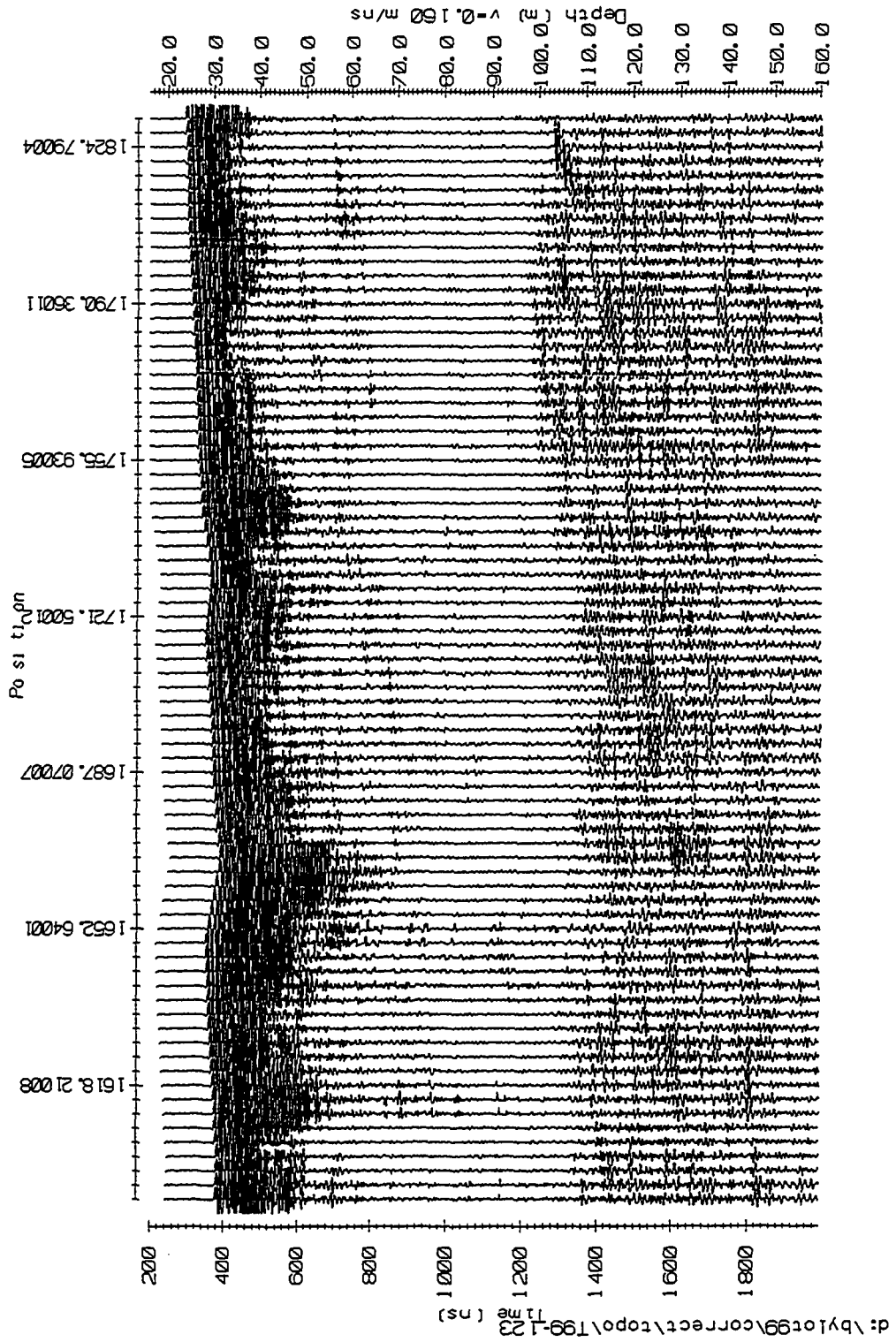






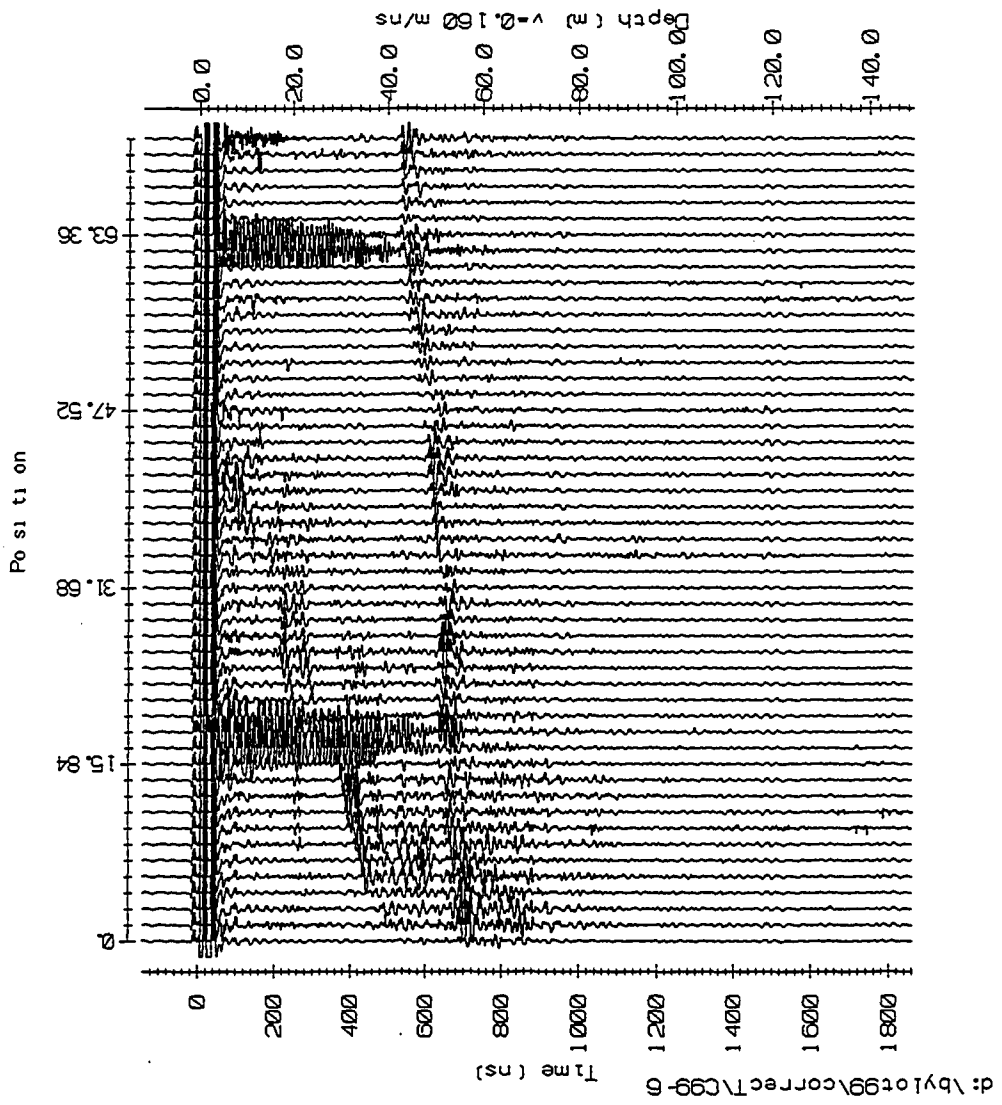
d:\bylot99\correct\topo\T99-123
Time (ns)

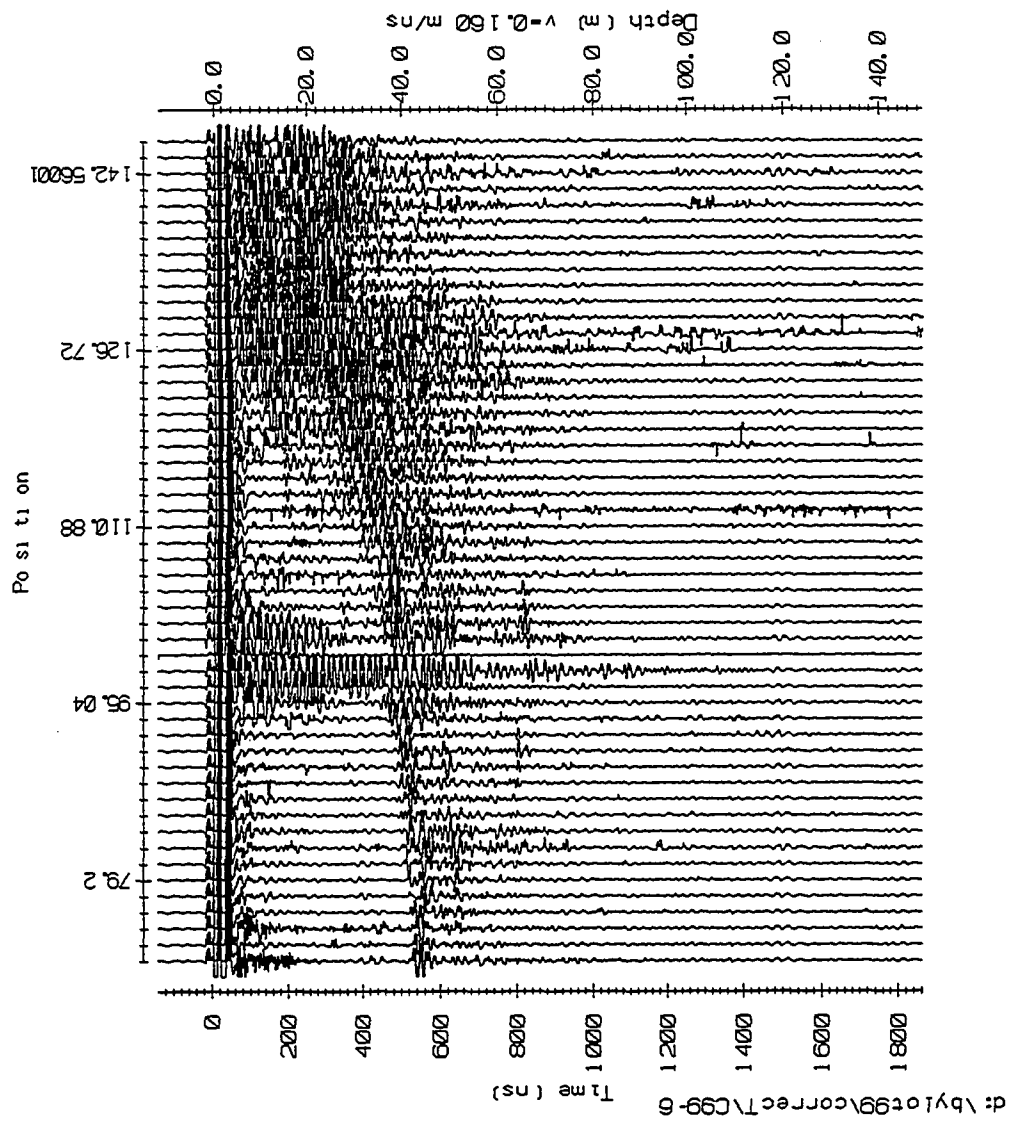


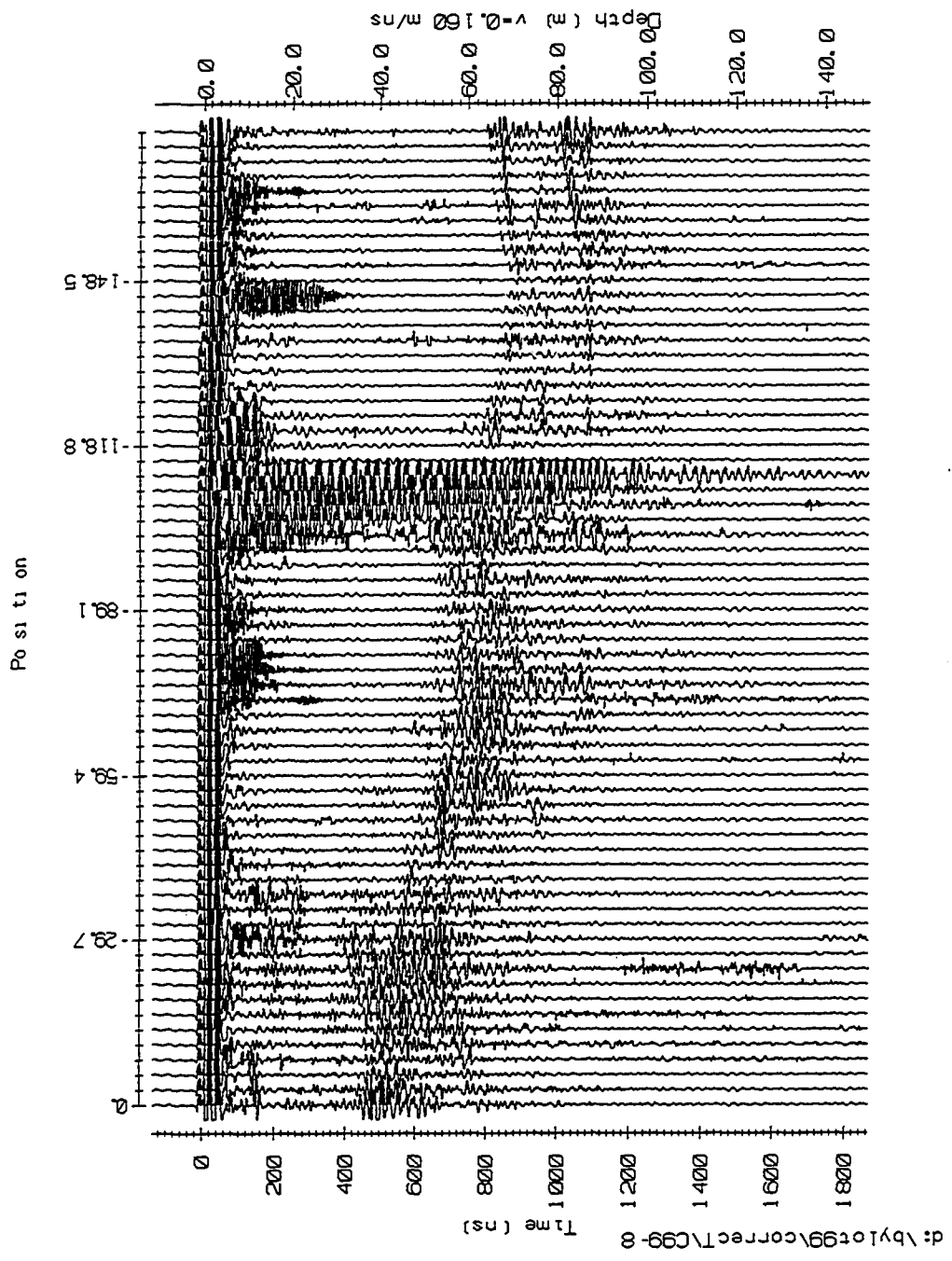




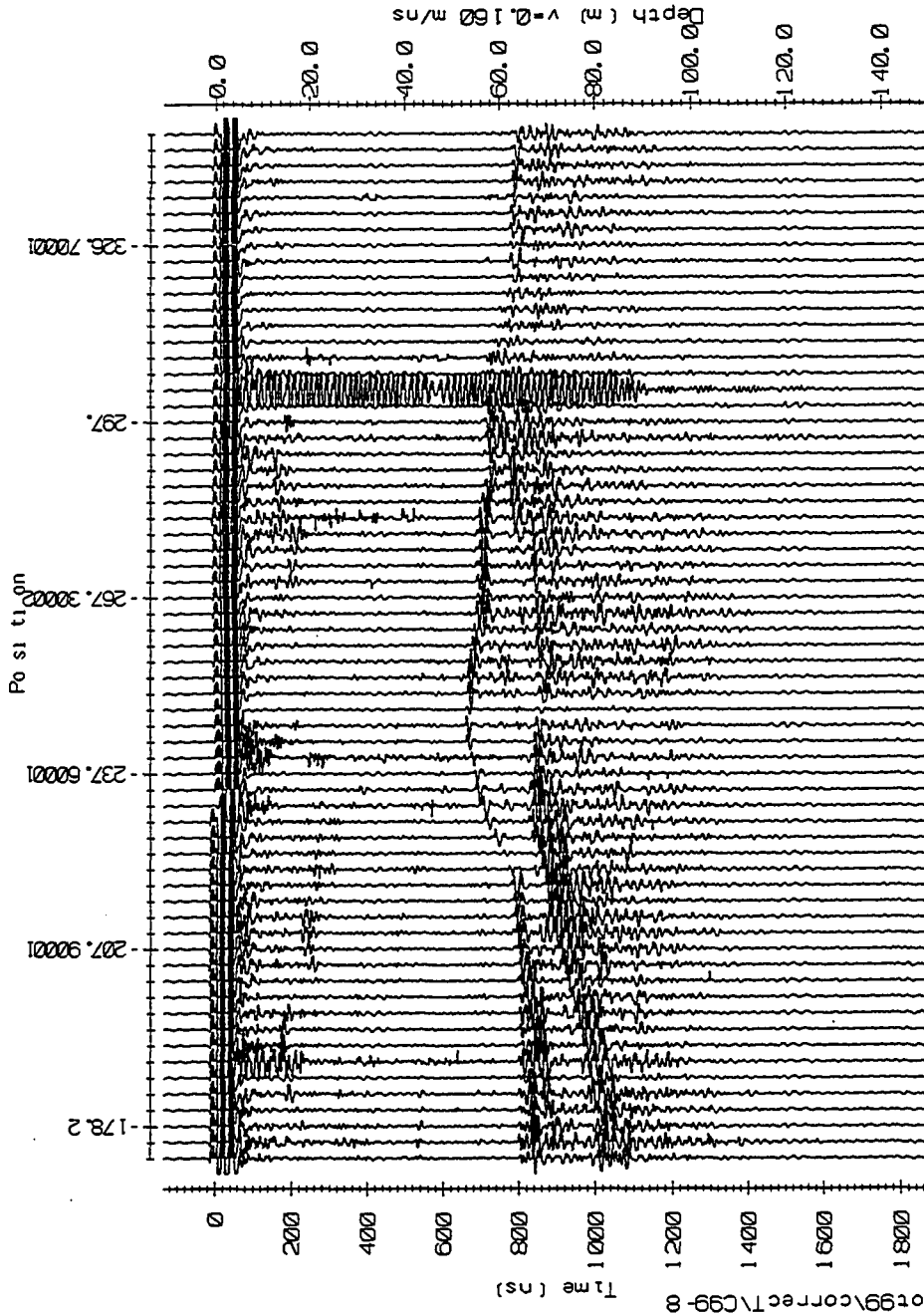
d:\bylot99\correct\topo\T99-123



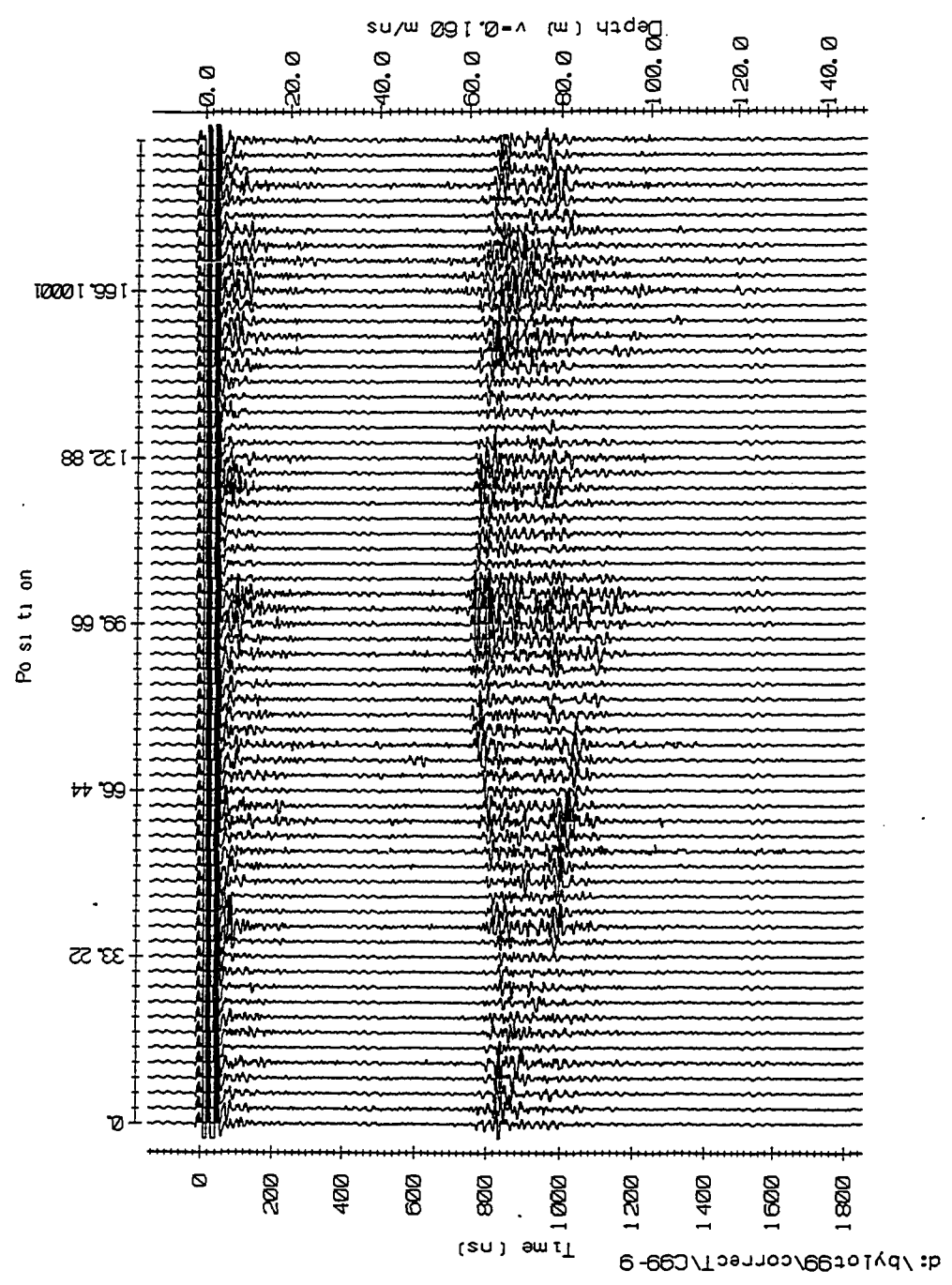


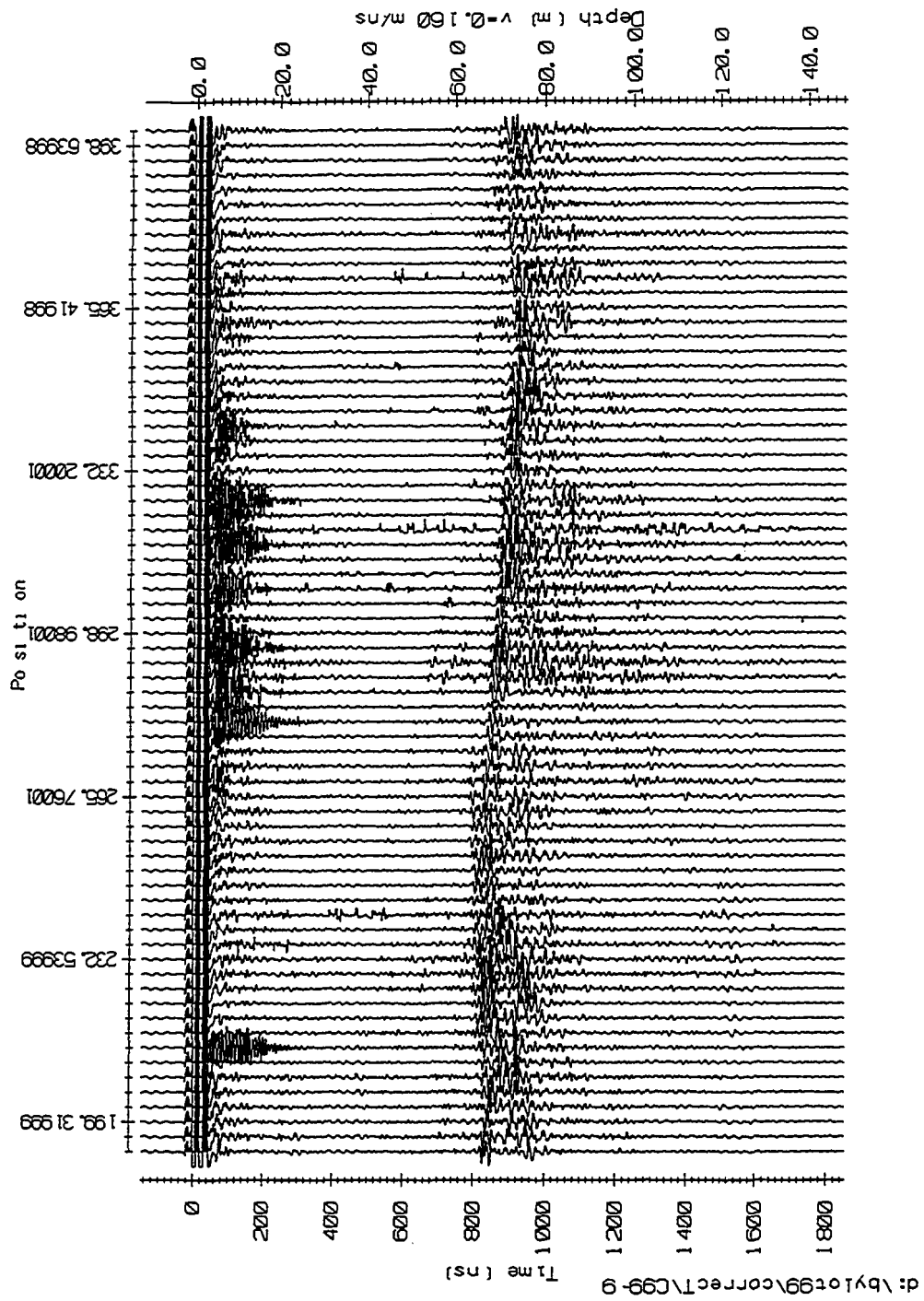


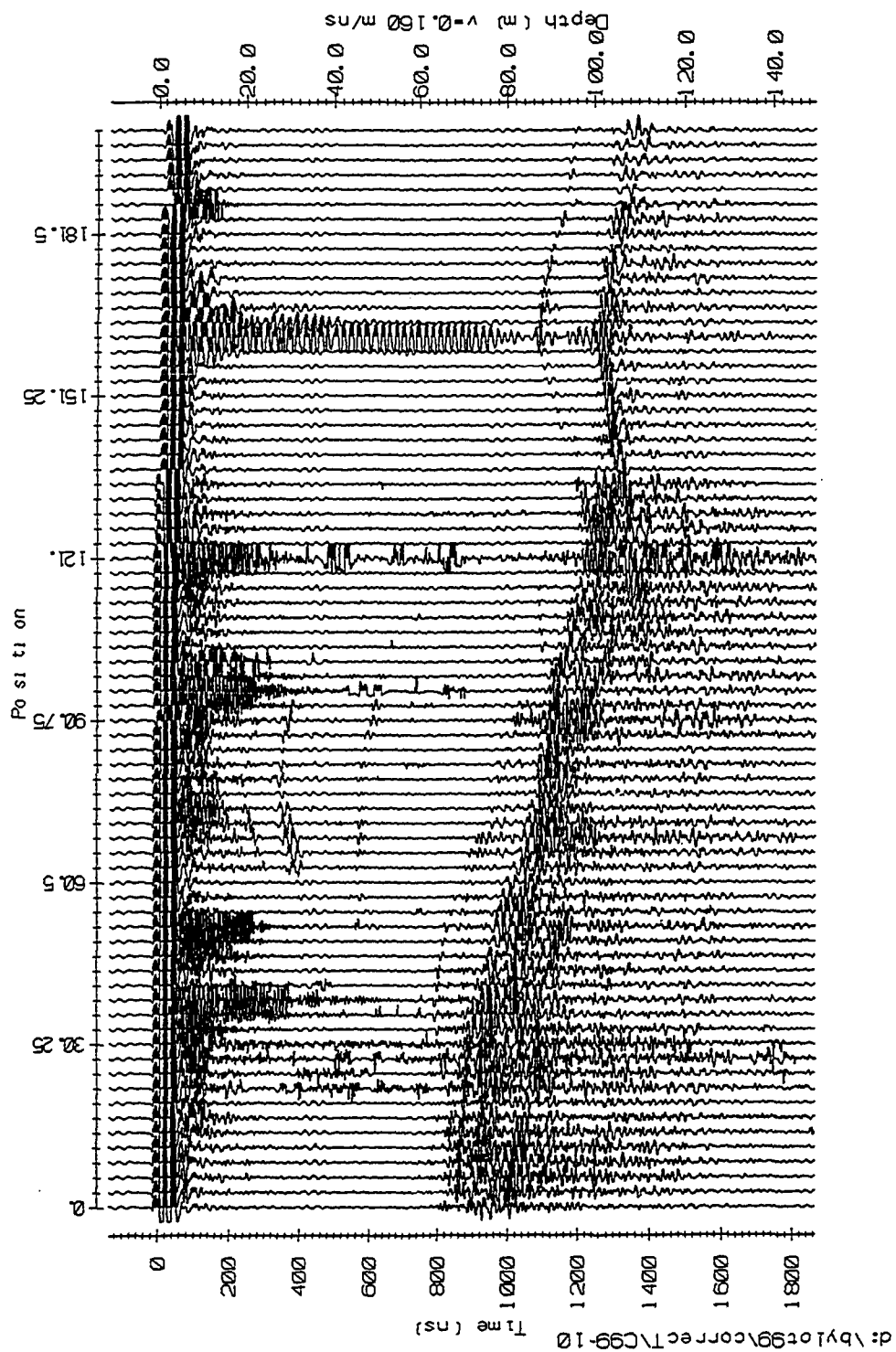
d:\bylot99\correct\C99-8

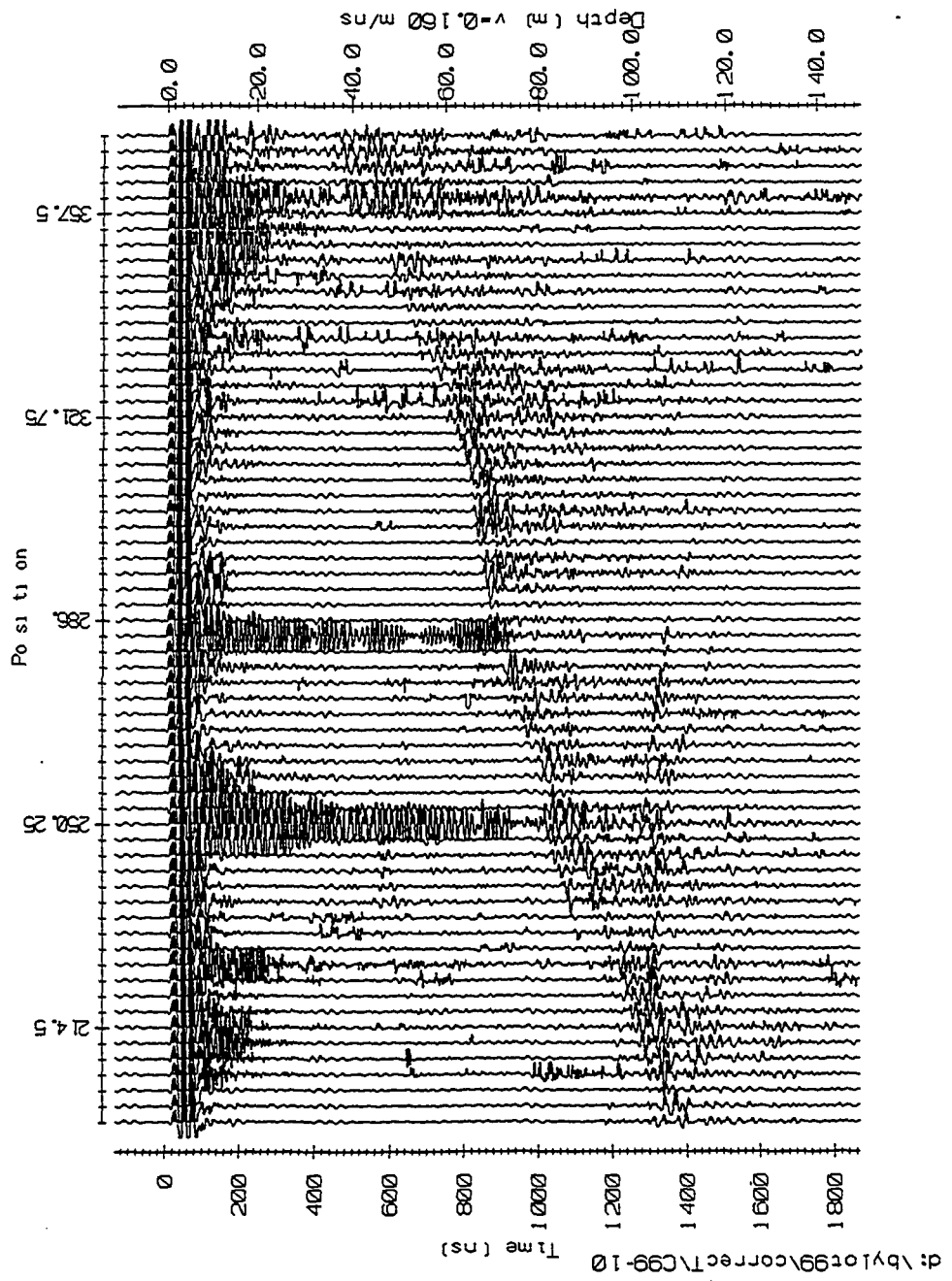


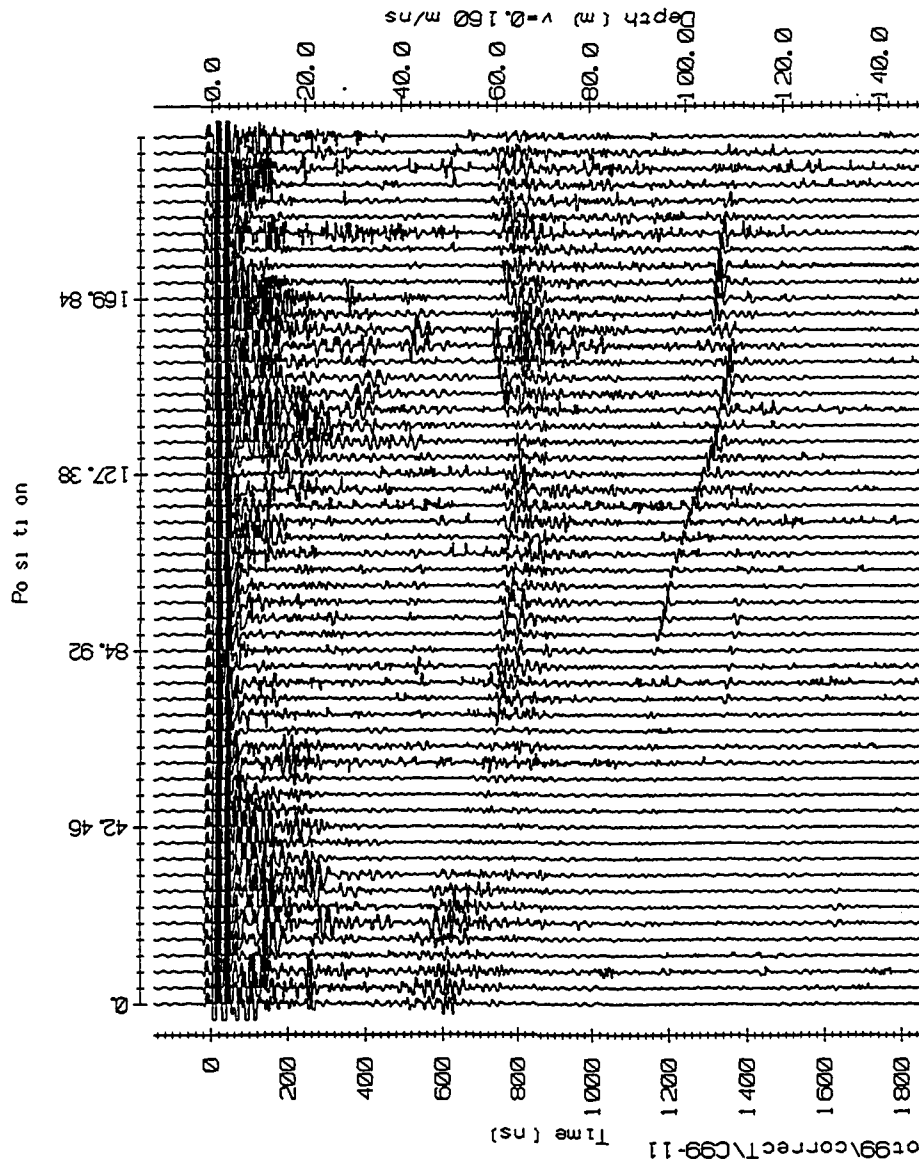
d:\vbylot99\correct\C99-8



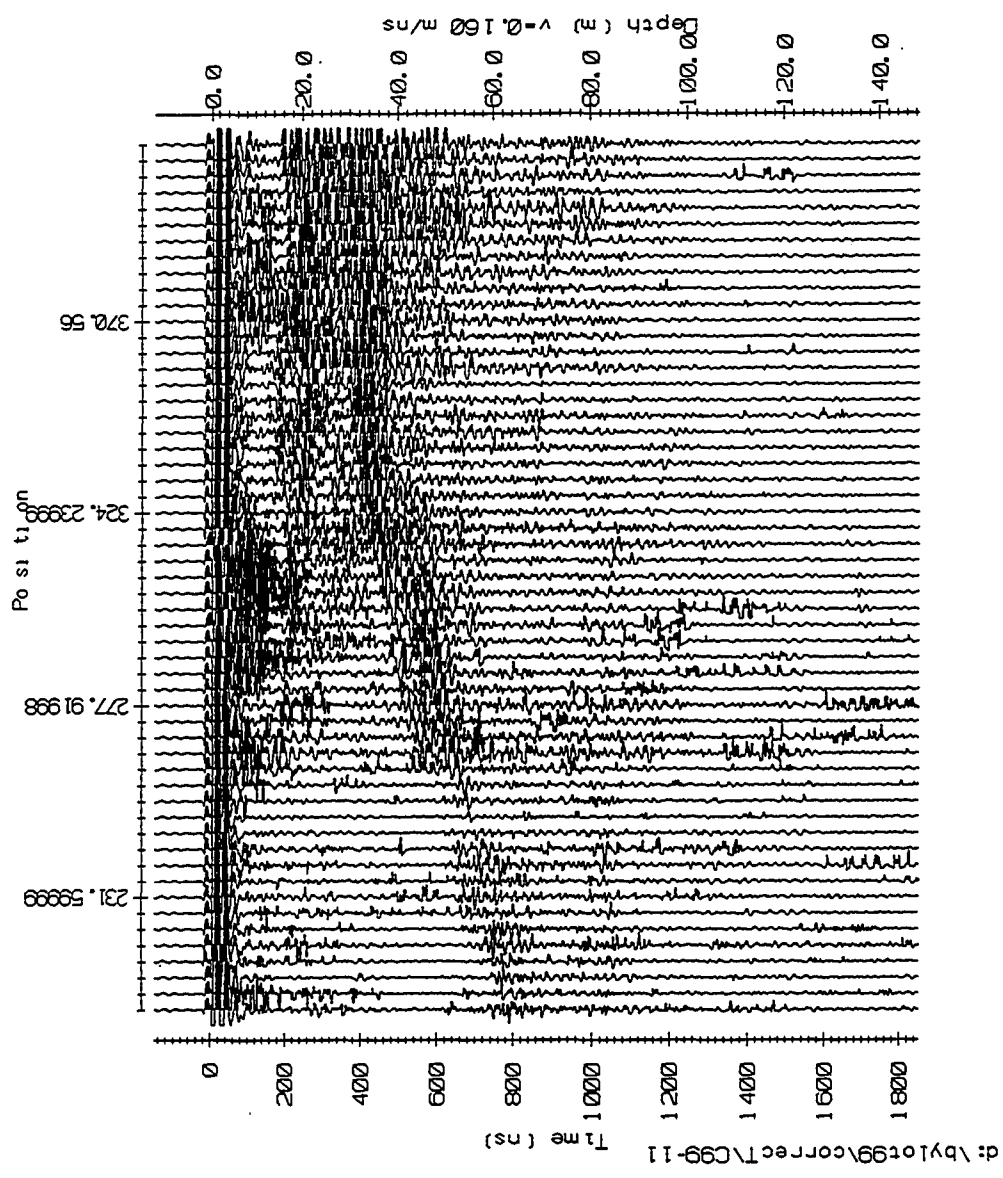


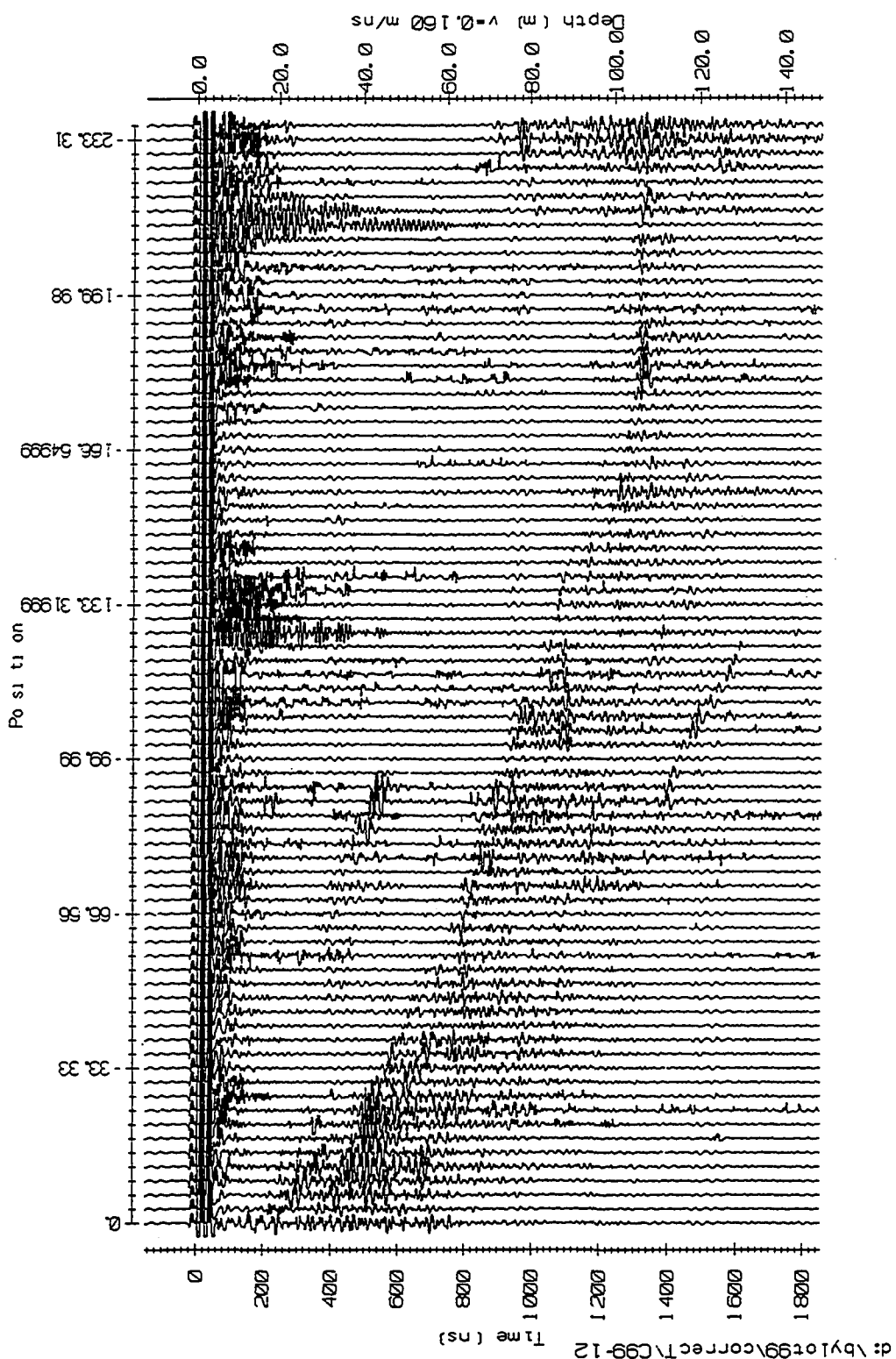


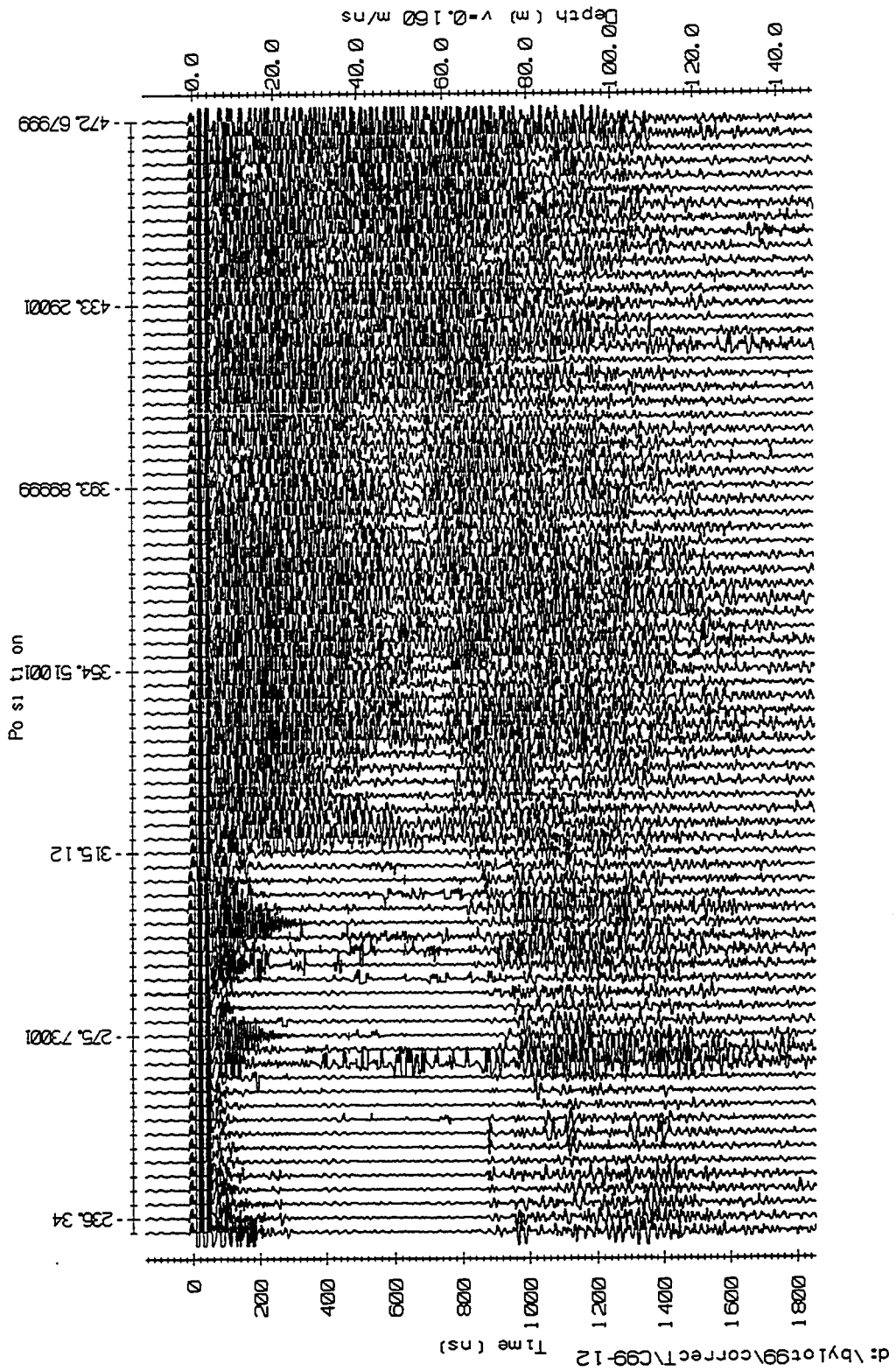


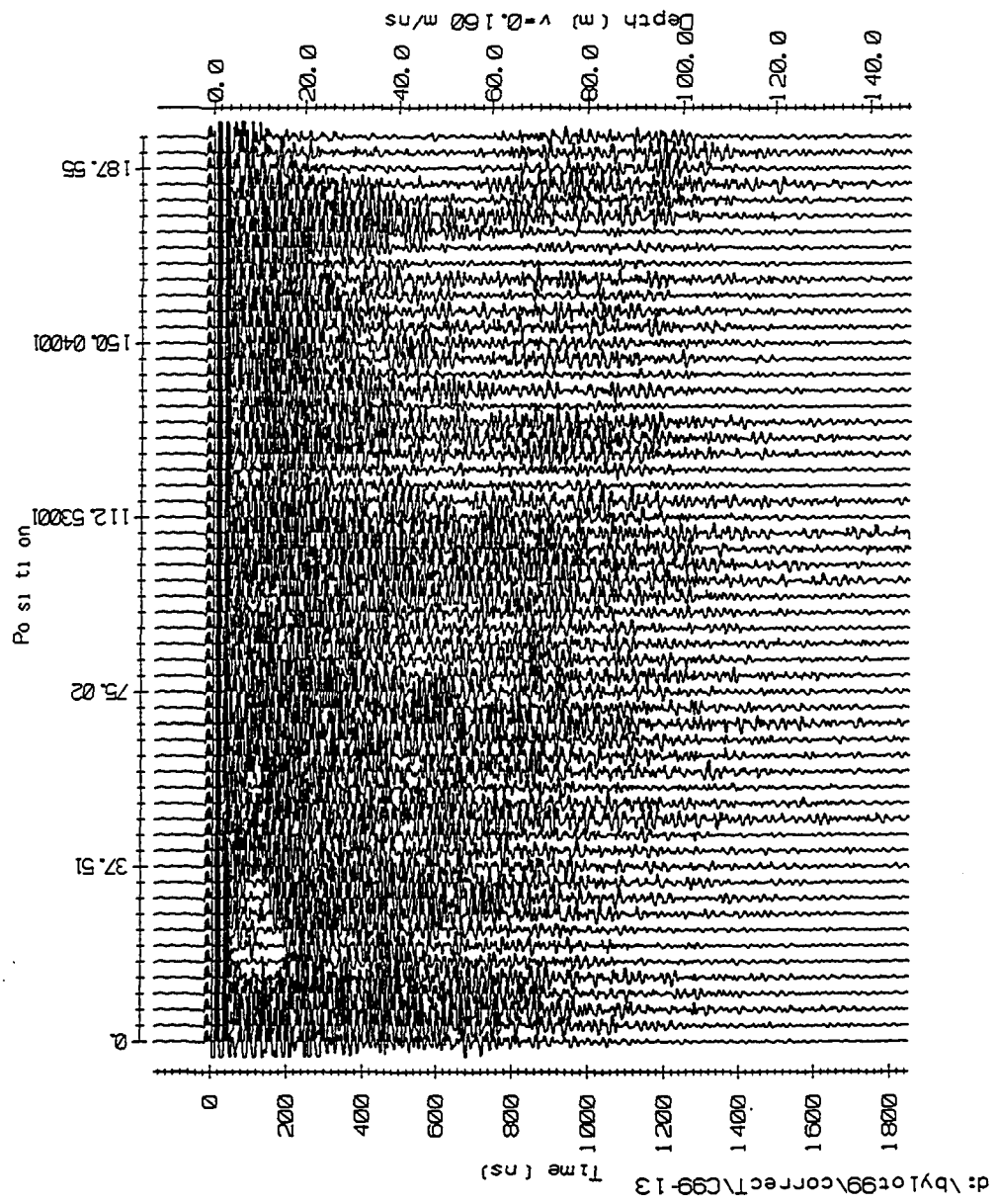


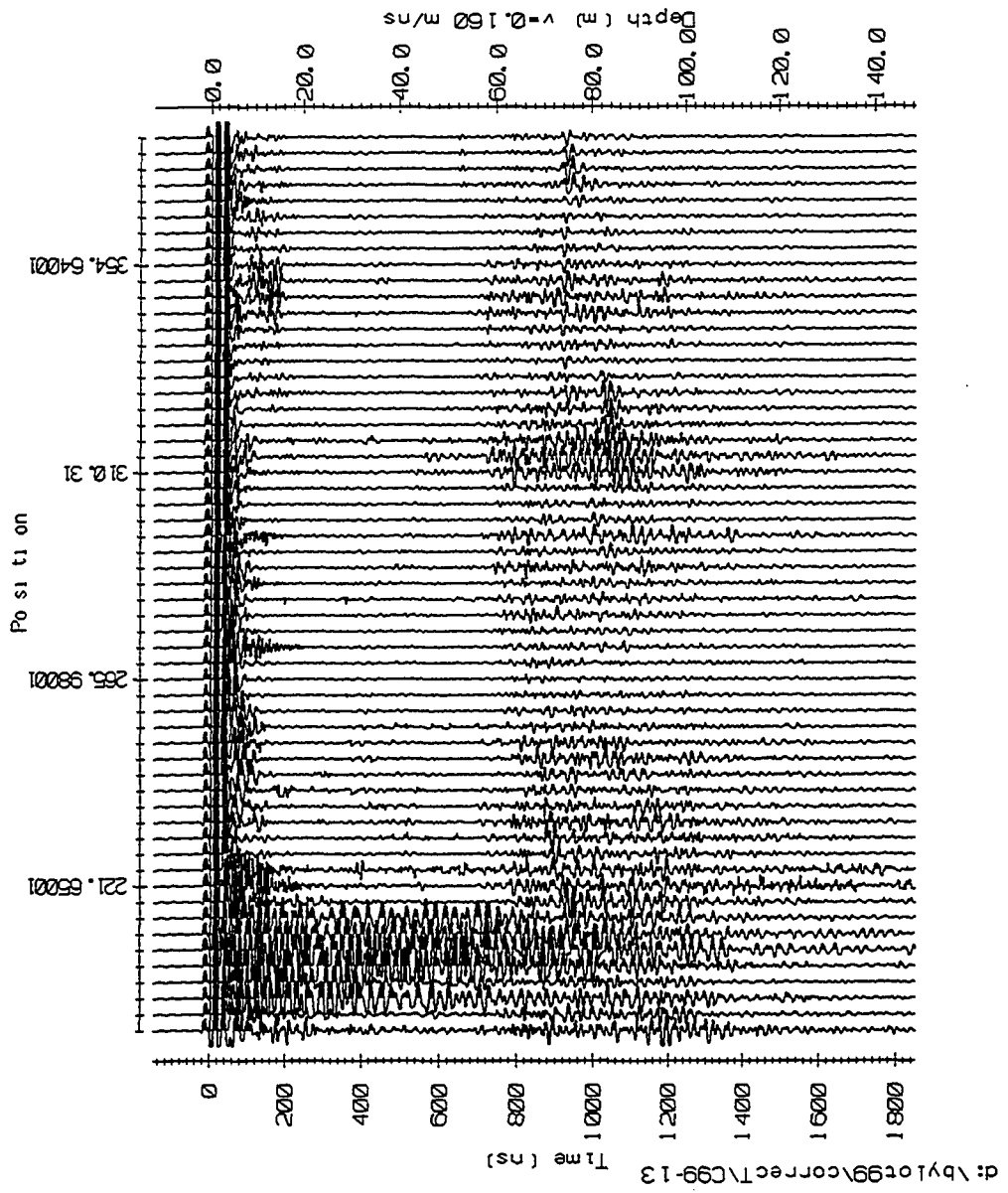
d:\bylot99\correct\C99-11

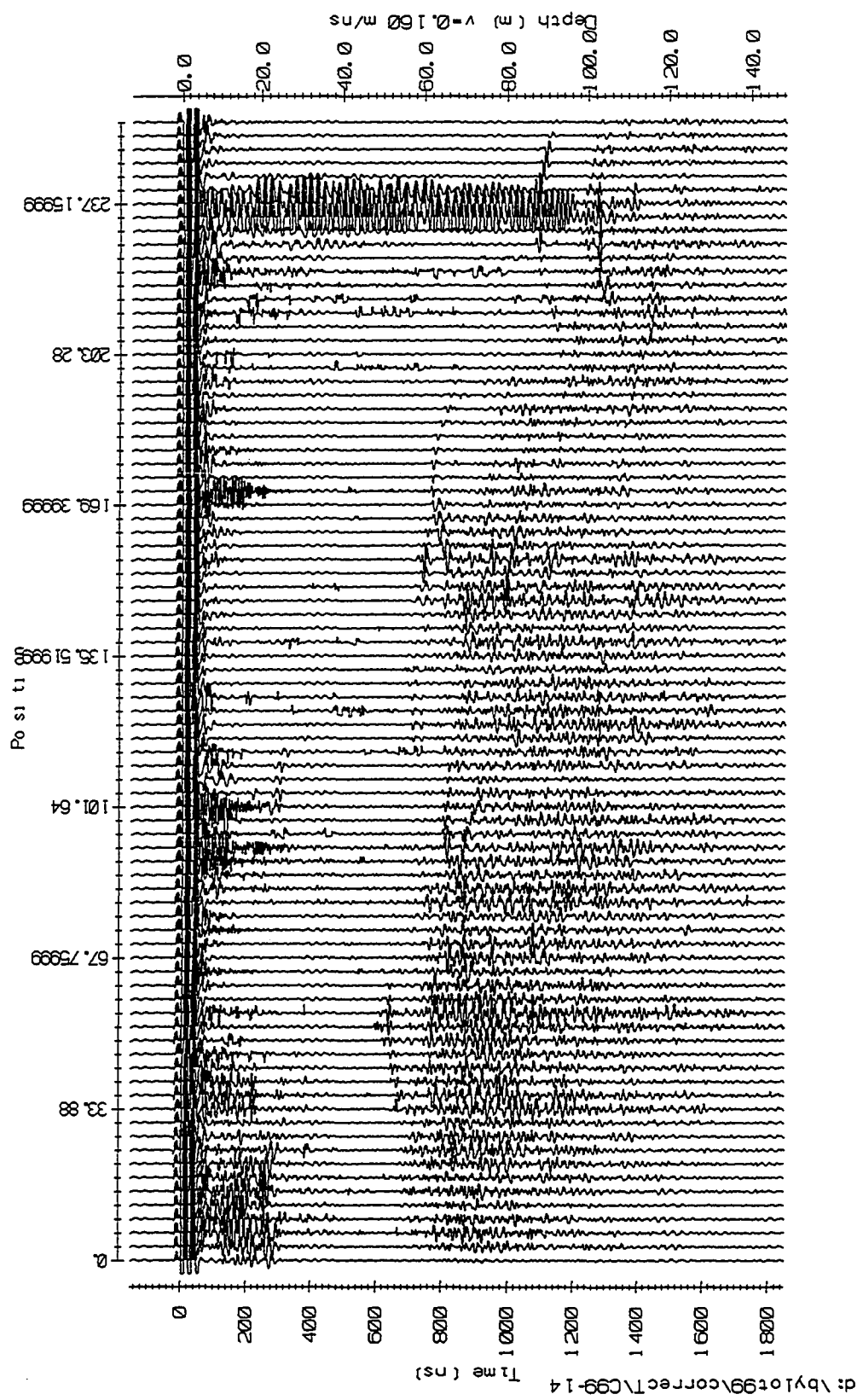




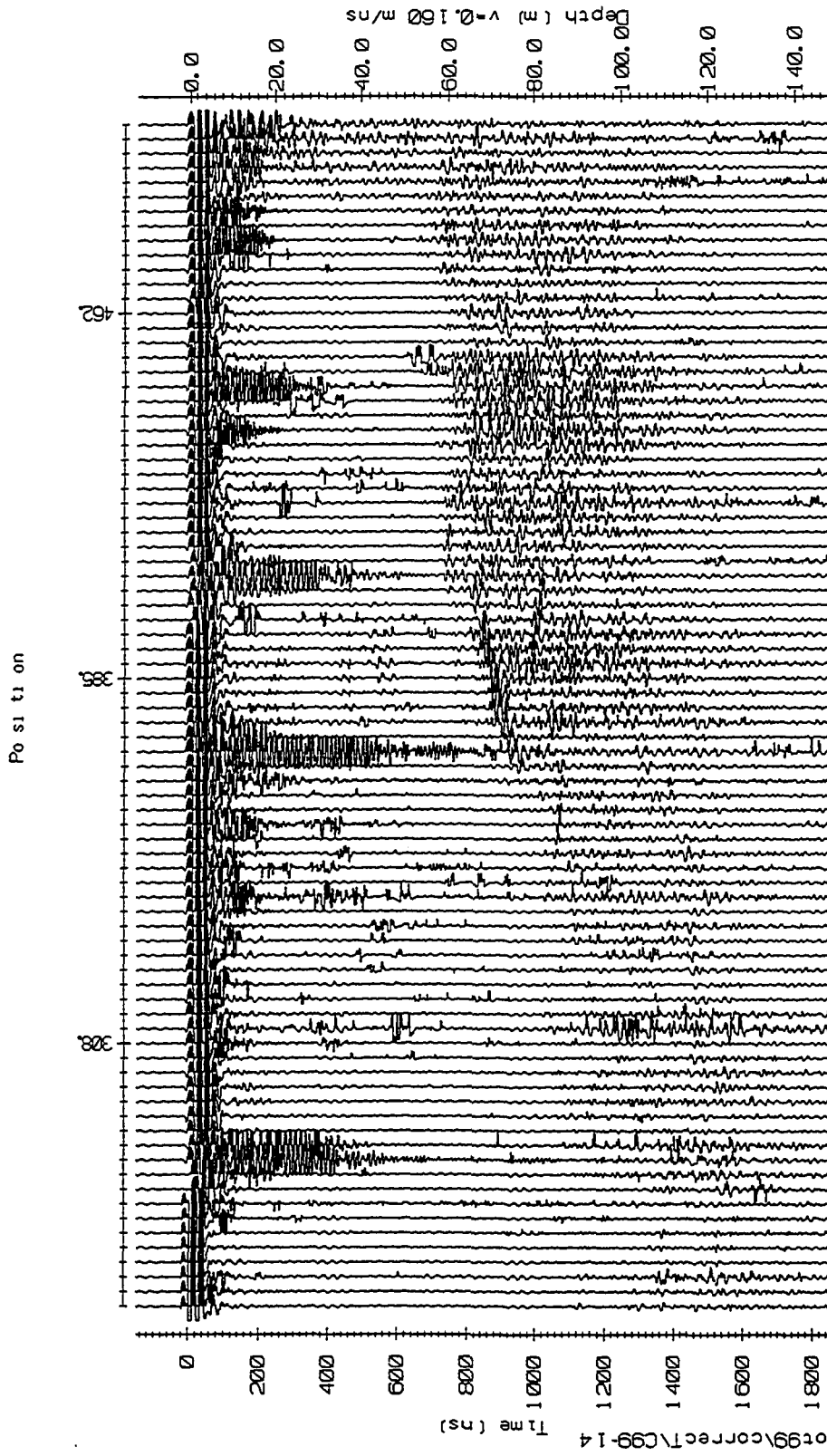








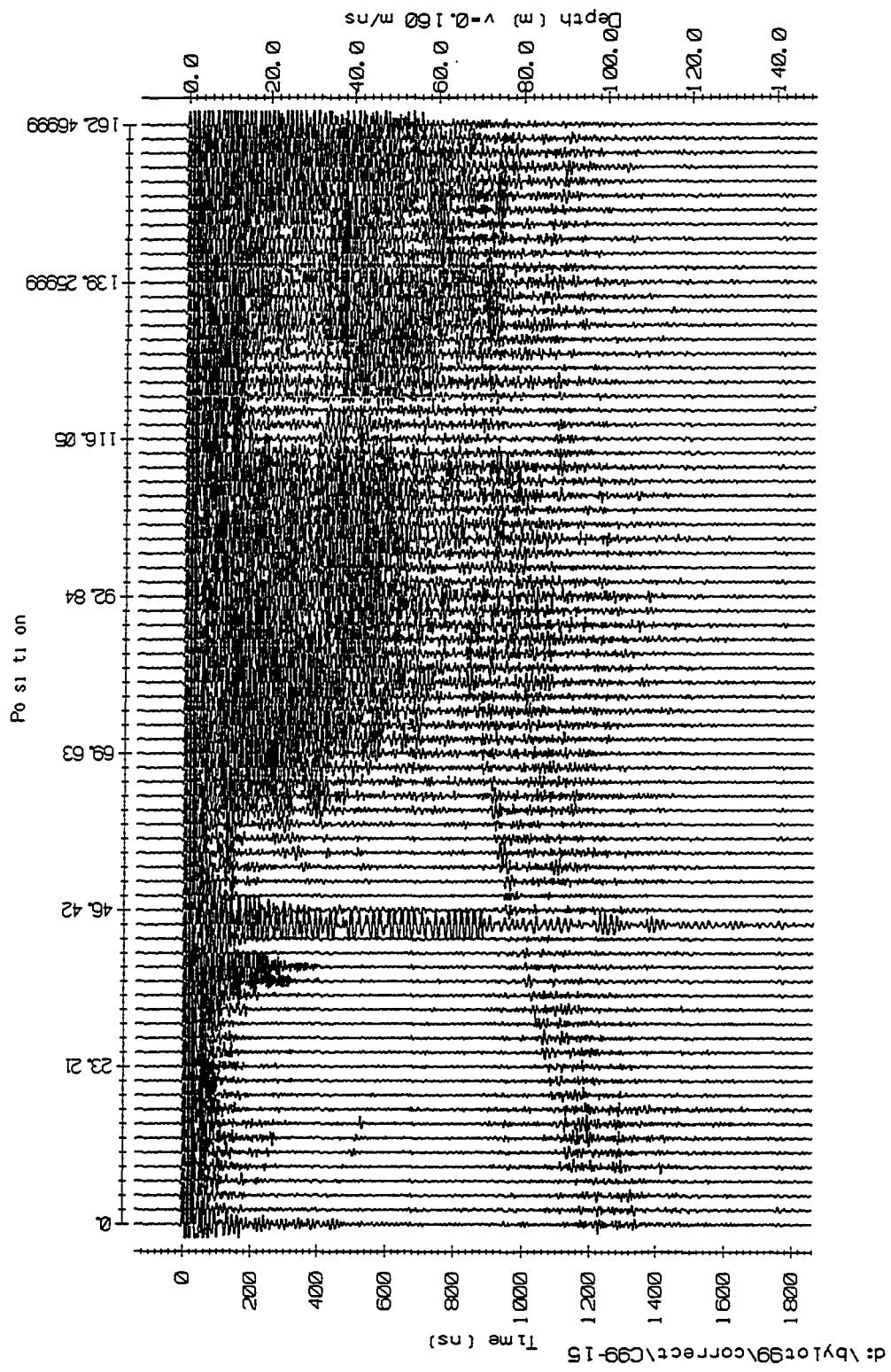
d:\bylot99\correct\C99-14

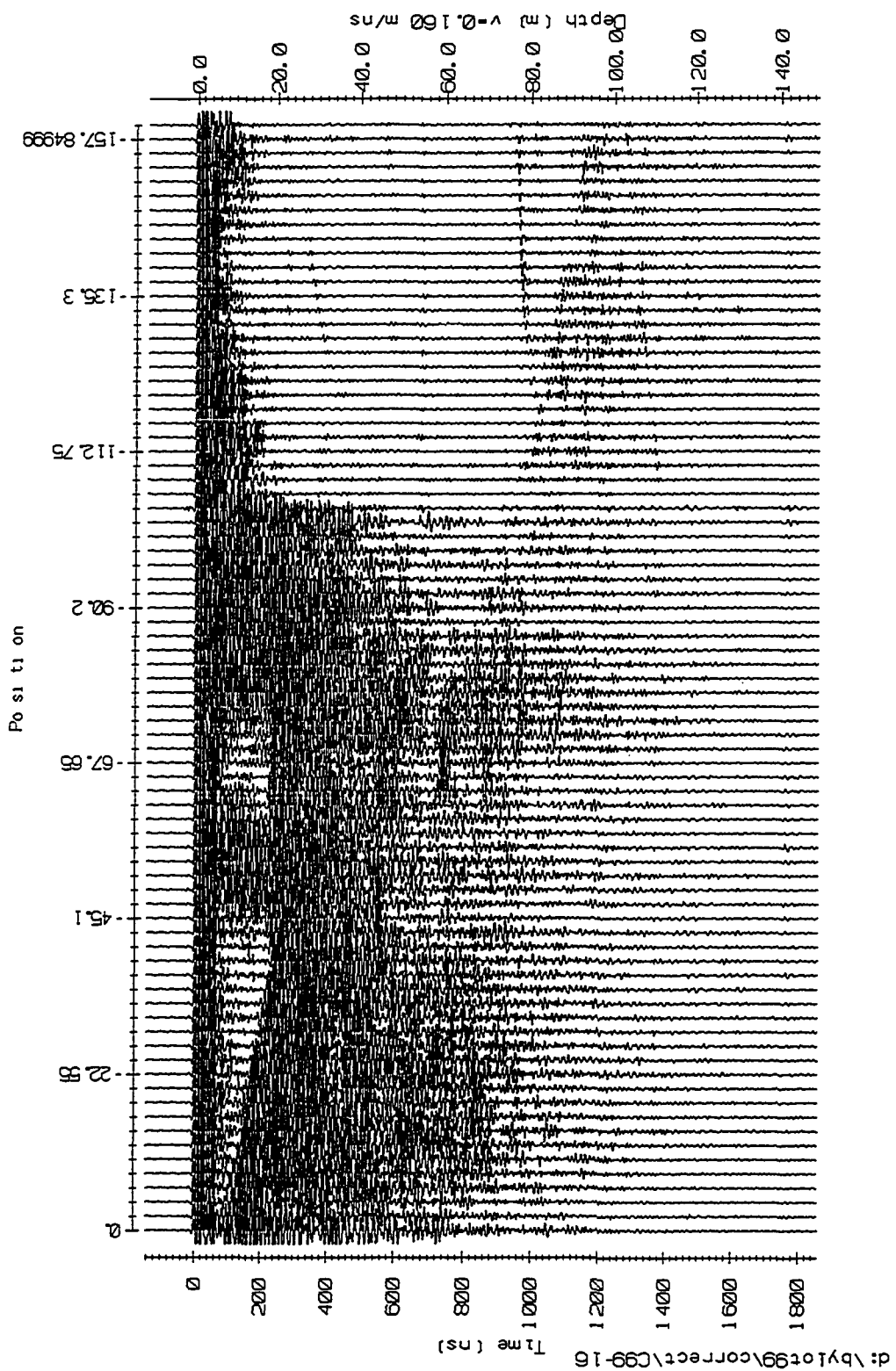


d:\bylot99\correct\C99-14

Time (ns)

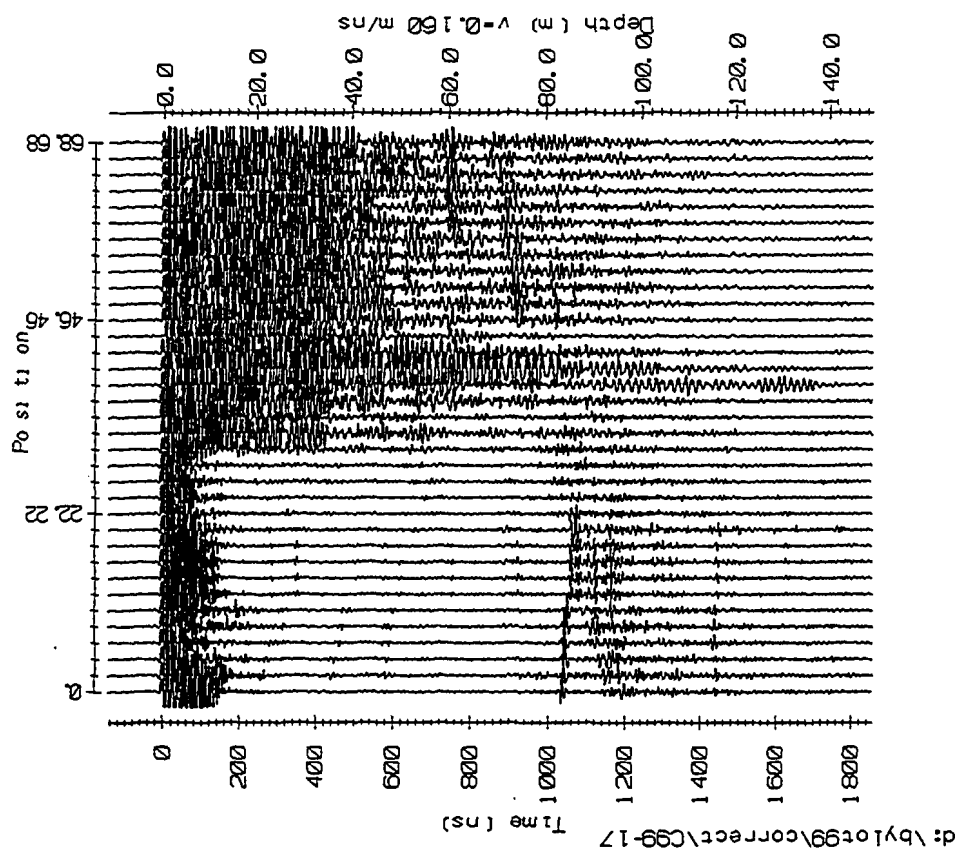
Position



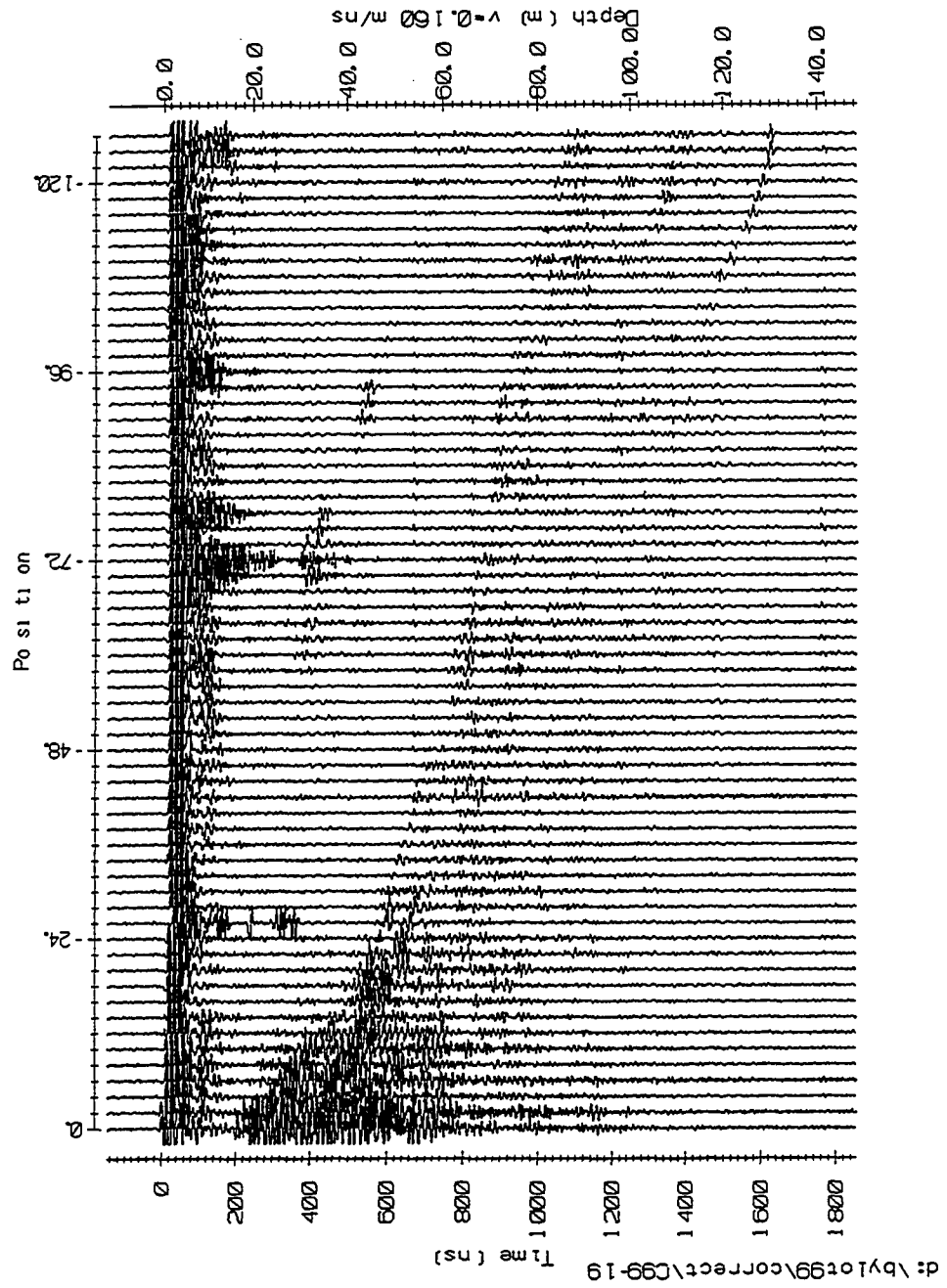


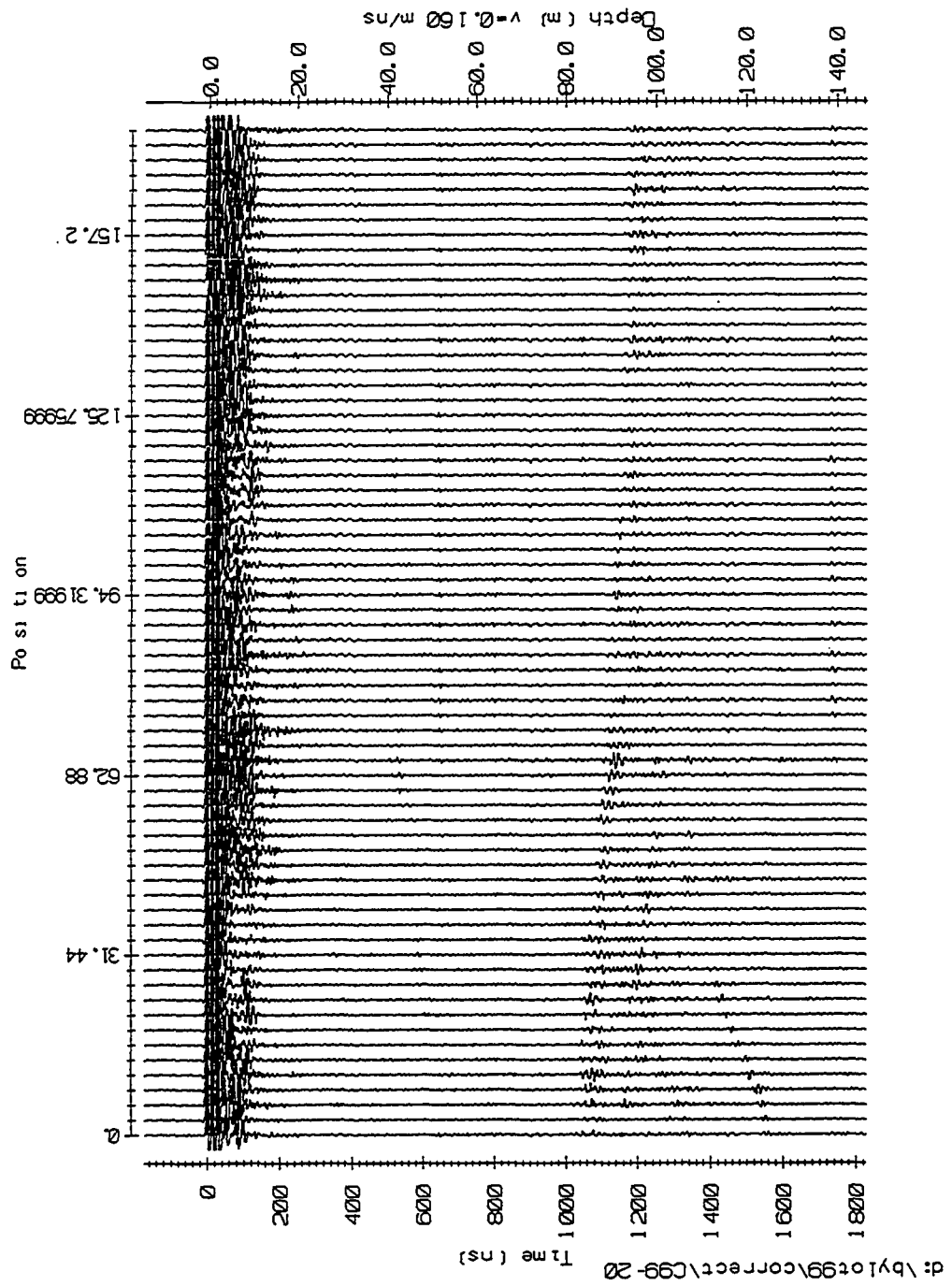
d:\bylot99\correct\C99-16

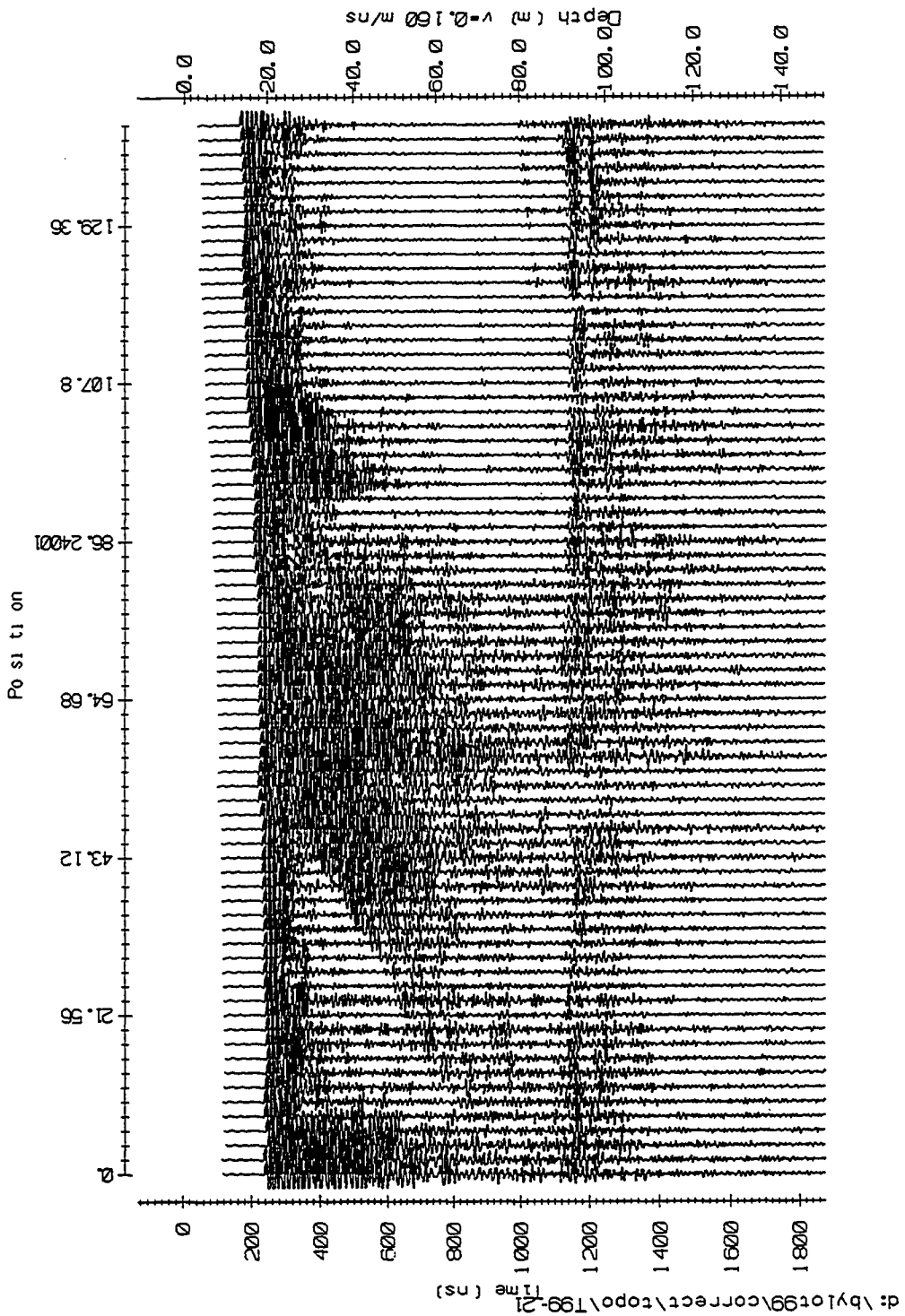
Position

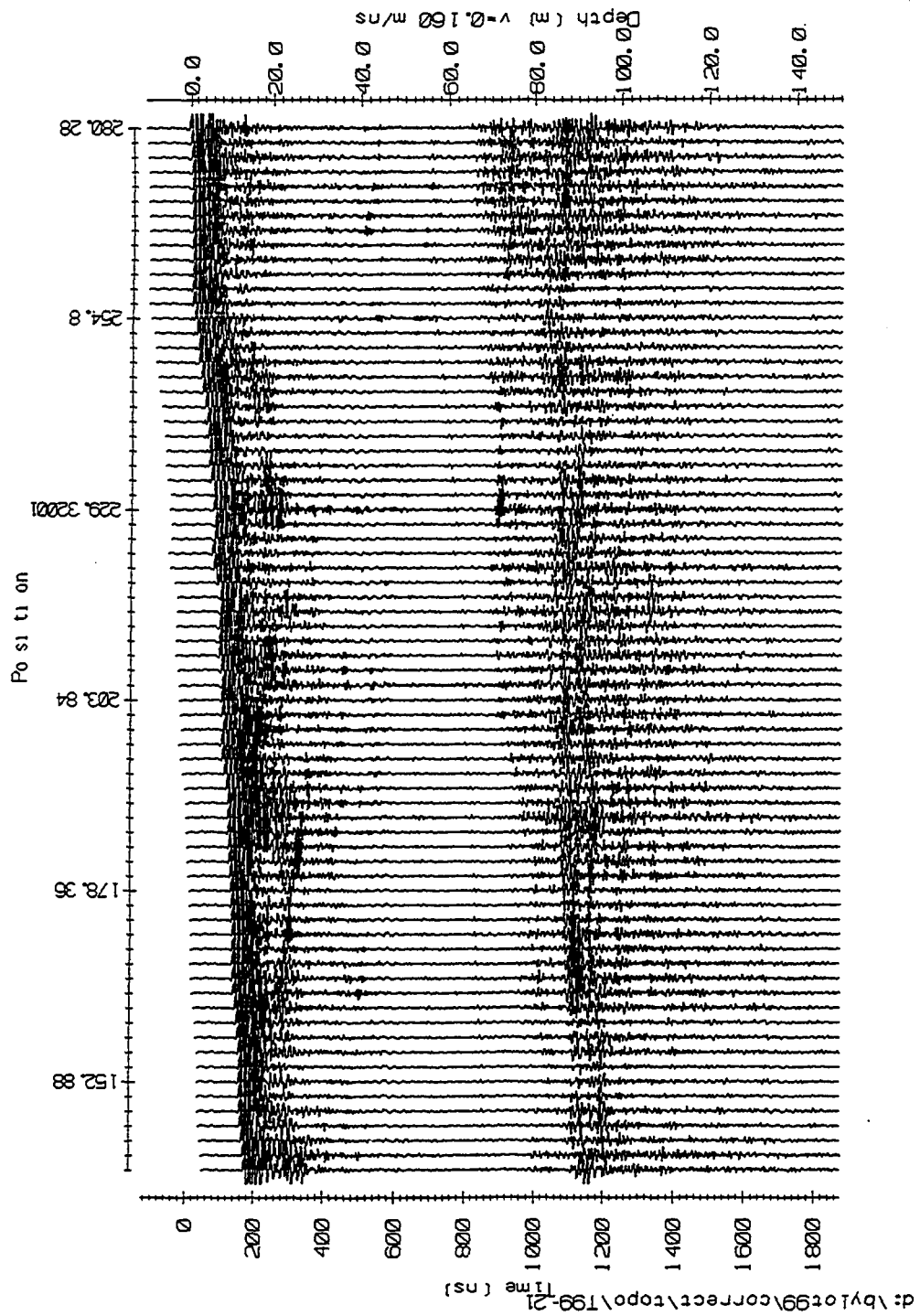


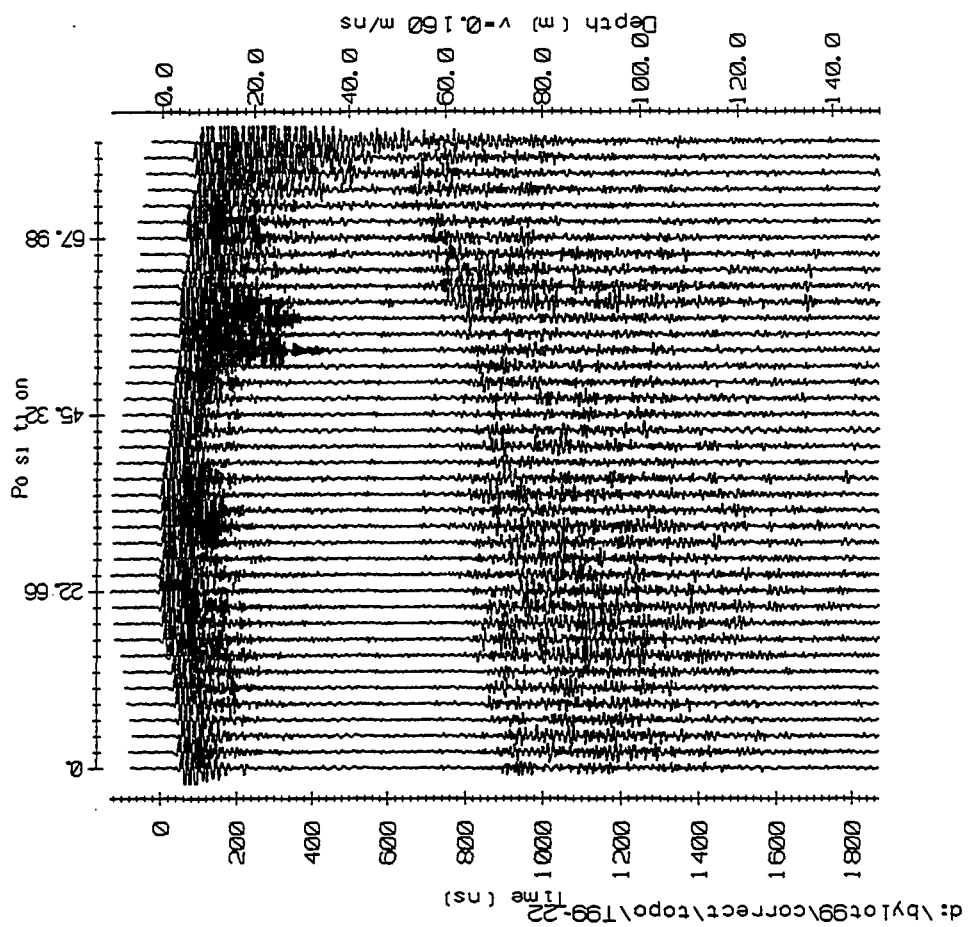


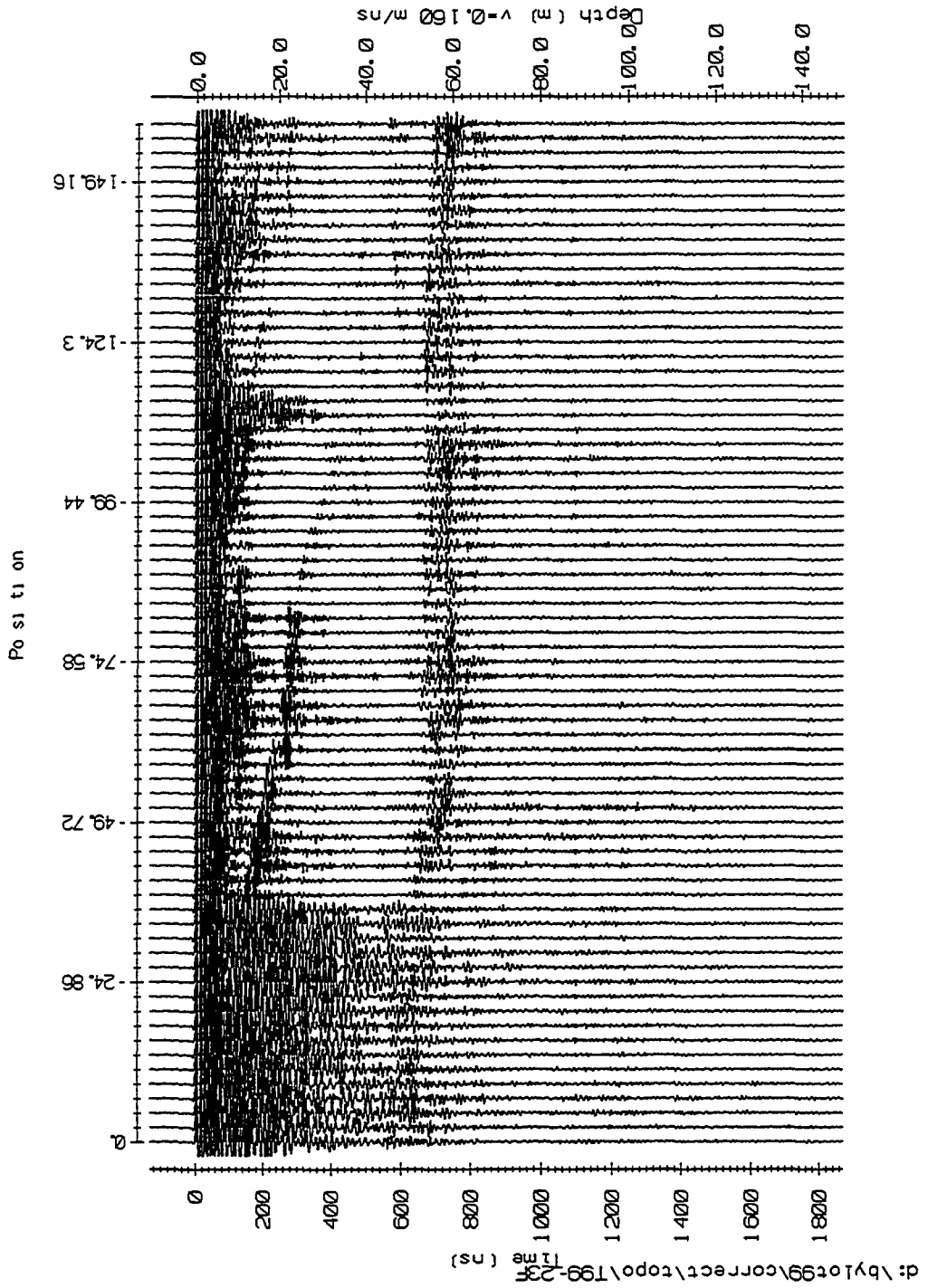


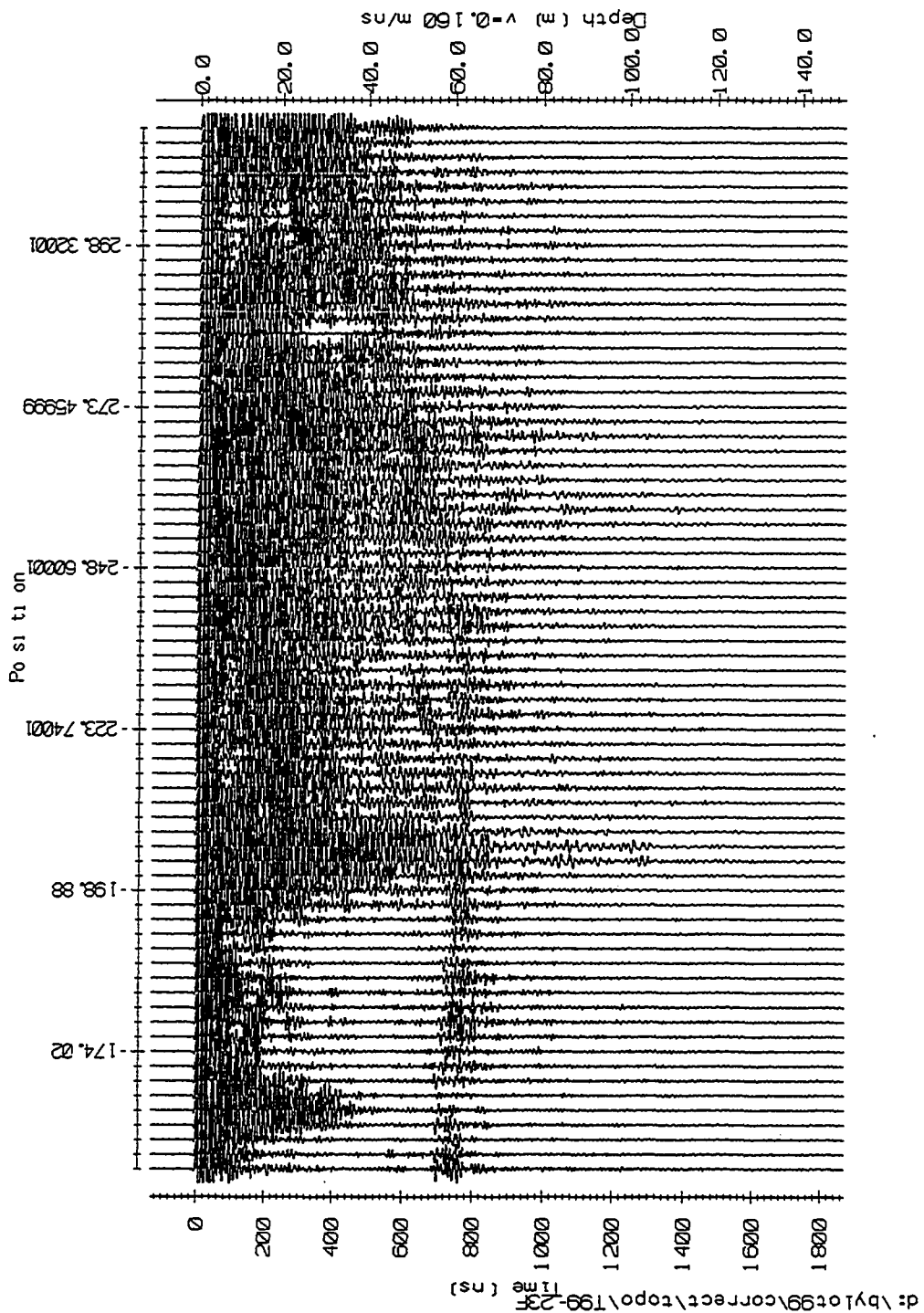


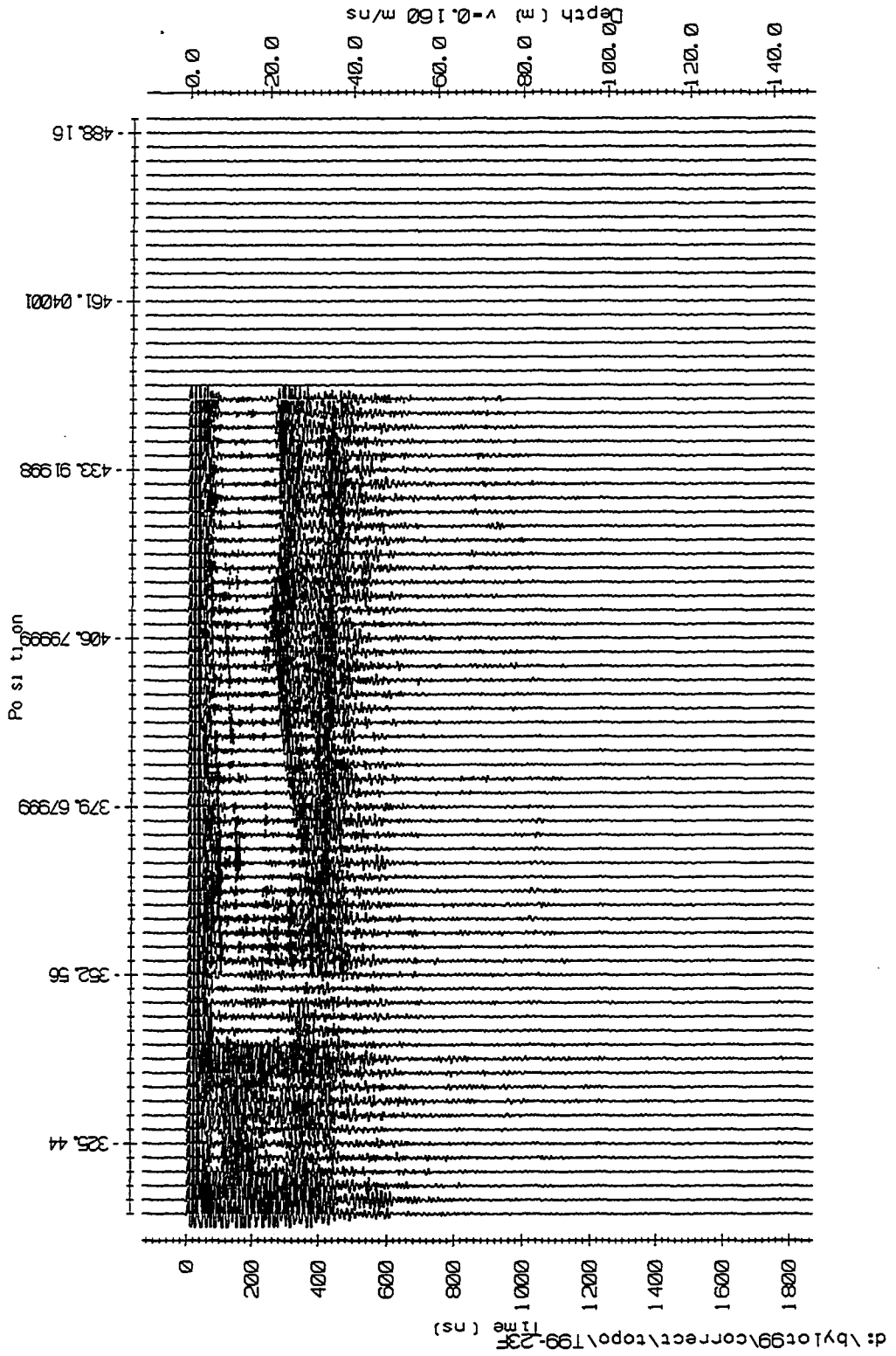


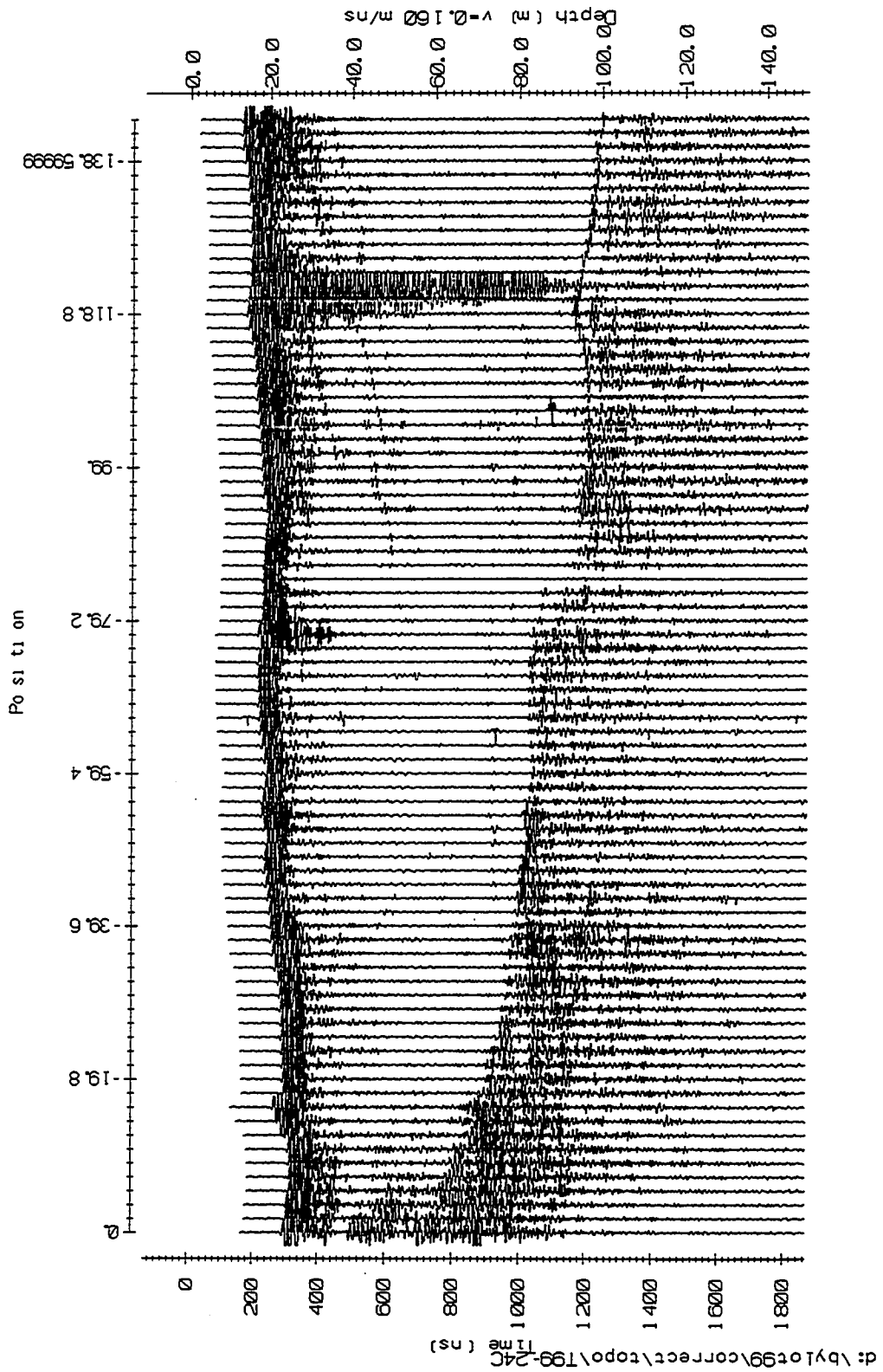


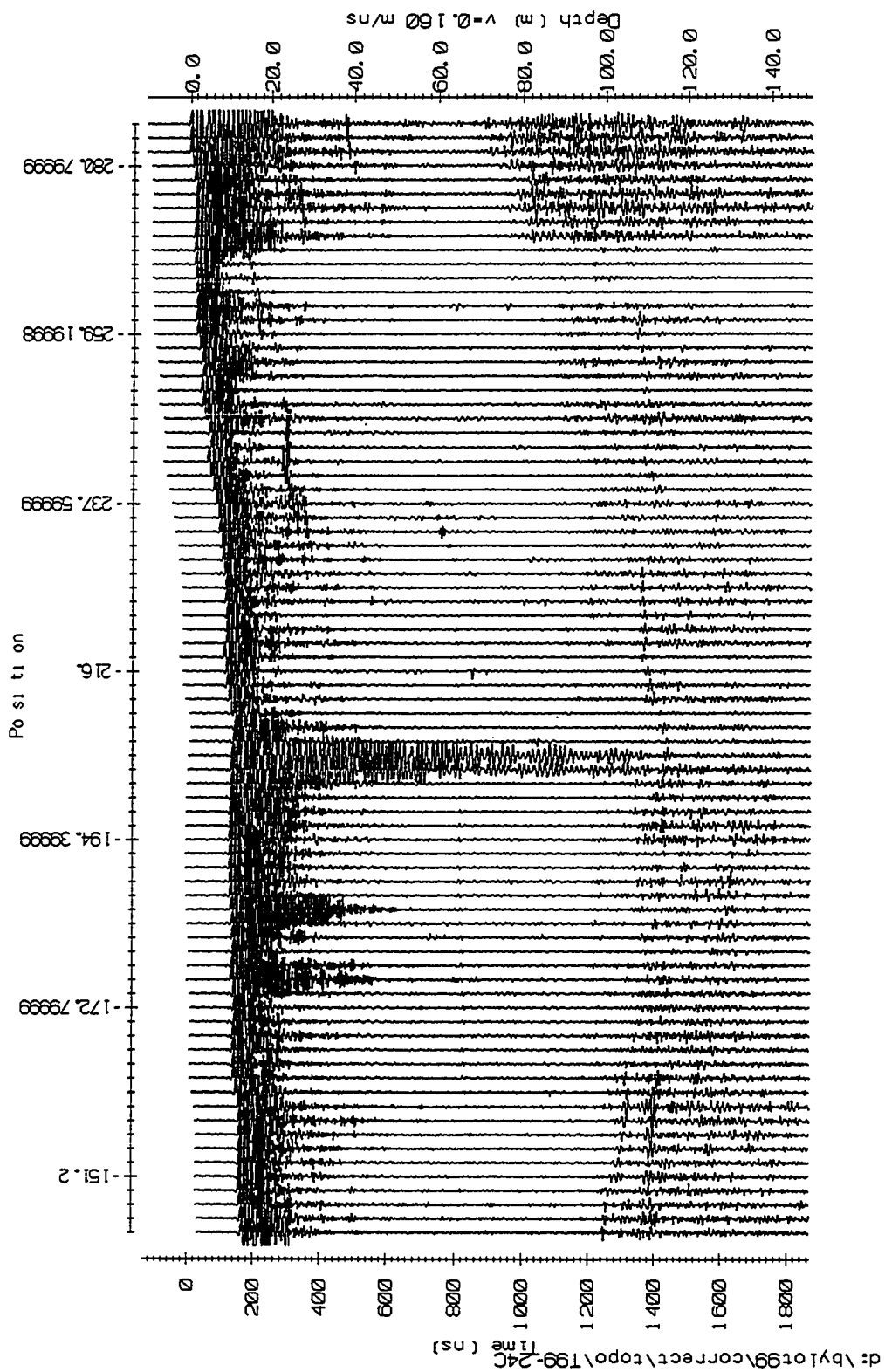




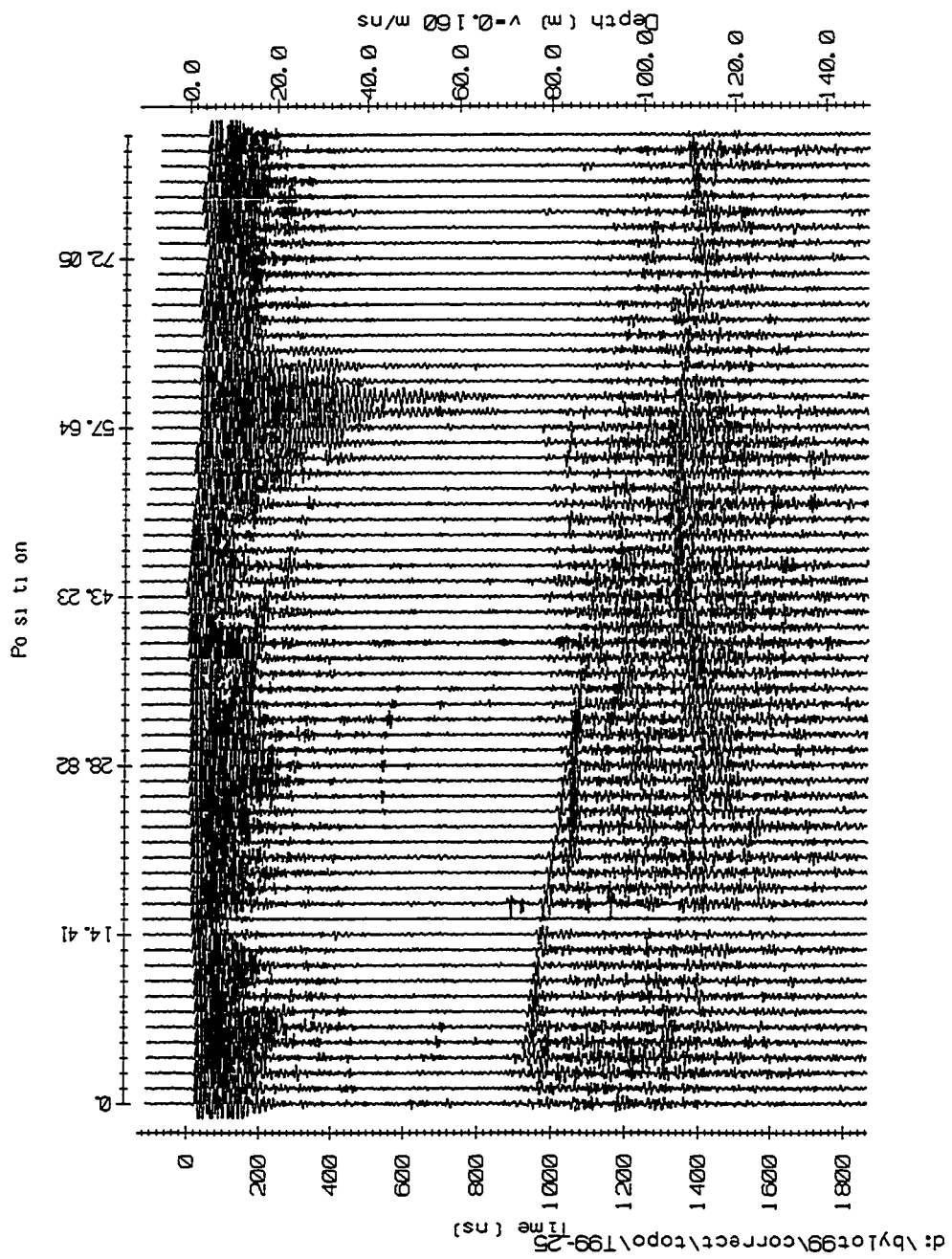


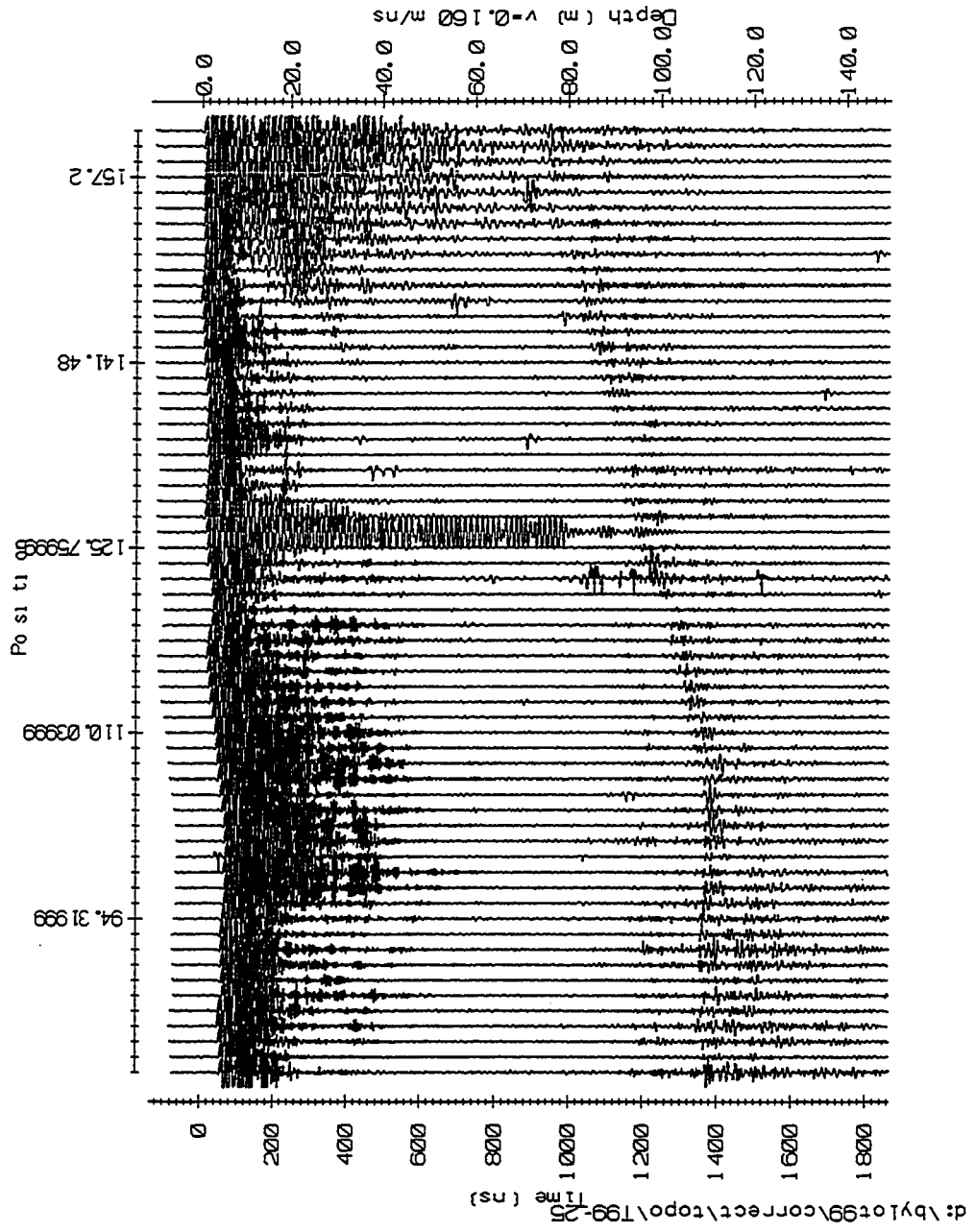


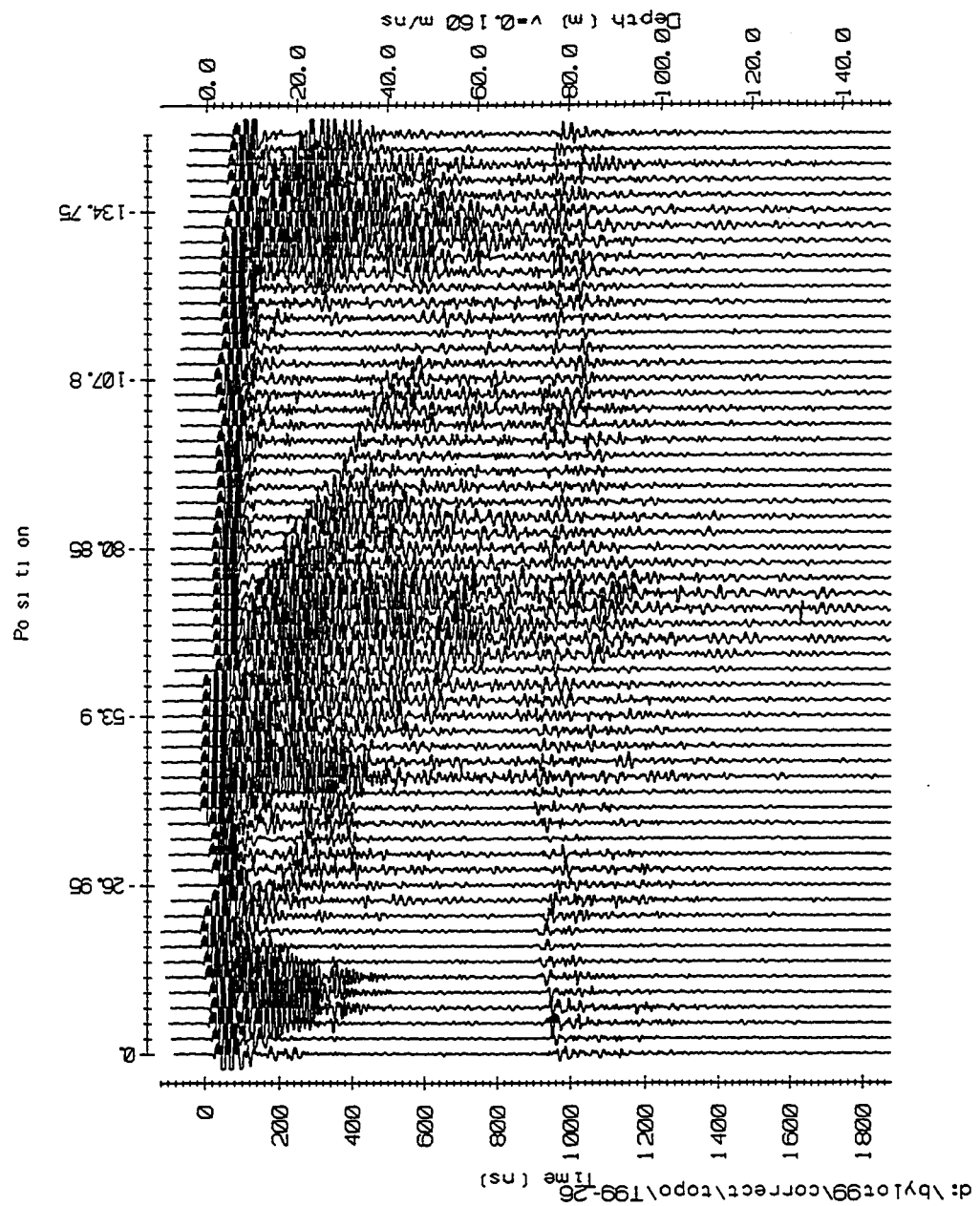


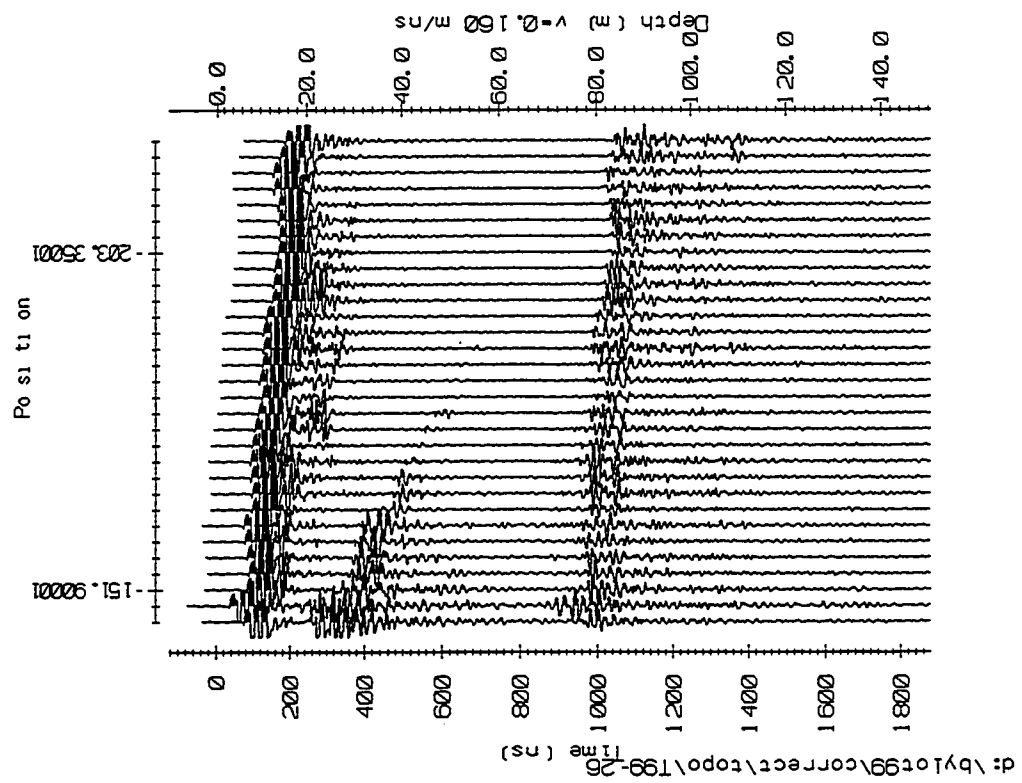


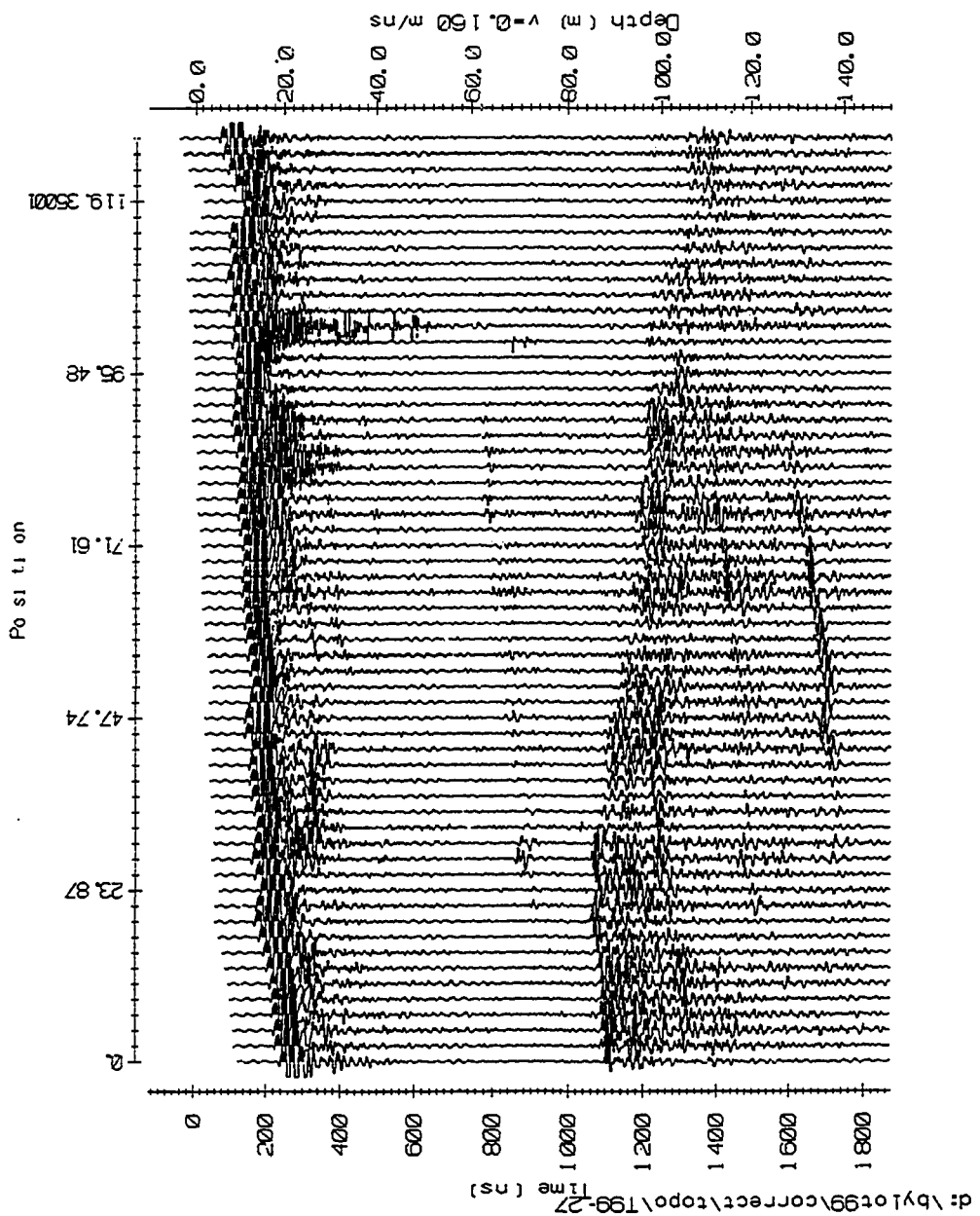
Position

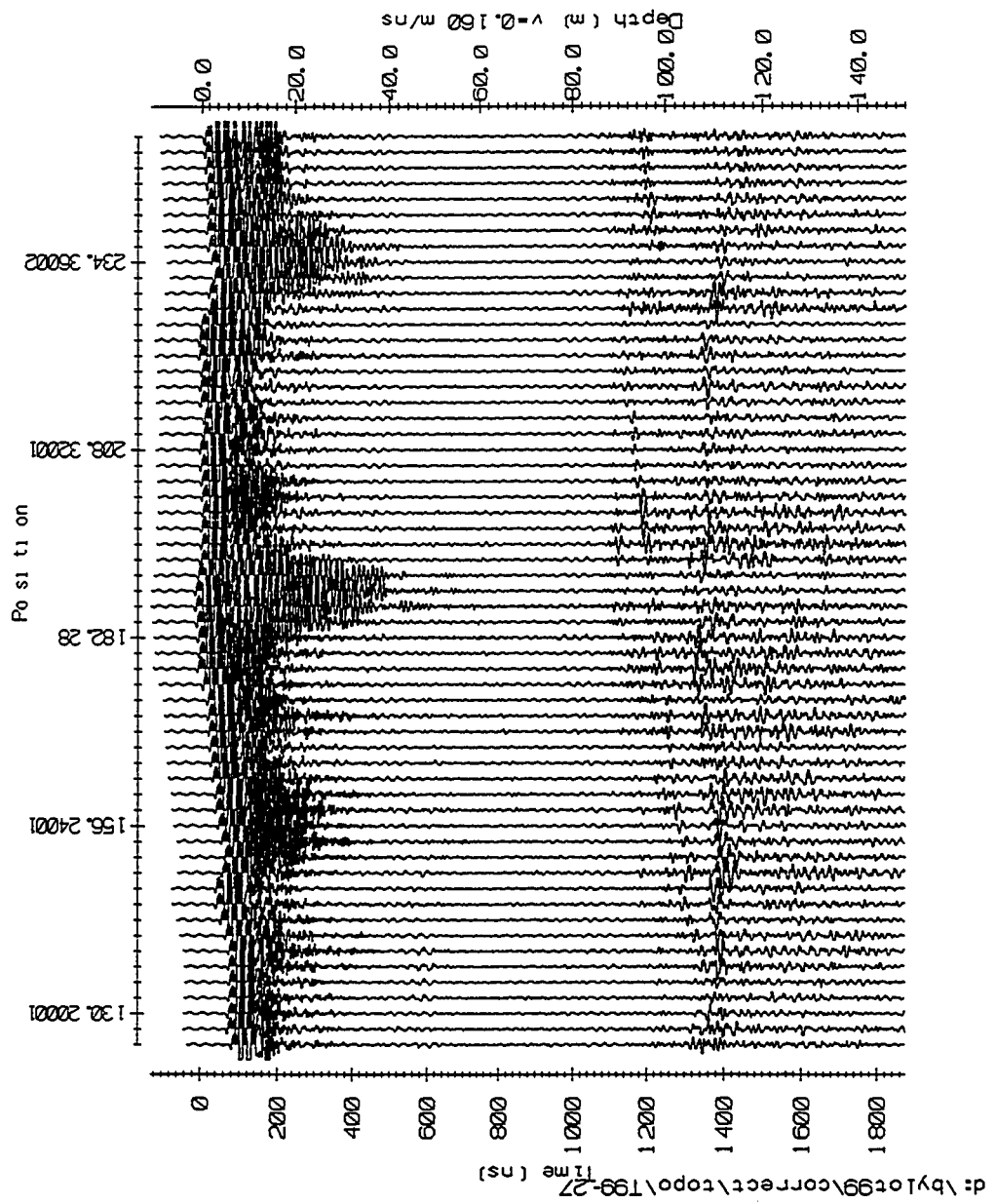


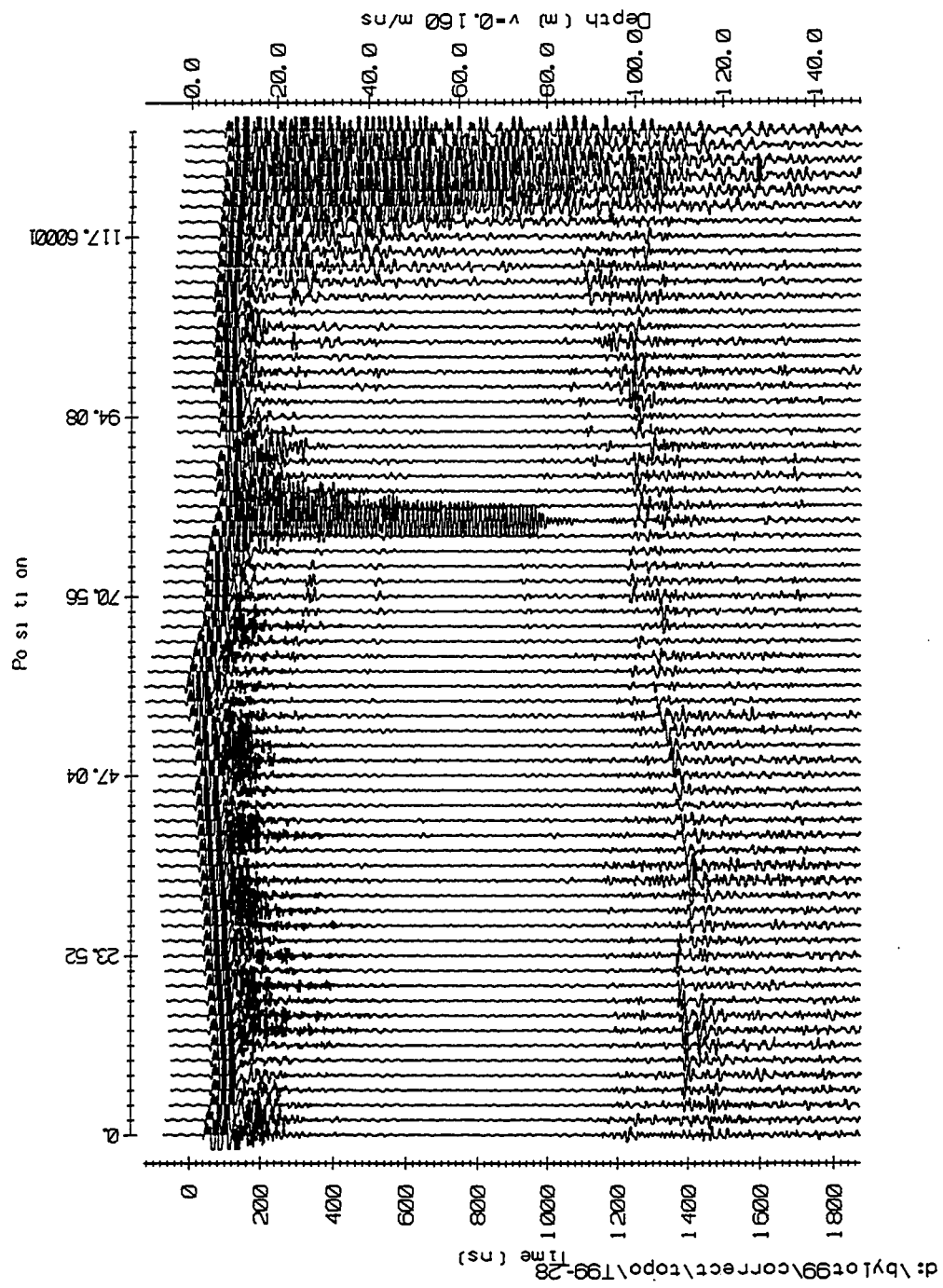


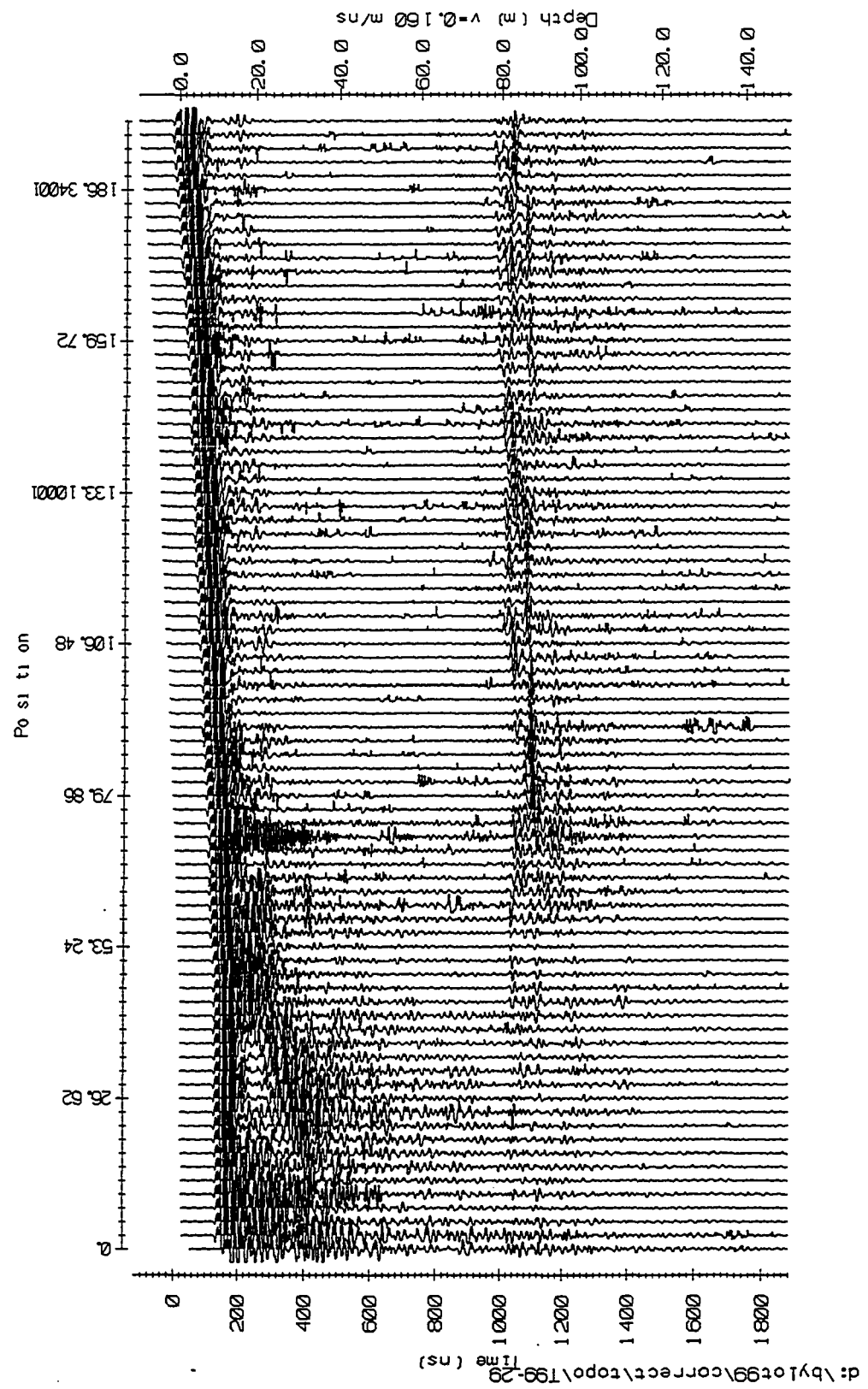


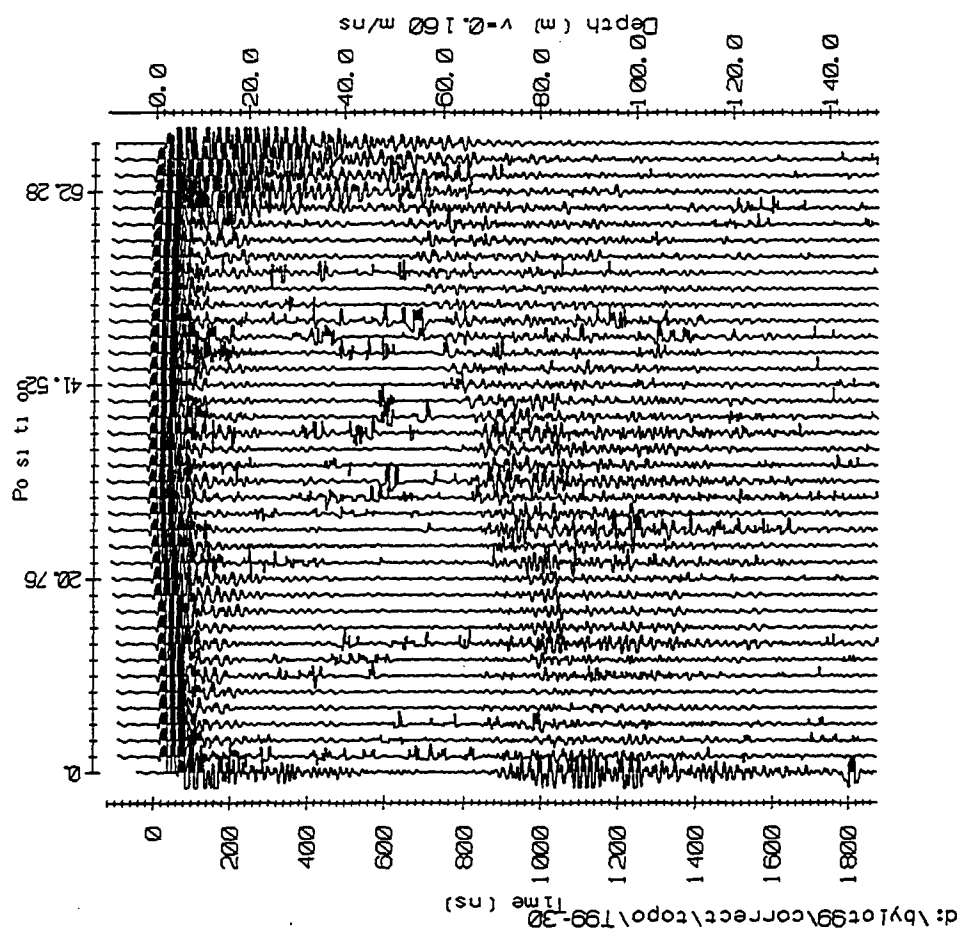


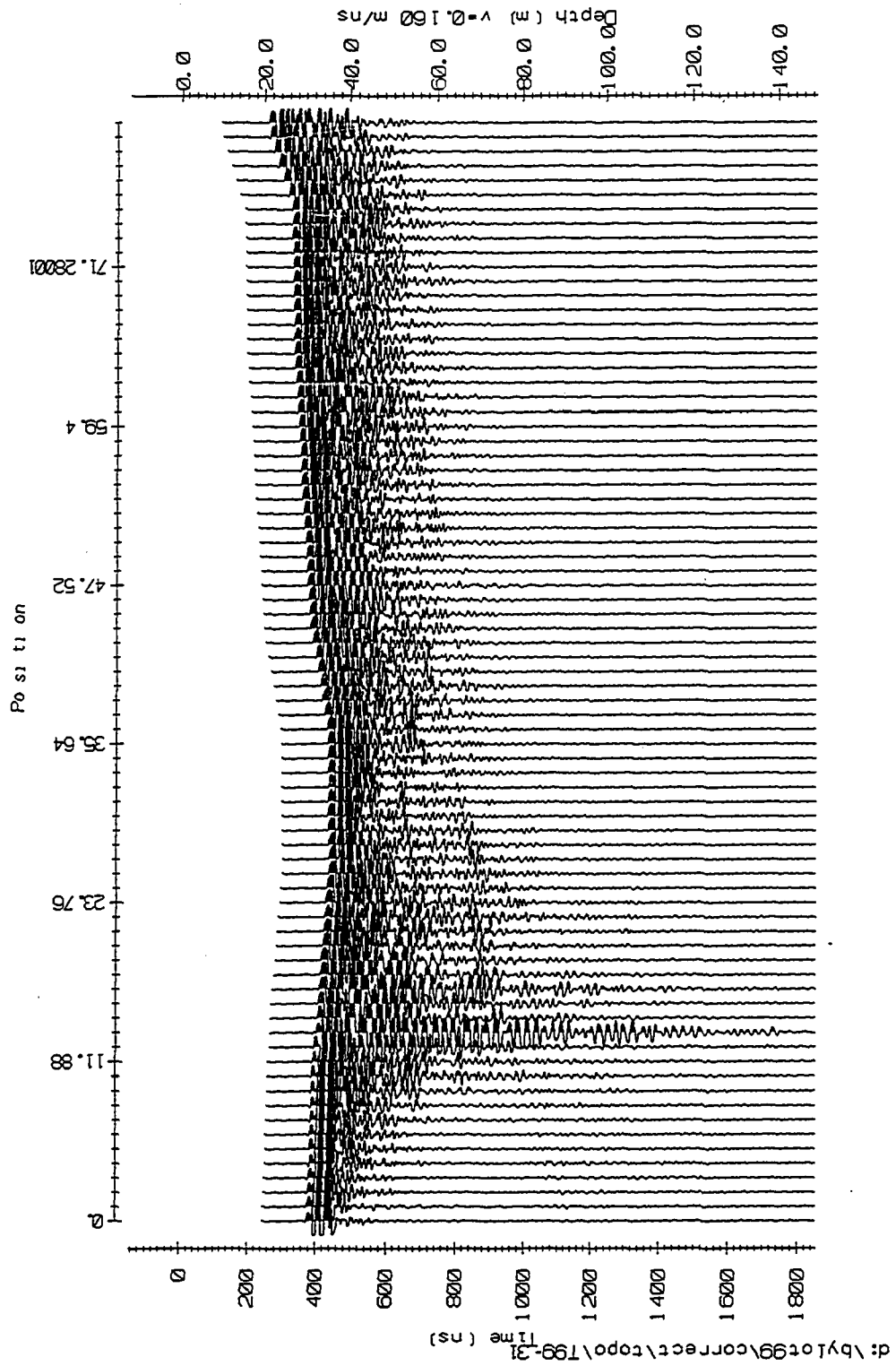


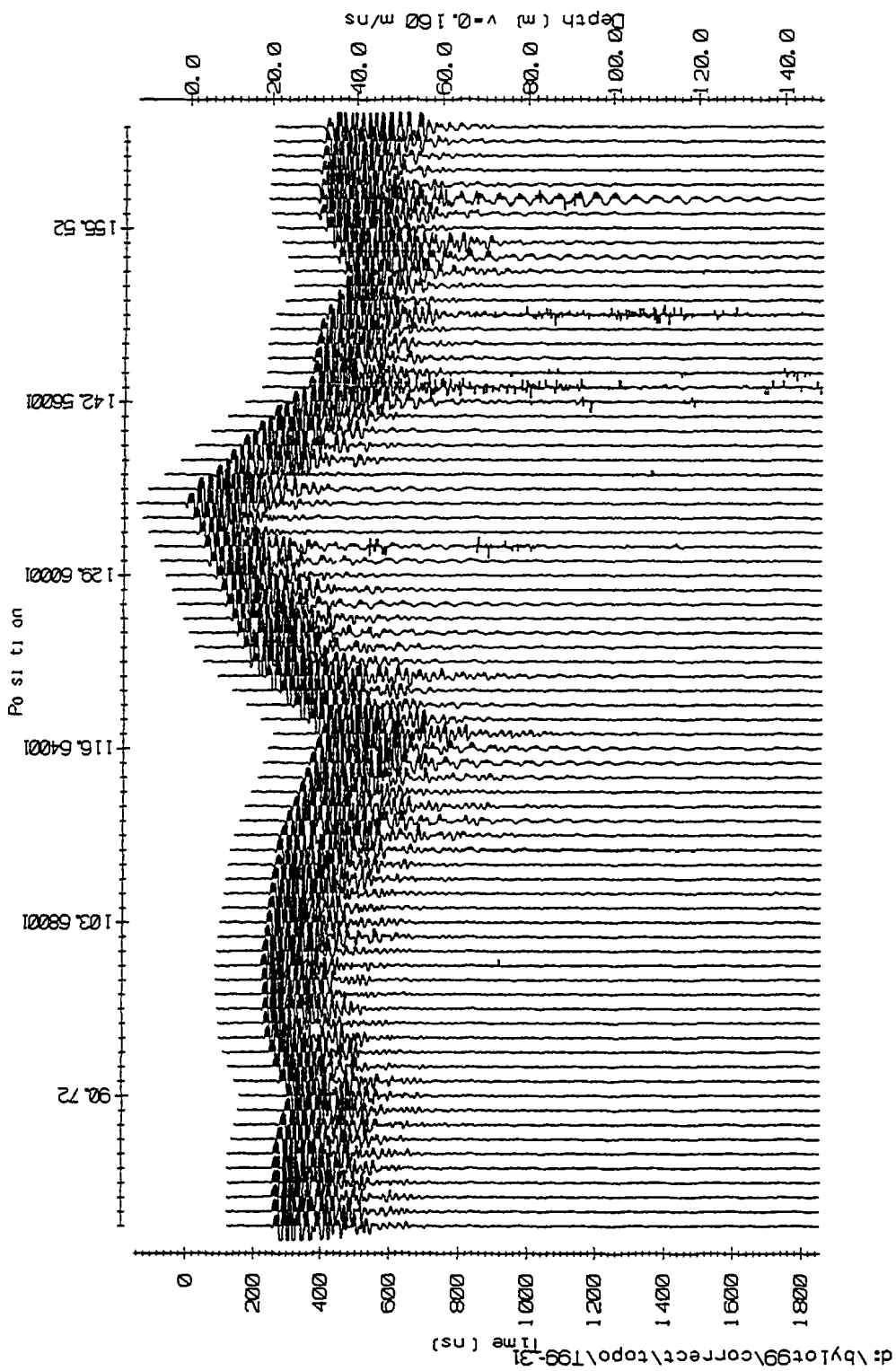


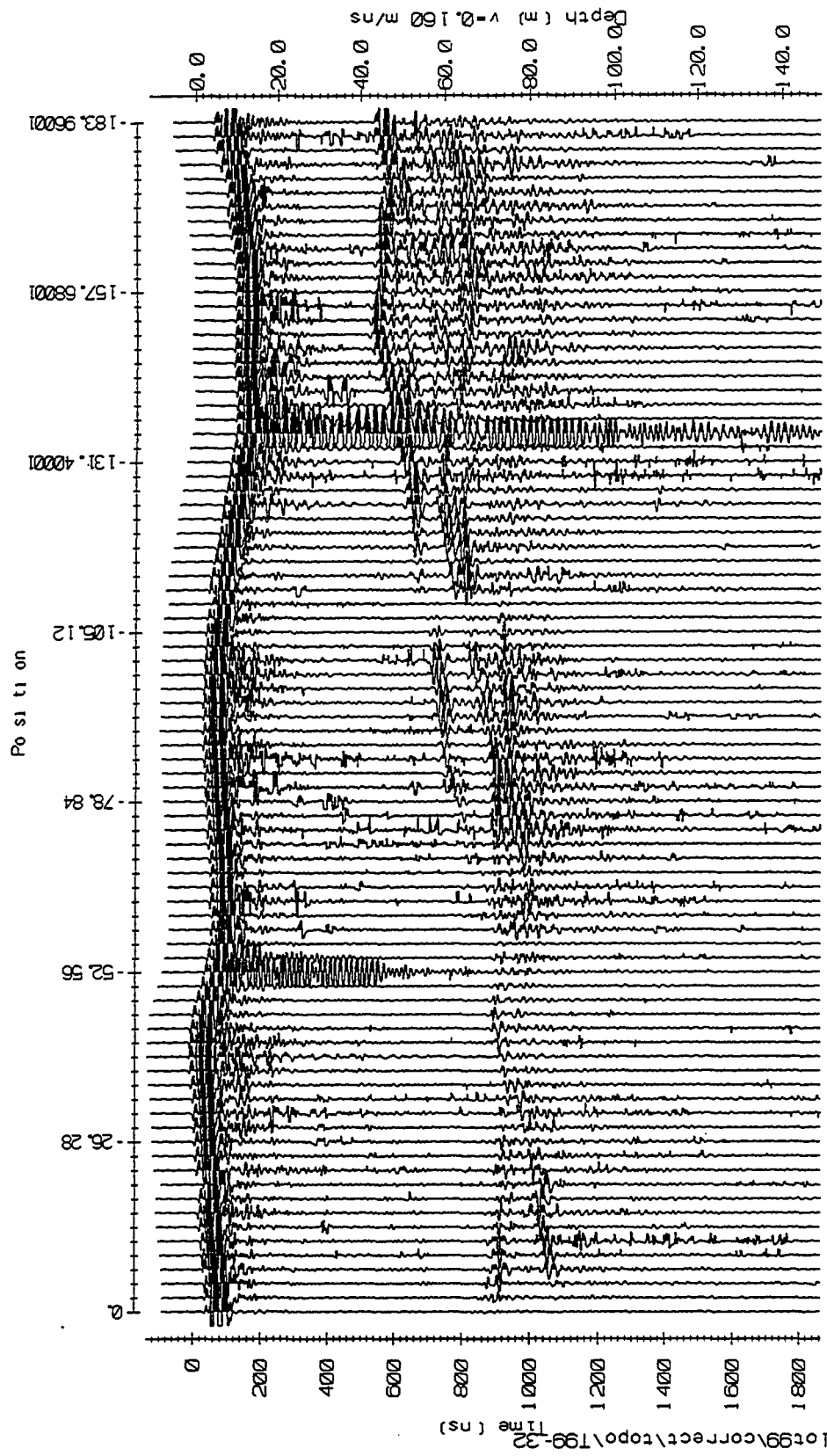




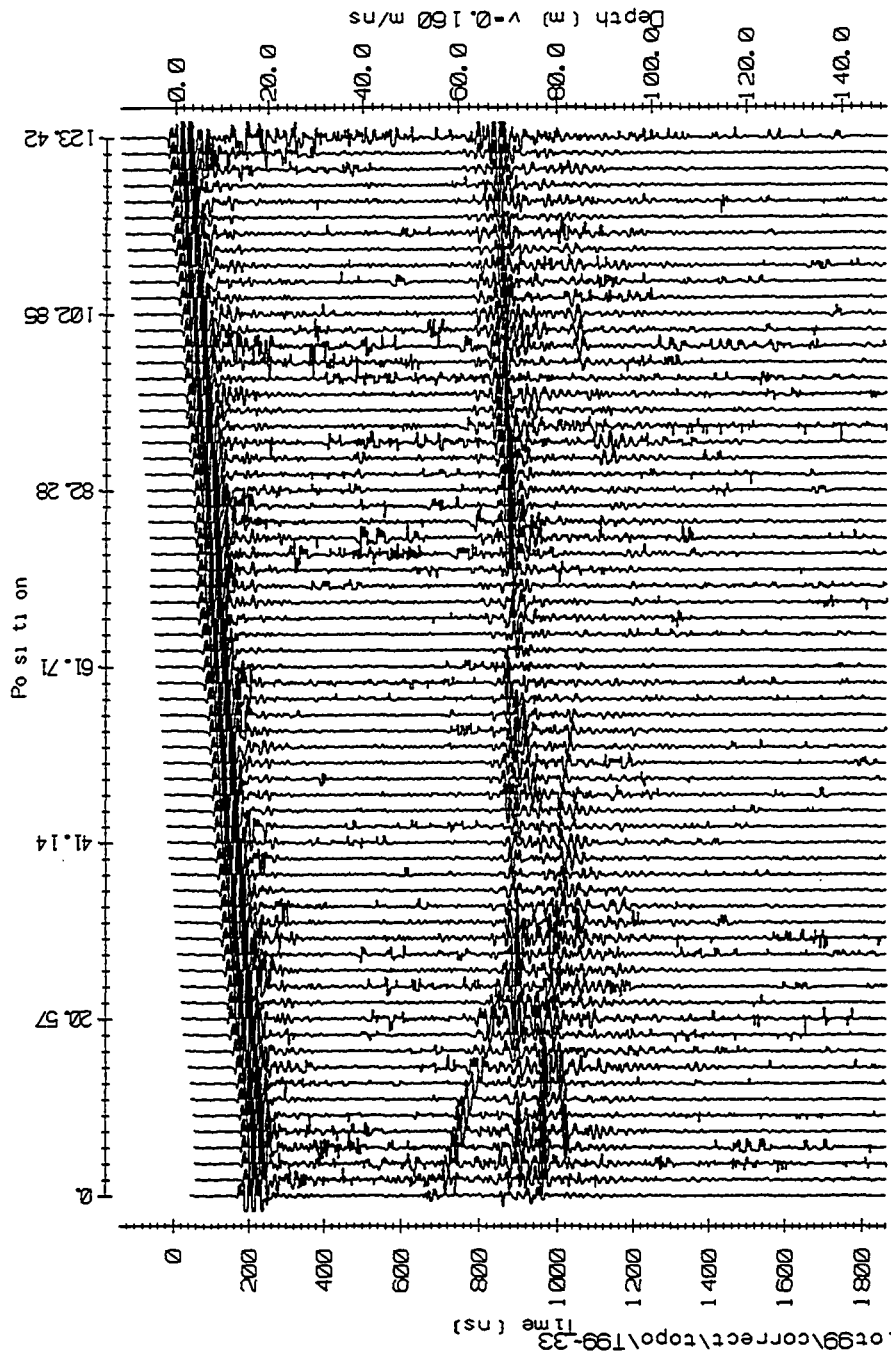




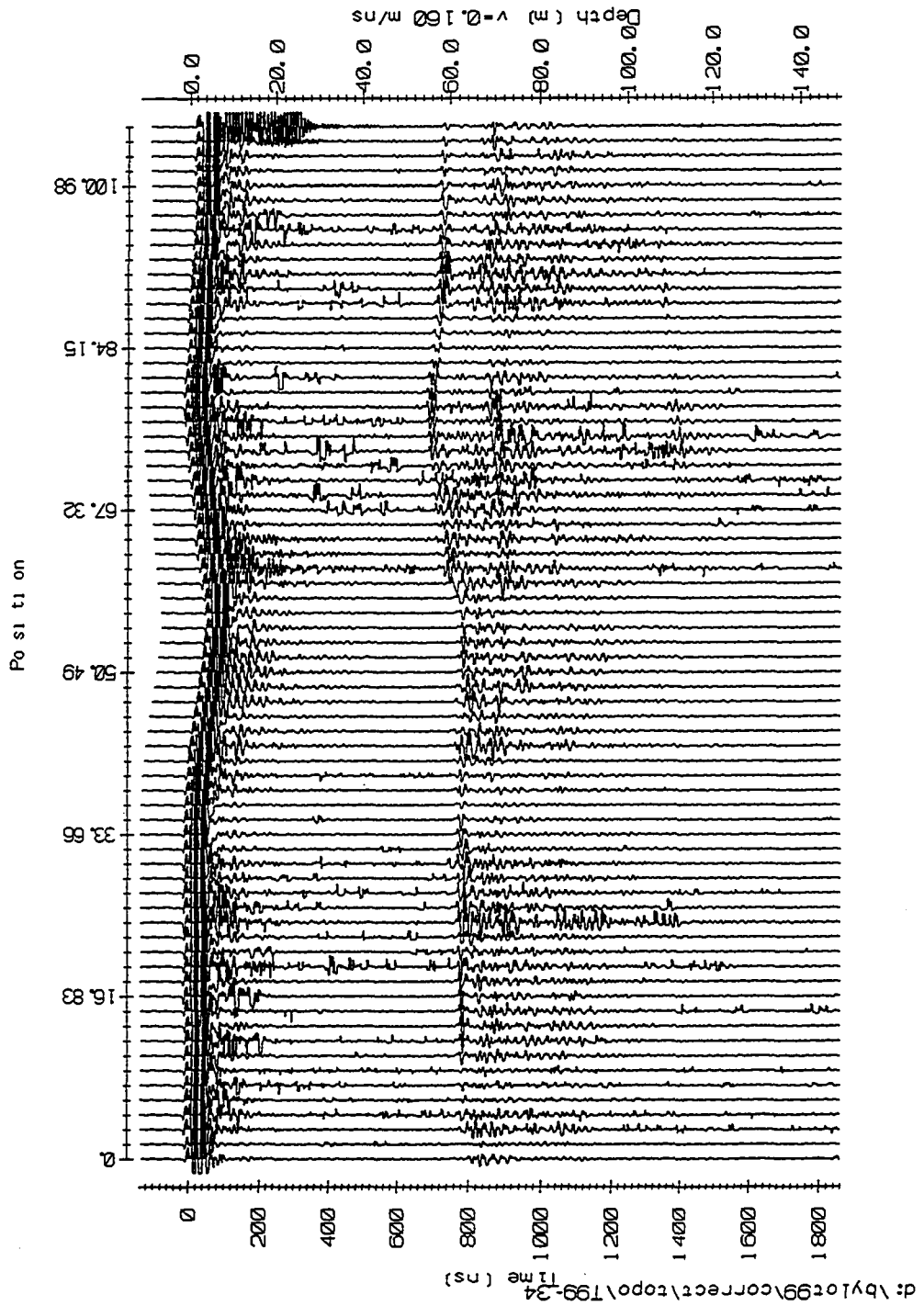


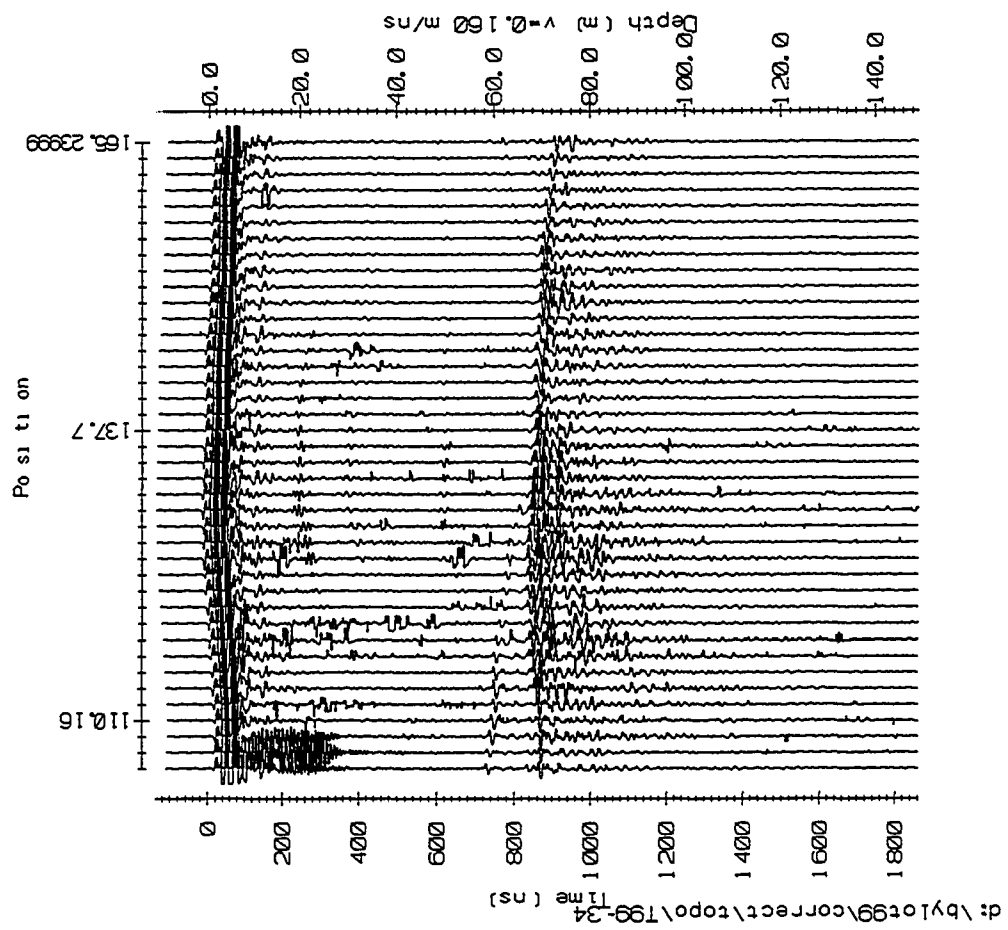


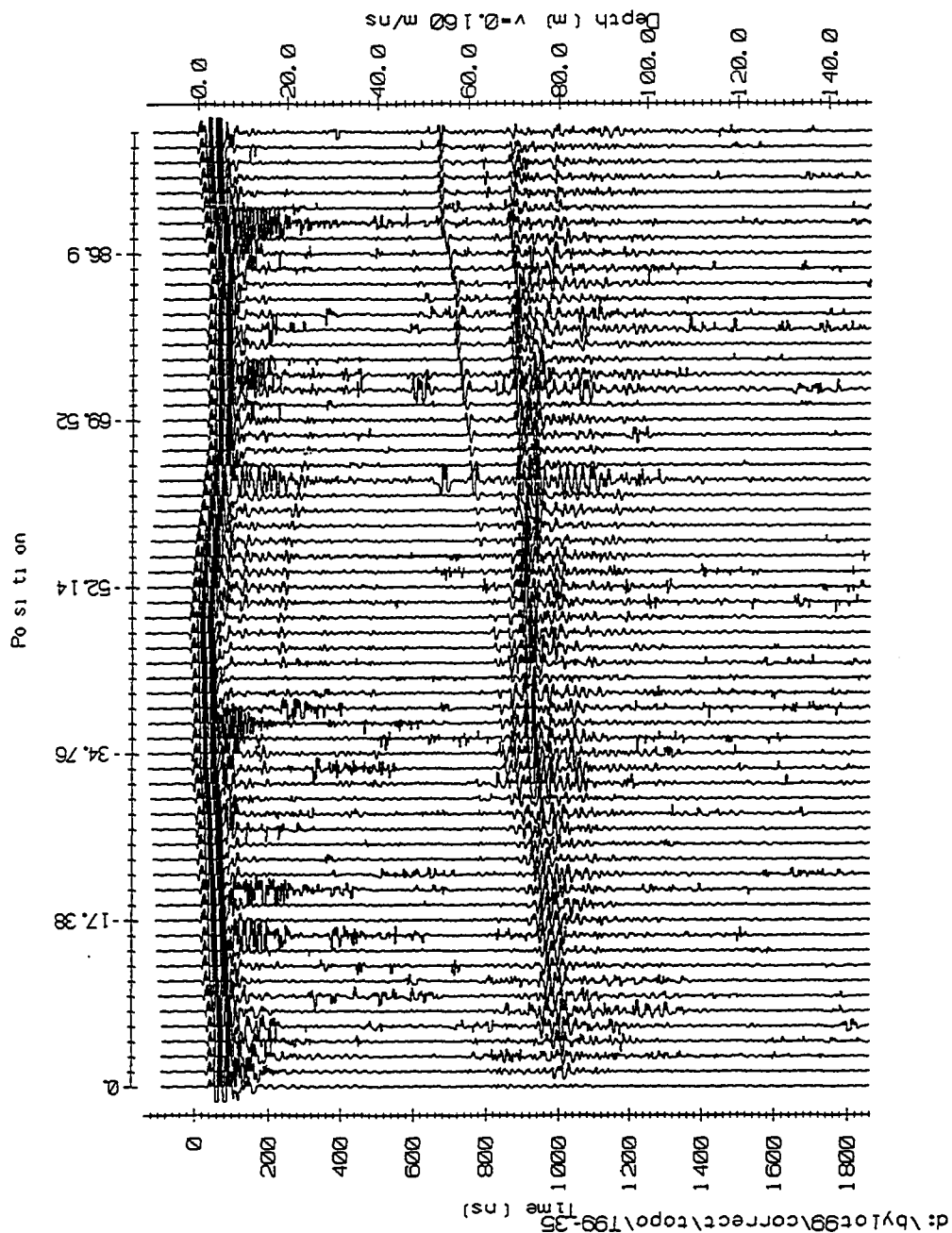
d:\bylot99\correct\topo\199-32

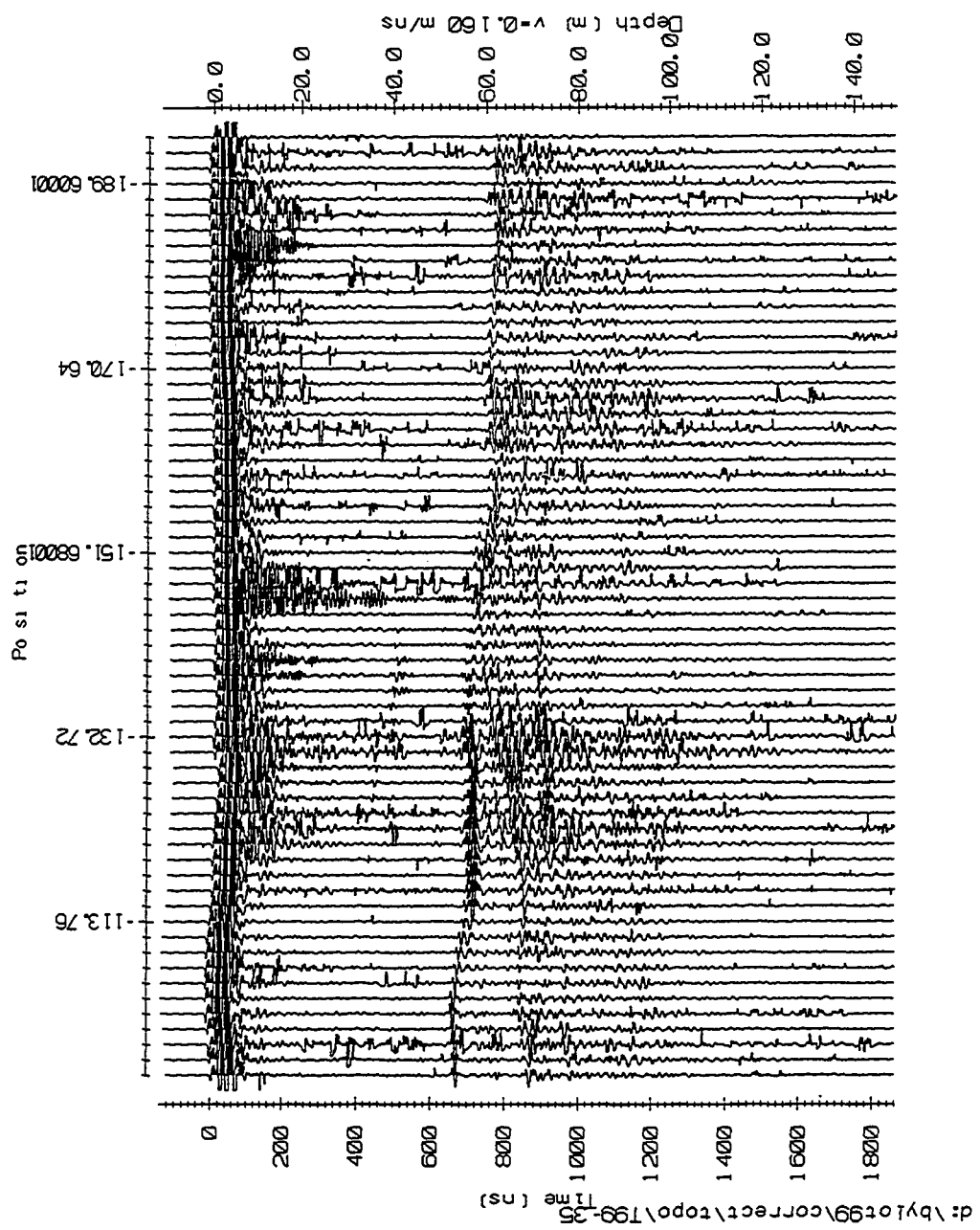


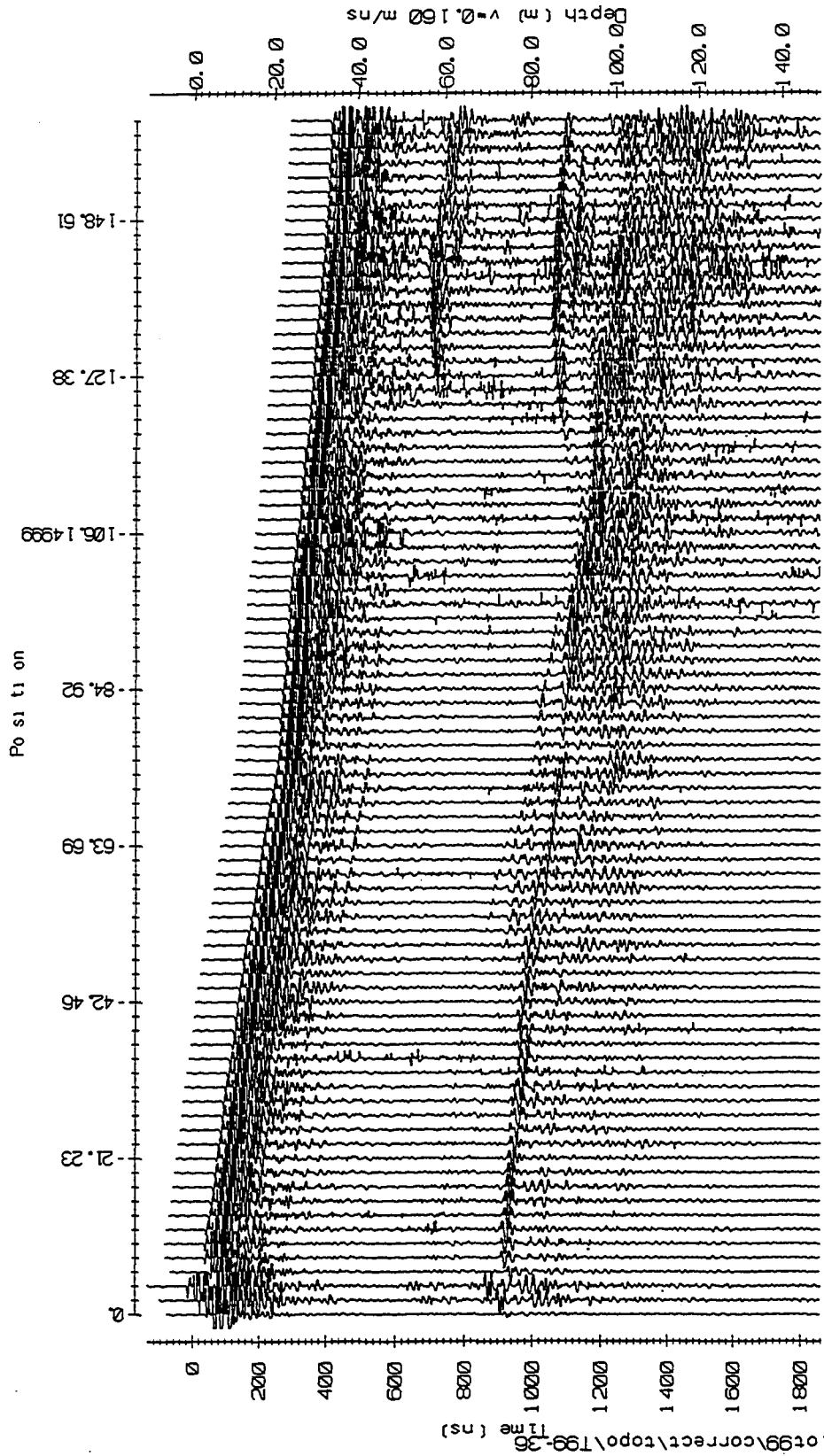
d:\bylot99\correct\topo\T99-33



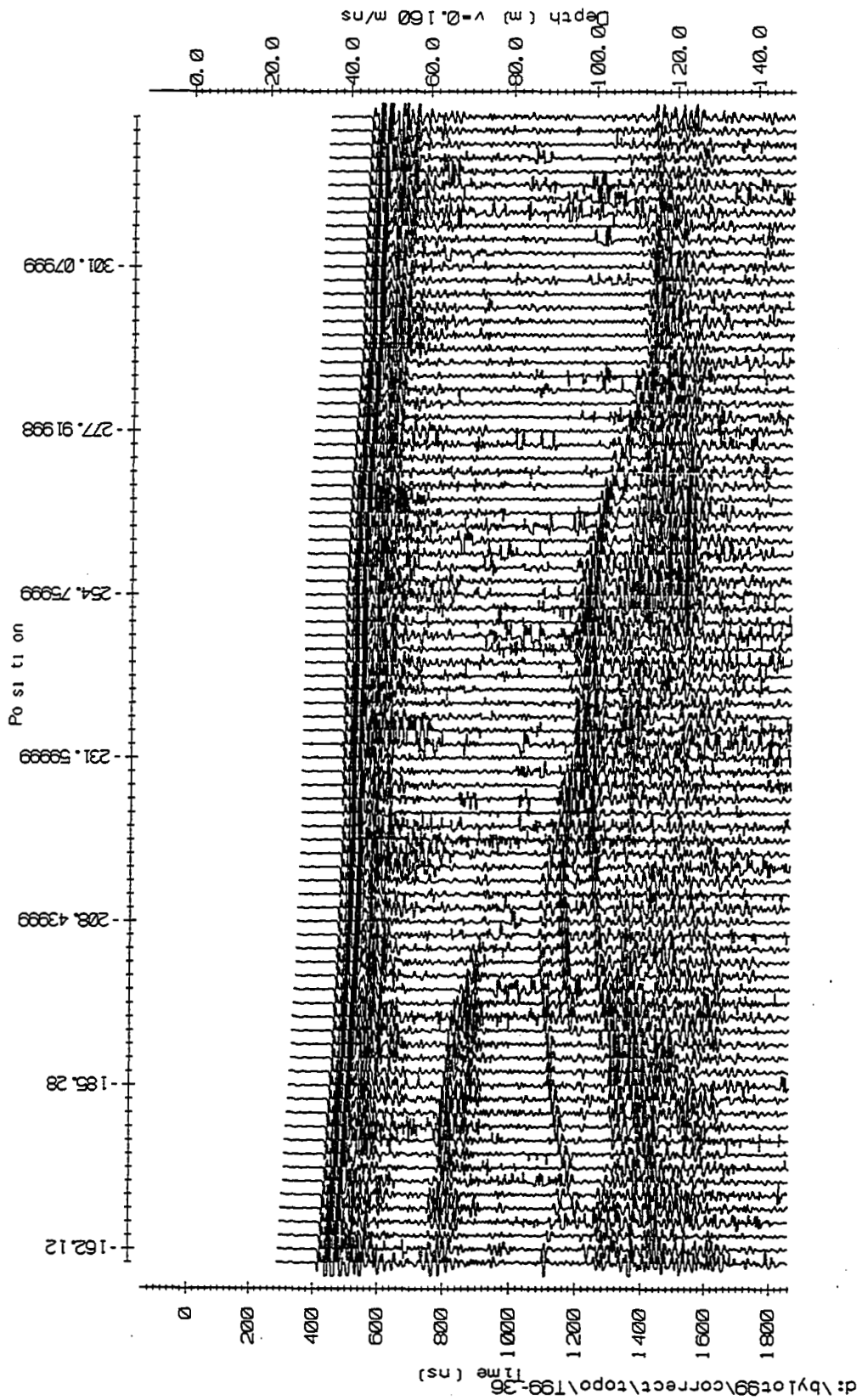


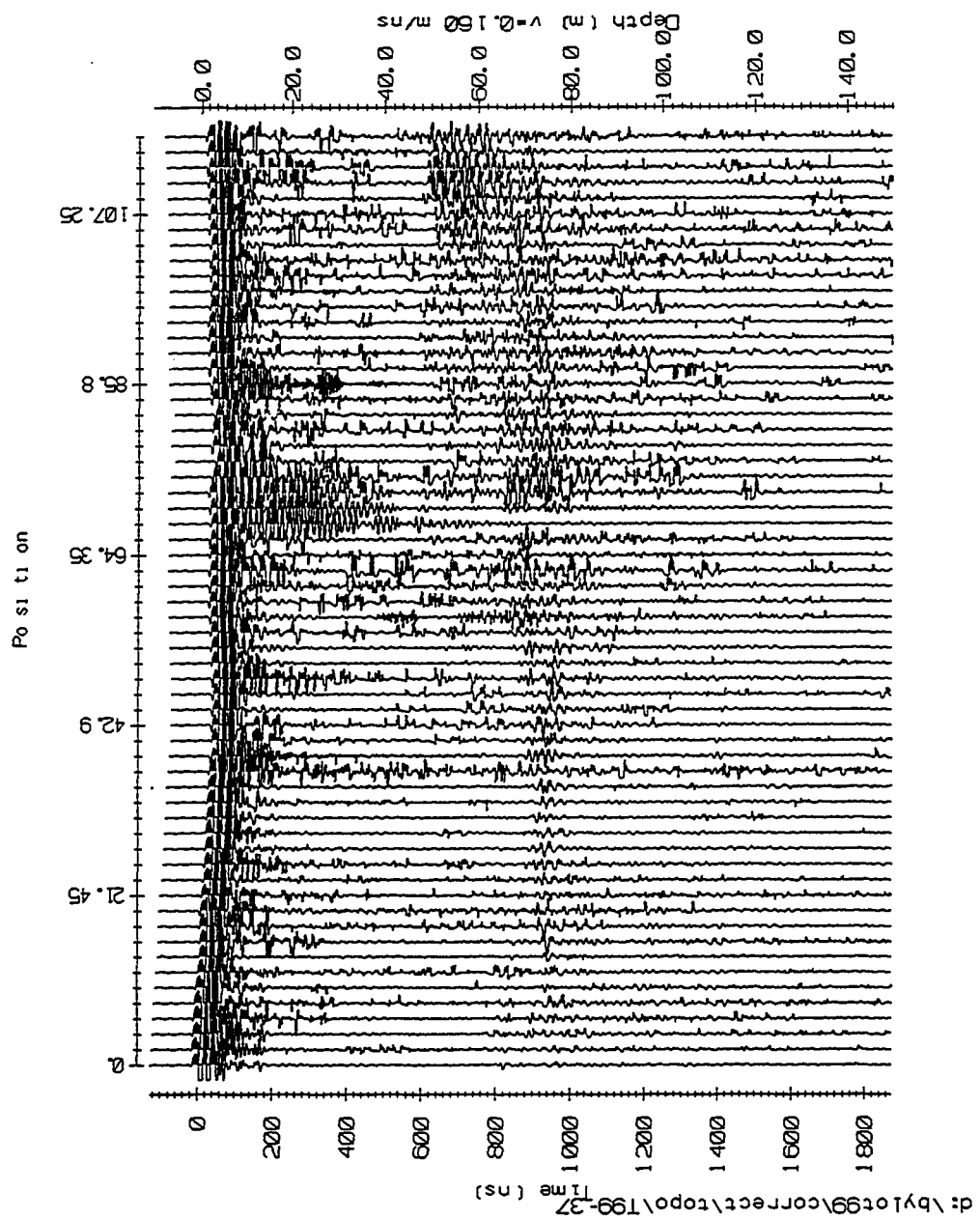


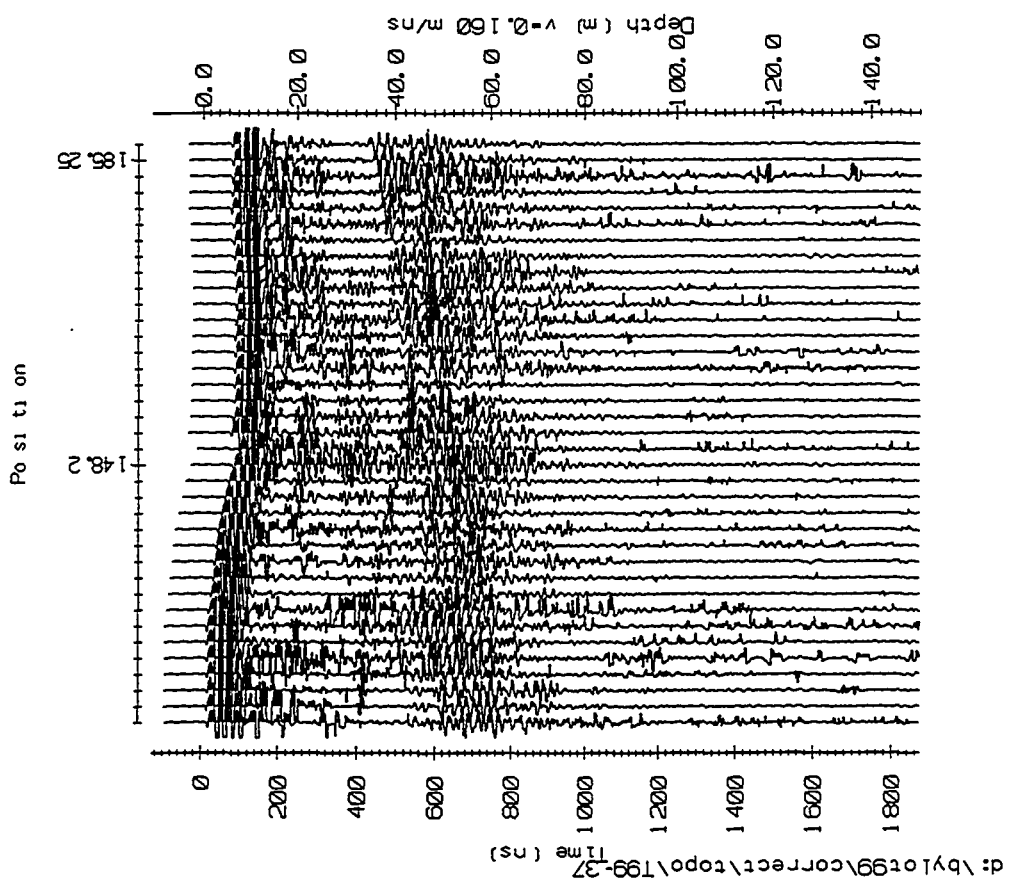


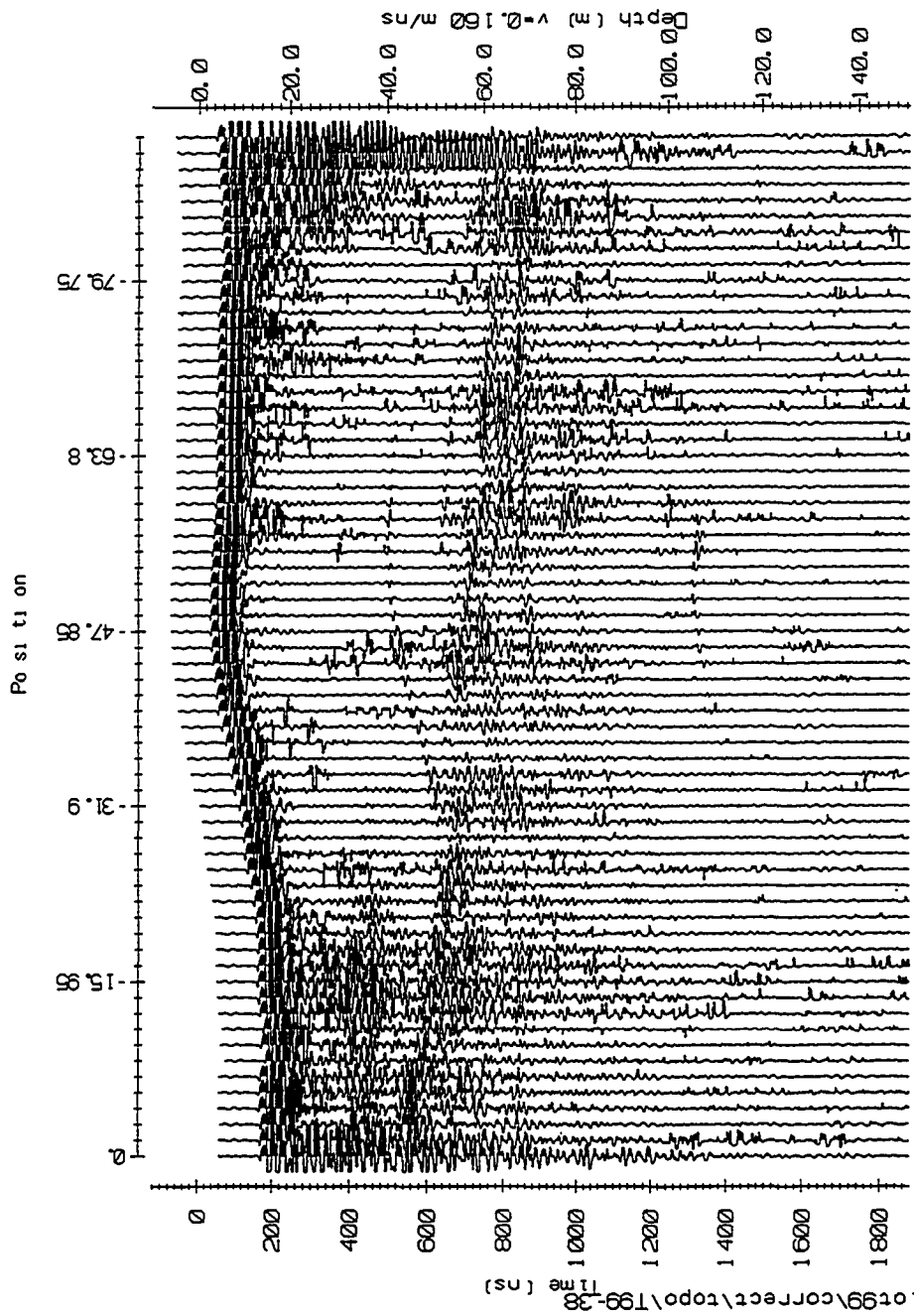


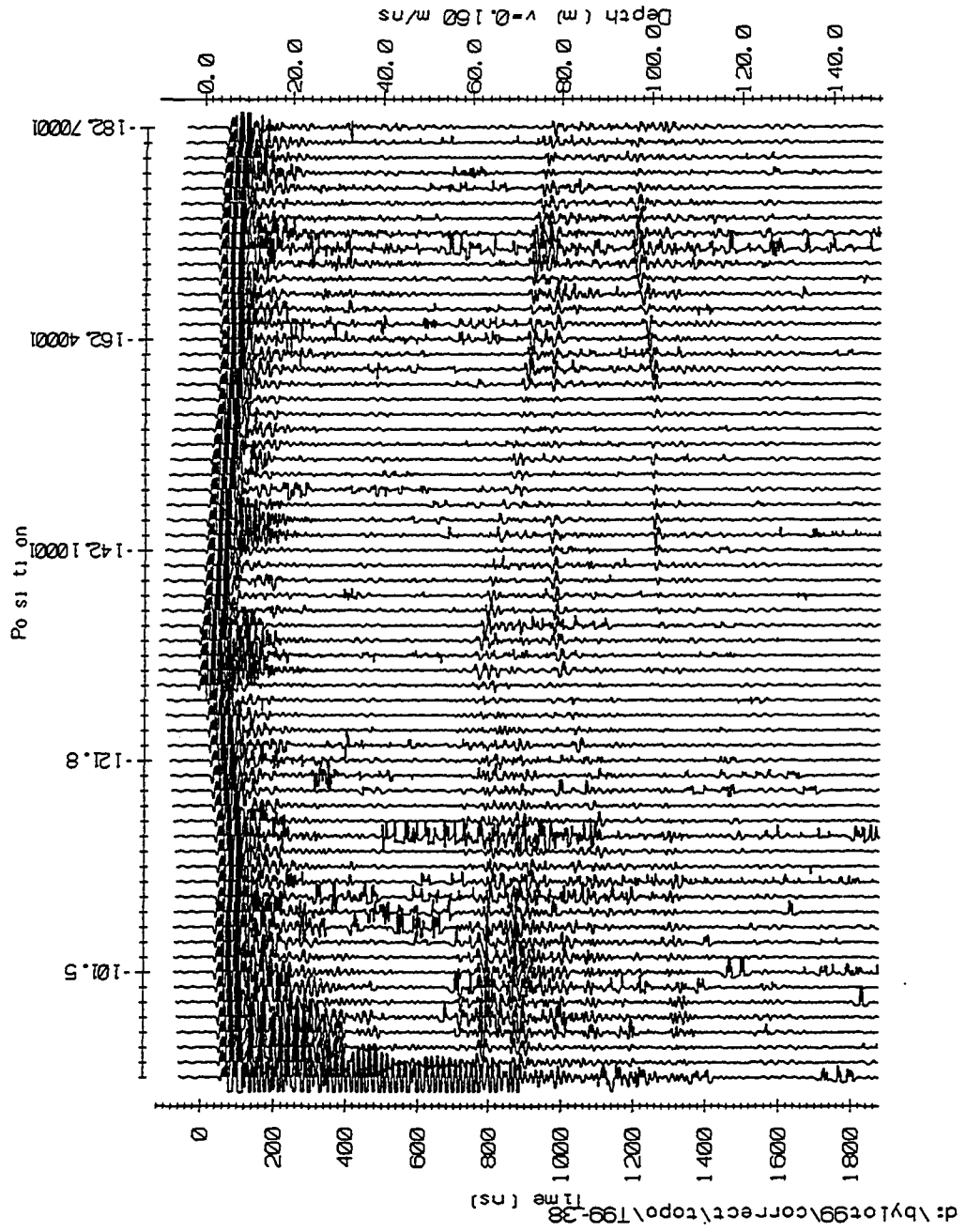
d:\bylot99\correct\topo\T99-36

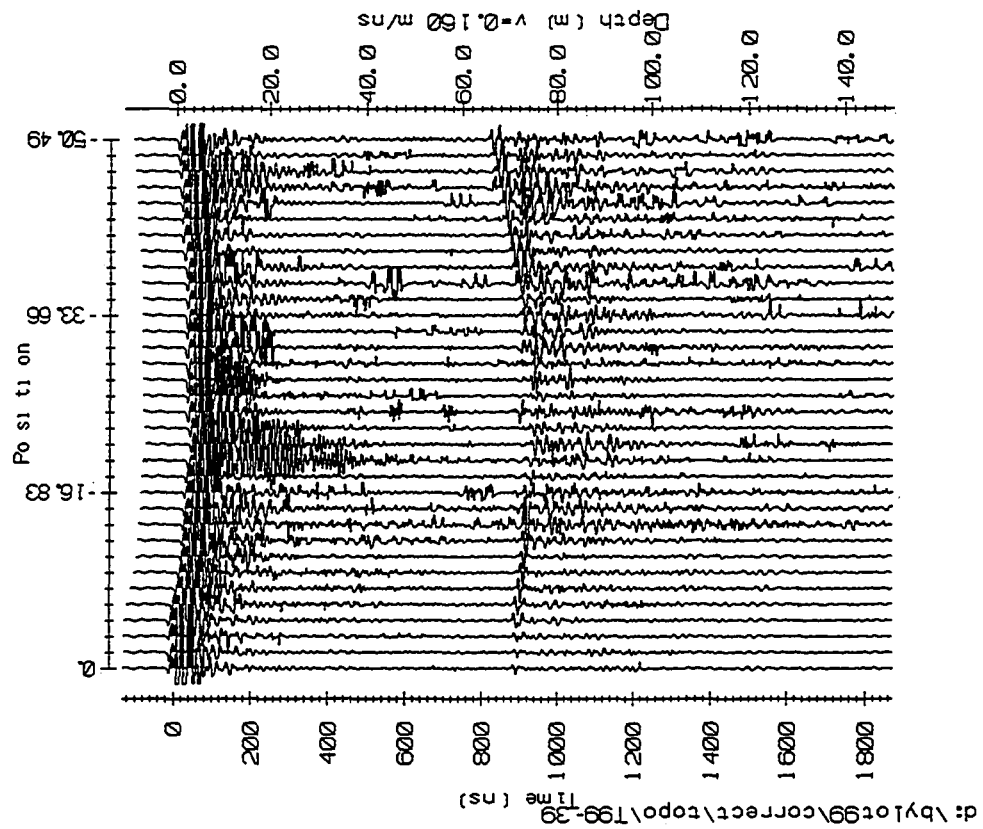


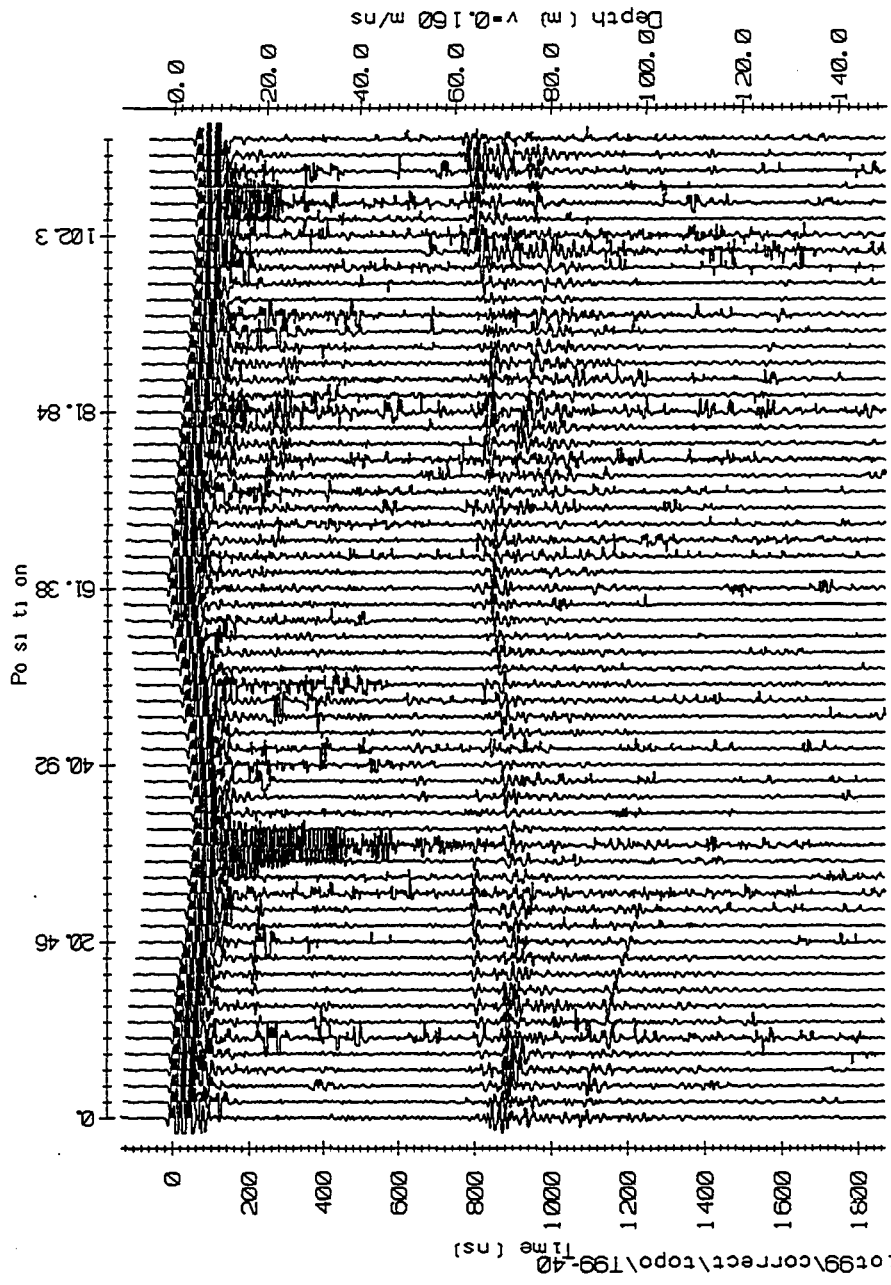






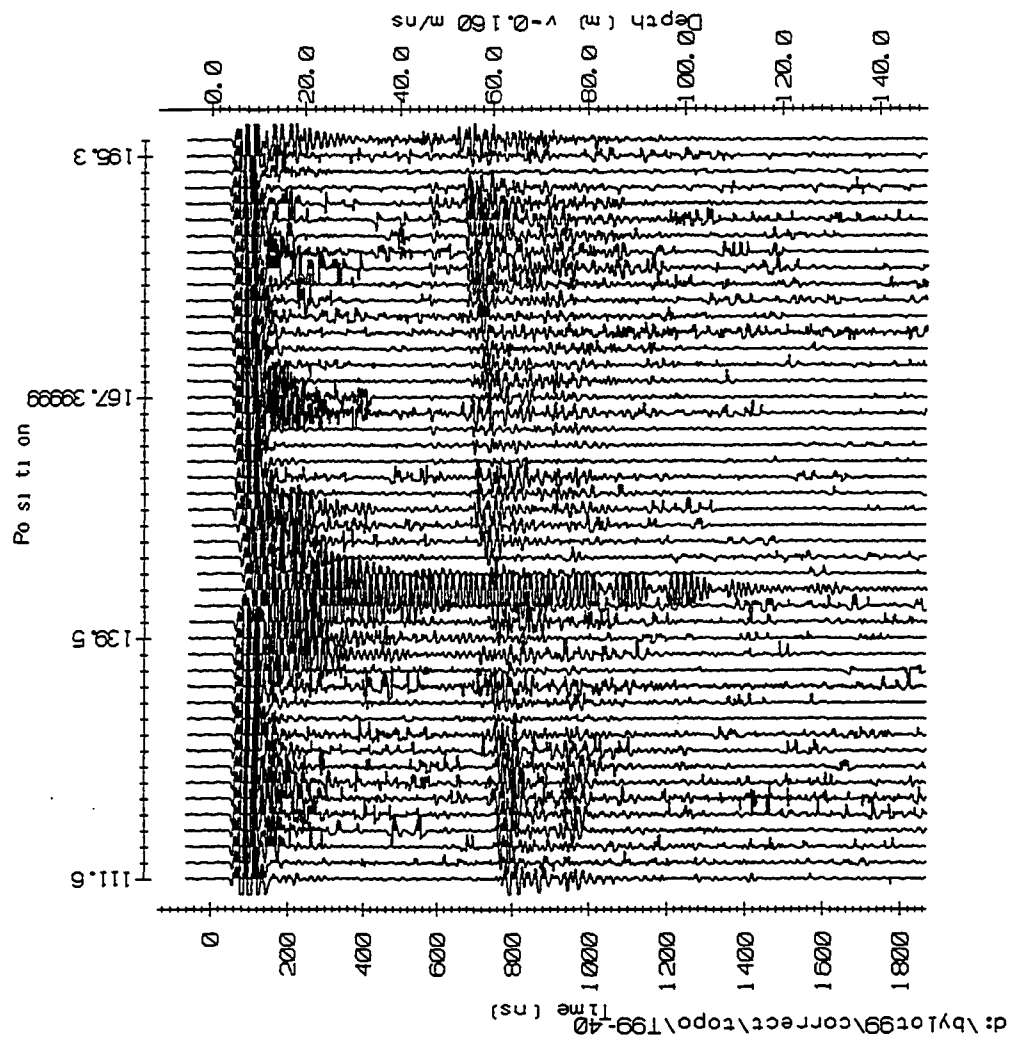






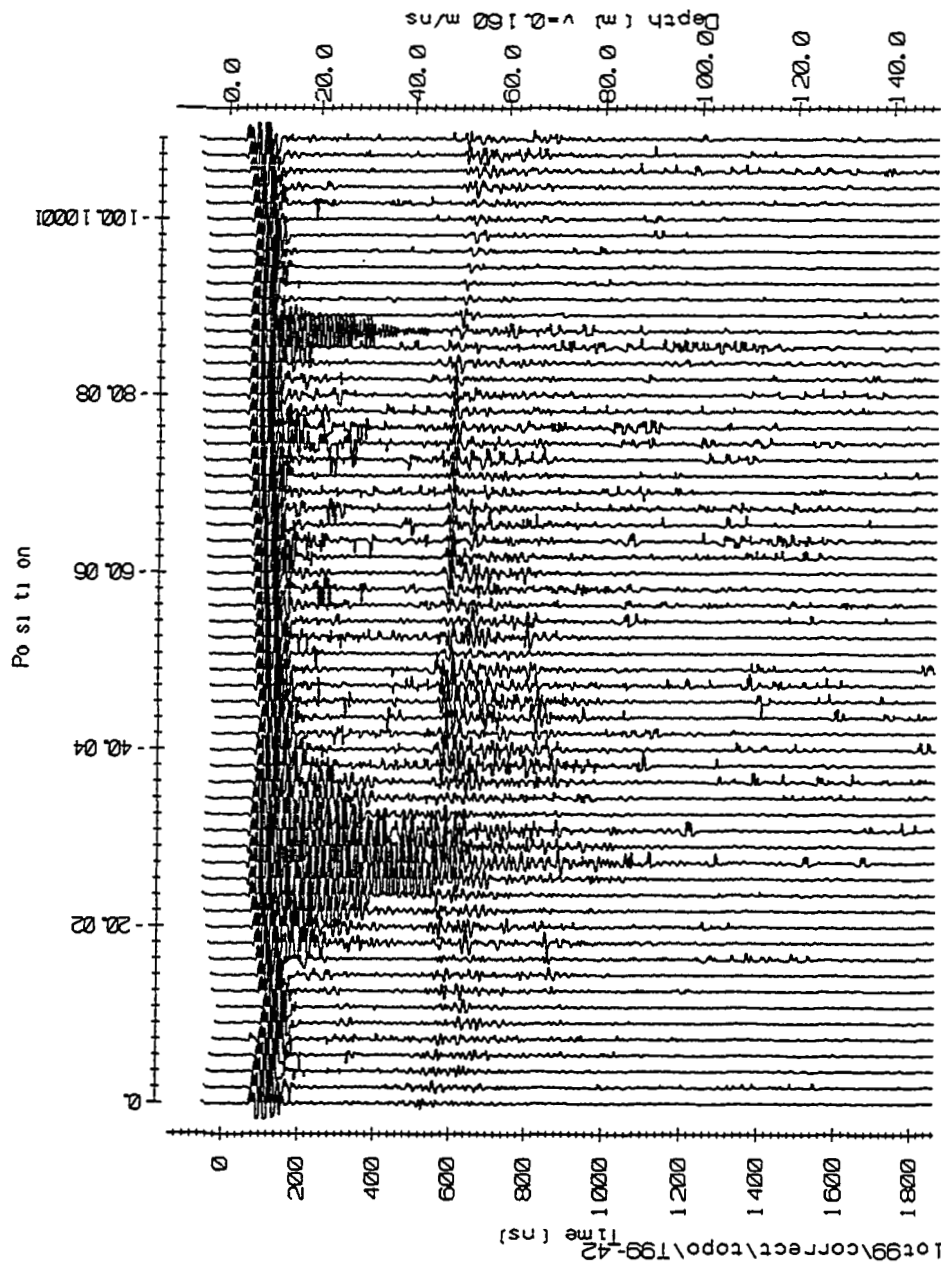
d:\bylot99\correct\topo\T99-40

Position



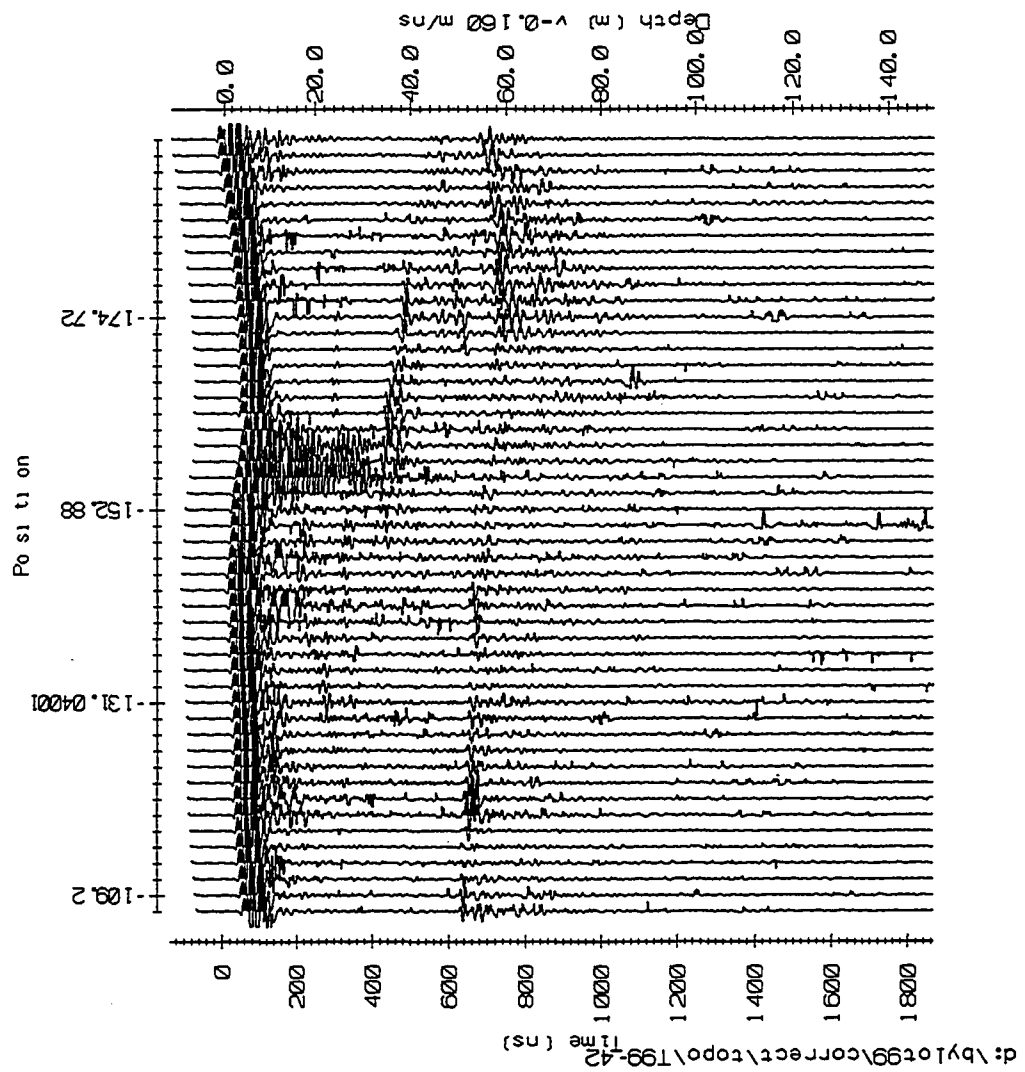
d:\bylot99\correct\topo\T99-40

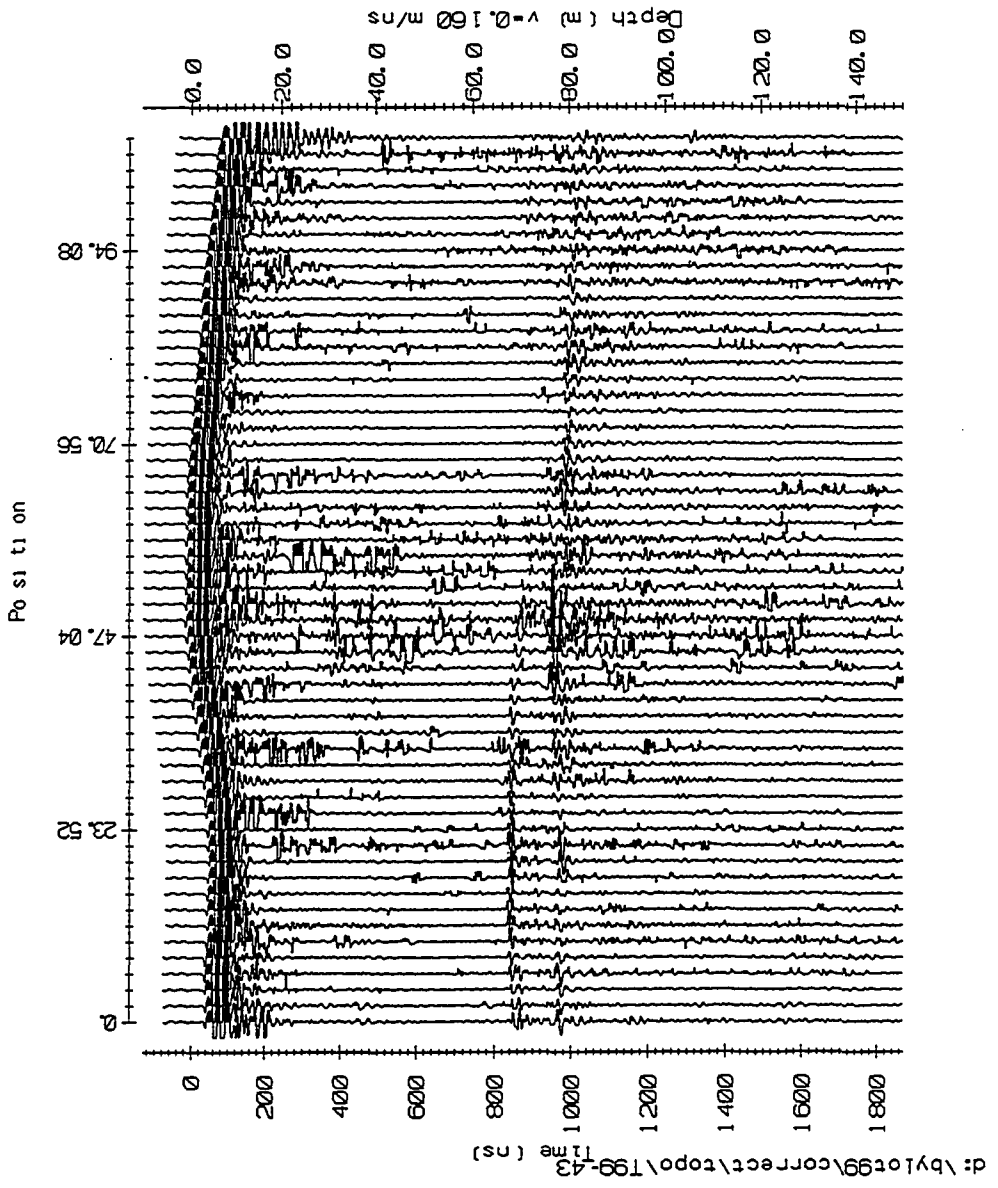
Position

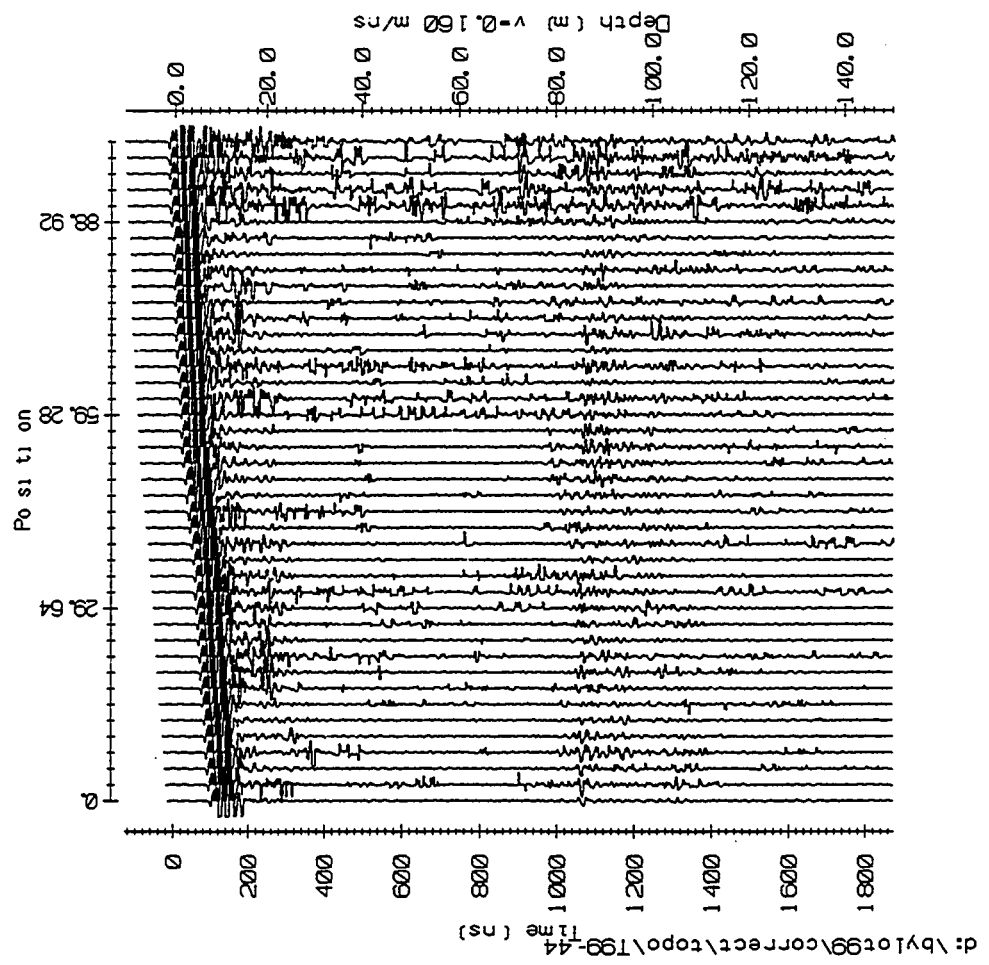


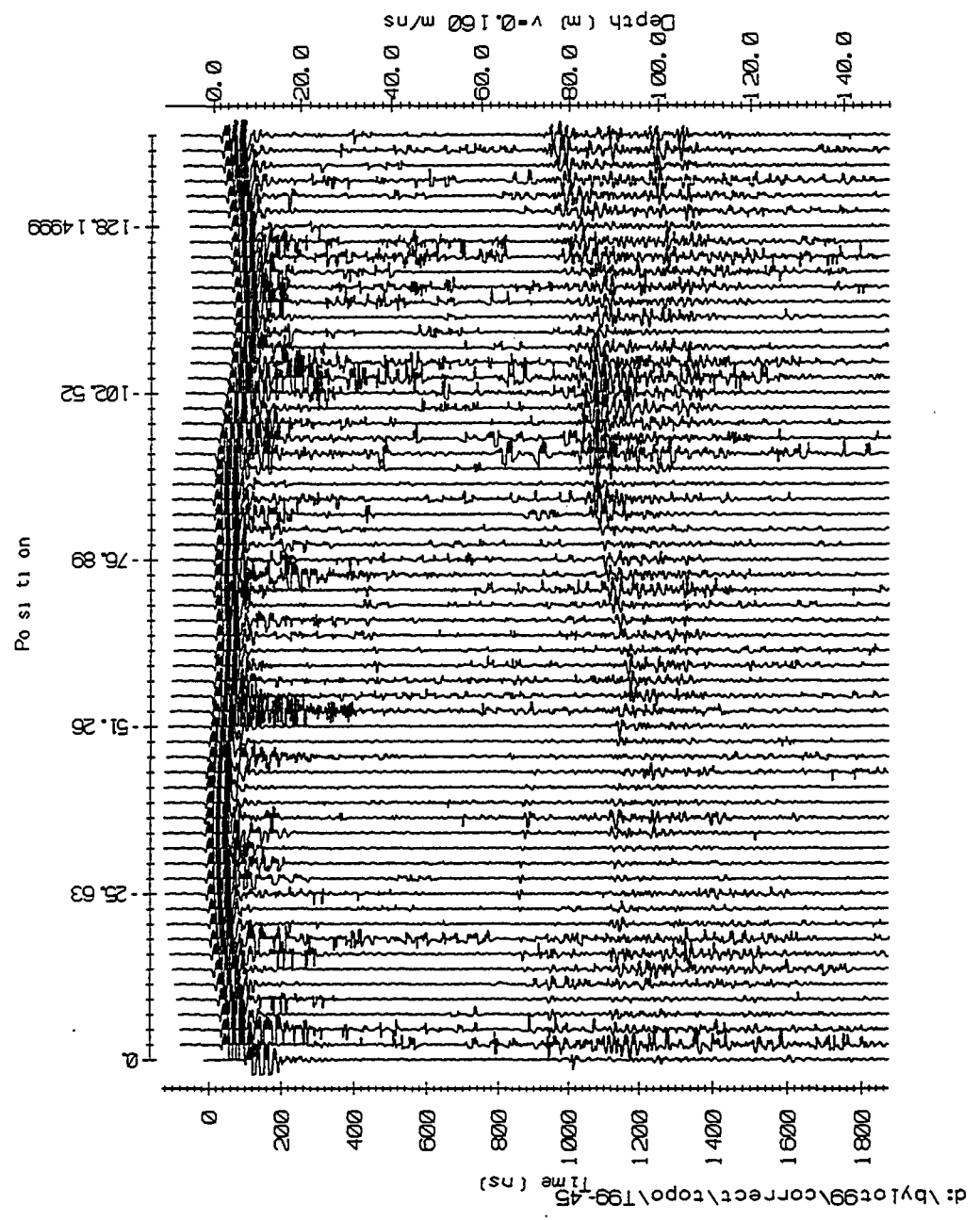
d:\bylot9\correct\topo\T99-42

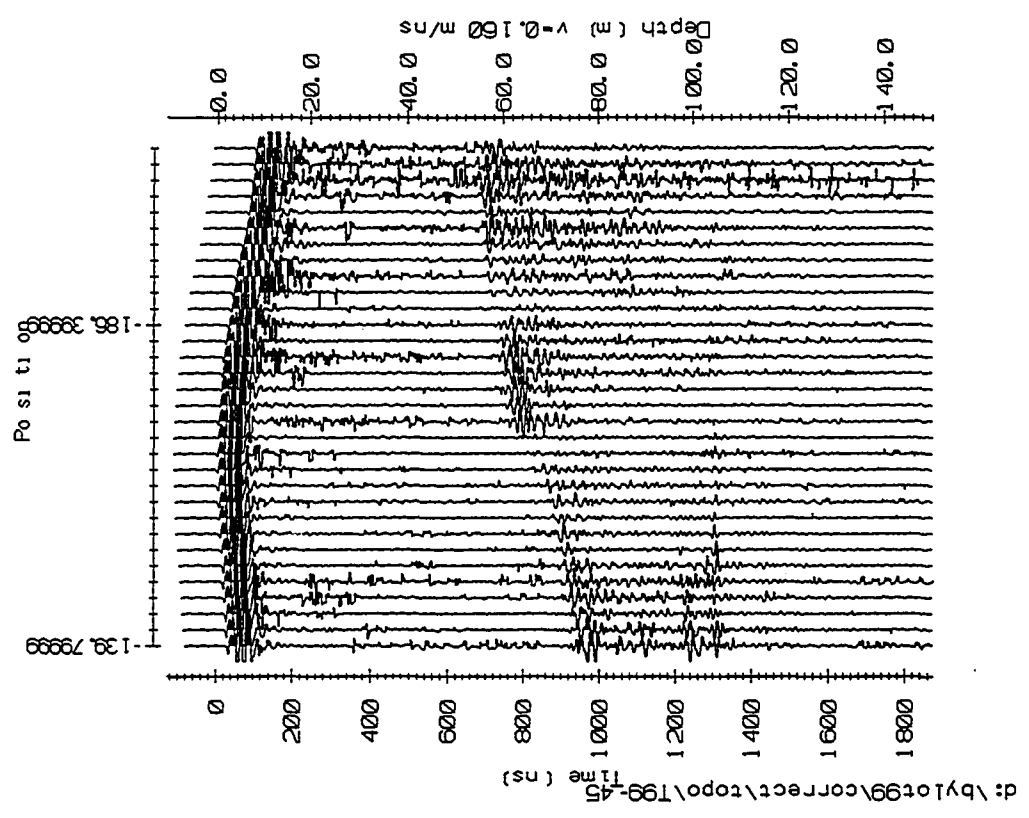
Position

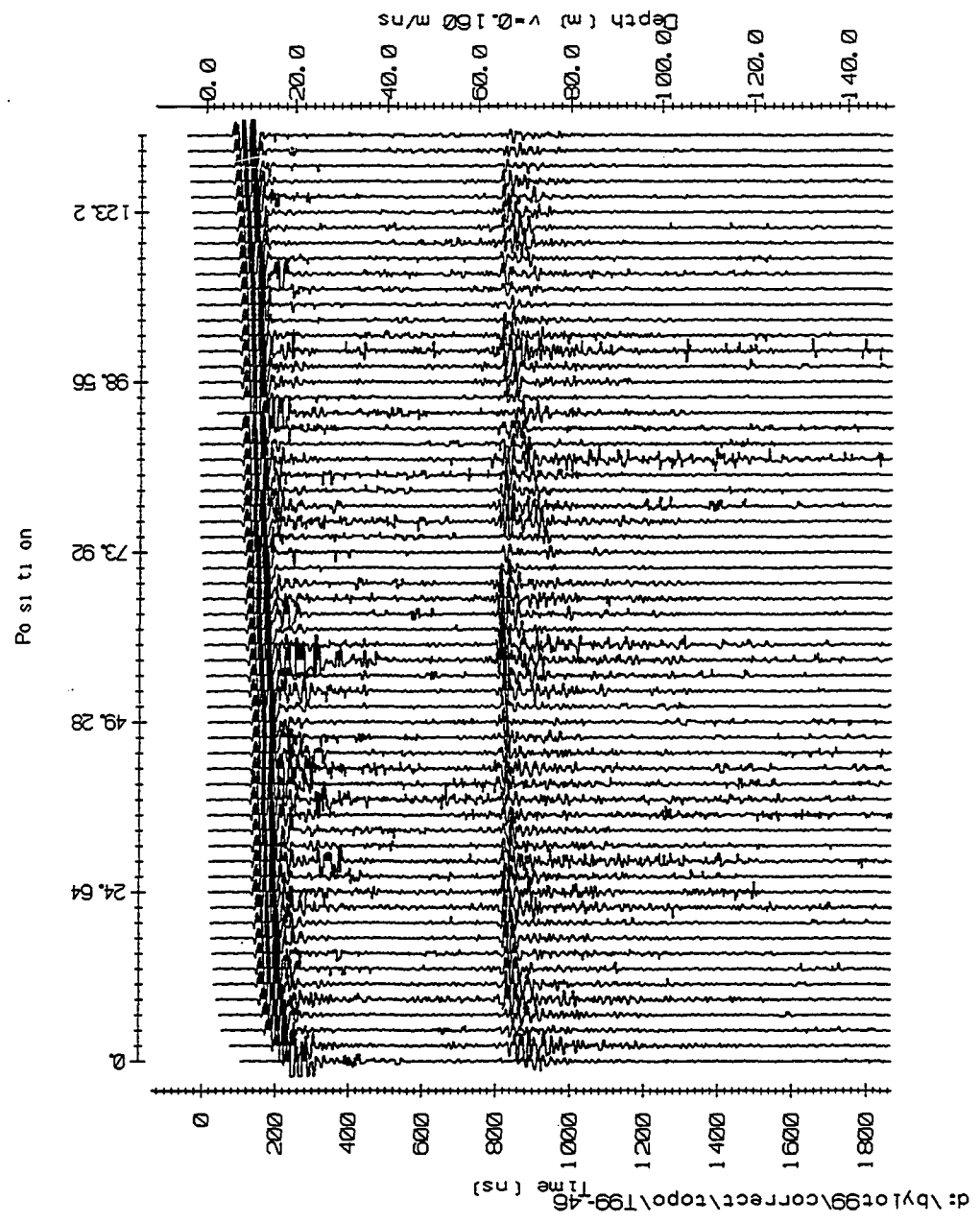




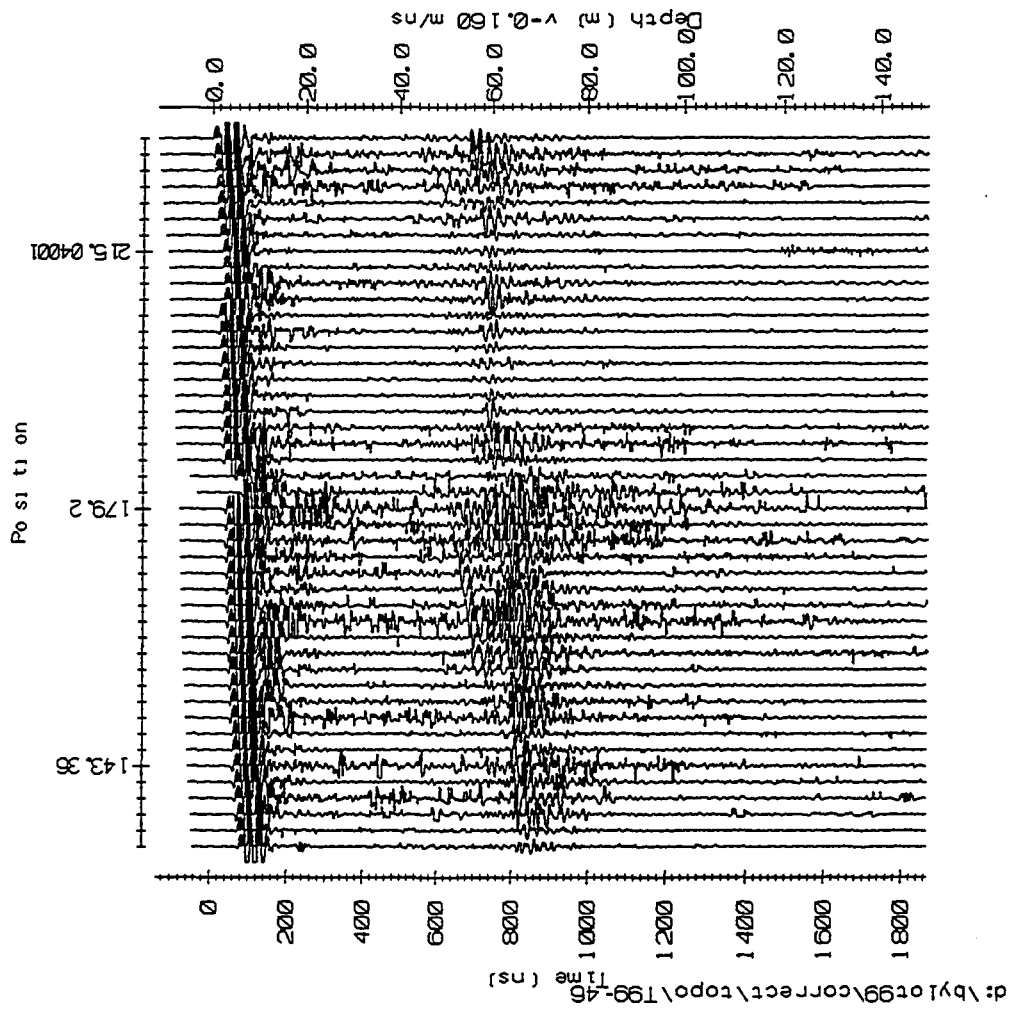


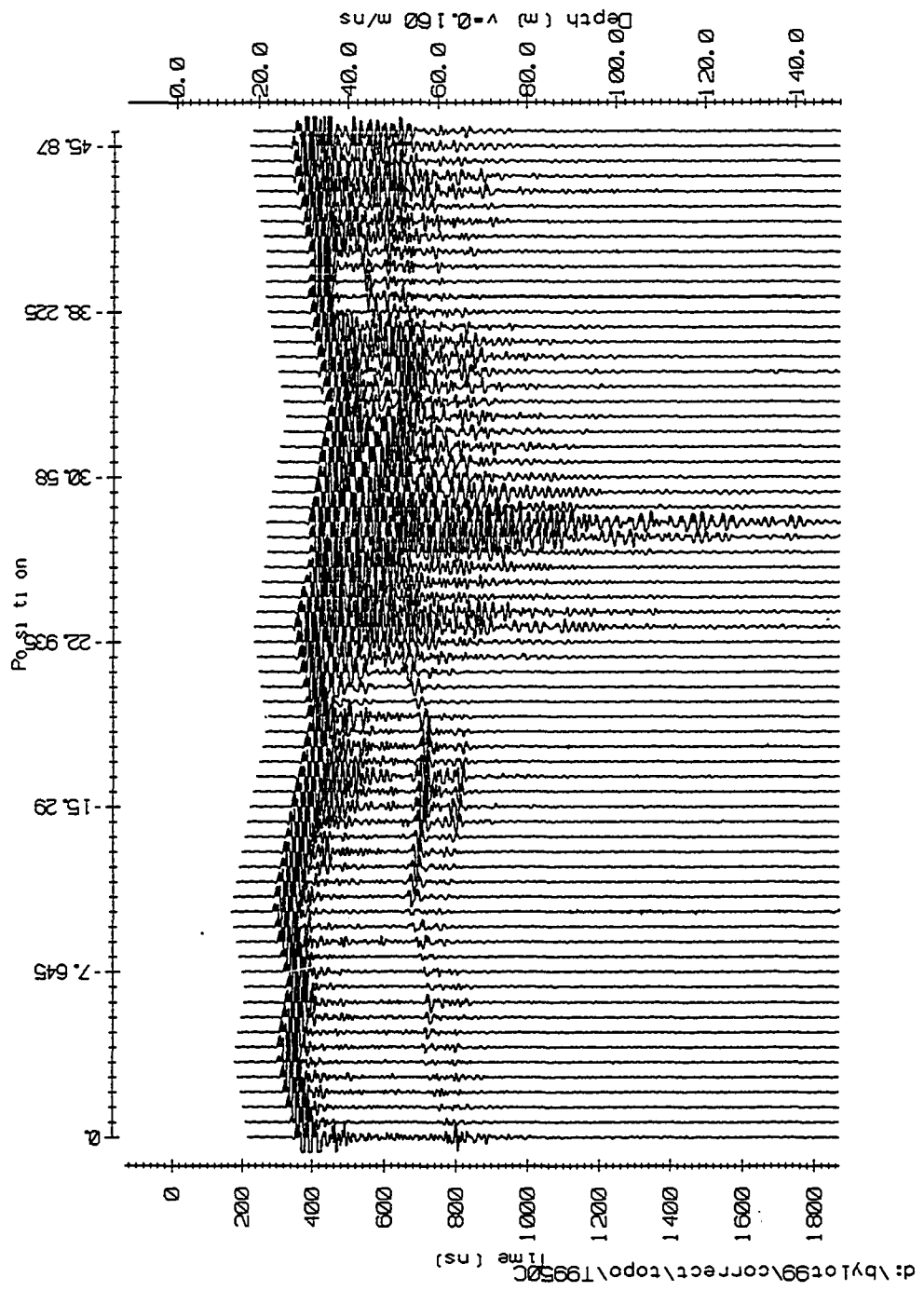


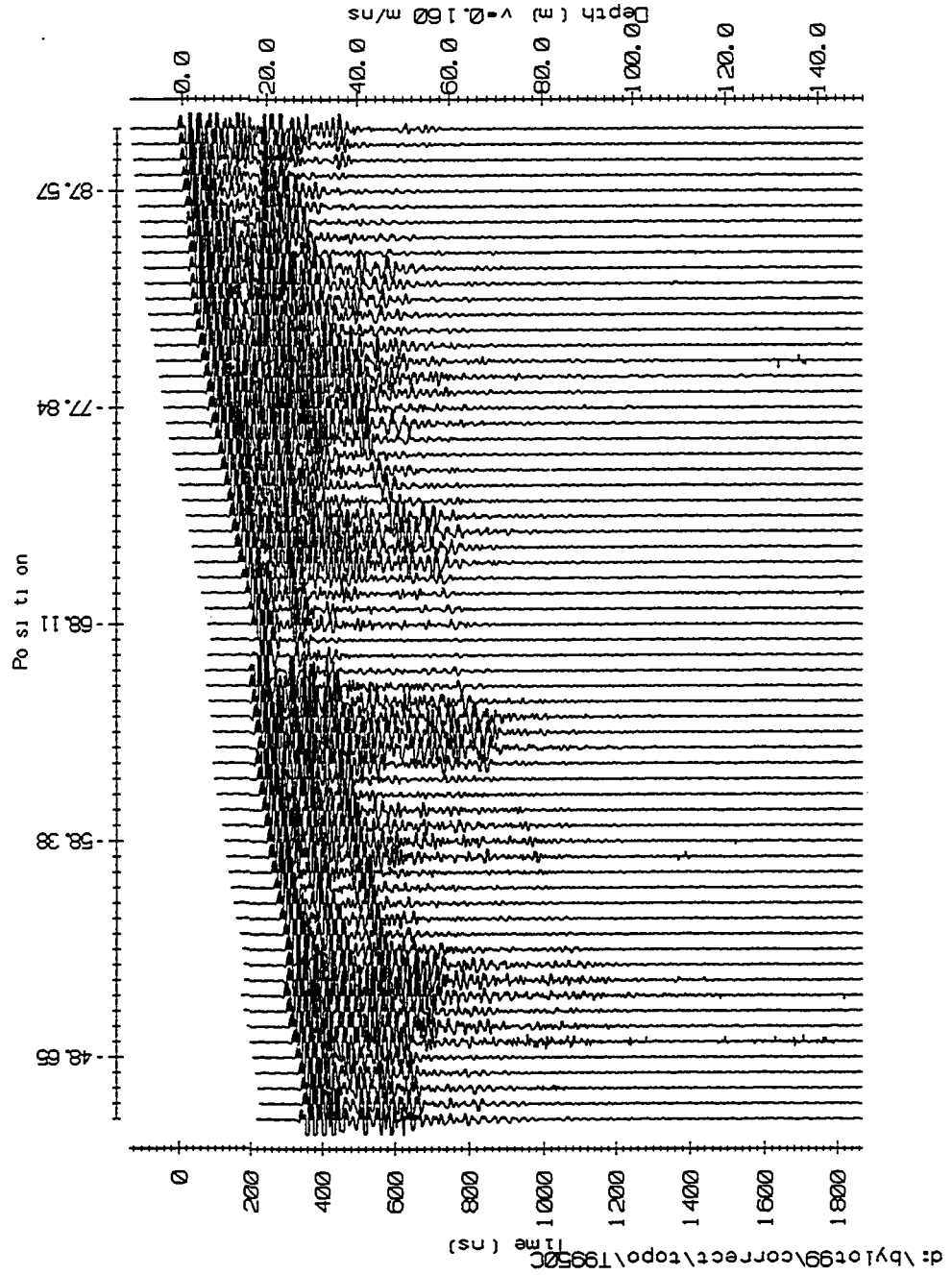


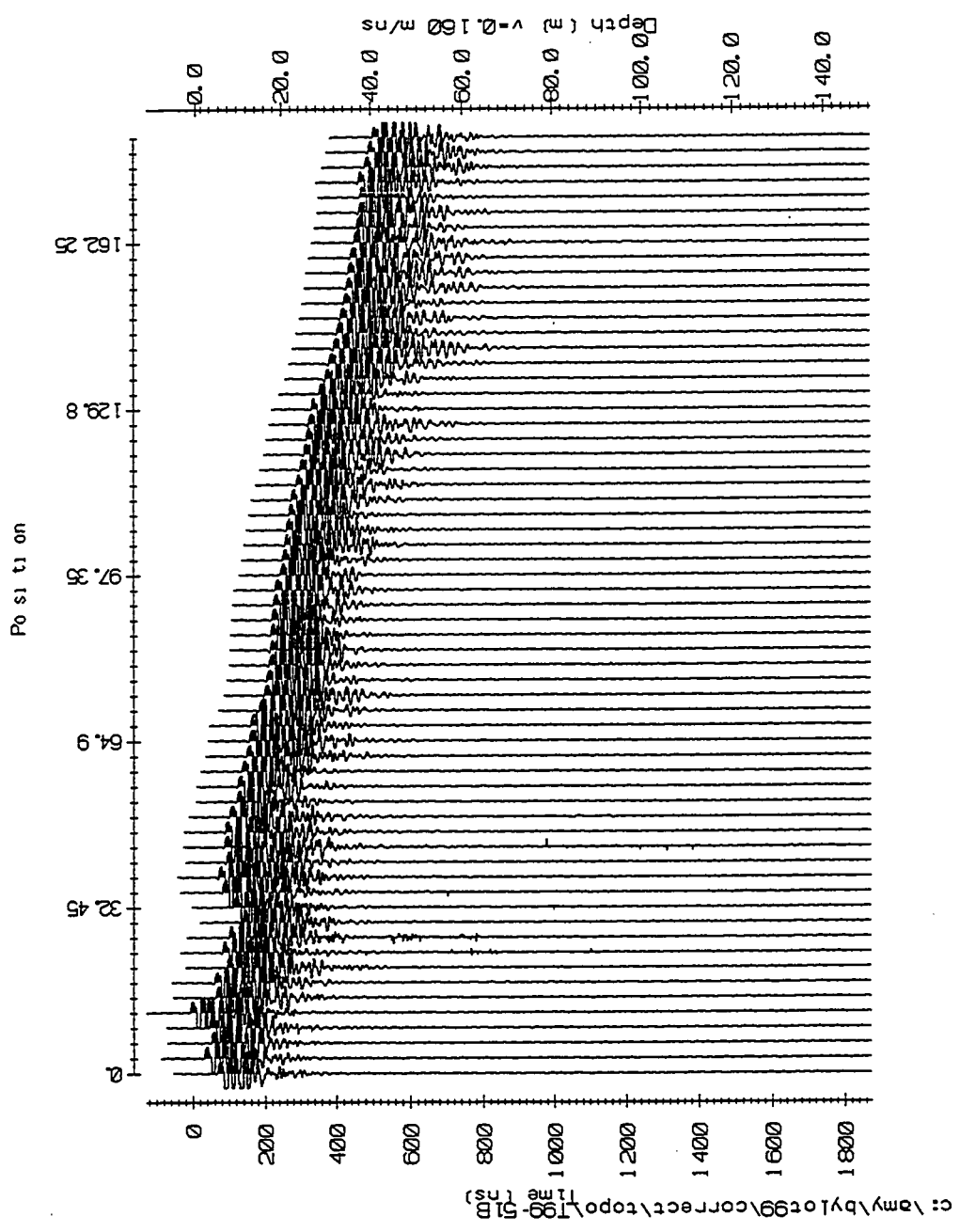


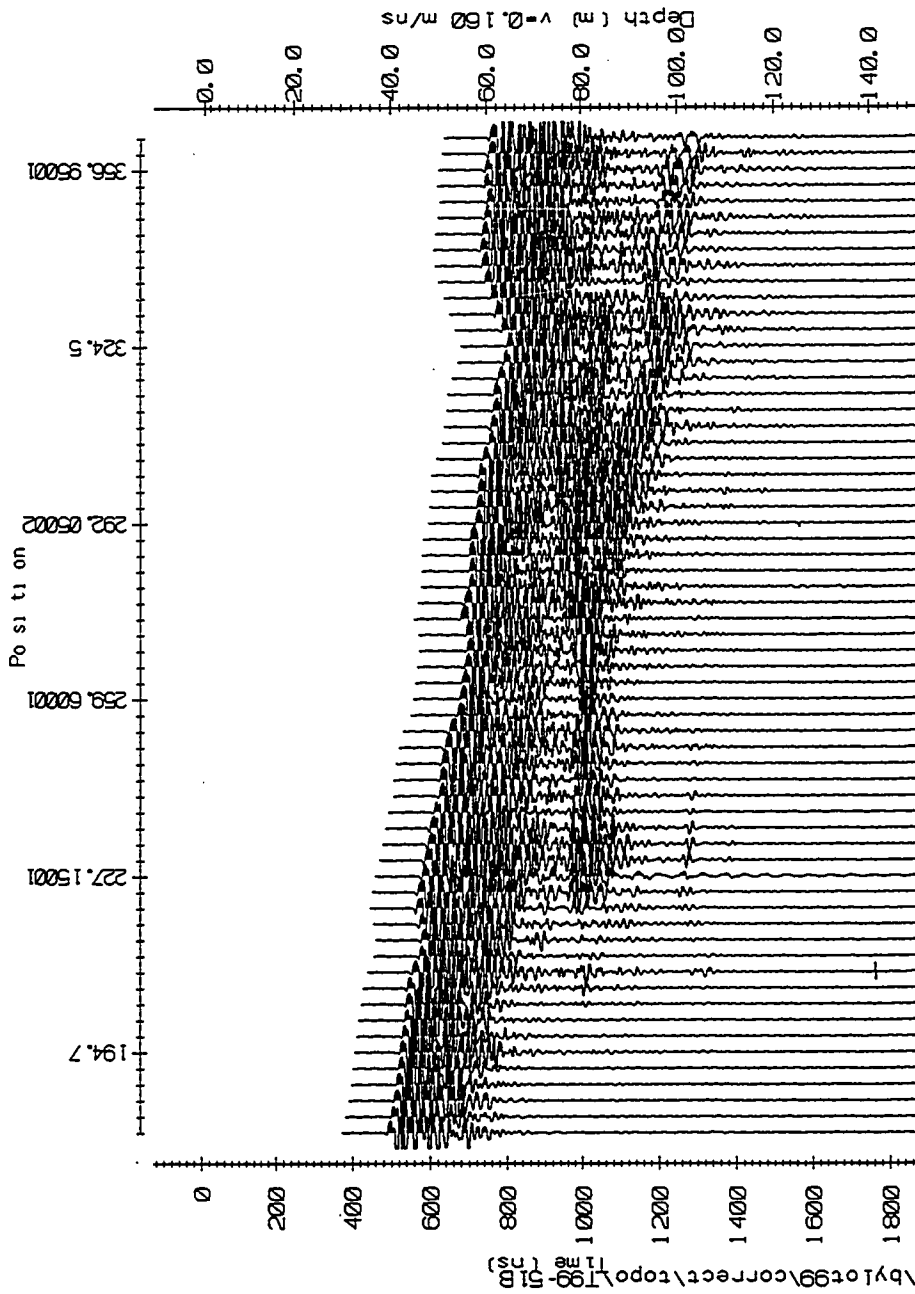
d:\bylot99\correct\topo\T99-46











c:\my\bylot99\correct\topo\T99-51B

